

Anaerobic Carbon Monoxide Dehydrogenase:
Mechanism of CO-Oxidation at the $[\text{NiFe}_4\text{S}_4\text{OH}_x]$ Cluster
and Nickel-Processing by its ATPase CooC

DISSERTATION

zur Erlangung des Doktorgrades
der Naturwissenschaften
(Dr. rer. nat.)

der Fakultät für
Biologie, Chemie und Geowissenschaften
der Universität Bayreuth
vorgelegt von

Jae-Hun Jeoung
aus Korea

Bayreuth 2008

Die Untersuchungen zur vorliegenden Arbeit wurden von April 2004 bis September 2008 an der Universität Bayreuth unter der Leitung von Herrn Prof. Dr. Holger Dobbek durchgeführt.

The investigations of the present work were accomplished from April 2004 until September 2008 at the University of Bayreuth under the supervision of Prof. Dr. Holger Dobbek.

Vollständiger Abdruck der von der Fakultät für Biologie, Chemie und Geowissenschaften der Universität Bayreuth genehmigten Dissertation zur Erlangung des akademischen Grades eines Doktors der Naturwissenschaften (Dr. rer. nat.).

Promotionsgesuch eingereicht am: 15.10.2008

Tag des wissenschaftlichen Kolloquiums: 08.12.2008

Erster Gutachter: Prof. Dr. Holger Dobbek

Zweiter Gutachter: Prof. Dr. Matthias Ullmann

Vorsitzender: Prof. Dr. Andreas Fery

Prof. Dr. Stephan Clemens

Teile der im zeitlichen Rahmen dieser Dissertation erzielten Ergebnisse sind in folgenden Publikationen veröffentlicht:

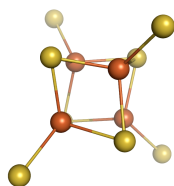
In the time frame of this thesis part of the obtained results have been published in the following publications:

Jae-Hun Jeoung and Holger Dobbek (2007) *Ni,Fe-containing Carbon Monoxide Dehydrogenase*, **Handbook of Metalloproteins**, A. Messerschmidt (ed.), John Wiley & Sons, DOI: 10.1002/0470028637.met213, Article in Online.

Jae-Hun Jeoung and Holger Dobbek (2007) *Carbon Dioxide Activation at the Ni,Fe-Cluster of Anaerobic Carbon Monoxide Dehydrogenase*, **Science** (318), 1461-1464.

Jae-Hun Jeoung, Diana A. Pippig, Berta M. Martins, Nadine Wagener and Holger Dobbek (2007) *H₂THP: A Novel Class of Hexameric, Tyrosine-coordinated Heme Proteins*, **Journal of Molecular Biology** (368), 1122-1131.

ACKNOWLEDGEMENTS



Bioinorganic Chemistry

First, I would like to thank my supervisor, **Prof. Dr. Holger Dobbek**, for giving me the opportunity to work with this fantastic topic and for having confidence in me. I am grateful for his enthusiastic and friendly supervision during the past four years. I am greatly indebted to him for the work we have carried out and the successes we have achieved.

I hereby thank for Prof. Dr. Dr. h.c. Robert Huber, FRS, Dr. Sofia Macieira and Mr. Snežan Marinkovic for giving me the opportunity to work with them and for sharing their experiences at the beginning of my research. My time at the Max Planck Institute of biochemistry (Structure Research, February – June 2004) has been a wonderful and rewarding experience. I am forever indebted to these people for their contributions to my scientific growth over the years.

I wish to thank Dr. Berta Martins for her constant encouragement, support and guidance, not only for the scientific work but also for the beginning of my life in Martinsried and Bayreuth. I am also grateful for her proofreading of my thesis.

I would also like to acknowledge the former Diploma students, Diana Pippig (worked with HTHP), Till Giese and Marlene Grünerwald (worked with CooC proteins) and Christian Gerhold (worked with HGO). I wish them great success in their Ph. D. work.

I greatly thank Roman Jacob for helping in measurement and interpretation of CD spectra.

I thank PD. Dr. Vitali Svetlitchnyi for helpful advise during *E. coli* cultivation and activity measurements of CODH, and for his kind donation of *C. hydrogenoformans* cells.

I wish to acknowledge the entire Lab members of the Bioinorganic Chemistry team (formerly Protein Crystallography) for their resources and for providing such a supportive and inspiring work environment.

To my parents in Korea, I would like to thank them for their patience, encouragements and endless supports during my life.

Last but not least I want to acknowledge my family: my wife **Hea-Suk**, my son **Hyun-Bin** and my daughter **Ye-Rin** for their support, patience and love.

CONTENTS

ABBREVIATIONS	1
ZUSAMMENFASSUNG	3
SUMMARY	5
INTRODUCTION	6
1. CHEMISTRY OF CARBON MONOXIDE AND CARBON DIOXIDE	6
1.1. CARBON MONOXIDE (CO)	6
1.2. CARBON DIOXIDE (CO ₂)	7
2. CARBON MONOXIDE DEHYDROGENASES (CODHS)	9
2.1. MO-,CU-CONTAINING CODH	10
2.2. NI-,FE-CONTAINING CODH	14
3. NICKEL ENZYMES AND NICKEL PROCESSING SYSTEMS	20
3.1. HYDROGENASE SYSTEM	22
3.2. UREASE SYSTEM	24
3.3. CODH AND ACETYL-COA SYNTHASE SYSTEMS	26
4. STRUCTURAL COOC HOMOLOGUES IN THE SIMIBI CLASS	28
5. AIM OF STUDY	32
MATERIALS AND METHODS	33
1. CHEMICALS	33
2. ANAEROBIC WORK	33
3. BACTERIAL STRAINS AND CULTURE MEDIA	34
3.1. CARBOXYDOTHERMUS HYDROGENOFORMANS Z-2901	34
3.2. ESCHERICHIA COLI AND CULTURE MEDIA	34
4. MOLECULAR BIOLOGY	34
4.1. CLONING AND MUTAGENESIS OF COOC1	35
4.2. CLONING AND MUTAGENESIS OF COOSII	36
5. HETEROLOGOUS EXPRESSION OF PROTEIN	36
5.1. EXPRESSION OF COOC1	36
5.2. EXPRESSION OF REC-CODHII	37
6. PURIFICATION OF PROTEIN	38
6.1. PURIFICATION OF COOC1	38

6.2. PURIFICATION OF REC-CODHII	39
7. MEASUREMENTS OF ENZYMATIC ACTIVITIES	40
7.1. NTPASE ACTIVITIES OF COOC1	40
7.2. CO-OXIDATION/CO ₂ -REDUCTION ACTIVITIES OF REC-CODHII	40
7.2.1. CO-OXIDATION ACTIVITY	40
7.2.2. CO ₂ -REDUCTION ACTIVITY	41
8. SPECTROSCOPIC ANALYSIS	41
8.1. UV-VISIBLE SPECTROSCOPY	41
8.1.1. COOC1 SPECTRA	42
8.1.2. REC-CODHII SPECTRA	42
8.2. CIRCULAR DICHROISM (CD) SPECTRA OF COOC1	42
8.2.1. FAR-UV CD SPECTRA	42
8.2.2. THERMALLY INDUCED UNFOLDING CD SPECTRA	43
9. SPECTROSCOPIC DETERMINATION OF NICKEL-BINDING TO COOC1	43
10. OLIGOMERIC STATES ANALYSIS OF COOC1	44
11. CRYSTALLOGRAPHIC METHODS	45
11.1. CRYSTALLIZATION OF COOC1 AND REC-CODHII	45
11.2. MANIPULATION OF CRYSTALS	46
11.3. DATA COLLECTION	47
11.4. STRUCTURE DETERMINATION	47
11.5. STRUCTURE REFINEMENT AND EVALUTION	47
12. MISCELLANEOUS METHODS	48
12.1. DETERMINATION OF PROTEIN CONCENTRATION	48
12.2. SDS-PAGE	48
12.3. COMPUTER SOFTWARES	48
RESULTS	49
1. CLONING	49
1.1. CLONING OF COOC1	49
1.2. CLONING OF COOSII	49
2. PROTEIN EXPRESSION AND PURIFICATION	50
2.1. EXPRESSION AND PURIFICATION OF COOC1	50
2.2. EXPRESSION AND PURIFICATION OF REC-CODHII	52
3. ATPASE AND GTPASE ACTIVITIES OF COOC1	55
4. SPECTROSCOPIC CHARACTERIZATION OF WILD-TYPE AND CLUSTER C-MISSING REC-CODHII	57
5. SPECTROSCOPIC DETERMINATION OF NI-BINDING AND NI-TITRATION OF COOC1	58

6. FAR-UV CD SPECTRA AND THERMAL UNFOLDING TRANSITIONS FOLLOWED BY CD OF COOC1	61
7. OLIGOMERIC STATES OF COOC1 STUDIED BY GEL FILTRATION	62
8. CRYSTALLIZATION	64
8.1. <i>CRYSTALLIZATION OF COOC1</i>	64
8.2. <i>CRYSTALLIZATION OF REC-CODHII</i>	65
9. STRUCTURES OF REC-CODHII	65
9.1. <i>OVERALL STRUCTURE OF REC-CODHII</i>	65
9.2. <i>STRUCTURES OF THREE-REDOX STATES IN REVERSIBLE CO₂-REDUCTION</i>	65
9.3. <i>PROTON CHANNEL MUTANT H96D AND WATER NETWORK IN REC-CODHII</i>	69
9.4. <i>STRUCTURE OF CLUSTER C-MISSING REC-CODHII</i>	71
10. STRUCTURES OF COOC1	72
10.1. <i>OVERALL STRUCTURES</i>	72
10.2. <i>NUCLEOTIDE BINDING SITE</i>	80
10.3. <i>METAL BINDING SITE</i>	84
DISCUSSION	87
1. CARBON DIOXIDE ACTIVATION AT THE Ni,Fe-CLUSTER OF ANAEROBIC CO DEHYDROGENASE	87
2. SUBSTRATE AND PRODUCT TRANSFER PATHWAYS IN CO DEHYDROGENASE	92
3. IMPLICATIONS OF CLUSTER C-MISSING CO DEHYDROGENASE	93
4. COOC1 IS AN ATPASE	94
5. COOC1 IS A NICKEL-BINDING PROTEIN	95
6. COOC1 UNDERGOES Ni- AND NUCLEOTIDE-DEPENDENT DIMERIZATION	98
7. FUNCTIONAL MODEL FOR Ni-PROCESSING OF COOC1	100
OUTLOOK	103
REFERENCES	104
APPENDIX	116
1. APPENDIX TABLES	116
2. APPENDIX FIGURES	122

ERKLÄRUNG (DECLARATION)**132**

ABBREVIATIONS

ADP	Adenosine-5'-diphosphate
APS	Ammoniumperoxo-disulfate
ATP	Adenosine-5'-triphosphate
BSA	Bovine serum albumin
Cam	Chroloamphenicol
CCP4	Collaborative Computational Project
CO	Carbon monoxide
CO ₂	Carbon dioxide
CN	Cyanide
CNS	Crystallography and NMR System
DT	Sodium dithionite
DTT	Dithiothreitol
EDTA	Ethylene diamine tetraacetic acid
FAD	Flavin-adenine-dinucleotide
Fig.	Figure
HEPES	4-(2-hydroxyethyl)-1-piperazineethanesulfonic acid
K_{cat}	Catalytic rate constant
K_d	Dissociation constant
K_m	Michaelis constant
Km	Kanamycine
LB	Luria Bertani
MBS	Metal-binding site
MCD	Molybdopterin-cytosine dinucleotide
MES	2-(N-morpholino) ethanesulfonic acid
mTB	Modified Terrific Broth
MV	Methyl viologen
MW	Molecular weight
n-BIC	n-Butyl isocyanide
OH _x	Water or hydroxo
OD	Optical density
ox	Oxidized
PAGE	Polyacrylamide gel electrophoresis
PCR	Polymerase chain reaction
PDB	Protein data bank

PEG	Polyethylene glycol
Rec-CODHII	Recombinant CO dehydrogenase II
red	Reduced
rpm	Rotation per min
SDS	Sodium dodecyl sulfate
SHE	Standard hydrogen electrode
SHP	Sepharose High Performance
SIMIBI	Signal recognition particle MinD and BioD
Subscript of protein	Indicative of source organism (XXX _{Ch} : <i>C. hydrogenoformans</i>)
Tab.	Table
TCEP	Tris (2-carboxyethyl) phosphine hydrochloride
TEMED	<i>N,N,N',N'</i> -Tetramethylethylenediamine
Tet	Tetracycline
T _m	Melting temperature
TRAFAC	Translation factor-related
Tris	Tris (hydroxymethyl) aminomethane
U	Unit
UV-vis	Ultra-violet visible
v/v	Volume per volume
w/v	Weight per volume

ZUSAMMENFASSUNG

Anaerobe CO-Dehydrogenasen (CODH) katalysieren die reversible Oxidation von CO zu CO₂ an einem komplexen Metallzentrum, das Ni, Fe und S enthält und als Cluster C bezeichnet wird. In dieser Arbeit wird ein heterologes Expressiossystem für CODHII aus *Carboxydotherrnus hydrogenoformans* in *E. coli* vorgestellt sowie Kristallstrukturen von CODHII in verschiedenen Zuständen. In einem reduzierten Zustand mit einer exogen zur Verfügung gestellten CO₂-Quelle wurde CO₂ beobachtet, das Ni und Fe1 verbrückt und das durch die Bindung an Cluster C reaktiv aktiviert wird. Der Ligand CO₂ komplettiert die quadratisch-planare Koordination des Ni-Ions und ersetzt den H₂O/OH⁻-Ligand an dem Fe1-Ion in den zwei anderen Zuständen. Der bei der Katalyse verbrauchte H₂O/OH⁻-Ligand wird stets durch ein benachbartes Netzwerk aus Wassermolekülen ersetzt. Der Ausstoß der Protonen, die bei der reversiblen CO-Oxidation produziert werden, erfolgt durch einen semikonservierten Histidinkanal. Die Mutation von His96, eines von vier halbkonservierten Histidinen, zu Asp verringerte die Aktivität der CO-Oxidation auf 2,7 % des Wildtyps, was auf eine essentielle Rolle dieser Aminosäure bei der Katalyse hindeutet. Die Struktur von H96D-CODHII zeigt, dass das Verschwinden der Aktivität nicht auf einer Fehlfaltung des Proteins und/oder auf der Abwesenheit von Metallzentren im Protein beruht. Eine andere Variante von CODHII, die nicht Cluster C, sondern nur die Cluster B und D enthält, wurde strukturell charakterisiert. Die Struktur der CODHII ohne Cluster C ist identisch mit der Struktur des aktiven Enzyms. Auch die Reste, die die Metalle von Cluster C koordinieren, befinden sich an den gleichen Positionen wie in dem aktiven Wildtypenzym. Von allen Metallen in Cluster C zeigt nur das Fe1-Ion eine alternative Position, was anscheinend der Grund für die beobachtete Heterogenität von Cluster C ist. Die Strukturen, die in dieser Arbeit vorgestellt werden, bestätigten den Mechanismus der CO-Oxidation/CO₂-Reduktion am Ni-Fe1-Paar von Cluster C. Außerdem zeigen sie die Kanäle, die einen Substrat- / Produkttransfer während der Katalyse ermöglichen.

Die ATPase CooC1 aus *C. hydrogenoformans* gehört zu der MinD-Familie aus der Klasse der SIMIBI-NTPasen, die ein abgewandeltes Walker A-Motiv enthalten. Es wurde vorgeschlagen, dass das Protein an der Reifung von Cluster C der CODH beteiligt ist (Jeon et al., 2001). Gereinigtes CooC1 liegt in Lösung als Monomer mit einem Molekulargewicht von 32 kDa vor. Die Anwesenheit von Ni(II) induziert eine Dimerisierung von CooC1, wobei das Protein ein Ni(II)-Ion pro Dimer mit nanomolarer Affinität bindet. Die Kristallstruktur von CooC1 mit gebundenem Metall identifizierte das konservierte CXC-Motiv eindeutig als Metallbindungsstelle, das für die Dimerisierung verantwortlich ist. In Lösung unterliegt CooC1 auch einer Nukleotid-abhängigen Dimerisierung. Es bildet ein stabiles Dimer in Gegenwart von

ATP. Die K8A-CooC1-Mutante, bei der ein Ala das charakteristische Lys ersetzt, kann weder ATP hydrolysieren noch ATP-abhängig ein stabiles Dimer bilden. Vergleiche mit strukturellen Homologen der MinD-Familie ergaben, dass die ATP-induzierte Dimerstruktur von CooC1 eine andere Konformation besitzt als das Ni-induzierte Dimer. Auf der Basis von biochemischen Daten und Strukturen von CooC1 in Kombination mit einem Modell für die ATP-induzierte Dimerisierung, wird ein Reaktionszyklus vorgeschlagen, wie die Ni-Prozessierung in CooC1 für die Reifung von Cluster C ablaufen könnte.

SUMMARY

Anaerobic CO dehydrogenases (CODH) catalyze the reversible oxidation of CO to CO₂ at a complex metal center containing Ni, Fe and S called cluster C. In this work, a heterologous expression system of CODHII from *Carboxydotherrmus hydrogenoformans* in *E. coli* and the crystal structures of CODHII in different states are reported. CO₂ bridging the Ni-Fe1 site is observed in a reduced state with exogeneously supplied CO₂-source, and is reductively activated by binding to cluster C. The ligand CO₂ completes the square-planar coordination of the Ni ion and replaces the H₂O/OH⁻ ligand at the Fe1 ion in the other two states. The H₂O/OH⁻ ligand is replenished by a neighboring network of water molecules. Protons produced from the reversible CO oxidation are expelled through a semi-conserved histidine channel. The mutation of His96, one of four semi-conserved histidines to Asp diminished CO-oxidation activity to 2.7% of wild-type, indicating its essential role in catalysis. The structure of H96D CODHII reveals that the abolished activity is not originated from protein misfolding and/or absence of metal centers in the protein. Another variant of CODHII devoid of cluster C, but containing clusters B and D, was structurally characterized. This cluster C-missing CODHII shows an identical protein scaffold to the structure of active enzyme, and the residues coordinating the metals of cluster C display the same location as the active wild-type enzyme. From all metals of cluster C, only the Fe1 ion displays an alternative position, which appears to be the reason for the observed cluster C heterogeneity. The structures presented in this work define the mechanism of CO oxidation/CO₂ reduction at the Ni-Fe site of cluster C and show the channels that facilitate the transport of substrate/product during catalysis.

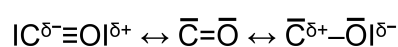
The ATPase CooC1 from *C. hydrogenoformans* belongs to the MinD family of the SIMIBI class NTPases containing a deviant walker A motif. The protein has been proposed to participate in the maturation of cluster C of CODH (Jeon et al, 2001). As-isolated CooC1 shows monomeric state in solution with a molecular weight of 32 kDa. The presence of Ni(II) induces dimerization of CooC1, and the protein binds one Ni(II) per dimer with nanomolar affinity. The crystal structure of Metal-bound CooC1 clearly identified the conserved CXC motif as the metal-binding site, which is responsible for the dimerization. In solution, CooC1 also undergoes nucleotide-dependent dimerization and forms a stable dimer in the presence of ATP. The K8A CooC1 mutant, where Ala replaced the signature Lys is incapable of both ATP hydrolysis and ATP-dependent stable dimer formation. Compared to other structural homologues of the MinD family, the ATP-induced dimer structure of CooC1 shows a different conformation than the Ni-induced dimeric state. On the basis of biochemical data and structures of CooC1 in combination with a model of ATP-driven dimerization, a reaction cycle of CooC1 in Ni-processing for the maturation of cluster C is presented.

INTRODUCTION

1. Chemistry of Carbon Monoxide and Carbon Dioxide

1.1. Carbon Monoxide (CO)

Carbon monoxide (CO), a $10e^-$ molecule, is a toxic, colorless, odorless, and tasteless gas. The difference in formal charge and electronegativity cancels each other out producing a small dipole moment with its negative end on the carbon atom {Kutzelnigg, 2002}, which can be represented by three resonance structures (Scheme 1).



Scheme 1

Because of a partial triple bond (the most left form) that is likely to pull the six-shared electrons closer to oxygen than carbon atom, $C\equiv O$ is a weak Lewis base and an unsaturated soft ligand that can accept metal d_{π} electrons by a process called π back-bonding. Thus, CO acts as a σ donor and π acceptor that can form stable complexes with the low valent states of the metals, which the π -bonding weakens the carbon-oxygen bond compared with free carbon monoxide. Because of the multiple bond character of the M-CO linkage, the distance between the metal and carbon is relatively short. This property also classifies CO as a toxic chemical since metalloproteins containing low valent metals such as iron or nickel can be inhibited by binding of CO to their metals. The carbonyl ligand is versatile and displays a range of bonding modes in metal carbonyl cluster chemistry (Fig. 1) (McIndoe, 2000). The most frequently encountered mode is terminal, but bridging between two (μ_2) or three (μ_3) metals also occurs. The increased π -bonding due to back-donation from more metal centers results in further weakening of the C-O bond. Much less common in bonding modes is that both C and O bind to the metal, e.g. $\mu_3-\eta^2$.

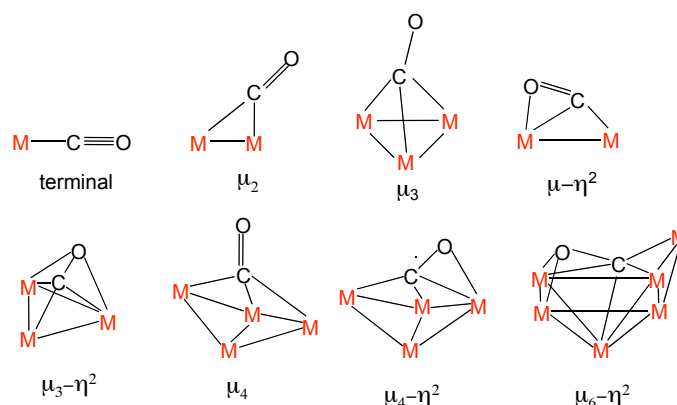


Figure 1. Bonding modes of transition metal carbonyl complex. Redrawn from the reference (McIndoe, 2000).

In organometallic chemistry, conversion of CO to CO₂ and H₂ from water at high temperature with varieties of metal catalysts is known as the water-gas shift reaction (WGSR, Eq. 1 and Fig. 2) (Ford & Rokicki, 1988; Aresta & Dibenedetto, 2007). In this reaction, a metal carboxylate intermediate is formed by nucleophilic attack of the activated water by metal hydride (-OH) on carbon of M-CO and CO₂ is eliminated leaving a metal-hydride. The metal-hydride then attacks water to generate the hydroxide nucleophile and the active catalyst.

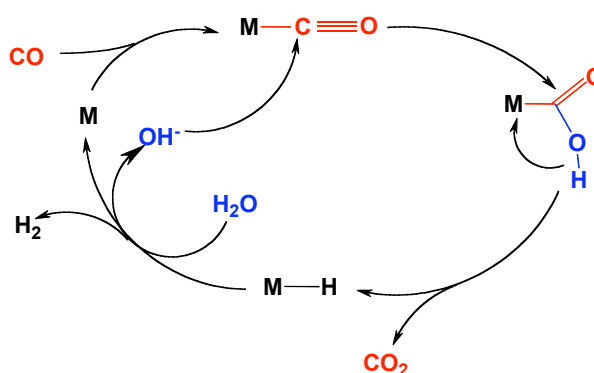
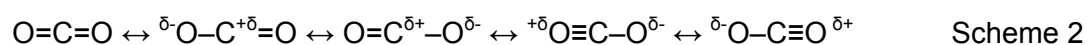


Figure 2. The water-gas shift reaction.

1.2. Carbon Dioxide (CO₂)

Carbon dioxide, CO₂, is a 16e⁻ molecule and is linear in its ground state. The molecule itself is nonpolar although it contains two polar C–O bonds: charges in the C–O bonds are separated in opposite direction with equal intensity (Scheme 2; Aresta & Dibenedetto, 2007).



Because of the polarity of the CO₂ molecule, it exhibits two quite different reaction sites. The carbon atom behaves electrophile (Lewis acid), while the oxygen atoms are mildly nucleophilic (weak Lewis base), which makes CO₂ a bi-functional catalyst (Dibenedetto, 2002) for its activation and conversion. Since the electrophilicity of carbon is higher than the nucleophilicity of each oxygen atoms, CO₂ commonly behaves as an electrophile. When the carbon atom of CO₂ is bonded to a third atom, the linear geometry in the ground state changes to a bent geometry with the O–C–O angle close to 133° to minimize the electrostatic repulsion and the molecular energy (Rabalais et al, 1971). Several theoretical calculations and X-ray structural analysis on modes of CO₂ coordination to metals in organometallic chemistry have been

reported and reviewed (Gibson, 1999, Aresta & Dibenedetto, 2007, and Gibson, 1996). The bonding modes of CO₂ to metal centers can be classified and are shown in Tab. 1.

Table 1. Bonding modes and structural types of metal-CO₂ complexes.

Bonding Mode	Structural types	M ¹	O-C-O angle ²	C-O bond length (Å) ²
$\eta^1\text{-O}$ (end-on)		U	180°	1.122 / 1.277
$\eta^1\text{-C}$		Rh	126°	1.20 / 1.25
$\eta^2\text{-C,O}$ (side-on)		Ni	136.2°	1.211 / 1.257
$\mu_2\text{-}\eta^2$		Fe-Re	121.9°	1.226 / 1.298
$\mu_2\text{-}\eta^3$ (class I)		Re-Re	113.2°	1.289 / 1.296
$\mu_2\text{-}\eta^3$ (class II)		Re-Sn	116.8°	1.26 / 1.31
$\mu_3\text{-}\eta^3$		Os-2Rh	116.3°	1.300 / 1.309
$\mu_3\text{-}\eta^4$		Co-2K	134.9°	1.20 / 1.24
$\mu_4\text{-}\eta^4$		Ru	120.9°	1.245 / 1.283
$\mu_4\text{-}\eta^5$		Rh-Zn	112.2°	1.322 / 1.29

¹ M indicates metal types and examples are chosen based on the X-ray structural analysis. ² Values of angle and length are adapted from (Gibson, 1996) and references are therein.

The simplest type of CO₂-bridged bimetallic complex is the $\mu_2\text{-}\eta^2$ bonding mode that involves coordination of the carbon atom to one metal and bonding of one oxygen atom to a second metal center. However, there are many variations depending on whether the two metal centers are bound together, bridged by other groups, totally independent or bridged CO₂ as a repeating unit in a polymer chain (Gibson, 1996). Nevertheless, all of the $\mu_2\text{-}\eta^2$ complexes show one short and one long C–O bond and present a relatively large O–C–O bond angle, varying from 117 to 124°. There are two distinct types of compounds in the $\mu_2\text{-}\eta^3$ type having the carbonyl carbon bound to one metal center and both carbonyl oxygens bound to a second metal. The distinguishing feature for class I and class II is the unequal nature of the O–M₂ bond lengths in class II compounds. In addition, the shorter C–O bond always is paired with the longer O–M₂ bond. Additional feature is that the O–C–O bond angles in class I compounds are usually shorter than those in class II. One general characteristic in all bonding modes of CO₂-metal complexes is that the carbon-oxygen bond order decreases and the length of the C–O bond increases, moving from the η^1 to the $\mu_4\text{-}\eta^5$ mode (Aresta & Dibenedetto, 2007; Gibson, 1996).

2. Carbon Monoxide Dehydrogenases (CODHs)

CO is a constituent of the atmosphere, with the majority of it produced by human (e.g., automobile and industrial emissions (Ascone & Marcy, 2005)) as well as by microorganisms (Ragsdale, 2007). CO contributes to global warming and is a potent human poison. The microbial CO metabolism plays an essential role in the balance between emission and removal of CO in the atmosphere, since 10⁸ tons of CO are removed from the lower atmosphere of the earth by bacterial oxidation every year (Bartholomew & Alexander, 1979), helping to maintain ambient CO below toxic levels. Despite its deleterious effects on many species, CO is an important carbon and energy source since the earliest life on Earth. Microbes use carbon monoxide dehydrogenase (CODH, EC 1.2.99.2, CO: *acceptor oxidoreductase*) to utilize CO as their sole source of carbon and energy. CODH is the key biological catalyst for the reversible oxidation of CO to CO₂ with water as the source of oxygen (Eq. 2).



There are two principal types of CODHs that can be classified according to their cofactor composition, structure and stability in the presence of dioxygen. One is a Mo-, and Cu-containing iron-sulfur cluster flavoprotein found in aerobic carboxidotrophic bacteria such as *Oligotropha carboxidovorans* (Dobbek et al, 1999; Dobbek et al, 2002) and *Hydrogenophaga pseudoflava* (Hänzelmann et al, 2000). The other class, oxygen sensitive Ni-, and Fe-containing CODHs are found in diverse groups of anaerobic bacteria and archaea (*Carboxydothemus hydrogenoformans*, *Rhodospirillum rubrum*, *Moorella thermoacetica* and *Moorella thermophila*)

[(Dobbek et al, 2001; Drennan et al, 2001; Doukov et al, 2002; Darnault et al, 2003); for review, see (Ragsdale, 2004)]. The CO/CO₂ redox reaction (Eq. 2) of CODH uses a ping-pong mechanism (Ragsdale & Kumar, 1996): oxidation of CO to CO₂ producing two electrons reduced CODH in the ping step and reoxidation of the CODH by transferring two electrons to an external electron acceptor in the pong step. Despite their identical principle reaction, the rate of CO-oxidation to CO₂ varies between CODHs. Ni,Fe-containing CODH from *C. hydrogenoformans* reaches a turnover number of 40,000 s⁻¹ (Svetlitchnyi et al, 2001), while the turnover number of the Mo,Cu-containing *O. carboxydovorans* CODH is 107 s⁻¹ (Dobbek & Huber, 2002). The CODH reaction (Eq. 2) is formally equivalent to the WGSR (Eq. 1 and Fig. 2) except the former produces two protons and two electrons and the latter produces hydrogen. This section describes the structural diversity of the two classes of CODHs with their different cofactor composition related to CO-oxidation mechanism.

2.1. *Mo-,Cu-containing CODH*

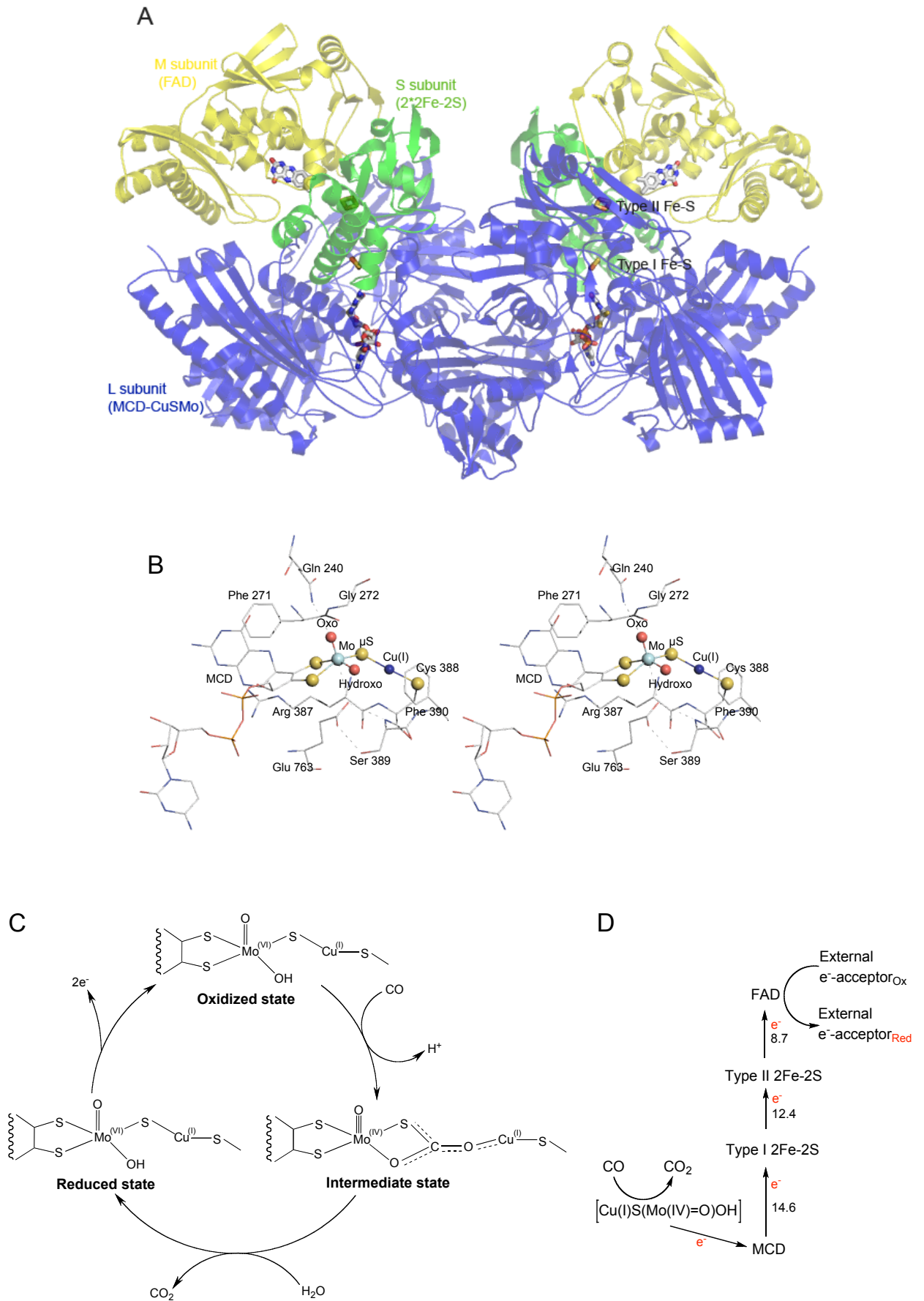
CODH_{oc} from the aerobic bacterium *O. carboxydovorans* is a Mo- and Cu-containing iron-sulfur cluster flavoprotein that belongs to the molybdenum hydroxylase family (Schubel et al, 1995; Hille, 1996). It is the key enzyme responsible for the oxidation of CO to CO₂ (Eq. 2) in the energy conserving reaction when *O. carboxydovorans* grows with CO as sole carbon and energy source (Meyer et al, 2000). CODH_{oc} is structurally characterized by a butterfly shaped 277 kDa dimer of heterotrimers consisting of three subunits in a (LMS)₂ arrangement as shown in Fig. 3A (Dobbek et al, 1999; Dobbek et al, 2002). Each heterotrimer is composed of an 88.7 kDa molybdoprotein (L subunit) carrying the molybdopterin-cytosine dinucleotide (MCD) type of molybdenum cofactor harbouring the active site of the enzyme, a 30.2 kDa flavoprotein (M subunit) that carries a noncovalently bound flavin-adenine dinucleotide (FAD) cofactor and a 17.8 kDa iron-sulfur protein (S subunit) containing two types of [2Fe-2S] clusters, type I and II, distinguished by electron paramagnetic resonance (EPR) spectroscopy (Gremer et al, 2000). Each L subunit in the two heterotrimers possesses a Mo ion bound to MCD. The two independent CO-oxidation active site of the dimer are at a Mo-Mo distance of 52.9 Å without any interconnecting other cofactors.

Recent crystal structure of fully active CODH_{oc} (23.2 units/mg) at true atomic resolution (Dobbek et al, 2002) revealed that the active site is comprised of a MoSCuS binuclear center. The Mo ion is connected to the enedithiolate group of the pyran-ring of the molybdopterin and two oxygens and is bridged via a μ -sulfido ligand (formerly identified as an oxygen) to a Cu ion covalently bound to S_γ atom of a cysteine residue (Cys₃₈₈) in its oxidized state (Fig. 3B). The [CuSMo(=O)OH] active site also interacts noncovalently with residues of the unique VAYRC₃₈₈SFR active site loop (Dobbek et al, 1999; Hänzelmann et al, 2000). The geometry

around Mo in the active site shows a distorted square pyramidal geometry, where the dithiolate group of two S7' and S8' from MCD, one O (hydroxo-group) and one S (sulfido-group) are positioned in the equatorial plane, and an oxo-group at the apical position, which further interacts with residue Gln₂₄₀ located in hydrogen-bonding distance. Glu₇₆₃ is in hydrogen-bonding distance to the equatorial hydroxo-group and the Mo ion. Furthermore, Ser₃₈₉ interacts with Glu₇₆₃ via hydrogen bonds. The Cu ion is linked to the Mo ion via a μ -sulfido ligand and interacts covalently with the protein via the S_v of Cys₃₈₈ in a distorted linear geometry, in which the distances and the angles of the Cu to the ligands corresponds to the oxidation state of Cu(I) from previously characterized biological metal cluster and an inorganic model compounds (Dobbek et al, 2002). When the oxidized active site is reduced regardless of the substrate or chemical reductant, the [CuSMo(=O)OH] has practically an identical geometry on the Mo and Cu sites with slightly increased distance between the Mo and the Cu and between the Mo and Glu₇₆₃, while the Mo-S dithiolate bond length decreases (Dobbek et al, 2002). The Cu(I) is cyanolysable and treatment with potassium cyanide inactivates CODH_{Oc} by altering the geometry of the active site, which the Cu-ion and μ -sulfide are removed (Dobbek et al, 2002). In the cyanide-inactivated structure, an O ligand occupies the former position of the μ -sulfido ligand and completes the geometry of the Mo ion, and Cys₃₈₈ and Glu₇₆₃ move away from the Mo (Dobbek et al, 2002). As cyanide, n-butylicyanide (n-BIC) acts as an inhibitor of CODH_{Oc} producing the EPR-silent Mo and Cu ions, which suggest the oxidation state of Mo(IV) and Cu(I) (Dobbek et al, 2002). Binding of n-BIC was characterized by structure analysis and shows large structural changes at the active site. The carbon atom of the bound-cyanide moiety is linked covalently to the μ -sulfido ligand and the hydroxo-group, while n-BIC nitrogen binds covalently to the Cu-ion with a bond length shorter than expected for single bond character. This forms an "open state" with an increase in the distance between Mo and Cu of more than 1.0 Å and between Mo and Glu₇₆₃ to 0.3 Å. The strongest bond shortening was observed for Mo=O (apical ligand) that showed a formerly double bond character in the other structures (Dobbek et al, 2002). In analogy to the thiocarbamate derivative derived from the n-BIC-bound structures, the authors proposed a CO oxidation mechanism at the active site [CuSMo(=O)OH] of CODH_{Oc} (Dobbek et al, 2002). As shown in the oxidized state of Fig. 3C, incoming substrate CO is inserted between Cu(I), the μ -sulfido ligand and the equatorial hydroxo-group of Mo(VI) producing the thiocarbamate intermediate state. Concomitant formation of the "open state" moves the Cu(I) away from the Mo ion. An increased electrophilicity of the carbon atom of CO results in its attack by the equatorial hydroxo-group that is deprotonated by Glu₇₆₃. Two electrons reduced the Mo ion from +VI to +IV via the sulfido ligand, which is presumably stabilized by Glu₇₆₃. The Cu(I) does not change oxidation state during the mechanism as shown by EPR (Dobbek et al, 2002). The product CO₂ is formed and released by replacement of the incorporated hydroxo ligand by water, closing the bimetallic cluster.

Reoxidation of the reduced Mo(IV) to Mo(VI) for the next round of reaction can be facilitated by transfer of electrons via chain of redox active cofactors to an external electron acceptor (Dobbek et al, 1999; Dobbek et al, 2002; Gremer et al, 2000). Fig. 3D depicts a postulated electron pathway composed of the type I [2Fe-2S] cluster placed 14.6 Å apart from the closest iron to the Mo-MCD, the type II [2Fe-2S] cluster with 12.4 Å distant from the type I, and the solvent exposed cofactor FAD positioned 8.7 Å apart from the type II [2Fe-2S] cluster.

Figure 3. (A) Three-dimensional cartoon-representation of the native CODH_{oc} structure showing a dimer of heterotrimers (PDB ID: 1N5W) adapted from the reference (Dobbek et al, 2002). Each molybdoprotein (L subunit) carrying a MCD-type of molybdenum cofactor with a binuclear CuSMo is presented in *blue*. Iron-sulfur proteins (S subunit) carrying two types, type I and II, of [2Fe-2S] clusters in each heterotrimer are shown in *green*. Each of the two flavoproteins (M subunits) containing FAD are shown in *yellow*. The cofactors are depicted in elemental color. (B) Stereo view of the active site [CuSMo(=O)OH] cluster of CODH_{oc}. (C) The proposed reaction mechanism of the oxidation of CO to CO₂ at the [CuSMo(=O)OH] site deduced from the crystal structures of the oxidized, reduced, and n-BIC-bound states (PDB ID: 1N5W, 1N63, 1N62, respectively) (Dobbek et al, 2002). Only the enedithiolate group of the molybdoprotein is shown here. Details are given in the text. (D) The postulated electron pathway in CODH_{oc} (Gremer et al, 2000). Two electrons generated on the active site Mo(IV) from CO oxidation pass through MCD, type I and II [2Fe-S] centers, and FAD to an external electron acceptor. The shortest distances between cofactors are drawn in Å. Figures are shown in the opposite page.



2.2. Ni-,Fe-containing CODH

Ni-,Fe-containing CODHs found in anaerobic bacteria and archaea are phylogenetically related and function in a variety of energy-yielding pathways (Ragsdale, 2004; Lindahl, 2002). They are O₂ labile and vary in terms of metabolic role, subunit composition, and catalytic activity, which permit their classification into four classes (for review see: Lindahl & Chang, 2001). Class I and II, found in methanogenic archaea such as *Methanosarcina thermophila*, *M. jannaschii*, *M. frisia* and *M. thermophila*, are bifunctional enzymes with a CODH protein that catalyzes CO/CO₂ redox reaction (Eq. 2) and a second protein acetyl-CoA synthase (ACS) that catalyzes the synthesis of acetyl-CoA. These bifunctional enzymes are called ACS/CODHs. Both class I and II enzymes form a multimeric ACS/CODHs with $\alpha\beta\gamma\delta\epsilon$ subunits where $\alpha\epsilon$ subunits possess CODH activity, while β and $\gamma\delta$ correspond to ACS and corrinoid cobalt iron-sulfur protein (CoFeSP), respectively. Class III, found in homoacetogens such as *Moorella thermoacetica* (formerly *Clostridium thermoaceticum*) are also formed a complex of $\alpha_2\beta_2$ heterotetramer of ACS/CODH, respectively, and $\gamma\delta$ of CoFeSP. Class IV CODHs are found in anaerobic CO-utilizing bacteria such as *R. rubrum* and *C. hydrogenoformans* and are monofunctional α_2 homodimers that catalyze exclusively the reversible reduction of CO₂ to CO (Eq. 2) but not the synthesis of acetyl-CoA. Sequence alignment and phylogenetic analysis of the four CODH classes reveals that the α subunit of Class I and II contains 2 extra [4Fe-4S] clusters that are not present in the class III and IV enzymes (Lindahl & Chang, 2001).

During the last few years, crystal structures of Ni-,Fe-containing CODHs from *C. hydrogenoformans* (CODH_{Ch}), *R. rubrum* (CODH_{Rr}) and *M. thermoacetica* (CODH_{Mt}), in which the last is characterized as bifunctional, have been reported (Dobbek et al, 2001; Dobbek et al, 2004; Drennan et al, 2001; Doukov et al, 2002; Darnault et al, 2003). The overall structures of CODH proteins were practically identical showing a mushroom shape formed by two intertwined and covalently linked subunits as shown in Fig. 4A. In the following text, descriptions of residue numbers are based on the structure of CODH_{Ch} (Dobbek et al, 2001). The homodimeric structure comprises five metal-clusters of three types, called B, C and D. The conventional cubane-type [4Fe-4S] cluster (cluster D) bridges two subunits covalently via two cysteines (Cys₃₉ and Cys₄₇) from each subunit. Another cubane-type [4Fe-4S] cluster, called cluster B (or B') coordinated through Cys₄₈, Cys₅₁, Cys₅₆ and Cys₇₀, is located 10 Å away from cluster D at the subunit interface. The active site, called cluster C (or C') is covalently linked by five cysteines (Cys₂₉₅, Cys₃₃₃, Cys₄₄₆, Cys₄₇₆ and Cys₅₂₆) and one histidine (His₂₆₁), is in a distance of 11 Å from cluster B' (or B) and is comprised of the mixed type Ni- and Fe-containing cluster. The residues coordinating these clusters are highly conserved between CODHs from different organisms (Lindahl & Chang, 2001) (see Fig. 31). Inverted V shape of intermolecular

arrangement between these clusters is depicted in Fig. 4B with orientation of cluster C to B' (or C' to B) to cluster D located in the two-fold rotation axis.

Despite of identical overall architecture, the active site cluster C shows significant differences between the reported structures (Dobbek et al, 2004; Volbeda & Fontecilla-Camps, 2005). The cluster C is comprised of an asymmetrical [Ni-4Fe-4/5S] mixed type metallocluster and can be divided into two part, a [3Fe-4S] subsite and a [Ni-X-Fe1] site. As shown in Fig. 4C, all [3Fe-4S] subsite structures display similar geometries, which are analogous to a standard cubane-type [4Fe-4S] with coordination of each iron via three μ^3 -S ligands and one S_V -Cys donor in tetrahedral geometry. The major differences come from the [Ni-X-Fe1] site depending on the presence or absence of a ligand at Ni and between Ni and Fe1. The Ni ion is basically coordinated by two μ^3 -S ligands and one S_V -Cys residue in all structures reported. The Fe1 was spectroscopically characterized as a high-spin ferrous component II (FCII) (Hu et al, 1996) and is unusually coordinated by one μ^3 -S ligand, a S_V from cysteine, a $N_{\epsilon 2}$ from histidine, and in some structures by an additional ligand. The cluster C structure of CO-treated CODH_{Rr} at 2.8 Å resolution (1JQK, Fig. 4C) shows a bridge between Ni and Fe1 by a cysteine ligand producing a distorted trigonal bipyramidal geometry on Ni with an exogenous ligand, which the authors interpreted as bound CO, while Fe1 has a distorted tetrahedral geometry (Drennan et al, 2001). Two structures of CODH_{Mt} from bifunctional ACS/CODH (1MJG and 1OAO, Fig. 4C) show both Fe1 and Ni ions of cluster C coordinated by only three ligands, where Ni ion in CO-treated cluster C shows a putative apical CO ligand (1OAO) (Doukov et al, 2002; Darnault et al, 2003). The cluster C structures of CODH_{Rr} and CODH_{Mt} have an asymmetric [Ni-4Fe-4S] as a basic constituent of the active site cluster. However, three out of four cluster C structures of CODH_{Ch} (1SU6, DTT-grown CO_{short}-treated; 1SU7, DTT-grown; 1SU8, Fig. 4C) analyzed with the highest resolutions among CODHs' structures, revealed an active site comprised of an unusual asymmetric [Ni-4Fe-5S] (Dobbek et al, 2001; Dobbek et al, 2004). The Ni ion is linked by an additional μ^2 -S to Fe1, which completes square-planar geometry of the Ni ion by coordination by two μ^3 -S ligands and a S_V from cysteine. Similar to the Fe1 site of CODH_{Rr}, the μ^2 -S ligand replaces the S_V atom from cysteine forming a tetrahedral geometry around Fe1 in CODH_{IIICh}. The labile μ^2 -S ligand is absent from any of the structures from CODH_{Rr} and CODH_{Mt} and can be removed by incubation of CODH_{IIICh} with CO leading to enzyme inactivation (Dobbek et al, 2004). The structure of cluster C of CO_{long}-treated CODH_{Ch} (1SUF, Fig. 4C) resembles the cluster C of CO-treated CODH_{Mt} (1MJG). The authors proposed that the presence of the μ^2 -S ligand bridged Ni and Fe1 in CODH_{IIICh} is an active form for catalysis derived from a positive correlation between the crystal structure of CO_{long}-treated missing the μ^2 -S ligand and the loss of enzymatic activity during prolonged incubation with CO in solution. In contrast to this observation, Feng and Lindahl reported that sulfide reversibly inactivates both CODH_{Rr} and CODH_{Mt} and that the inhibitory effect of sulfide can be reversed by reduction with CO and DT

(Feng & Lindahl, 2004b). Despite of discrepancy in structures of cluster C between CODHs, all structures treated with CO showed an undefined apical ligand on the Ni ion (1JQK-CODH_{Rr}, 1OAO-CODH_{Mt} and 1SUF-CODH_{Ch}), which has been proposed as a potential binding site for incoming CO substrate because of its direct accessibility through the substrate channel and its empty apical coordination site (Dobbek et al, 2001), but has to be further clarified. This structural heterogeneity of cluster C between diverse organisms could arise from differences in crystallization conditions, especially on the point of use of different reducing agents during crystallization and different initial conditions for crystal soaking experiments, or from the proteins themselves.

Before crystal structures of CODHs were available, many spectroscopic studies including EPR (electron paramagnetic resonance), Mössbauer and ENDOR (electron nuclear double resonance) spectroscopy have been applied to study the CO oxidation mechanism. CO oxidation/CO₂ reduction occurring at the active site cluster C of Ni-,Fe-containing CODHases is supposed to require three different redox states differing by one electron, termed C_{red1}, C_{int} and C_{red2} as shown in Fig. 4D (Lindahl, 2002; Ragsdale, 2004). In this model, C_{red1} is the electronic state of cluster C that is able to convert CO to CO₂ and is paramagnetic (S=1/2 spin state). This state is formed at redox potentials below -200 mV by one electron reduction for C_{ox}, which is diamagnetic (Feng & Lindahl, 2004a). In the C_{red1} state a distinct high spin Fe²⁺ ion (FCII equivalent to Fe1 in Fig. 4C) exists, which interacts with a water or hydroxo species, and CO binds to Ni (Hu et al, 1996; DeRose et al, 1998). CN⁻, a tight-binding inhibitor of CODH, also can bind to the FCII iron of C_{red1} by replacing the bound ligand and dissociates by CO (Hu et al, 1996; Anderson & Lindahl, 1996; DeRose et al, 1998). At pH 7.0, the midpoint potential for the conversion of C_{red1} to C_{red2} is -530 mV (Lindahl et al, 1990b; Lindahl et al, 1990a), which is similar to the normal potential of the CO₂/CO couple of -558 mV (Grahame & Demoll, 1995) and consequently C_{red2} is generated by a two-electron reduction of the C_{red1} state by either turnover with CO or reducing agents. CO₂ binds to C_{red2} and is reduced by two electrons for the reverse reaction, but is also able to bind to C_{red1} noncatalytically (Anderson & Lindahl, 1996). C_{int} is thought to exist as an intermediate redox state between C_{red2} and C_{red1} (Fraser & Lindahl, 1999). The proposed mechanism of CO/CO₂ redox reactions derived from spectroscopic studies (DeRose et al, 1998) is depicted in Fig. 4E. A water or hydroxo ligand binds to the FCII iron site and CO binds to the Ni ion in C_{red1}. The resulting nucleophilic hydroxyl group attacks the carbon of Ni-CO, forming a Ni-bound carboxylate. A base abstracts the proton of the carboxylate intermediate, leading to dissociation of CO₂ and two-electron reduction of the cluster C to yield the C_{red2} state.

After oxidation of CO with water at the active site cluster C, two electrons and two protons in addition to CO₂ are generated and have to be released. An intramolecular electron pathway suggested by Dobbek *et al.* (Dobbek et al, 2001), is built by three additional cubane type [4Fe-

4S] clusters (cluster B, B' and D), and their intramolecular arrangement and directions of electron transfer are shown in Fig. 4B. From cluster C (or cluster C'), buried 18 Å below the surface of the protein, the path continues cluster B' (or cluster B) at which point it diverges toward the protein surface, to cluster D. The distances between cluster C, B' and D are 10 to 11 Å apart, allowing an effective electron transfers in both monomers of the enzyme (Page et al, 1999). Studies using EPR and Mössbauer spectroscopy identified that cluster B undergoes redox change upon reduction (B_{red}), showing the typical paramagnetic signal of $[4Fe-4S]^+$ clusters (Fraser & Lindahl, 1999; Hu et al, 1996). The redox state of cluster D is still elusive. It was suggested that four semi-conserved histidine residues are relevant to transport the protons to the water reservoir near the surface of the protein (Drennan et al, 2001; Lindahl, 2002). Kim *et al.* showed that mutations of these conserved histidine residues (Fig. 31) abolished or diminished CO-oxidation activity without alterations of cluster C (Kim et al, 2004).

Figure 4. (A) Cartoon representation of the CODHII dimer of *C. hydrogenoformans* (PDB ID:1SU8; Dobbek et al, 2004). The subunits are colored by NH₂-terminal domain in *blue*, middle domain in *green*, and COOH-terminal in *red*. (B) Spatial arrangement of five metal clusters of CODHII_{Ch}. The shortest distances for electron transfer from cluster C via cluster B' (the prime denotes that the cluster is donated by the other subunit) possibly to cluster D are indicated. Fe in *red*, S in *yellow* and Ni in *cyan*. (C) Cluster C models of CODHs characterized by crystal structures with PDB codes: 1JQK, CO/Ar-grown CODH_{Rr} at 2.8 Å (Drennan et al, 2001); 1SUF, CO/DTT-grown CODH_{Ch} at 1.15 Å (Dobbek et al, 2004); 1SU8, N₂/DT-grown CODH_{Ch} at 1.10 Å (Dobbek et al, 2004); 1MJG, N₂/DTT-grown CODH_{Mt} at 2.2 Å (Doukov et al, 2002); 1OAO, DT/DTT-grown and CO-treated CODH_{Mt} at 1.9 Å (Darnault et al, 2003). Fe, S and Ni are colored in *red*, *yellow* and *cyan*, respectively. Residues involved in coordination of cluster C and the nearest lysine and histidine are indicated in elemental colors. (D) Mechanism of CO/CO₂ redox catalysis by CODH emphasizing three principle active redox states of the cluster C (Lindahl, 2002), (Ragsdale, 2004). Paramagnetic C_{red1} occurred at redox potential below -200 mV. C_{red2} is also a paramagnetic (E) Proposed mechanism of CO/CO₂ redox catalysis deduced from spectroscopic results. Figure is adapted from DeRose *et al* (DeRose et al, 1998). X and L are unidentified bridging and putative redox-active ligands detected spectroscopically, respectively. Details are given in the text.

Figure 4. (continued)

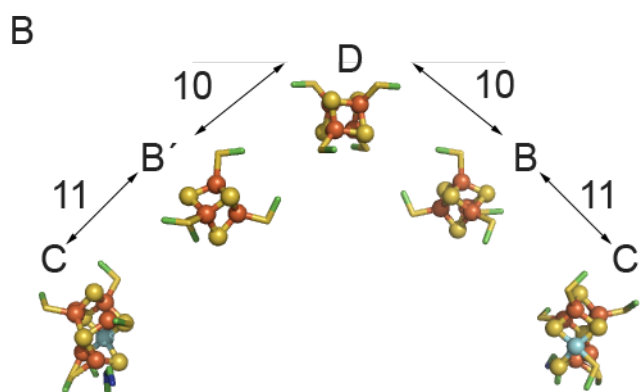
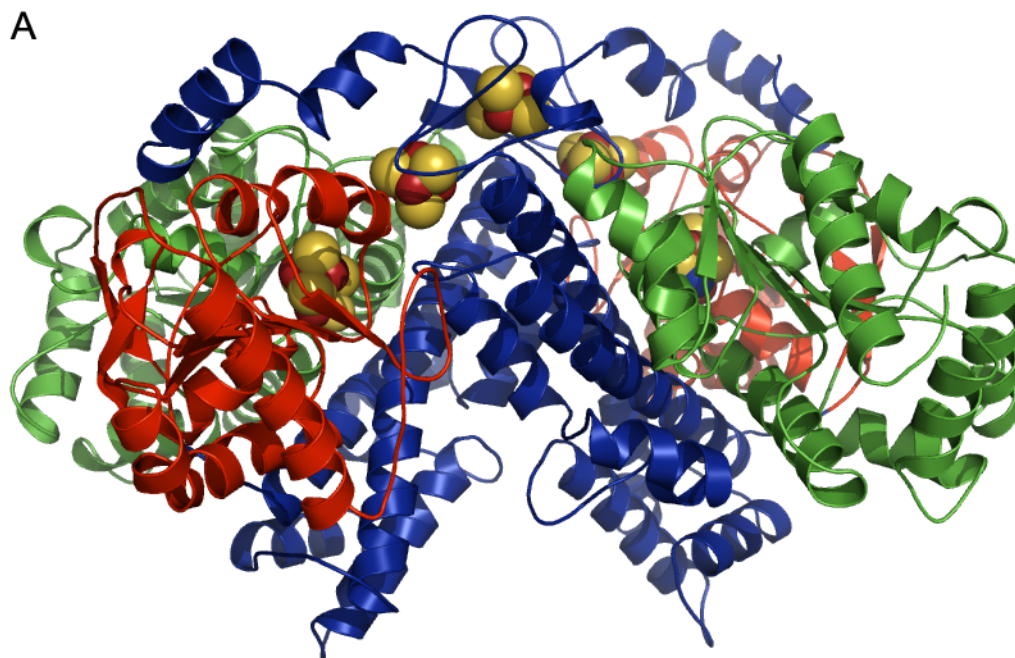
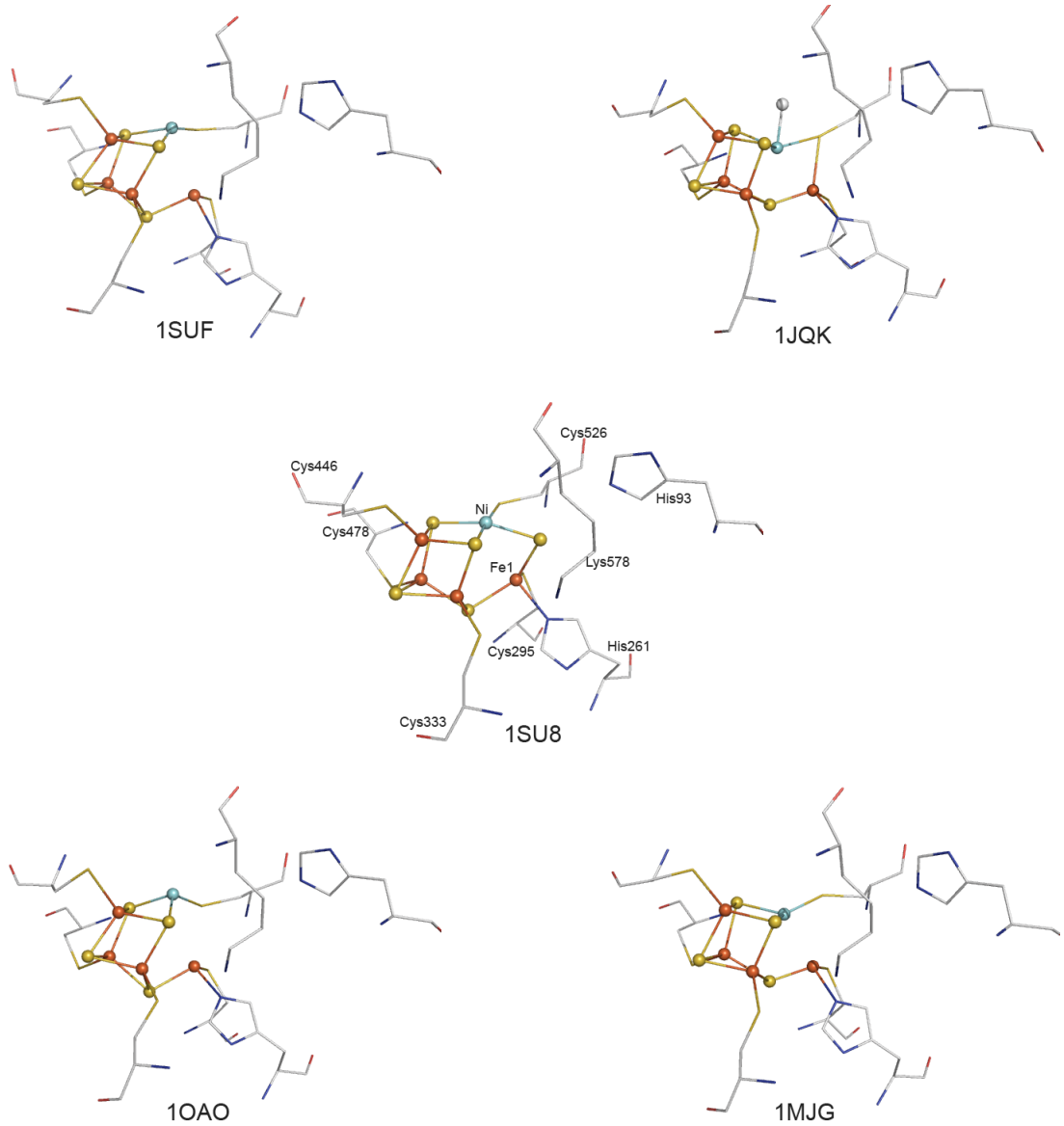


Figure 4. (continued)

C



D

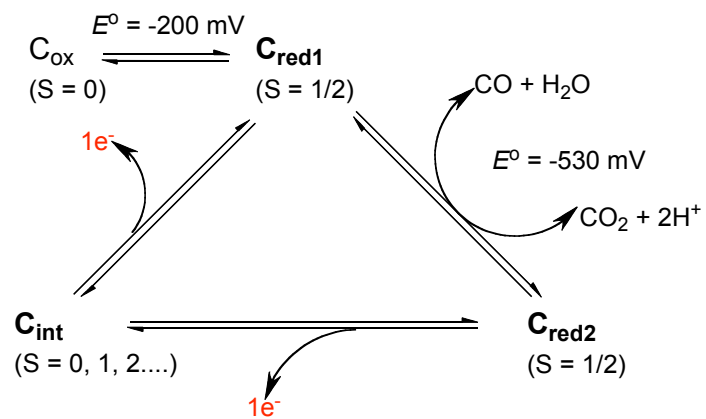
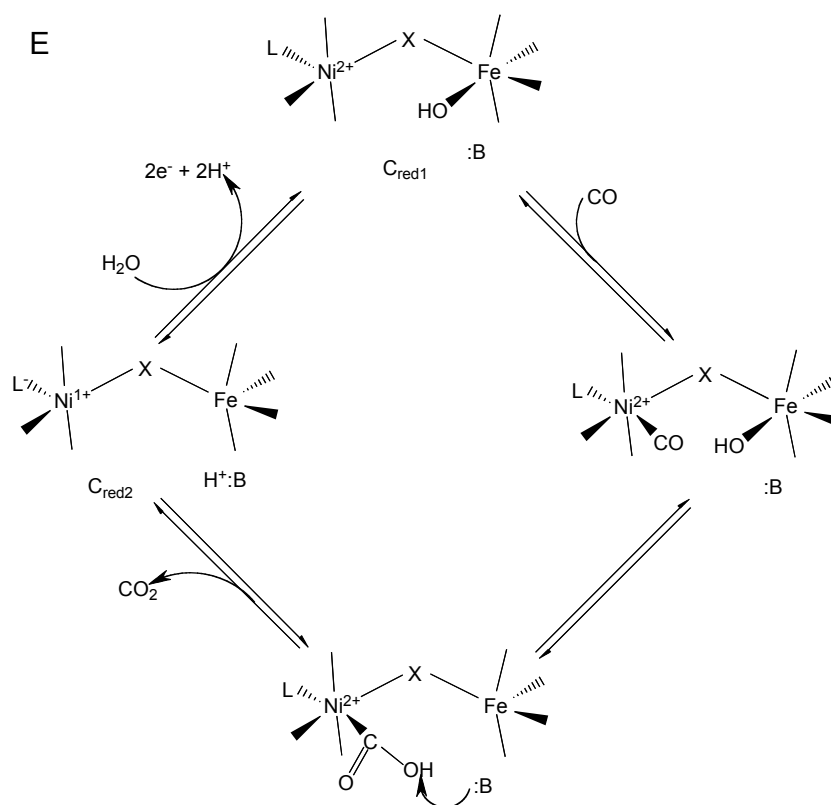


Figure 4. (continued)



3. Nickel Enzymes and Nickel Assembly Systems

Elucidating the mechanisms of metal cluster biosynthesis is one of the major challenges in the field of bioinorganic chemistry. Besides Ni-,Fe-containing CODH, seven other enzymes contain nickel as metalcenter constituent (Ni-superoxide dismutase (SOD), Ni-Fe hydrogenase, Ni-Ni acetyl-CoA synthase, methyl-coenzyme M reductase (MCR), glyoxalase I and acireductone dioxygenase) have been discovered and structurally characterized (Wuerges et al, 2004; Volbeda et al, 2005; Svetlitchnyi et al, 2004; Ermler et al, 1997; He et al, 2000; Xu et al, 2006). The active site structures and reactions catalysed are shown in Fig. 5. This section presents a brief description of the active site structures with corresponding catalytic reactions, for enzyme with reported Ni-assembly systems with a focus on Ni-binding and delivery proteins. Therefore, the enzymes whose Ni-assembly systems have not been identified or are relatively less defined, such as MCR, Ni-SOD, glyoxalase I and acireductone dioxygenase will not be described further and detailed reviews of the active site of these nickel enzymes and their catalysis are found elsewhere (Watt & Ludden, 1999; Ragsdale, 2006).

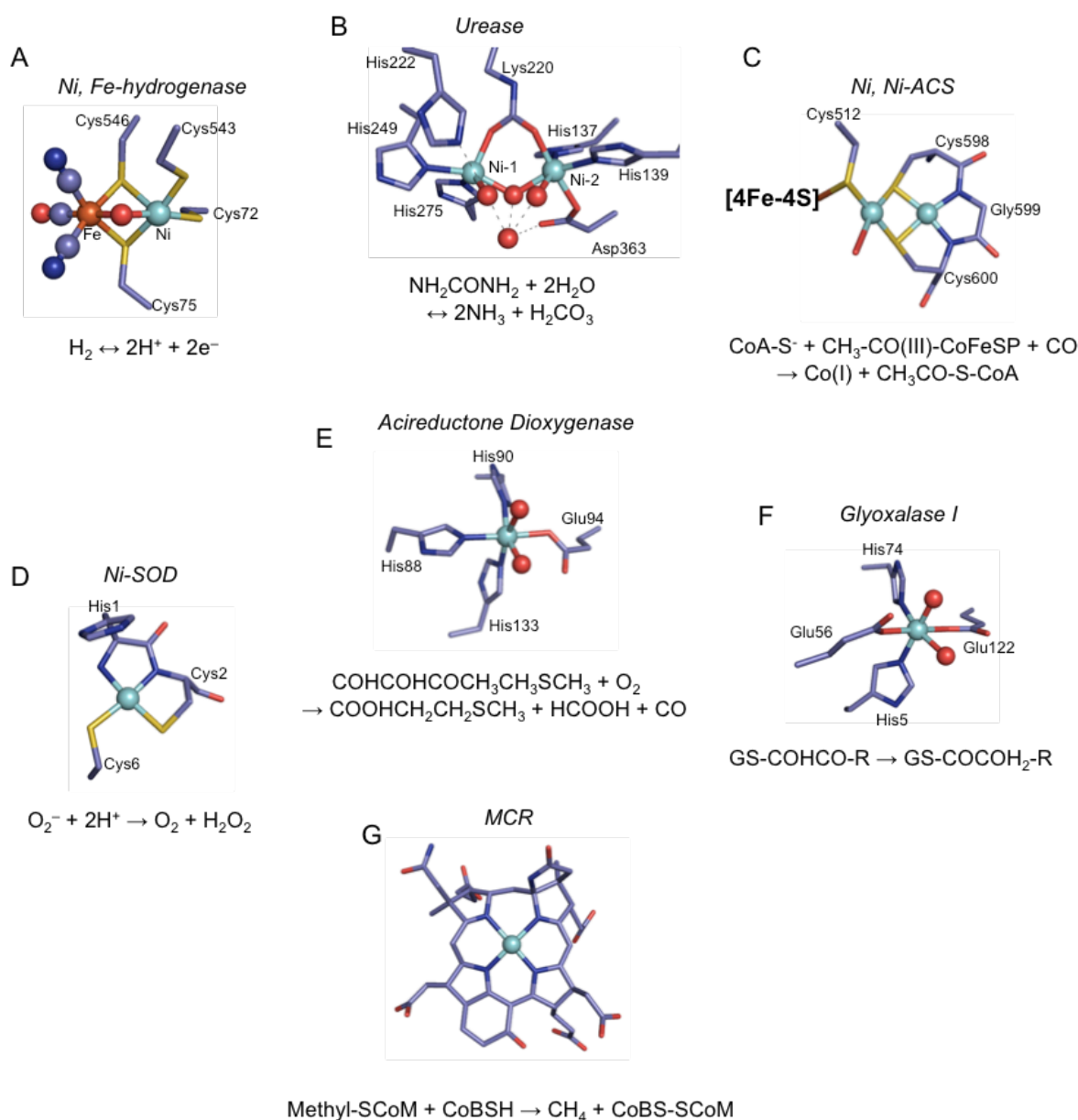


Figure 5. Overview of Ni metalcenters found in Ni-containing enzymes. (A) Dinuclear Ni-Fe active site of hydrogenase from *Desulfovibrio fructosovorans* (PDB ID: 1YRQ, ready oxidized form) catalyzing the two-electron redox chemistry of H_2 . The diatomic molecules bound to Fe are CO and two cyanide molecules. (B) Dinuclear Ni-Ni active site of urease from *Bacillus pasteurii* (PDB ID: 2UBP) involved in the hydrolysis of urea to carbamate. Lys₂₂₀ is the carbamylated residue coordinating two Ni sites. Metal-bound waters are shown as red spheres and hydrogen bonding as dotted line. (C) Dinuclear Ni-Ni-[4Fe-4S] active site cluster A of ACS from *C. hydrogeniformans* (PDB ID: 1RU3) catalyzing the synthesis of acetyl-CoA from a methyl group from CoFeSP with CO from CODH and CoA. Structure of [4Fe-4S] moiety linked by S_v atom of Cys₅₁₂ is not shown. (D) Active site structure of the reduced Ni-SOD from *Streptomyces seoulensis* (Wuerges et al, 2004) (PDB ID: 1Q0G) converting superoxide to oxygen and hydrogen peroxide. (E) The active site structure of the Ni-containing form of acidoreductone dioxygenase from *Mus musculus* (Xu et al, 2006) (PDB ID: 1VR3) transforming acidoreductone to methylthiobutyric acid, formate and CO in the methionine salvage pathway (Pochapsky et al, 2002). (F) Active site of *E. coli* glyoxalase I with two bound water molecules (PDB ID: 1F9Z) involved in the formation of thioesters by isomerization reaction in α -keto aldehyde detoxification. (E) Ni-tetrahydrocorphin (F₄₃₀) in methyl coenzyme M reductase from *Moorella marburgensis* (PDB ID: 1MR0) catalyzing the conversion of methyl-SCoM and N-7-mercapto-heptanoylthreonine phosphate (CoBSH) to methane and the CoB-SS-CoM heterodisulfide. All Ni atoms are shown in cyan, Fe atom in dark red, S in yellow, and O in red.

3.1. *Hydrogenase system*

Hydrogenases are enzymes that catalyze the two-electron redox chemistry of dihydrogen (Fig. 5A). Three different types of hydrogenases are known, Ni-Fe, Fe-only and metal-free hydrogenases designated by composition of metals in their active sites. The structures of the active site of Ni-Fe hydrogenases have been reported (Fontecilla-Camps et al, 2007). These structures revealed the presence of two distinct and inactive oxidized states, called Ni-B (unready) and Ni-A (ready), also proposed firstly from the corresponding Ni-based EPR signals (Teixeira et al, 1989), in which oxidation states of Ni undergoes between Ni(II) and Ni(III) states during catalysis. Furthermore, Fourier transform (FT) IR spectroscopic data (deLacey et al, 1997) supported crystallographic analysis, in which a heterodinuclear active site of both states is composed of a Ni center coordinated by four cysteines and a Fe center ligated by two CN ligands and a CO ligand (Fig. 5A; Volbeda et al, 2005). The dinuclear Ni and Fe sites are bridged by two cysteine ligands and additionally bridging exogenous ligand, thought to be (hydro-)oxo or sulphur in the ready state (Volbeda et al, 2005; Matias et al, 2001) and peroxide in the unready state (Volbeda et al, 2005). In addition to this bridging site to the Fe ion, the Ni ion contains a terminal site, which has been proposed to be a substrate-binding site shown by crystallographic identification of a hydrophobic route for H₂-access ending on the Ni site (Montet et al, 1997) and the binding of competitive inhibitor CO (Ogata et al, 2002).

The biosynthesis of Ni-dependent hydrogenase is a remarkably complex process as shown in Fig. 6A (Kuchar & Hausinger, 2004; Leach & Zamble, 2007). A precursor of the large subunit of hydrogenase 3 (pre-HycE) from *E. coli* is synthesized from an operon (*hycABCDEFGHI*). A five-gene operon (*hypABCDEFG*) that is located in a separated region from the *hyc* operon encodes accessory proteins (Lutz et al, 1991). A complex of HypC:HypD acquires an Fe ion by unknown mechanism. The HypEF complex generates the cyanide and CO ligands on the Fe ion of HypC by using carbamoyl phosphate and ATP in presence of reductant (Reissmann et al, 2003). HypC delivers the active site Fe-(CO)(CN)₂ (Fig. 5A) by forming a complex with pre-HycE (Drapal & Bock, 1998). The Ni ion is inserted into the Fe-(CO)(CN)₂ of the HypC:pre-HypE complex in a GTP-dependent process. This process requires HypB, a GTPase with Ni-binding activity (Gasper et al, 2006; Leach et al, 2005), and HypA, a weak Ni-binding protein (Atanassova & Zamble, 2005). Capacity and sites for Ni-binding in HypB proteins vary between microorganisms. For example, HypB containing a histidine-rich motif from *Bradyrhizobium japonicum* binds 9 Ni per monomer with GTPase activity (Fu et al, 1995). *E. coli* HypB possesses a conserved N-terminal CXXCGC motif (Leach et al, 2005) that is not conserved in bacterial HypB and is lacking in archaeal HypB proteins (Gasper et al, 2006). The structure of HypB from archaea *M. jannaschii* revealed that the protein has two metal binding sites per monomer, one of which is dependent on nucleotide binding in the dimer interface and

coordinates metals with highly conserved cysteine and histidine side chains (Fig. 6B) (Gasper et al, 2006).

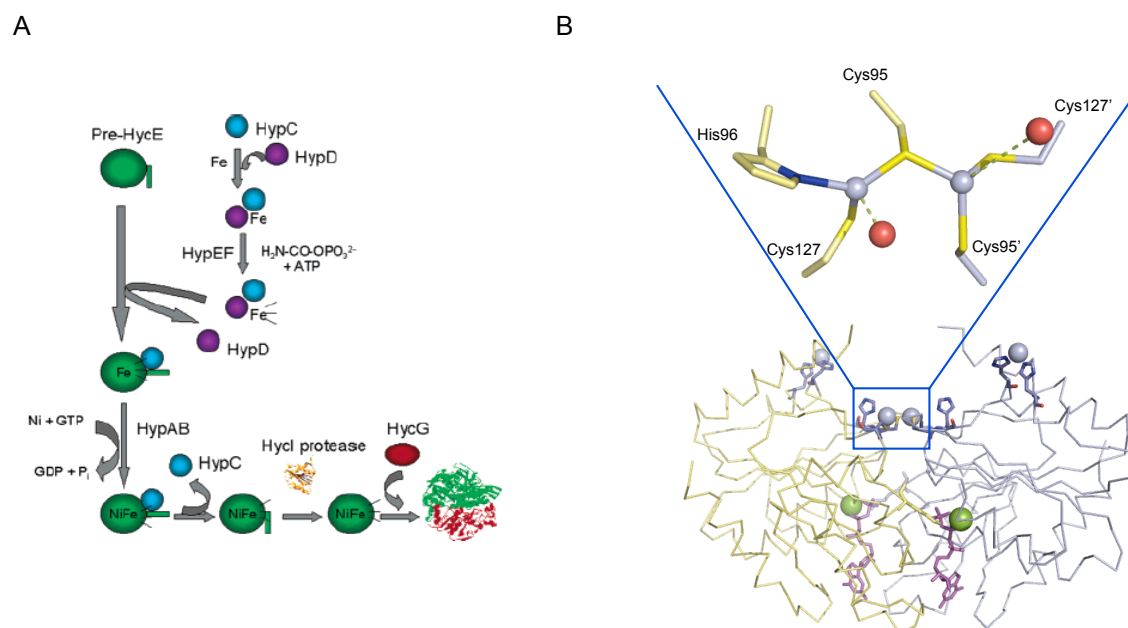


Figure 6. Biosynthesis and Ni-insertion model for Ni-Fe hydrogenases (A) and structure of HypB (B). The figure (A) is adapted from Kuchar *et al* (Kuchar & Hausinger, 2004) and details are given in the text. (B) Ribbon presentation of homodimeric structure of HypB from *Methanocaldococcus jannaschii* (Gasper et al, 2006) with GTPyS in violet, Mg²⁺ ion in green sphere, water in red sphere and Zn in gray sphere. Unusual asymmetric metal binding site in the dimerization interface is shown in enlarged figure. Prime denotes the coordination from other molecule.

It has been suggested that the nucleotide-dependent conformational changes in the switch II region, consisting a highly conserved ENV/IGNLV/ICP motif, releases a metal ion into hydrogenase and that HypB undergoes nucleotide-dependent dimerization (Gasper et al, 2006). *E. coli* HypB possesses two binding sites for nickel: a low-affinity site and a high-affinity site capable of binding one equivalent Ni with a K_d in sub-picomolar range (Leach et al, 2005). Mutational studies on conserved cysteine and histidine residues showed that the two binding sites are independently localized: the low-affinity site in the GTPase domain and the high-affinity site in the N-terminal CXXCGC motif (Leach et al, 2005). The proposed mechanism of nickel release of *E. coli* HypB to the hydrogenase postulated that the high-affinity site in the protein binds Ni tightly at low cellular Ni concentration and releases Ni to the pre-HycE by a trigger reaction. Although this trigger is not yet clearly known, it could be speculated to be an energy-evolving step during GTP hydrolysis and/or the cleavage of the C-terminal peptide of hydrogenase by Hycl (Maier et al, 1995). Cooperative actions of HypB with either HypA, a weak nickel binding protein (Atanassova & Zamble, 2005), or SlyD, a metal-binding peptidyl-propyl isomerase (Zhang et al, 2005), may provide Ni ion to the iron-loaded site of the hydrogenase (Leach et al, 2005). As the final steps in hydrogenase biosynthesis, the HypC protein

dissociates from the Ni and Fe-loaded pre-HycE, and HycG protein (the small subunit of hydrogenase) binds to HycE only after proteolytic removal of the C-terminal of pre-HycE by Hycl protease, generating the functional hydrogenase (Magalon & Bock, 2000).

3.2. Urease System

Urease catalyzes the hydrolysis of urea to carbamate and ammonia. The enzyme has been identified as the first nickel containing protein (Dixon et al, 1975). During the last decade, several structures of the enzyme consisting of a heterotrimeric $\alpha_3\beta_3\gamma_3$ subunits have been reported from *Klebsiella aerogenes* (Jabri et al, 1995; Pearson et al, 1997), *Bacillus pasteurii* (Benini et al, 1999), and *Helicobacter pylori* (Ha et al, 2001). These structures revealed that the active site is comprised of a dinuclear nickel center (Fig. 5B). One Ni atom (Ni-1) is bound by two protein ligands (His₂₄₉ and His₂₇₅ based on PDB ID: 2UBP). The second Ni atom (Ni-2) is coordinated by three protein ligands (His₁₃₇, His₁₃₉ and Asp₃₆₃) and a modified amino acid residue (a carbamylated Lys₂₂₀ produced by reaction with CO₂ in the presence of Ni (Park & Hausinger, 1995)) bridging the two Ni ions. Water molecules complete the coordination spheres of two Ni atoms: distorted square pyramidal for Ni-1 and distorted octahedral for Ni-2. Based on the structure of native urease together with the bound diamidophosphoric acid structure (Benini et al, 1999), it has been proposed that urea binds to the more electrophilic *penta*-coordinated Ni-1 site with the carbonyl oxygen, approaching the *hexa*-coordinated Ni-2 with one of its amino groups and eventually bridging the two metal ions. The bridging hydroxide plays a role as both nucleophile and general acid, while the newly identified His₃₂₃ acts as a general base stabilizing a positive charge in the transition state (Benini et al, 1999).

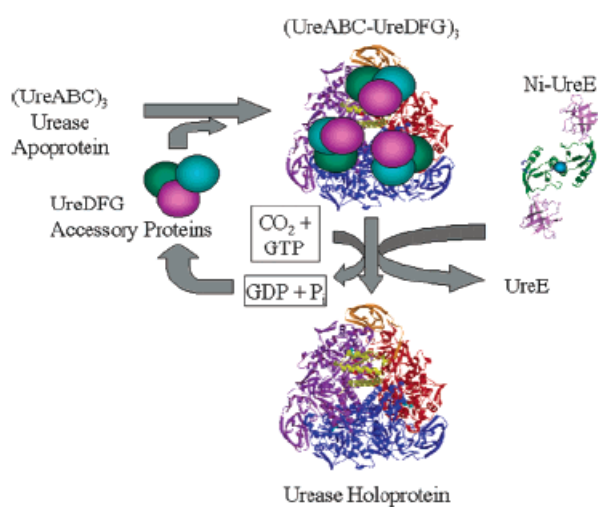


Figure 7. Model for nickel insertion into apo-urease. The figure is adapted from Kuchar *et al* (Kuchar & Hausinger, 2004). Details are given in the text.

Metallocenter assembly of the urease is a complex cellular process that requires Ni, carbon dioxide, several accessory proteins, and GTP hydrolysis (Kuchar & Hausinger, 2004). The majority studies on the urease activation are primarily derived from analysis of the *ureDABCEFG* gene cluster from *Klebsiella aerogenes* that encodes several proteins required to generate a mature active enzyme. As illustrated in Fig. 7, an apo-urease is synthesized from *ureABC* encoding three different subunits (γ , β , and α , respectively). The structure of the apo-urease is identical to native enzyme except lacking Ni and carbamylation of the lysine residue (Jabri & Karplus, 1996). In addition to the structural subunits for the apo-urease, this system encodes four accessory proteins, called UreD, UreE, UreF, and UreG (Mobley et al, 1995). UreD, UreF, and UreG form a series of complexes with apo-urease. Activation of apo-urease *in vitro* with the UreDFG complex requires high nickel and bicarbonate concentrations in the absence of GTP. However, the complex is able to activate apo-urease at low, physiologically relevant nickel and bicarbonate concentrations when GTP is present (Soriano & Hausinger, 1999). This Ni-activation process of apo-urease is dependent on GTP hydrolysis that is associated with a nucleotide-binding site on the UreG component (Soriano & Hausinger, 1999). UreG from *B. pasterurii* is the best characterized in structure and metal binding properties (Zambelli et al, 2005). It is a dimeric protein in solution with low GTPase activity. UreG binds stoichiometric amount of zinc with the high affinity site and four nickel per dimer in the low affinity site. NMR together with CD and fluorescent spectroscopic studies revealed that UreG is an intrinsically unstructured protein (Zambelli et al, 2005), which can be fully folded after it forms a complex with other accessory proteins (UreD and UreF) (Moncrief & Hausinger, 1997). Furthermore, it has been shown that UreG is involved in the delivery of CO₂ for the carbamylation of the lysine in the active site, which based on the observation of increasing activation level of apo-urease/UreDF complex with UreG in the presence of increasing nickel and carbonate concentrations (Soriano & Hausinger, 1999). UreG is similar to the HypB protein involved in nickel insertion into Ni-Fe hydrogenase. The roles of UreD and UreF in the activation of the apo-urease are not clearly known. It has been proposed that these accessory proteins act together as a GTP-dependent molecular chaperone that induces the conformational change of apo-urease to increase accessibility of both Ni and CO₂ to the buried active site. The Ni ion is delivered to a complex of apo-urease/UreDFG by the metallochaperone UreE (Lee et al, 1993). The UreE protein consists of peptide-binding, metal-binding and His-rich COOH-terminal domains, where the last two domains are responsible for the binding of 2 and 3 ~ 6 nickels per dimer, respectively (Soriano et al, 2000). Although the metal-binding domain of UreE alone is fully functional to transfer Ni to apo-urease, full activation of apo-urease in a complex with UreDFG requires full length UreE protein as demonstrated by *in vitro* studies (Soriano et al, 2000). After activation of urease, the accessory proteins dissociate and are probably recycled (Fig. 7).

3.3. CODH and Acetyl-CoA Synthase System

In contrast to the biosynthesis of nickel-containing enzymes like urease and hydrogenase as described previously, our knowledge about the assembly of the cluster C in Ni,Fe-containing CODHs is very limited. Among anaerobic bacteria and archaea containing CODH, the biosynthesis of cluster C in *R. rubrum* is the best studied system both at the genetic and physiological levels (Watt & Ludden, 1999; Hausinger, 1997). The five-gene operon (*cooFSCTJ*), located downstream of the CO-tolerant hydrogenase structural genes, encodes the ferredoxin-like protein CooF (*cooF*), CODH (*cooS*) and accessory proteins (CooC, CooT and CooJ) involved in the Ni-insertion into cluster C (*cooCTJ*) (Watt & Ludden, 1999). This *coo* operon is transcriptionally regulated by the CO-sensing heme protein CooA (Shelver et al, 1997). CooT_{Rr}, a 7.1 kDa protein, shows slight similarities to the chaperone-type HypC protein family (Kerby et al, 1997). CooJ_{Rr}, a soluble 12.6 kDa protein, contains a COOH-terminal histidine-rich region that is commonly found in UreE and HypB proteins containing the histidine-rich Ni-binding motif, and binds 4 Ni per monomer with a K_d of 4 μ M (Watt & Ludden, 1998). Insertion mutations in *cooT* and *cooJ* genes reduced Ni-activation of CODH but do not block it completely, suggesting that these proteins are not essential for nickel insertion (Jeon et al, 2001). CooC_{Rr}, a membrane-associated homodimer of 61-63 kDa protein, has a nucleotide-binding domain (P-loop) near the N-terminus and displays NTPase activity (Jeon et al, 2001). It has been reported that the P-loop mutated form of CooC_{Rr} having none of NTPase activities accumulates enzymatically inactive, Ni-deficient CODH *in vivo* (Jeon et al, 2001). The maturation of hydrogenase and urease by HypB (Maier et al, 1995) and UreG (Moncrief & Hausinger, 1997), respectively, depends on the nucleotide hydrolysis. According to the mutational studies on the *cooC* gene, CooC is an essential accessory protein for the insertion of nickel into cluster C of CODH and the maturation requires the use of energy by ATP hydrolysis. Although nickel activation of apoCODH_{Rr} by CooC_{Rr} during incubation with CooT_{Rr} and ATP has not been observed *in vitro*, addition of wild-type cell extract to *in vitro* activation mixture stimulated activation of apoCODH, suggesting that nickel incorporation of apoCODH *in vivo* requires all CooCTJ proteins and ATP-regeneration system (Jeon et al, 2001). In comparison to genetic studies of *R. rubrum*, three *cooC* genes encoding CooC1-3 isozymes, but none for CooT and J homologues, have been identified in *C. hydrogenoformans* (Fig. 8) (Wu et al, 2005). Up to date no further information about the biosynthesis of CODH from *C. hydrogenoformans* is available. All the nickel assembly systems for hydrogenase, urease and CODH require two common accessory proteins: a nickel-binding and a nucleotide-binding protein. CooC shows similarity to the HypB and UreG proteins involved in nickel insertion to hydrogenase and urease, respectively (Watt & Ludden, 1999) and to members of Mrp/MinD family in SIMIBI class GTPases including NifH, MinD, ParA, ArsA and Soj proteins (Leipe et al, 2002). The presence

of a P-loop in HypB, UreG and CooC may indicate that nickel-insertion requires energy consumption *in vivo*.

ACS catalyzes the synthesis of acetyl-CoA from a methyl group from CoFeSP (a cobalt-containing corrinoid iron-sulfur protein), CO, and CoA at the active site called cluster A (Svetlitchnyi et al, 2004). The functional cluster A of ACS_{Ch} contains a Ni-Ni-[4Fe-4S] as shown in Fig. 5C, in which dinuclear Ni ions show a square-planar coordination geometry through side-chain S atoms and backbone N atoms of cysteines (Svetlitchnyi et al, 2004). An open reading frame *acsF* within the *acs* operon in *C. thermoaceticum* encodes a 27 kDa AcsF protein that is a CooC homologue (Loke & Lindahl, 2003). Based on sequence similarity of AcsF to CooC and presence of ATPase activity, it was suggested that AcsF functions in the assembly of the cluster A in ACS though it is not experimentally proven yet (Loke & Lindahl, 2003). While nickel-binding activity of *R. rubrum* CooC has not been observed *in vitro*, a highly conserved region containing two cysteines (CXC) between AcsF and its homologues including CooC (see also Fig. 26) may be indicative of a potential metal-binding site.

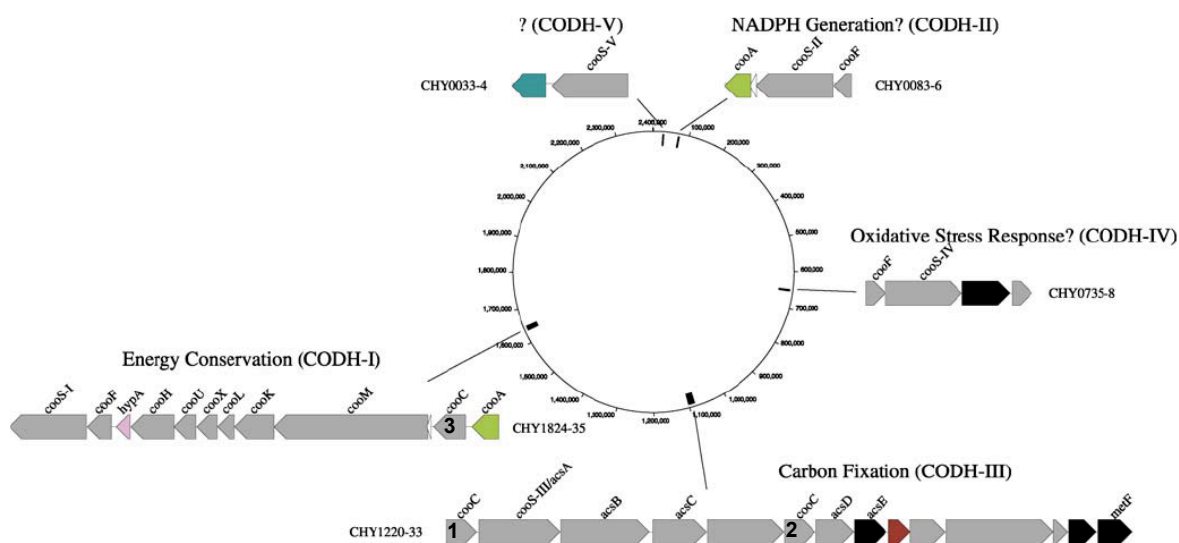


Figure 8. Locations of genes denoted as encoding CODHs and CooCs in the genomic DNA of *C. hydrogeniformans*. The genome locations of the genes encoding the five CooS homologs (labelled *cooS-I-V*) and the three CooC homologs (labeled *cooC 1-3*) are shown. This figure was adapted and modified from the reference (Wu et al, 2005).

4. Structural Homologues of CooC in SIMIBI Class

The GTPase superclass can be divided into two large classes, designated TRAFAC (translation factor-related) and SIMIBI (signal recognition particle, MinD and BioD), and shares a common core domain containing seven β -strands, designated strand 1 through 7 including Walker A (GxxxGK[ST]), Walker B (DxxG, Switch II region) and [NT]KxD (the GTPase specificity motif), shown in Fig. 9 (Leipe et al, 2002). Structurally, the distinctive feature of the TRAFAC class is that the strand that flanks the Walker B-containing strand 4 on the right-hand side is antiparallel to it, while this region forms two parallel β -strands in the SIMIBI proteins (Leipe et al, 2002). The SIMIBI class of GTPases and related NTPases, one of two distinct classes containing a unique set of sequence and structural signatures in GTPase superclass, has two broader subdivisions called the Mrp/MinD and the BioD-related superfamilies (Leipe et al, 2002). In addition to general similarity in sequence and structural levels, the SIMIBI class can be represented by three distinct and evolutionary derived sequence characters: a specific variation of the Walker A motif that includes a third conserved glycine residue (Walker A with GxxGxGK[ST]), a conserved aspartate residue at the COOH-terminus of strand 2 (Walker A' motif) that makes a hydrogen bond to the Mg ion and a conserved aspartate residue at the beginning of strand 4 (Walker B) (Leipe et al, 2002). An additional special feature that characterizes the Mrp/MinD family is a signature containing two lysines within the Walker A motif, one near the COOH-terminus of the P-loop that is common to the classical Walker A motif (underlined in xKGGxxK[T/S]) and a second at the beginning of the P-loop that is unique to this family, designated the deviant Walker A motif (underlined in xKGGxxK[T/S]) (Koonin, 1993).

The subgroups of Mrp/MinD family containing the deviant Walker A motif include proteins having diverse functions: NifH in nitrogen fixation, MinD in spatial regulation of cell division, Soj in plasmid and chromosome segregation and the anion pump ATPase ArsA (Lutkenhaus & Sundaramoorthy, 2003; Leipe et al, 2002). Soj, ArsA and MinD ATPases are structurally homologous to the nitrogenase iron protein NifH (Fig. 10) (Leonard et al, 2005), (Hayashi et al, 2001; Cordell & Lowe, 2001; Sakai et al, 2001; Schindelin et al, 1997; Zhou et al, 2000). All of these structures are dimeric, except MinD (Fig. 10B) that has been observed only in a monomeric form in all three published crystal structures (Cordell & Lowe, 2001; Sakai et al, 2001; Hayashi et al, 2001). MinD undergoes ATP-dependent dimerization in solution (Hayashi et al, 2001), which means that the protein forms a noncovalently-linked dimer upon binding of ATP as shown in the structure of dimeric Soj (Leonard et al, 2005), but dissociates upon ATP hydrolysis. However, the subunits of both NifH and ArsA are covalently linked. NifH is a homodimeric ATPase in which the constituent monomers are covalently linked by a [4Fe-4S] cluster (Fig. 10A).

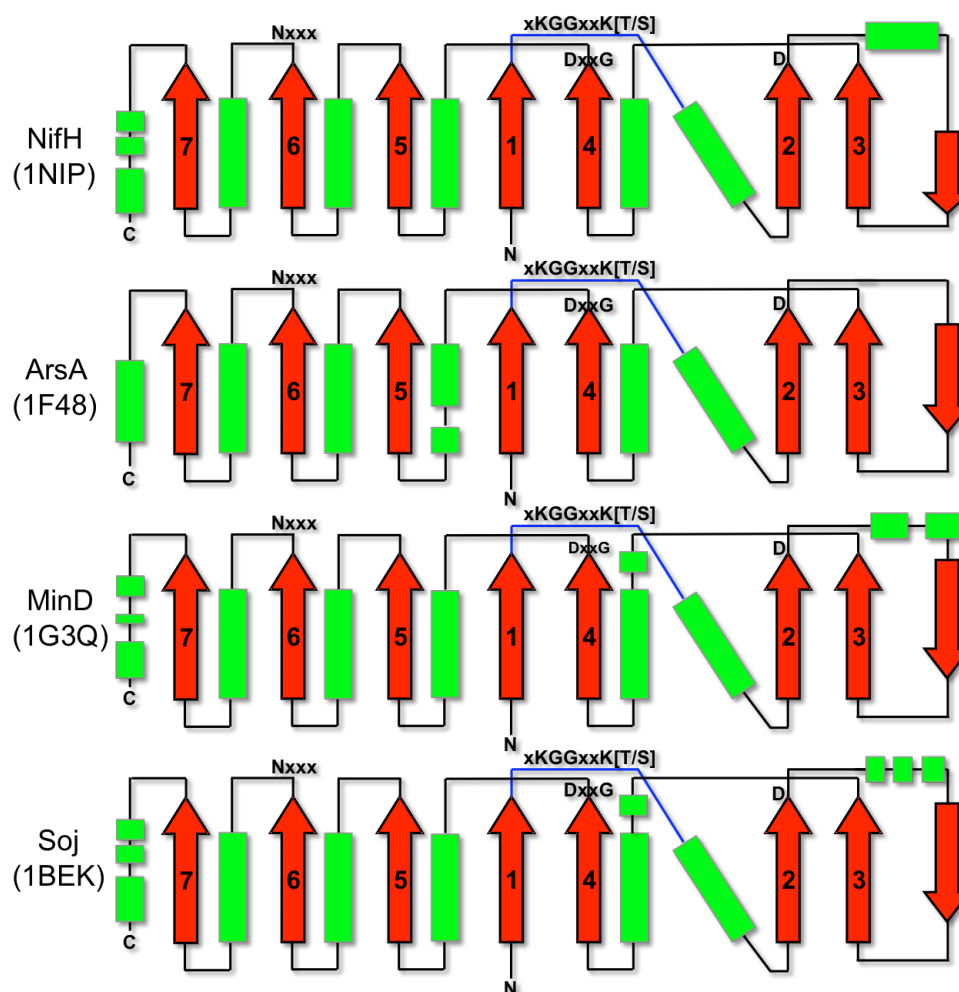


Figure 9. Schematic diagrams of topology found in P-loop containing NTPases of the Mrp/MinD family in the SIMIBI class. Strands and helices are shown as arrows with the arrowed head and rectangles, respectively. For simplification, only the core strands are numbered 1 through 7. The conserved sequence motifs xKGGxxK[T/S] (deviant Walker A), conserved D (Walker A'), DxxG (Walker B), and Nxxx that is similar motif of [NT]KxD in GTPases are shown. The P-loop is shown in *blue* line. Protein name with PDB ID in bracket is shown in the left column.

Formation of the transition state in the presence of ADP·AlF₄⁻ induces conformational change of the dimer from an open to a more compact, closed conformation in which the signature lysine of the opposing subunit stabilizes the β-phosphate across the dimer interface (Fig. 10, inset). This results in the rotation of the subunits by approximately 13° towards their nucleotide-bound dimer interface (Schindelin et al, 1997). Although ArsA is monomeric, it has twice the size of the others consisting of two similar domains connected by a short linker, such that each ArsA monomer behaves functionally as pseudodimer (Fig. 10D; Zhou et al, 2000). The most recent crystal structure and biochemical data from the hydrolysis-deficient Soj mutant showed conclusively that the proteins in the Mrp/MinD family containing the deviant Walker A motif undergo, indeed, ATP-dependent nucleotide sandwich dimer formation, in which the developing negative charge on the β-phosphate of each monomer during the hydrolysis is stabilized by the signature lysine (Fig. 10C and inset; Leonard et al, 2005).

Sequence alignment of CooC to homologues of the Mrp/MinD family in SIMIBI class (See Fig. 35) shows highly conserved Walker A and B motifs including the signature lysine and aspartate in both motifs, classifying the CooC protein as a member of the Mrp/MinD family. Furthermore, HypB and UreG, functional homologues of CooC containing P-loop in Ni-assembly process, belong to the G3E family of the BioD related superfamily in the SIMIBI class (Leipe et al, 2002).

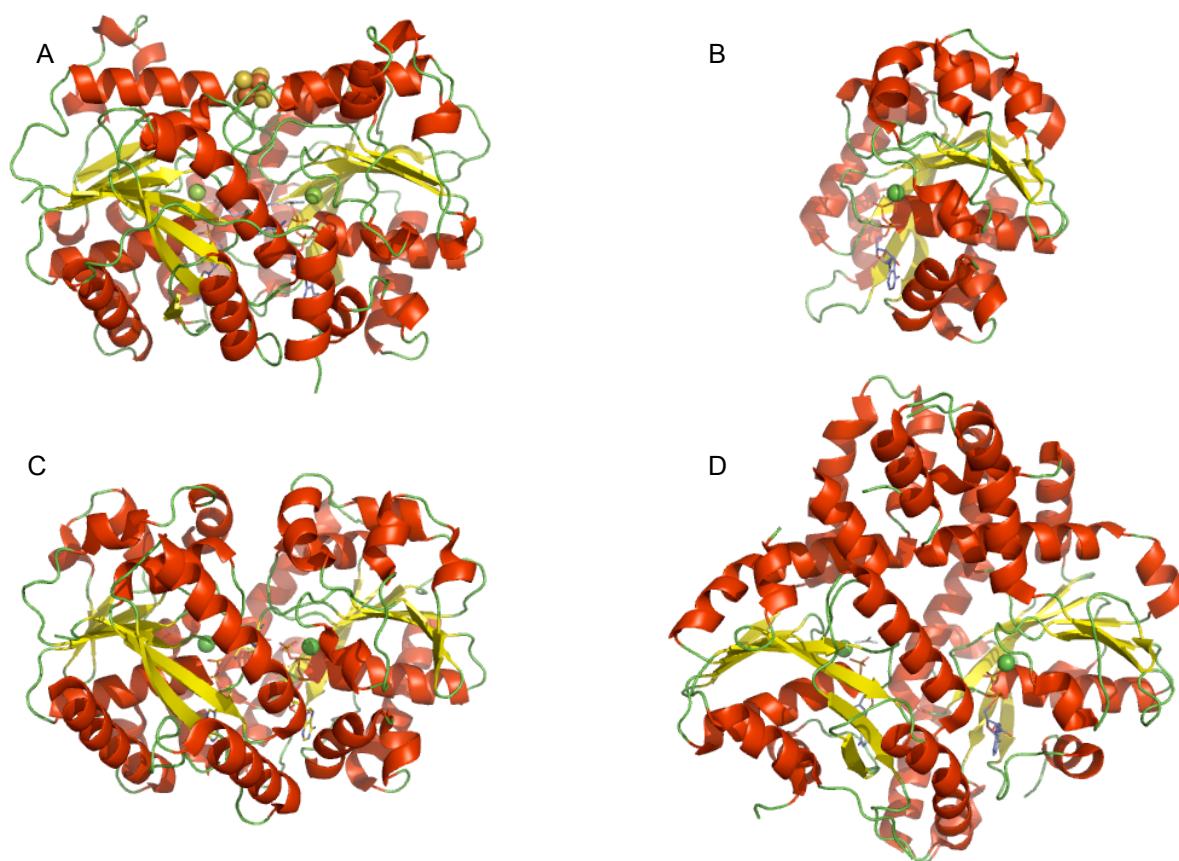
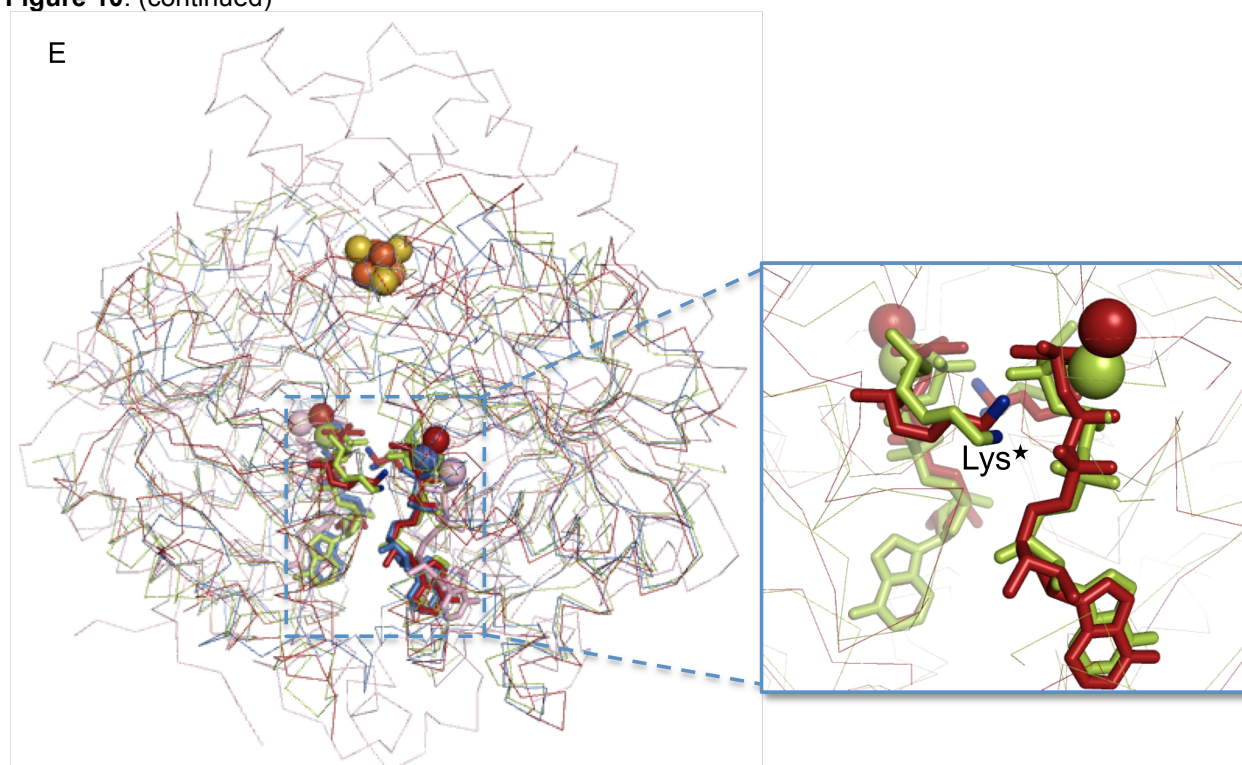


Figure 10. Structures of the deviant Walker A motif-containing proteins, (A) NifH, (B) MinD, (C) Soj, and (D) ArsA, in the Mrp/MinD family. Bound nucleotides are shown in element colored stick model, Mg ion in *green* spheres. The [4Fe-4S] cluster of NifH is shown as Fe in *red* spheres and S in *brown* spheres. Helices and strands are shown in *yellow* and *red* colors, respectively. (E) Superposition of four homologues by C α atoms. NifH in *red*, MinD in *blue*, Soj in *green*, and ArsA in *violet*. Inset box shows the dimer interface of NifH and Soj with the conserved signature lysines (N ζ atom in *blue*) stabilizing phosphate groups of nucleotides on the opposing molecule. Superposition was obtained using COOT (Emsley & Cowtan, 2004).

Figure 10. (continued)



5. Aim of Study

- In contrast to the wealth of spectroscopic and biochemical information accumulated over a decade, our understanding about the function of the catalytic active cluster C based on structural analysis is still limited. Several structures of CODHs have been reported, but they showed a high degree of heterogeneity of cluster C. Currently, the proposed mechanism for CO oxidation/CO₂ reduction at cluster C postulates the activation of water and CO as well as the stabilization of a metal bound intermediate. However, the structure of these states remained elusive. One of the main goals of this work is to elucidate the CO oxidation mechanism using protein X-ray crystallography. For this, a heterologous expression system for CODHIII in *E. coli* has to be constructed and developed because of the difficulty in obtaining native enzyme from *C. hydrogenoformans*. Crystal structures of CODHIII in different states will be analyzed in order to verify the proposed reaction mechanism at cluster C.

- Compared to other Ni-containing enzymes, the assembly of cluster C of CODH is poorly understood. The second main goal of this work is to gain biochemical and structural informations about the CooC1 protein from *C. hydrogenoformans* that is proposed to be involved in maturation of cluster C. Investigation of Ni-binding activity of CooC1 is essential to gain insight into how the protein interacts with nickel. Furthermore, biochemical characterizations of CooC1 on nucleotide hydrolysis and nucleotide-dependent oligomerization will be investigated. Finally, the crystal structures of CooC1 in different states will be analyzed. This will allow further advance in understanding the function of CooC1 in Ni-processing for cluster C assembly.

MATERIALS AND METHODS

1. Chemicals

N₂ (99.999%, O₂ ≤ 3 ppm), CO (99.997%), and N₂/H₂ (95%/5%) gases were obtained from Riessner-Gase (Lichtenfels, Germany). DNase-free water for molecular biology was obtained from Fermentas. All restriction enzymes were purchased from Fermentas. T4 DNA ligase, Klenow Fragment (exo-, the Large Fragment of DNA Polymerase I), *Taq* and *Pfu* DNA polymerase were obtained from Fermentas. Herculase DNA polymerase was obtained from Stratagene. Plasmid preparation kit was obtained from Fermentas. Kits for PCR purification and Gel Extraction were purchased from Qiagen. All gene amplifications were achieved using Master Cycler Personal from Eppendorf. All chromatography columns and materials were obtained from GE Healthcare except for the macro-prep ceramic hydroxyapatite (Type I, 20 μm) material that was obtained from BIO-RAD. Electrophoresis materials were supplied by Roth. Size markers for SDS-PAGE were purchased from Roth (RotiMARK standard) and Fermentas (unstained protein molecular weight marker). All other chemicals used were of at least analytical grade and obtained from Fluka, Sigma or Merck. Anaerobic reaction tubes (15 ml), EPA vials (20 ml), glass vials (2 ml), butyl or silicon septa and other anaerobic glass equipments were purchased from SUPELCO, OCHS or CZT (<http://www.czt.de/>). Metal-free water and buffers were prepared by passing over Chelex 100 Resin (50-100 mesh, sodium form, BIO-RAD). pASKIBA17 plus vector (strep tag with TEV protease cutting site) was purchased from IBA. Novagen supplied other pET vectors used in this work. A stock solution of 50 mM aluminum tetra fluoride (AlF₄) was prepared by mixing equivalent volumes of 100 mM AlCl₃ and 500 mM NaF and filtering the solution through a 0.45 μm filter. A stock solution of vanadate (V_i) was prepared from Na₃VO₄ (Sigma-Aldrich; Goodno, 1979). The solution was adjusted to pH 10 with 6 M HCl and boiled until the solution got colorless indicating the depolymerization of yellow poly-vanadate species.

2. Anaerobic Work

Purification, crystallization and crystal soaking experiments were done in an anoxic glove box (model B, COY Laboratory Products Inc., Michigan, USA) under an atmosphere of 95% N₂/5% H₂ at 17 °C except for the purification of CooC1 which was performed at room temperature. EPA vials and 2 ml vials with silicon-coated butyl rubber septum were used for storage of cell pellet and proteins samples, respectively. All anaerobic solutions were prepared in a container (bottle, tube, or cuvette) equipped by screwed cap with butyl rubber or silicon septum either by vigorous sparging of N₂ gas or by successive cycles (at least 4 cycles) of evacuating and flushing with N₂ gas at a vacuum-gas line.

3. Bacterial Strains and Culture Media

3.1. *Carboxydotherrnus hydrogenoformans* Z-2901

Cells of *C. hydrogenoformans* Z-2901 were a gift from PD. Dr. V. Svetlitchnyi (Mikrobiologie, Universität Bayreuth).

3.2. *Escherichia coli* and culture Media

Escherichia coli DH5 α {F⁻ ϕ 80 Δ lacZ Δ M15 Δ (lacZYA-argF)U169, *deoR*, *recA1*, *endA1*, *hsdR17*(*rK*⁻, *mk*⁺), *phoA*, *supE44*, λ ⁻, *thi-1*, *gyrA96*, *relA1*} was usually grown at 37 °C in LB medium (10 g/l trypton, 5 g/l yeast extract, 5 g/l NaCl) for cloning of genes used in this study. Expression strains, BL21(DE3) {F⁻ *ompT* *hsdSB*(*rB*⁻ *mB*⁻) *gal dcm* (DE3)} and Rosetta(DE3) {F⁻ *ompT* *hsdSB*(*rB*⁻ *mB*⁻) *gal dcm* (DE3) pRARE6 (Cam^R)} were cultivated either at 37 °C in TB (12 g/l trypton, 24 g/l yeast extract, 4 ml/l 87% glycerol) for CooC1 expression or at 30 °C in modified TB medium (12 g/l trypton, 24 g/l yeast extract, 10 ml/l 87% glycerol) for CODHII expression containing antibiotic(s) depending on the harboured plasmid(s). Concentrations of antibiotics are described in Table 2.

Table 2. Concentrations of antibiotics used in this study.

Antibiotic	Stock	Final concentration
Cb (Carbenicillin)	50 mg/ml H ₂ O and sterilised by filtration (0.2 μ m)	50 μ g/ml
Tet (Tetracyclin)	12.5 mg/ml 100% ethanol	12.5 μ g/ml
Cam (Chloroamphenicol)	50 mg/ml 100% ethanol	50 μ g/ml
Km (Kanamycin)	50 mg/ml H ₂ O and sterilised by filtration (0.2 μ m)	50 μ g/ml

4. Molecular Biology

The circular genomic DNA of 2,401,892 bp from *Carboxydotherrnus hydrogenoformans* Z-2901 (Wu et al, 2005) was isolated as described by Sambrook *et al* (Sambrook, 1989). Gene amplification by PCR followed a standard protocol (Tab. 3).

PCR fragments used for cloning were extracted from 1% (w/v) agarose gels. DNA restrictions and ligations followed the protocols supplied with enzymes used. DNA sequencings were done by MWG Biotech (Martinsried, Germany). Electrocompetent cells of *E. coli* strains were prepared as described in (Sambrook, 1989).

Site-directed mutants were constructed using the Quick Change site-directed mutagenesis method from Stratagene. PCR conditions are described in Tab. 3. Conditions of thermal cycle and templates are described in the following text for each gene. PCR products were incubated for 60 min at 37 °C with *DpnI* (2 U/ μ l) to remove the parental plasmid. The *DpnI*-treated plasmid

was purified and transformed into *E. coli* DH5 α strain. Point mutations were verified by DNA sequencing.

Table 3. Standard PCR conditions used in this study.

	End Concentrations in 50 μ l total reaction volume
Water	variable ¹
Template	variable ²
Forward primer in 50 pmol/ μ l	[0.5 μ M]
Reverse primer in 50 pmol/ μ l	[0.5 μ M]
2.5 mM each dNTPs	Each [250 μ M]
10-fold specific buffer for DNA Polymerase	1-fold
DNA polymerase	variable ³

¹ Rest of the reaction volume was filled up to 50 μ l by ddH₂O. ² Amount of template DNA was ~ 100 ng of genomic DNA and ~ 1 ng of plasmid DNA for gene amplification, ~20 ng of plasmid DNA for site-directed mutagenesis and single colony dissolved in 6 μ l water for colony PCR were used as template. ³ End concentrations of *Pfu* and *Herculase* DNA polymerases were used as 0.05 U/ μ l and *Taq* DNA polymerase was used as 0.025 U/ μ l.

4.1. Cloning and Mutagenesis of *cooC1*

The *cooC1* gene was amplified by PCR from the genomic DNA of *C. hydrogenoformans* Z-2901 using *Pfu* DNA polymerase with the primers; Fw_C1 with *Nde*I restriction sites and Rv_C1 designed with *Eco*31I restriction sites producing a *Bam*HI-compatible ligation site (Tab. A1 and A2). A 791 bp fragment was isolated from 1% (w/v) agarose gel and ligated into *Nde*I/*Bam*HI-digested pET11a vector (Novagen). Ligation products were transformed into *E. coli* DH5 α and positive colonies were selected by colony PCR. Digestion analysis with *Nde*I/*Bam*HI single and double digestion after plasmid purification confirmed positive plasmid from the colony PCR. The positive plasmid was sequenced, checked for the absence of mutations and named pPKC1.

To obtain CooC1 with N-terminal strep-tag, the *cooC1* gene was amplified with a set of Fw_C1strep and Rv_C1strep primers with *Eco*31I restriction sites using pPKC1 as template (Tab. A1 and A2). *Eco*31I-digested 791 bp PCR product was ligated into *Eco*31I-digested pASKIBA17 plus vector (N-terminal strep-tag). A positive plasmid was selected by digestion analysis as detailed above, sequenced and named pPKC1-Strep.

Site-directed mutagenesis was used to change Lys8 to Ala. Two primers, Fw_C1K8A and Rv_C1K8A, were used for PCR amplification using pPKC1 plasmid as a template (Tab. A1 and A2). A plasmid was isolated and nucleotide sequencing confirmed double point mutations at aaa (Lys8) to gca (Ala) resulting in pPKC1K8A.

4.2. Cloning and Mutagenesis of *cooSII*

All primer sequences and thermocycler conditions used for cloning and mutagenesis of *cooSII* gene are shown in Tab. A3 and A4. An operon (*cooFISII*) encoding CooFI and CODHII (Wu et al, 2005) was amplified by PCR with *Herculase* DNA Polymerase using Fw_PR1 and Rv_PR2 primers with the genomic DNA of *C. hydrogenoformans* Z-2901 as template. The 2.5 kb PCR product was ligated into blunt-ended pET15b vector generated by filling of 3'-recessed ends using Klenow fragment with 2.5 mM dNTPs after digestion of pET15b by *XbaI* and *BamHI*. The resulting plasmid carrying *cooFISII* genes (pPKFISII) contained a point mutation for a stop codon at the position of *gaa* for Glu140, identified by sequence analysis. The point mutation was reverted to *gaa* for Glu140 by using the mutagenesis method described above. *Pfu* DNA polymerase amplified the pPKFISII plasmid as template with Fw_140E and Rv_140E primers. PCR products were treated with the *DpnI* restriction enzyme and transformed into *E. coli* DH5 α . A plasmid was isolated and sequenced, resulting in the complete wild-type sequence named pPKFS2. A 1.9 kb of *cooSII* gene from the pPKFS2 plasmid that was amplified with Fw_PR12 and Rv_PR6 primers using *Pfu* DNA polymerase was digested *BamHI* resulting blunt-end at one side and sticky-end at the other. pET28a vector (N-terminal 6His-tag) was restricted with *NheI* and filled at 3'-recessed end with Klenow fragment. The resulting blunt-ended pET28a was digested with *BamHI*. The previously *BamHI*-digested 1.9 kb of *cooSII* gene was ligated into the blunt-ended and *BamHI*-digested pET28a vector. Two fragments, 1.56 kb and 0.34 kb, after *NdeI* restriction confirmed an insert as *cooSII* gene. The plasmid was sequenced by using four primers (Fw_PR12, Fw_Seq1, Fw_Seq2 and Rv_T7Ter) and a codon for Lys3 was changed to Arg3 as intended and named pPKS2.

A mutant of H96D was generated by using the Stratagen method as described above. *Pfu* DNA polymerase amplified mutant strands from pPKS2 as the parental strand using the primers, Fw_H96D and Rv_H96D. Plasmids were isolated from the *E. coli* DH5 α transformants and a PCR reaction was performed to identify the presence of mutation by using T7-forward primer and R_missH96D-reverse primer that makes miss-pairing at the 3'-end of wild-type sequence. A positive plasmid was isolated and DNA sequencing verified mutation of *cac* to *gat* resulting in pPKS2H96D.

5. Heterologous Expression of Protein

5.1. Expression of CooC1

The pPKC1 encoding wild-type CooC1 was transformed into *E. coli* BL21(DE3) and cultivated in TB medium containing Cb by compressed-air flushing at 37 °C. When OD₆₀₀ reached 0.7 ~ 0.8, 0.2 mM IPTG was added to the culture to induce expression of CooC1. The culture was further

incubated for 20 h at 37 °C after induction and harvested aerobically. Cell pellet was collected inside of the anaerobic tent, frozen in liquid N₂ and kept at -30 °C.

For expression of CooC1K8A, pPKC1K8A plasmid was transformed, cultivated and expressed identically as described above for the wild-type CooC1.

The pPKC1-strep plasmid was transformed into *E. coli* BL21(DE3). Culture was grown as same as that of wild-type CooC1. When the culture reached the beginning of exponential phase (OD₆₀₀ = 0.7 ~ 0.8), the CooC1-strep protein was expressed by adding anhydrotetracycline (200 µg/L). Cultures were cultivated for further 20 h, harvested and stored as same as described in the pPKC1 expression.

5.2. Expression of Rec-CODHII

The pPKS2 plasmid encoding recombinant CODHII with 6 histidines at the N-terminal (Rec_CODHII wild-type) was transformed into *E. coli* Rosseta(DE3) harbouring additionally pRKISC (Nakamura, 1999). This strain was cultivated aerobically by shaking at 37 °C on TB medium containing 0.5 mM NiCl₂, 1 mM Na₂S, 1 mM FeSO₄, and 2 mM Cysteine. Expression of Rec-CODHII was induced by adding 0.5 mM IPTG when the culture reached an OD₆₀₀ of 0.7 ~ 0.8. At 30 h after induction, additional 0.2 mM NiCl₂, 1 mM Na₂S and 1 mM FeSO₄ were added to the culture, which was harvested aerobically 50 h after induction. This cultivation mode produced cluster C-missing Rec-CODHII (C-miss Rec-CODHII) analysed later by UV-visible spectroscopy, CO-oxidation activity and crystal structure (See Results).

To obtain active CODH from *E. coli*, another cultivation mode was attempted by changing cultivation from aerobic to anaerobic. Initially, culture inoculated by over-night culture of *E. coli* Rosseta(DE3) harbouring pPKS2 and pRKISC plasmids was grown aerobically at 30 °C on the modified TB medium containing Tet/Cam/Km antibiotics with addition of 0.02 mM NiCl₂, 0.1 mM Na₂S, 0.1 mM FeSO₄, and 2 mM Cysteine. Expression of Rec-CODHII wild-type was induced by addition of 0.2 mM IPTG supplemented with 0.5 mM NiCl₂, 1 mM Na₂S, 1 mM FeSO₄, and 50 mM KNO₃ when the culture reached an OD₆₀₀ of 0.7 ~ 0.8. Cells were cultivated further anaerobically by gas N₂ flushing. Using the efficient purification of His-tagged protein, the specific activity of CO oxidation from a sample at different time was used to monitor the expression of active protein by using 0.1 ml of Ni-sepharose High Performance (Ni-SHP) material. Purification of the culture sampling was done as described in Materials and Methods (6.2) except for cell breaking. The cell pellet from 2 ml culture was resuspended and incubated for 10 min in lysis buffer (50 mM Tris-HCl pH 8.0, 20 mM NaCl, 20 mM Imidazole, 0.9% (v/v) DCA and 2 mM DT), and the supernatant was loaded onto the Ni-sepharose column. CO-oxidation activities of the purified Rec-CODHII of the sampling were measured as described in Materials and Methods (7.2.1) during time course of cultivation. Cells were immediately

harvested anaerobically either under nitrogen gas flushing or inside the anaerobic tent when the growth reached the highest specific activity around 20 to 22 h after induction (Fig. 12) by centrifugation at 6,000 rpm for 10 min. Cell pellet was collected in the anaerobic tent, frozen in liquid N₂ and kept at -30 °C.

Expression of Rec-CODHIIIH96D was obtained as described above for the wild-type protein. Monitoring for expression of active CODH was performed by cultivating the wild-type strain simultaneously under identical condition. Cells were harvested anaerobically around 20 to 22 h after induction when the wild-type showed the highest activity. Cell pellet was frozen in liquid N₂ and stored at -30 °C until needed.

6. Purification of Protein

6.1. *Purification of CooC1*

All solutions used in purification were prepared as in Materials and Methods (1. and 2.) The purification was performed under anaerobic conditions either under nitrogen atmosphere or inside the anaerobic tent (95% N₂/5% H₂). Frozen cell paste was resuspended in 100 ml buffer QW (50 mM Tris-HCl pH 8.0 and 1 mM TCEP) by addition of small amount of lysozyme and DNase I. After 20 min stirring at room temperature, cells were broken in a glass rosette on ice by 5 cycles of 2 min sonication and 2 min cooling with 50% duty cycle and 6-output control (Branson sonifier) under N₂ atmosphere. Cell extracts were further stirred for 30 min at room temperature. The clear supernatant was prepared by centrifugation for 60 min at 40,000 rpm at 9 °C.

The supernatant was subjected to anionic exchange chromatography (30 ml Source 30Q) on a column equilibrated with buffer QW, followed by washing the column with the same buffer until the absorption at 280 nm reached zero. Protein was eluted with 300 ml of a linear gradient of 0 to 1 M NaCl in buffer QW. CooC protein was identified in flow-through, washing, and the beginning of elution (~100 mM NaCl) fractions by SDS-PAGE as shown in Fig. A1. Fractions containing CooC1 protein were pooled, applied to Blue sepharose fast flow material (18 ml) equilibrated with buffer QW, and eluted with 20 ml of buffer QW followed by 200 ml of a increasing linear gradient of 0 to 1 M NaCl in buffer QW. Fractions containing CooC1 protein eluted at 150 mM NaCl were combined (Fig. A1) and applied to 20 ml Macro-prep ceramic hydroxyapatite equilibrated with buffer HAW (5 mM NaH₂PO₄·2H₂O pH 6.8 and 1 mM TCEP). CooC protein was eluted at 200 mM phosphate concentration by applying 200 ml of a linear gradient with buffer HAE (500 mM NaH₂PO₄·2H₂O pH 6.8 and 1 mM TCEP) as shown in Fig. A1. The fractions containing CooC1 were concentrated in 1.5 ml by spin-concentrator Vivaspin 70 (10 kDa MWCO, Vivascience GmbH) equipped with rubber sealing of screwed cap. The

concentrated CooC1 was subjected to Superdex™ 200 prep-grade gel filtration chromatography equilibrated in 50 mM Tris-HCl pH8.0, 300 mM NaCl and 1 mM TCEP. The fractions corresponding to monomer size (29 kDa) were collected (Fig. A1) and the buffer was exchanged by gel filtration on Sephadex G-25 to metal-free buffer of 20 mM Tris-HCl pH 8.0 and 2 mM TCEP. CooC1 was further concentrated to an appropriate concentration, frozen in glass vials equipped with butyl-rubber septum in liquid N₂ and stored at -70 °C.

Protein samples used to crystalize metal-bound forms were prepared as described above, except that all purification steps were performed aerobically with 2 mM TCEP and gel filtration with Superdex™ 200 prep-grade was excluded.

Purification of the K8A CooC1 mutant was performed identically to that of the wild-type CooC1 as described above. The mutant CooC1 behaved as the wild-type protein in all steps of chromatography.

6.2. Purification of Rec-CODHII

The following purification steps were performed in an anoxic glove box (model B, COY Laboratory Products Inc., Michigan, USA) under an atmosphere of 95% N₂/5% H₂ at 17 °C except that sonication was done under N₂ atmosphere on ice. The cell pellet was resuspended in buffer A (50 mM Tris-HCl pH 8.0 and 20 mM NaCl) containing 20 mM Imidazole and 2 mM DT, disrupted by Branson sonifier with condition: 3 cycles of 1 min sonification and 1 min pause with 30% duty cycle and 6 output control. The cell free extract was centrifuged at 13,400 rpm for 10 min at 17 °C and the supernatant was loaded into Ni-SHP material. The following purification was performed using a syringe. Before purification, free and weakly bound nickel in 1 ml Ni-SHP material was removed by blank run as following: washing column with 5 ml of buffer A followed by washing with 5 ml of buffer A containing 250 mM imidazole. The supernatant after centrifugation was subjected to 1 ml Ni-SHP material equilibrated in buffer A containing 20 mM imidazole and 1 mM DT followed by washing the column with 10 ml of the equilibration buffer. His-tagged Rec-CODHII was eluted by 3 ml of buffer A containing 250 mM imidazole and 1 mM DT. Dark brown eluant containing CODH was subsequently loaded onto Sephadex G-25 (10 by 60 mm) equilibrated in 20 mM Tris-HCl pH 8.0 and 2 mM DT to remove imidazole. The enzyme was further concentrated by Vivaspin 500 (30 kDa MWCO, Vivascience GmbH). Purity of the Rec-CODHII was verified as homogeneous by SDS-PAGE (Fig. 13). Because Rec-CODHII was very sensitive, it was frozen in liquid N₂ using a double vial system made by a 2 ml glass vial with butyl rubber septum, which was transferred into an EPA vial equipped with screwed cap with butyl rubber septum and over-pressurized by N₂ gas. This way, the protein can be stored at -70 °C up to 1 month without a significant loss of activity.

7. Measurements of Enzymatic Activities

A circulating water bath (Haake F8/C25) was attached to the sample holder of an AnalytikJena SPECORD 30 spectrophotometer to control the reaction temperature when described.

7.1. *NTPase Activities of CooC1*

NTPase activities of CooC1 were determined by measuring the amount of inorganic phosphate (P_i) released by ATP or GTP hydrolysis. The amount of released P_i was determined with a procedure modified from the malachite green assay (Lanzetta et al, 1979) by spectrophotometrically detecting an absorbance from the phosphomolybdate-malachite green complex at 630 nm.

All solutions were prepared freshly on the day of use. A mixed malachite green and ammonium molybdate (MG-AM) reagent was prepared by mixing 2 parts of 0.0812% (w/v) malachite green with 1 part of 2.32% (w/v) polyvinyl alcohol prepared by boiling, 1 part of 5.72% (w/v) ammonium molybdate dissolved in 6 M HCl and 2 parts of deionized water. This reagent was allowed to stand at room temperature for 30 min at least or until it turned golden yellow and stable at least for 10 h.

For measurements of the ATPase and GTPase of CooC1, 400 μ l of assay solution was prepared in 50 mM Tris-HCl pH 8.0 containing 100 mM NaCl, 2 mM $MgCl_2$, 2.5 mM ATP or GTP and 2 mM TCEP. ATP or GTP hydrolysis was initiated by adding 10 μ M CooC1 monomer to the assay solution and the reaction continued for 90 min at room temperature. During time course of measurement, 25 μ l reaction solutions were taken, diluted with 75 μ l water and mixed with 800 μ l MG-AM reagent. Colorimetric reaction was quenched by immediately adding 100 μ l 34% (w/v) sodium citrate. After 15 min incubation at room temperature, absorbance at 630 nm was recorded. An amount of P_i released from the hydrolysis was calculated from a standard curve prepared by 1 to 9 nmol of inorganic phosphate KH_2PO_4 (Figure A2). Auto-hydrolysis of nucleotides in the absence of CooC1 as a control was measured and abstracted from the protein-catalyzed reaction. The unit of activity (U) was defined as one μ mol P_i released per minute. The specific activities of enzyme were designated in mU ($mg\ protein^{-1}$). As dioxygen didn't have a significant effect in the NTPase activities, all reactions were performed under aerobic condition except for the ATP hydrolysis of Ni-incubated CooC1 that was measured under anaerobic condition.

7.2. *CO-oxidation/CO₂-reduction Activities of Rec-CODHII*

7.2.1. *CO-oxidation activity*

CO-oxidation activity was assayed as described (Svetlitchnyi et al, 2001) at 70 °C by following the CO-dependent reduction of oxidized methyl viologen (MV_{ox}) spectrophotometrically using an ϵ_{578} of $9.7 \text{ mM}^{-1} \text{ cm}^{-1}$. One ml assay solution containing 20 mM MV_{ox} and 2 mM DTT in 50 mM HEPES-NaOH pH 8.0 was filled in screw-capped cuvette sealed with either a butyl rubber or a silicon septum under CO flushing into the atmosphere. Stock solutions of enzyme (mostly 10 mg/ml) were diluted in an appropriate concentration (approximately 10-thousand fold) with dilution buffer of 50 mM HEPES-NaOH pH 8.0, 2 mM DTT and 2 mM DT. Reactions were initiated by injecting Rec-CODHII with a gas-tight syringe (HAMILTON Bonaduz AG, Switzerland). The unit of activity (U) was defined as one μmol CO consumption per minute. The pH-dependent CO-oxidation activities of Rec-CODHII wild-type and H96D was measured in a pH range 5.56 to 8.96 prepared with 50 mM buffers (MES-NaOH for pH 5.56 and 6.10, HEPES-NaOH for pH 7.0 and 8.0, and Tris-HCl for pH 8.96).

7.2.2. *CO₂-reduction activity*

CO₂-reduction activity was assayed spectroscopically by monitoring the formation of carboxyhemoglobin as described previously by (Ensign, 1995) with modifications. Assays were performed in 2 ml anaerobic quartz cuvettes sealed by silicon septum with screw cap without free headspace. Reaction conditions were designed to be identical as in the crystal soaking condition for $-600 \text{ mV} + \text{CO}_2$ (See Material and Methods 11.2). Two ml of Assay mixture containing 50 mM Tris-HCl pH 8.0, 0.2 mg/ml hemoglobin (Fluka), 5 mM Ti(III) citrate, and 50 mM NaHCO_3 as CO₂ source was filled into cuvettes by gas-tight syringe. This reaction mixture was equilibrated for 2 min at 25 °C leading to no spectral changes. Reaction was initiated by addition of Rec-CODHII. The production of CO from CO₂ by the enzyme was monitored by formation of carboxyhemoglobin with the increase in absorbance at 419 nm. Standard curve was prepared by titrating samples of a saturated CO solution in water at 25 °C in assay cuvette and measuring spectral changes between 400 nm and 460 nm (Fig. A3). 1.04 mM of saturated CO in water at 25 °C was adapted from (Ensign, 1995; Wilhelm et al, 1977). The unit of activity (U) was defined as one μmol CO production per minute.

8. Spectroscopic Analysis

8.1. *UV-visible Spectroscopy*

All UV-visible spectra were obtained on an AnalytikJena SPECORD 40 spectrophotometer with screw-capped quartz cuvette (1 cm path length, Hellma GmbH & Co) sealed with butyl or silicon septum. Metal-free buffers and water used in all spectroscopic analysis of CooC1 were prepared as described in Materials and Methods (1.).

8.1.1. *CooC1 spectra*

To prepare apo-CooC1, as-isolated protein (50 μM dimer) was treated with 10 mM EDTA and 2 mM TCEP for 2 days in an anoxic glove box at 17 °C. EDTA was removed by PD10 column (GE Health Care) equilibrated with buffer R (50 mM Tris-HCl pH 8.0 and 100 mM NaCl) in the absence of 1 mM TCEP. Spectra of as-isolated and apo-CooC1 were obtained with buffer R in the presence or absence of 1 mM TCEP.

8.1.2. *Rec-CODHII spectra*

Spectrum of the as-isolated Rec-CODHII under N_2/H_2 was recorded after removing DT by Sephadex G25 (10 by 60 mm). Characteristic spectra of the reduced enzyme were obtained from reduction either by 2 mM DT under N_2/H_2 or pure CO. Spectra were measured by wavelength scanning from 250 to 600 nm at room temperature.

8.2. *Circular Dichroism (CD) Spectra of CooC1*

All CD measurements were recorded on a JASCO J600 spectropolarimeter with HAAKE K thermostat and a PTC348 W1 Peltier element with N_2 gas flushing. In all experiments, CooC1 was prepared in buffer G (20 mM Na-Phosphate pH 7.5, 100 mM NaCl and 2 mM TCEP).

8.2.1. *Far-UV CD spectra*

The standard Far-UV CD spectra of the as-isolated, Ni-, ATP- and ADP-bound CooC1 were collected at 20 °C using a 1 cm path-length cell with a 1 nm bandwidth, 2 s response times and a scan speed of 20 nm/min. End protein concentrations of Apo- and Ni-CooC1 were 5 μM monomer in buffer G. 10 μM NiCl_2 was added for Ni-CooC1. Effect of presence of ATP or ADP were carried out by adding 200 μM nucleotide to the protein solution. Ten individual scans taken from 190 to 260 nm were added and averaged, followed by subtraction of the solvent CD signal. The average of recorded ellipticity (θ) in degree was converted to a average molar ellipticity per amino acid $[\theta]_{MRW}$ using Eq. 3.

$$[\Theta]_{MRW} = \frac{\Theta}{c \cdot d \cdot N_{AS} \cdot 10} \quad (\text{Equation 3})$$

$[\theta]_{MRW}$	average molar ellipticity per amino acid in degree $\text{cm}^2 \text{dmol}^{-1}$
θ	recorded ellipticity in mdeg
c	protein concentration in M
d	path-length of cuvette in cm
N_{AS}	number of amino acid

8.2.2. Thermally induced unfolding CD spectra

Thermal denaturation was monitored by measuring the CD signals at 222 nm for as-isolated and Ni-CooC1 and at 225 nm for the ATP- and ADP-CooC1 with increasing temperature from 20 to 80 °C with a temperature scan rate of 60 °C/h. End protein concentrations of Apo- and Ni-CooC1 were 1 μM monomer in buffer G. 10 μM NiCl₂ and 200 μM ATP or ADP were added for Ni-CooC1 and ATP- or ADP-CooC1, respectively. The values of T_m and $\Delta H_{v.H.}$ were calculated by a non-linear least-square fit of the experimental data to Eq. 4 with the heat capacity, ΔC_p , of 20,000 J mol⁻¹K⁻¹ (Mayr et al, 1993).

$$y_{obs} = \frac{(y_n^o + m_n T) - (y_u^o + m_u T)}{1 + \exp\left[-\frac{\Delta H_{v.H.}}{R} \left(\frac{1}{T} - \frac{1}{T_m}\right) - \frac{\Delta C_p}{R} \left(1 - \frac{T_m}{T} + \ln \frac{T_m}{T}\right)\right]} + y_u^o + m_u T \quad (\text{Equation 4})$$

y_{obs}	observed experimental absorbance
y_n^o	absorbance values for the native protein at 0 Kelvin
y_u^o	absorbance values for the unfolded protein at 0 Kelvin
m_n	slopes of the pre-transitional baselines
m_u	slopes of the post-transitional baselines
T_m	midpoint of thermal transition
$\Delta H_{v.H.}$	van't Hoff enthalpy of the transition at T_m

9. Spectroscopic Measurement of Nickel Binding to CooC1

All metal-free buffers and water used in this study were prepared as described in Materials and Methods (1.). Ionic strength in the measurements was adjusted to 100 mM NaCl. Total 1 ml reaction solution was prepared by dissolving 16 ~ 18 μM dimer of the wild-type and K8A CooC1 in buffer R (50 mM Tris-HCl pH 8.0 and 100 mM NaCl) with or without 100 μM ATP or ADP supplemented with 1 mM TCEP inside of the anoxic glove box. For Ni-titration in the presence of a nucleotide, reaction solution was incubated for 10 min. After taken the cuvette out of the anoxic glove box, nickel titration was achieved by adding 1 ~ 5 μl of 1 mM NiCl₂ stock solution into the titrating solution with a gas-tight syringe (Hamilton) in each step at room temperature. After slight mixing of the solution, spectra of different nickel concentrations at the wavelength from 250 to 500 nm were recorded against the buffer titrating with nickel without protein as the measurement. During titration, whole spectra of apo-form (as-isolated) and Ni-bound (prepared by adding 1 equivalent nickel to dimer) wild-type and K8A CooC1 were measured from 250 nm to 900 nm to be able to detect spectral change at the lower energy wavelength. Each spectrum was measured in 5 min. Spectra were corrected with dilution factors, absorption was transformed into extinction coefficient [M⁻¹ cm⁻¹] and difference at a specified wavelength was plotted against nickel concentrations added. Titration data were fitted to a non-linear equation (Eq. 5) using the program GraFit 5 (Leatherbarrow, 2001).

$$\delta A(sw) = \frac{\delta A_{\max}(sw)}{2nE_T} \left[(L_T + nE_T + K_d) - \sqrt{\left((L_T + nE_T + K_d)^2 - (4L_T nE_T) \right)} \right] \quad (\text{Equation 5})$$

$\delta A(sw)$	absorption difference at a specified wavelength
$\delta A_{\max}(sw)$	maximum absorption difference at a specified wavelength
n	number of nickel binding sites at dimer CooC1
E_T	concentration of dimer CooC1
L_T	concentration of Ni ²⁺ Ion
K_d	dissociation constant

10. Oligomeric States Analysis of CooC1

All buffers used in this study were freed from metal according to Materials and Methods (1.). Gel filtration experiments were performed at room temperature using Superdex™ 200 prep-grade column (16 mm x 600 mm) inside the anaerobic glove box. Aliquots of wild-type and K8A CooC1 were dissolved in the running buffer (50 mM Tris-HCl pH 8.0, 100 mM NaCl, and 2 mM TCEP), injected onto the column equilibrated in the running buffer with or without a ligand as noted below and run with a 1 ml/min flow rate by ÄKTAprime (GE Health Care). Elution chromatograms of experiments were recorded by detecting absorbance at 280 nm. Approximately 0.5 mg/ml (9 µM dimer state) of the EDTA-incubated wild-type as described in Materials and Methods 8.1.1 and 1 mg/ml (18 µM dimer) of the as-isolated wild-type CooC1 were subjected to the gel filtration column equilibrated in the running buffer with or without 1 mM EDTA. For the Ni-bound wild-type, 1 mg/ml of the as-isolated CooC1 was incubated in the running buffer with equimolar concentration of Ni and incubated for 10 hrs at 17 °C in the anoxic glove box. Binding of Ni was detected by the presence of a peak at 330 nm in the absorption spectrum, and the protein was injected on the column in the running buffer containing 2 mM Ni. To investigate nucleotide-dependent oligomeric states, 1 mg/ml of the as-isolated wild-type and 2 mg/ml K8A CooC1 were dissolved in the running buffer and loaded on the column equilibrated in the running buffer containing 1 mM ATP or ADP. Proportions of different oligomeric states were calculated by using a peak integration function in PrimeView Evaluation Software. The molecular weights of different states of CooC1 in solution were determined by loading known-molecular weight standards in the running buffer: 5 mg/ml catalase (250 kDa), 1 mg/ml aldolase (161 kDa), 1 mg/ml cobalbumin (75 kDa), 1 mg/ml carbonic anhydrase (29 kDa) and 1 mg/ml ribonuclease I (13.7 kDa). A Standard curve of molecular weight sieves was generated by plotting elution volume against log MW and fitted to a linear equation (Fig. A4).

11. Crystallographic Methods

11.1. *Crystallization of CooC1 and Rec-CODHII*

All crystallizations were carried out in the anoxic glove box as described in Materials and Methods 3. The crystallizations of CooC1 and Rec-CODHII were performed with the hanging drop vapor diffusion method (McPherson, 1982) by mixing equivalent volumes of protein solution and reservoir buffer, and equilibrated against 0.5 ml of reservoir buffer.

Crystals of different states of CooC1 were obtained by mixing 2 μ l of 8 ~ 10 mg/ml protein in 20 mM Tris-HCl pH 8.0 with 2 mM TCEP with or without incubation of a ligand and 2 μ l of a reservoir buffer (see *conditions* below) containing 5 mM TCEP as noted below. Protein samples purified aerobically and anaerobically (see Materials and Methods 6.1) were used for crystals with and without metal, respectively. A crystal for phasing by thiomersal-derivative was grown in *condition I* (0.1 M tri-ammonium citrate pH 8.0, 15-23% (w/v) PEG 3350 and 3% MPD) within a few days. A crystal of Apo-form CooC1 was grown in *condition II* (0.2 M L-proline, 0.1 M HEPES-NaOH pH 7.5 and 7-10% (w/v) PEG 3350) in the presence or absence of 2 mM ADP, 10 mM MgCl₂ and 4 mM V_i in a week. ADP-bound CooC1 crystal was obtained by mixing the protein with *condition III* (0.2 M lithium citrate tribasic tetrahydrate, 13-15% (w/v) PEG 3350, 5% (v/v) glycerol and 1 mM ADP) in a few days and grown for 2 – 3 weeks. A crystal of Metal-bound CooC1 appeared in *condition IV* (0.25 M lithium citrate tribasic tetrahydrate and 12-14% (w/v) PEG 3350) after one week and needed additional 2 – 3 weeks to reach its final size. A crystal of Metal- and ADP-bound CooC1 was obtained in *condition V* (0.2 M lithium citrate tribasic tetrahydrate, 9-11% (w/v) PEG 3350, 5% (v/v) glycerol, 10 mM AlF₄, 10 mM MgCl₂ and 1 mM ADP) within one week.

Cluster C-missing or wild-type Rec-CODHII were crystallized by mixing 2 μ l of 10 ~ 15 mg/ml protein solution with 2 μ l of reservoir buffer of either *formate condition* (250 mM Mg-formate, 15 ~ 20% (w/v) PEG 3350, and 2 mM DT) or *sulfate condition* (15 - 18% (w/v) PEG 3350 or PEG 2000, 200 mM ammonium sulfate, 100 mM Bis-Tris pH 6.5, and 2 mM DT). Rec-CODHIIH96D crystals were grown from a mixture of 2 μ l of 10 mg/ml protein and 2 μ l of reservoir buffer (0.15 ~ 0.25 mM MgCl₂, 0.1 M Bis-Tris pH 6.5, 20 ~ 23% (w/v) PEG 3350, and 2 mM DT). Crystals appeared in few days or further grown up to 21 days. During this period of crystallization over 90 % of CO oxidation activities were maintained. As an additional control to exclude a trace of oxygen, colours of MV_{red} (blue; E_h \approx -430 mV) or resazurin_{red} (colorless; E_h \approx -110 mV), which were prepared by adding 0.1 mM DT, in reservoir and/or drop were used as indicators of reducing conditions during crystallization.

11.2. *Manipulation of Crystals*

To solve the phase problem of CooC1, diffraction data of a crystal grown in *condition I* was collected as native. Another crystal was soaked by adding a little bit of thiomersal powder for 30 min and data set was collected (Tab. A5).

Different redox intermediates of CODH crystals were prepared as following below. Stock solutions of DT and DTT were prepared freshly in water as 1 M concentration. 83 mM Ti(III) citrate was prepared as reference (Seefeldt & Ensign, 1994) as following: 1 ml TiCl_3 (Merck) was dissolved in 4.8 ml 0.5 M Na_3 -citrate and buffered by adding 6.2 ml 1 M Tris-HCl pH 8.0.

To obtain different redox states, single crystals of Rec-CODHII were incubated in buffer A (25% PEG 3350, and 50 mM Tris-HCl pH 8.0) with different redox potentials adjusted with either 5 mM Ti(III) citrate solution to -600 mV vs. SHE or with 7 mM DTT solution to -320 mV vs. SHE. Redox potentials of the soaking solutions were measured with an EMC 130 redox electrode containing an integrated Ag/AgCl reference system (Sensortechnik Meinsberg GmbH, Germany). The reported three states (-320 mV, -600 mV, and -600 mV+ CO_2) were obtained from crystals grown for 10 days as follows. All crystals were washed three times with the -600 mV solution and remained in this solution for three hours. After this procedure one crystal was shock frozen in liquid nitrogen giving the -600 mV state. Another crystal was soaked for 30 min in the -600 mV solution containing 45 mM NaHCO_3 after which it was shock frozen to give the -600 mV+ CO_2 state. At a pH of 8.0 approximately 1% of the total carbonate concentration is present as dissolved CO_2 . The -320 mV state was prepared by transferring one crystal from the -600 mV solution into a solution containing 7 mM DTT and 0.5 mM MV_{ox} as electron acceptor for reoxidation; after no further reduction of MV_{ox} to the blue colored MV_{red} was detectable the crystals were incubated in the -320 mV solution containing 7 mM DTT for 2 hours. Between all steps crystals were washed extensively for at least three times with the subsequent soaking solution.

The influence of soaking experiments on Rec-CODHII activity was monitored by measuring the specific activities of dissolved crystals. After 40 days of crystallization, all crystals from one 24 well plate were treated in the same way as the crystals for structure determination. Specific activities of dissolved Rec-CODHII crystals were: as-isolated state, 10,999 units mg^{-1} ; -600 mV state, 11,317 units mg^{-1} ; -320 mV state, 13,427 units mg^{-1} ; -600 mV+ CO_2 state, 13,808 units mg^{-1} .

A reservoir solution containing 15% (v/v) 2*R*, 3*R*-butandiol (Sigma) was used as a cryoprotectant for all crystals. Crystals of Rec-CODHII were shock frozen in soaking solutions containing the cryoprotectant and stored in liquid nitrogen until the diffraction experiments were carried out.

11.3. *Data Collection*

The data statistics reported in Tables A6 and A7, for CooC1 and CODH structures, respectively, are given for the crystals with highest diffraction limit. Diffraction experiments were carried out on an X-ray generator with rotating Cu-anode (Nonius FR591, Bruker AXS, Karlsruhe, Germany) equipped with an image plate detector (mar345dtb, marresearch GmbH, Hamburg, Germany). Data were collected at 100 K. For each of the reported-three states (-320 mV, -600 mV, and -600 mV+CO₂) of CODH crystals at least two independently prepared crystals were measured and analyzed. All diffraction data were indexed, integrated, scaled and merged using XDS package (Kabsch, 1993). All Rec-CODHII crystals belonged to space group C2 with one monomer in the asymmetric unit and cell constants of $a = 112$, $b = 74$, $c = 70$ Å and $\alpha = \gamma = 90^\circ$, $\beta = 111^\circ$.

11.4. *Structure Determination*

The structure of CooC1 was solved by using SIRAS (single isomorphous replacement with anomalous scattering) with diffraction data sets of native and thiomersal-derivative crystals (see Materials and Methods 13.1.). Both diffraction data sets were integrated and scaled using XDS program (Kabsch, 1993). Phasing was carried out using SOLVE (Terwilliger & Berendzen, 1999) and the resulting phases were modified using RESOLVE (Terwilliger et al, 2006) and further optimized by cyclic averaging of the electron density. Model building was done with MAIN 2000 (Turk, 1992). Refinements were carried out using CNS (Brunger et al, 1998). The crystallographic statistics of phasing and refinement are reported in Tab. A5. However, this structure was used only for solving the phase problem and was not used for structure examination because electron density was missing for some regions.

The structure of CODH was solved by Patterson search techniques with homologous search model using the program Phaser (Mccoy et al, 2007). The crystal structure of native CODHII_{Ch} (PDB ID:1SU8) (Dobbek et al, 2004) served as search model.

11.5. *Structure Refinement and Evaluation*

All other CooC1 structures reported here were solved by Patterson search techniques with homologous search model using the program Phaser (Mccoy et al, 2007). The crystal structure of the thiomersal-derivative served as an initial search model (see above). Models for CooC1 and Rec-CODHII structures were built with MAIN 2000 (Turk, 1992) and/or COOT (Emsley & Cowtan, 2004). Positional and temperature factor refinements were carried out using CNS (Brunger et al, 1998) for CooC1 structures with NCS restraints in case of two molecules in asymmetric unit (ADP-bound and Metal/ADP-bound), and Refmac5 (Murshudov et al, 1997) for

the different states of Rec-CODHII structures. Restraints for the different states of cluster C were generated by iterative cycles of refinement with weak restraints and generation of new parameters using Refmac5 and SHELX (Sheldrick & Schneider, 1997). Individual occupancies of atoms from cluster C were adapted to show comparable B factors (Tab. A9). In the final refinement cycles the B factors of iron and nickel ions were refined anisotropically, alternative conformations of several side chains and Fe1 were included and restraints for bond length and angles of cluster C were practically excluded. The final refinement statistics are shown in Table A7. Simulated annealing omit maps were used to validate the reported structures. The stereochemistry of each structure was analyzed by PROCHECK (Laskowski et al, 1993). Refinement statistics of all reported structures are shown in Tables A6 and A7 for structures of CooC1 and Rec-CODHII, respectively.

12. Miscellaneous Methods

12.1. *Determination of Protein Concentration*

Protein concentration of Rec-CODHII was determined by Bradford (Bradford, 1976) with BSA as a standard. Concentration of CooC1 was calculated from an extinction coefficient ϵ_{280} of 19,285 $M^{-1} cm^{-1}$ derived from reference (Pace et al, 1995).

12.2. *SDS-PAGE*

SDS-PAGE was prepared according to Laemmli (Laemmli, 1970). The denatured samples were loaded on the gel with Roti-Mark Standard (Roth: Myosin, 200 kDa; β -Galactosidase, 119 kDa; Serum albumin, 66 kDa; Ovalbumin, 43 kDa; Carbonic anhydrase, 29 kDa; Trypsin inhibitor, 20 kDa; Lysozyme, 14.5 kDa) or unstained protein molecular weight marker (Fermentas: β -Galactosidase, 116 kDa; Bovine serum albumin, 66.2 kDa; Ovalbumin, 45 kDa; Lactate dehydrogenase, 35 kDa; REase Bsp98I, 25 kDa; β -Lactoglobulin, 18.4 kDa; Lysozyme, 14.4 kDa). The separated proteins were stained with a 0.025% (w/v) coomassie brilliant blue G-250 for 20 minutes and then transferred into 10% (v/v) acetic acid of destaining solution until background got colourless.

12.3. *Computer Softwares*

Spectra measured in this work were analyzed and presented by Grafit 5 (Leatherbarrow, 2001) or Microcal™ Origin 6.0. Amino acids sequences were aligned with ClustalW (Chenna et al, 2003) and edited manually. All pictures of reported structures in this study were prepared using PyMol (DeLano).

RESULTS

1. Cloning

1.1. Cloning of *cooC1*

Carboxydotherrnus hydrogenoformans Z-2901 possesses 3 genes encoding CooC isozymes (CooC1-3) (Wu et al, 2005). As shown in Fig. 8, each gene is located in a specific region where genes encoding Ni-containing enzymes (Ni-CODHs (*cooSI-V*), Ni-Ni-actyl-CoA synthase (*acsA*) and CO-induced Ni, Fe-hydrogenase (*cooHUXLKM*)) are placed. Among them, *cooC1* (locus_tag: CHY_1823) is located in front of genes encoding CODH/ACS complex. A 765 bp of gene denoted as *cooC1* encoding 254 amino acids of CooC1 was cloned into pET11a vector without an affinity tag and named pPKC1. The nucleotide sequence from DNA sequencing and its amino acids sequences deduced from it confirmed no mutation compared to the published sequence (Wu et al, 2005). The *cooC1* gene was subcloned into pASKIBA17 plus vector containing an N-terminal strep-tag for one-step purification and named pPKC1-strep. The amino acid sequence of CooC1 was blast at NCBI (<http://blast.ncbi.nlm.nih.gov/Blast.cgi>) using the *blastp* algorithm and aligned to its homologues from *C. hydrogenoformans* and other microorganisms that have a Ni-containing CODH or CODH/ACS complex as shown in Fig. 26. CooC1 belongs to an ATPase family of the SIMIBI class with a deviant Walker A motif (XKGGXXK[T/S]) in the P-loop where the first lysine is the “signature lysine”. This deviant Walker A motif including the signature lysine is highly conserved. In order to investigate the role of the conserved lysine among CooC homologues, K8 in CooC1 was changed to Ala by site-directed mutagenesis producing the pPKC1-K8A plasmid. CooC1 shows high sequence similarity to other CooCs (over 30% identities) except CooC2_{Ch}. While the genomic DNA of *C. hydrogenoformans* does not contain a gene annotated as encoding AcsF that is a putative accessory protein of Ni insertion to ACS (Loke & Lindahl, 2003), CooC2_{Ch} has 52% sequence identity to AcsF_{Mt} and corresponding genomic location at vicinity to *acsA* (Figures 8 and 26), suggesting that CooC2_{Ch} functions as AcsF in *C. hydrogenoformans*.

1.2. Cloning of *cooSII*

The genomic DNA of *C. hydrogenoformans* Z-2901 encodes 5 structural genes for CODH (I-V) as shown in Fig. 8 (Wu et al, 2005). Because of sequence similarities of the five *cooS(I-V)* genes and low GT content of a region for *cooS-II* gene, a specific primer set was designed to amplify an operon of *cooFS-II* genes. This operon was cloned into a pET15b vector, mutated for an occasional stop codon, sequenced and named pPKFS2. 1911 bp of the *cooS-II* from pPKFS2 was cloned into pET28a vector containing N-terminal His₆-tag. Finally DNA sequencing

resulted in a complete *cooS-II* gene encoding 636 native amino acids excepting Lys3 to Arg, which named pPKS2 plasmid. The pPKS2 plasmid encodes totally 656 amino acids including N-terminal His₆-tag with a short linker.

During CO-oxidation of CODH reaction, two protons are produced and must be released out of protein using a channel. Drennan and co-authors proposed that several semi-conserved histidines placed structurally close to cluster C take protons after CO-oxidation reaction (Drennan et al, 2001). To investigate the role of the histidine residues on CO oxidation mechanism, the most highly conserved histidine residue (His₉₆ in CODHII, shown in Fig. 32) among sequences from CODHs was mutated to Aspartate. This plasmid was named pPKS2-H96D and further used for studies of H96D mutation affecting CO oxidation activity and the structure of the putative proton channel.

2. Protein Expression and Purification

2.1. *Expression and Purification of CooC1*

For test expressions, *E. coli* BL21(DE3) harbouring pPKC1 was cultivated in TB or LB medium with Cb at 30 ~ 37 °C. Synthesis of the wild-type CooC1 protein was induced by adding 0.2 ~ 1 mM IPTG as final concentration in the test expressions. Overexpression of soluble protein did not depend on the concentration of IPTG and the time point of induction showing similar expression level at the very early (OD₆₀₀ = 0.4 ~ 0.8) and the beginning (OD₆₀₀ = 0.8 ~ 1.0) of exponential growth phase. However, cultivation temperature, cultivation time after induction and types of media influenced yield of protein expression and the purification strategy. Among all conditions tested, the best condition for the yield and purity were obtained when *E. coli* strain harbouring pPKC1 cultivated in TB at 37 °C, were induced by 0.2 mM IPTG at OD₆₀₀ 0.7 ~ 0.8 and harvested after 20 h of further cultivation at 37 °C (Fig. 11, Lane 1). Approximately over 90% of total overexpressed CooC was identified in the soluble fraction from cell extract judged from SDS-PAGE (Fig. A1). This condition was highly reproducible.

Fig. 11 (Lane 2 ~ 5) shows SDS-PAGE of the fractions collected from four chromatography steps used in the purification of the wild-type CooC1. Since approximately 50 ~ 80% of soluble CooC were not bound on the anionic exchanger Source 30Q, several tests were performed to bind CooC to the anionic exchanger for increase in purity and yield. Several attempts of adding small amounts of NiCl₂ in TB media during cultivation, addition of EDTA and change of pH value of buffers used in cell lysis and purification of Source 30Q did not improve the binding strength of CooC1 to the anionic exchanger. This phenomenon is still not fully understood, but this effect seems to be dependent on the cultivation and not on the materials used for purification. Even though cultivation was done identically each time, the amount of CooC1 in the flow-through from

Source 30Q varied between cultivations. Nevertheless, the optimized expression condition described above as in Materials and Methods (5.1.) was quite reproducible and the flow-through and washing fractions containing CooC1 were to be around 80% of total soluble protein (Fig. 11, Lane 2 and Fig. A1-A, Lanes 3 and 4). Fractions containing CooC1 (flow-through, washing and elution from 0 to 70 mM NaCl, see Fig. A1-A) from Source 30Q were collected and loaded on Blue sepharose column for further purity. CooC1 was bound to the column and eluted between 50 and 100 mM NaCl concentration (Fig. 11, lane 3 and Fig. A1-B).

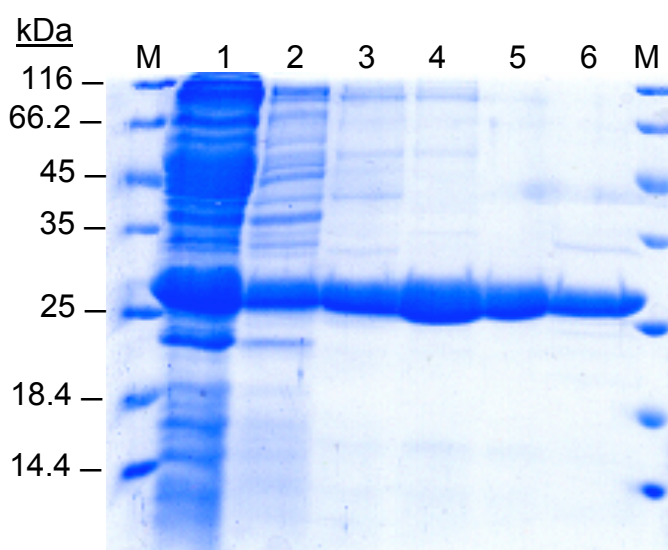


Figure 11. Coomassie blue-stained 12 % (w/v) SDS-PAGE of overexpression and chromatography steps used in purification of the wild-type and K8A CooC1. Lane 1, whole cell pellet from the overexpression of wild-type CooC1 at 20 h after induction; Lane 2, 5 μ l of pooled-fractions of wild-type CooC1 from Source 30Q (total volume 150 ml), Lane 3, 5 μ l of a pool containing wild-type CooC1 from Blue sepharose, Lane 4, 5 μ l of a pool containing wild-type CooC1 from Hydroxyapatite; Lane 5, ~12 μ g of the wild-type CooC1 after SuperdexTM 200 gel filtration; Lane 6, ~12 μ g of the purified K8A CooC1 after SuperdexTM 200 gel filtration; M, Unstained protein molecular weight marker from Fermentas. Because of the identical behaviors between wild-type and K8A mutant in purification steps, pictures of three steps (Source 30Q, Blue sepharose and Hydroxyapatite) from the purification of the mutant are not shown.

Further purification with hydroxyapatite material removed major impurities and CooC1 eluted with 180 to 220 mM phosphate (Fig. 11, lane 4 and Fig. A1-C). Structural homogeneity of CooC1 was achieved after SuperdexTM 200 prep-grade gel filtration as shown in Fig. A1-D. CooC1 showed two conformations in solution, monomer and dimer during gel filtration but only monomeric fractions were collected. Homogeneity (over 95% pure) of the as-isolated CooC1 was identified in the coomassie-blue stained SDS-PAGE (Fig. 11, Lane 5). With conditions for expression and purification steps described above, approximately 30 mg of CooC1 was purified out of 2 L culture (~18 g wet cell paste). The mutant form of CooC1 K8A behaved similarly on the level of expression and the yield and purity of purification (Fig. 11, Lane 6).

To achieve high yield and purity of protein in one-step, a strep-tag was applied to the NH₂-terminal of CooC1. However, overexpression of strep-tagged CooC1 was not obtained by

different expression conditions tested including different *E. coli* strains, different media, amount of AHT, and temperature of cultivation. Regardless of the expression level, soluble cell extracts were loaded on a Strep-tactin column. Over 95% of total soluble CooC1 was identified in the flow-through fraction and protein yield was approximately 1 mg out of 1 L culture with less homogeneity (data not shown) when compared with the native purification.

2.2. Expression and Purification of Rec-CODHII

The gene encoding structural CODHII from *C. hydrogeniformans* was cloned into a pET28a vector containing an NH₂-terminal His₆-affinity tag, resulting in the pPKS2 plasmid. Codon usage analysis (Graphical Codon Usage Analysis: <http://gcu.schoedl.de/>) of the *cooS-II* gene indicated abnormal codon usage different from *E. coli*. The pPKS2 plasmid was introduced into Rosseta(DE3) strain harbouring the pRARE plasmid providing six rare codons, and expression of full length CODHII (69 kDa) was identified by SDS-PAGE (Fig. 12). Because homodimeric CODHII requires 20 moles of Fe, 22 moles of S, and 2 moles of Ni for active species as identified by crystal structure (Dobbek et al, 2001), additional metal and sulfide sources were added at a concentration below the toxic effect for *E. coli* growth (Spain, 2003). Aerobic cultivation under these conditions followed by anaerobic purification produced the protein with less Fe-S cluster contents (Fig. 16-B) comparing to the native enzyme as judged by the absorption ratio of 418 nm to 280 nm from UV-visible spectrum (Svetlitchnyi et al, 2001), corresponding to inactive species (~ 0.3 U/mg protein of CO-oxidation activity). Later this species were identified as an enzyme that is lacking cluster C (cluster C-missing Rec-CODHII) by X-ray crystal structure (see Result). An attempt to produce active enzymes was carried out by applying complete anaerobic cultivation and expression with media containing glycerol as carbon source and nitrate as an artificial electron acceptor to support anaerobic respiratory growth of *E. coli* (Uden & Bongaerts, 1997). However, enzymes purified anaerobically from this cultivation showed only 2,000 ~ 3,000 U/mg protein of CO-oxidation activities.

An expression system of active Rec-CODHII was established in *E. coli* by applying the fact that *E. coli* is a facultative microorganism that can grow aerobically and anaerobically in the presence of an appropriate carbon and energy source. All conditions for cultivation and expression were the same as the complete anaerobic system described above, but *E. coli* cells initially were cultivated aerobically by air-flushing before IPTG-induction, followed by turning to anaerobic expression supported by N₂-flushing (Fig. 12). However, a mode of the anaerobic cultivation by leaving culture in a bottle closed by screw capped butyl rubber septum in this system resulted in the same as the complete anaerobic system. ISC (Iron Sulfur Cluster) operon is comprised of 6 genes (*iscSUAhscBAfdx*) and encodes the proteins playing key roles in the Fe-S cluster assembly in *E. coli* (Nakamura, 1999). To support the formation of large

numbers of Fe-S clusters required for overexpression of the protein in *E. coli*, pPRKISC plasmid (Nakamura, 1999) was coexpressed together with supplementation of iron and sulfur sources, thus enhancing production of holo and active forms of CODHII.

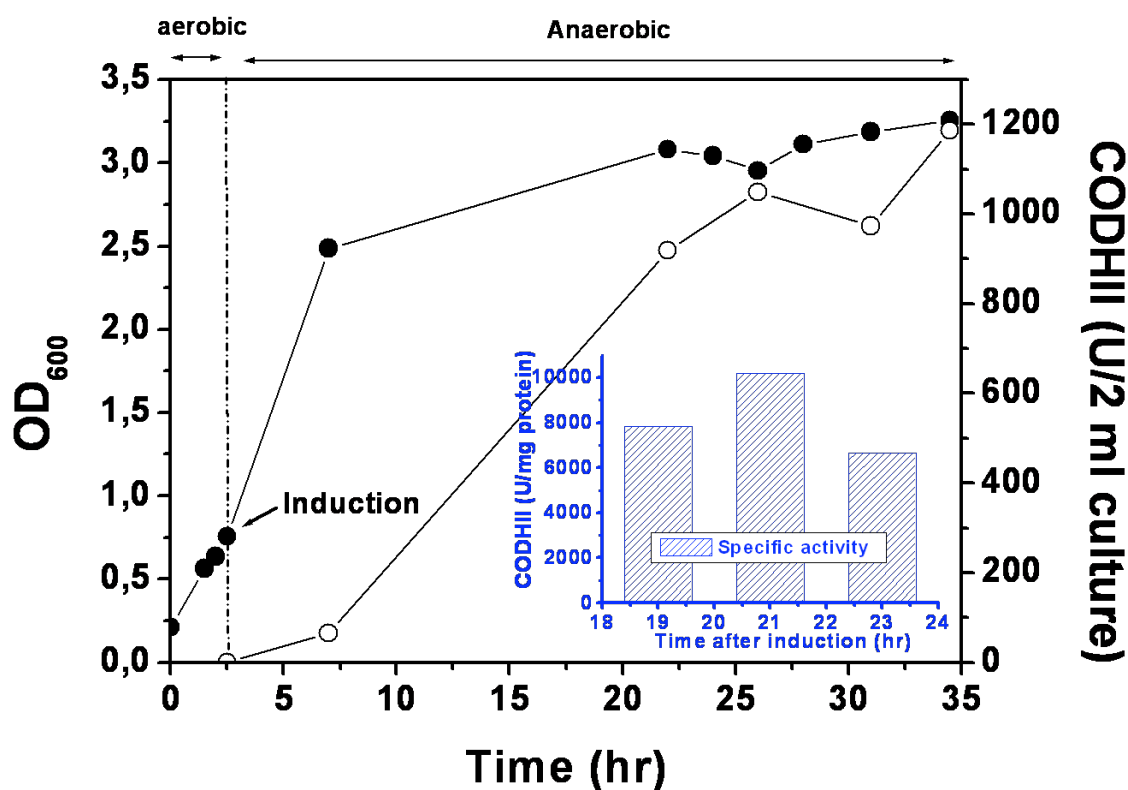


Figure 12. Growth and activity monitoring of Rec-CODHII expressed in *E. coli* Rosseta(DE3) harboring pRKISC (Nakamura, 1999). Inset shows average specific activity of Rec-CODHII purified at different time from three independent cultivations; 10182 U (mg protein)⁻¹ as the highest activity around 21 hours after induction was measured from three independent cultivations. Change of cultivation mode is indicated as dashed line with induction. Filled-circle indicates optical density at 600 nm and empty-circle denotes volumetric activity of CO-oxidation measured during the time course of cultivation.

Monitoring of the increasing CO-oxidation activity after induction of expression was essential to get active enzyme as shown in Fig. 12. Monitoring of production of active enzyme by measuring volumetric activity was not reliable because of increasing activity with decreasing specific activity after certain time (data not shown in Fig. 12). Specific activity of samples during the time course of cultivation was monitored, which was important to get a highly active enzyme. By using the benefit of his-tag, Rec-CODHII could be purified during cultivation with Ni-SHP material and the specific activities of samples from different times were measured. The specific activity was highest between 19 to 23 hrs after induction (Fig. 12, inset). When the culture reached the highest specific activity, it was immediately harvested under anaerobic condition. Otherwise Rec-CODHII lost activity within few hours. The frozen cells were kept at -30 °C for several months without loss of activity.

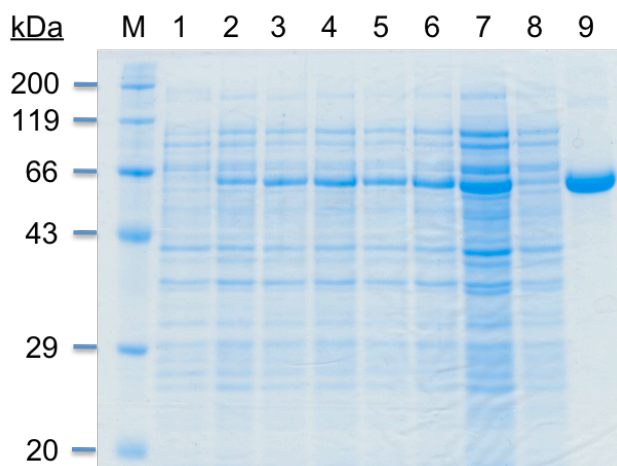


Figure 13. Coomassie blue-stained 12% (w/v) SDS-PAGE of expression and purification of Rec-CODHII. Lane 1, 0 h; Lane 2, 4.5 h; Lane 3, 18.5 h; Lane 4, 23.5 h; Lane 5, 28.5 h; Lane 6, 32.5 h; Lane 7, supernatant from centrifugation after cell-breaking; Lane 8, pellet from centrifugation after cell-breaking; Lane 9, ~ 10 μ g of as-isolated Rec-CODHII; M, Roti-Mark Standard. The time indicated here is sampling after induction. From Lane 1 ~ 6, 5 μ l out of the dissolved cell pellet from 1 ml sampling at the specified time in 100 μ l water was loaded on SDS-PAGE.

Changing cultivation mode from aerobic to anaerobic as described above was the only way to produce active Rec-CODHII in *E. coli*. In view of practical aspect, the best approach to increase yield and specific activity is to use several parallel cultivations in 1L volume (2 – 4) by using the same preculture, monitoring one culture and harvesting all cultures at the same time when the culture shows the highest activity. Total volumetric activities of CO oxidation from the supernatant, eluates from Ni-SHP and Superdex G-25 were measured to check the influence of Ni leakage during purification resulting in no significant change during these steps (data not shown). In this way, Rec-CODHII can be purified with a specific activity of the native protein (Svetlitchnyi et al, 2001) within two hours. Another advantage of this system is that the amount of *E. coli* proteins expressed is relatively small compared to aerobic cultivation, meaning CODH could be purified to a more pure state with his-tag affinity purification even without high overexpression as shown in Fig. 13.

Frozen cells were dissolved at 17 °C and Rec-CODHII containing a 6-histidine tag was purified in one-step purification using high capacity Ni-SHP material. One Liter culture yielded approximately 10 ~ 12 mg of proteins. SDS-PAGE (Fig. 13) showed protein homogeneity of more than 95%. As-isolated Rec-CODHII showed 11,000 ~ 13,000 U (mg of protein)⁻¹ CO-oxidation activities that slightly varied between cultivations and 1.9 ± 0.2 U (mg of protein)⁻¹ CO₂-reduction activity at 25 °C from the enzyme possessing 12,300 U (mg of protein)⁻¹ CO-oxidation activity. This is a relatively lower CO₂-reduction activity compared to CODH from *R. rubrum* having approximately 13 U (mg of protein)⁻¹ at the same temperature (Ensign, 1995).

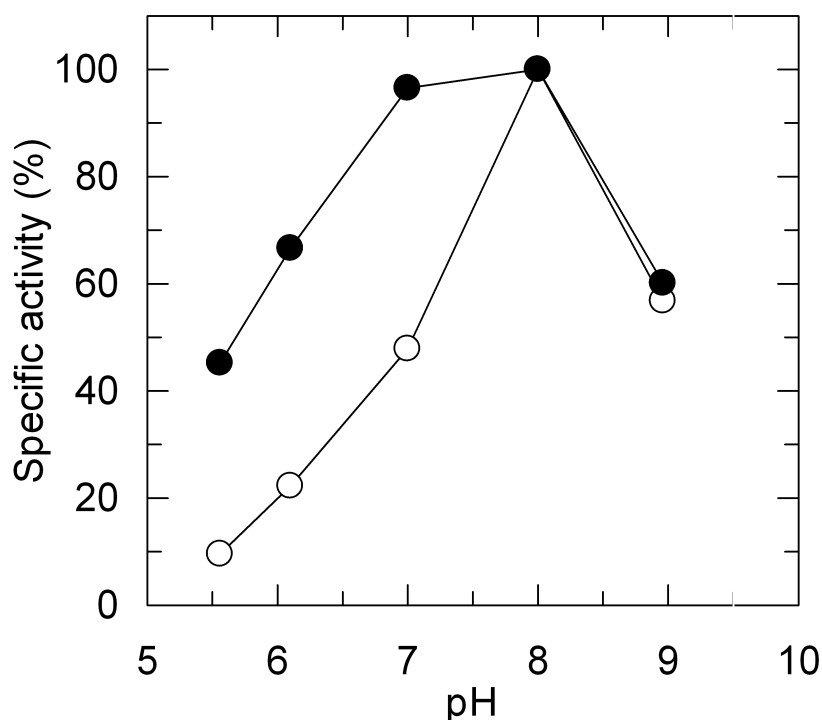


Figure 14. pH profile of CO-oxidation activities of wild-type (open-circle) and mutant H96D (filled-circle) CODH. 100 % specific activity of the wild-type and H96D were 10,760 and 291 U (mg protein)⁻¹, respectively. Middle values are plotted from two independent measurements. Activity measurements at pH value larger than 9.0 were not possible because of spontaneously reduction of MV_{ox}.

The mutant H96D Rec-CODHII was expressed and purified in the same way as the wild-type. The as-isolated mutant H96D, reported as the most effective single mutant in the proton transfer chain (Kim et al, 2004) exhibited 291 U (mg of protein)⁻¹ in this study. If H96 is involved in proton transfer, the overall CO-oxidation activity versus pH profile may be affected and might be saved at higher pH than 4.0 (pK_a of Asp = 3.9). As shown in Fig. 14, both enzymes showed a pH optimum at 8.0 as described previously for the native enzyme (Svetlitchnyi et al, 2001). Mutant enzyme indeed showed gradual increase in activity at higher pH ranges than 5.5. Although the activity of H96D Rec-CODHII diminished to 2.7 % of the wild-type activity at pH 8.0, it did show a practically identical pH profile as wild-type. In comparison, the same mutant of CODH_{Mt} exhibited an increased activity as pH increased with the same as the wild type, even though it showed nearly abolished activity at the optimum pH (pH 9.0) (Kim et al, 2004), indicating that H96D Rec-CODHII functions similarly in proton abstraction during CO-oxidation catalysis.

3. ATPase and GTPase Activities of CooC1

CooC1 contains the Walker A motif (P-loop) and belongs to the MinD family in the SIMIBI Class NTPases. Activities of ATP and GTP hydrolysis of CooC1 were investigated by colorimetric detection of inorganic phosphate released from nucleotide hydrolysis with malachite green solution (Materials and Methods 7.1.). NTPase activities of wild-type CooC1 are shown in Fig.

15-A. Wild-type CooC1 showed specific activities of ATP and GTP hydrolysis of 5.1 ± 0.6 and 0.14 ± 0.09 nmol min^{-1} ($\text{mg of protein}^{-1}$), respectively. It seems that CooC1 is an intrinsic ATPase, not a GTPase. Wild-type CooC1 when incubated with Ni^{2+} exhibited slightly lower activity, 4.4 ± 0.3 nmol min^{-1} ($\text{mg of protein}^{-1}$). CooC_{Rr} from *R. rubrum* showed approximately 12-fold higher ATPase activity (58.7 nmol min^{-1} ($\text{mg of protein}^{-1}$); Jeon et al, 2001) than CooC1. This difference in ATPase activity could arise from the different methods and temperature, since CooC_{Rr} activity was measured at 37 °C while CooC1 was assayed at 25 °C. Similarly, HypB, the accessory protein for Ni-insertion into Ni-Fe hydrogenase, is an intrinsically weak GTPase (Maier et al, 1995).

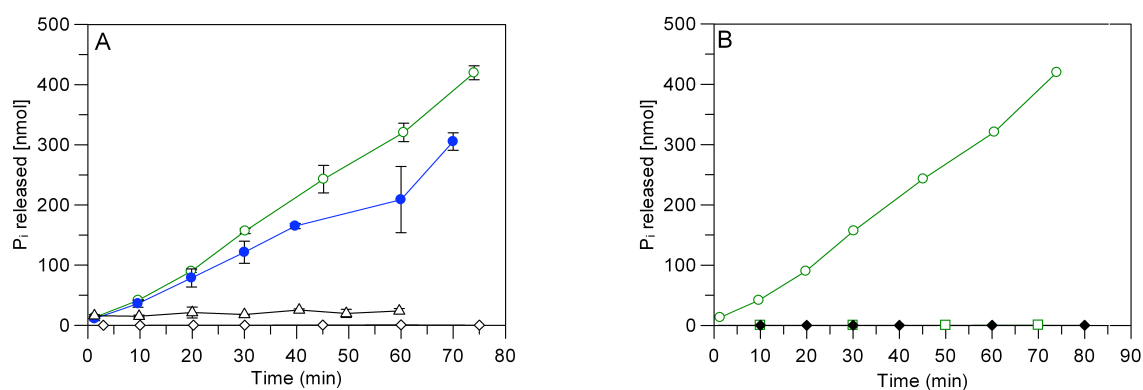


Figure 15. ATPase and GTPase activities of CooC1. (A) ATP and GTP hydrolysis of wild-type CooC1 in the presence of MgCl_2 are shown as empty-circle with *green* line and empty-triangle, respectively. ATPase activity of Ni-incubated wild-type CooC1 is shown as filled-circle with *blue* line. (B) Comparison of ATP hydrolysis of wild-type with (empty-*green* circle) and without (empty-*green* square) MgCl_2 and K8A CooC1 (filled-square). Given P_i values were corrected for the autohydrolysis of the nucleotides (empty-square). Assay solution contained 100 mM NaCl, 2 mM MgCl_2 , 2.5 mM ATP or GTP and 2 mM TCEP in 50 mM Tris-HCl pH 8.0, in which influence of Mg^{2+} on ATPase activity was measured in the absence of MgCl_2 (empty-*green* square). Reactions were initiated by adding 10 μM CooC1 monomer into the assay solution at room temperature. Aliquots (25 μl) of the reaction were withdrawn during the time course of the reaction as indicated in A and B. The amount of P_i released during the reaction was determined using the malachite green/molybdenum assay. The error bars were calculated from three independent measurements.

ATPases of the MinD family contain a special P-loop, carrying the deviant Walker A motif with a highly conserved Lys involved in hydrolysis of ATP by dimer formation. It was previously shown for MinD from *E. coli* (Zhou et al, 2005) and the Fe protein of nitrogenase (NifH) from *Azotobacter vinelandii* (Schindelin et al, 1997), homologues of CooC1, that the signature Lys is necessary for ATP hydrolysis. The mutant protein carrying Ala instead of Lys₈ (the signature lysine in CooC1 is shown in Fig. 26) was generated, expressed and purified as the wild-type (see Materials and Methods). As shown in Fig. 15B, change of Lys₈ to Ala completely abolished ATPase activity of K8A CooC1. This indicates Lys₈ in CooC1 plays the key role in ATP hydrolysis, and that like for the other homologues the deviant Walker A motif is important in nucleotide hydrolysis. Influence of the Mg ion in ATP hydrolysis by CooC1 was investigated by

measuring the activity in the absence of $MgCl_2$, showing that ATPase activity of CooC1 is absolutely dependent on the presence of Mg ion.

4. Spectroscopic Characterization of Wild-Type and Cluster C-missing Rec-CODHII

Characteristic UV-visible absorption spectra of wild-type and cluster C-missing Rec-CODHII were examined under various conditions. When DT was removed from as-isolated wild-type and cluster C-missing enzymes by Sephadex G-25 gel filtration (spectra in Fig. 16A and B, respectively), a shoulder was detected extending from 350 nm to 550 nm with a maximum at 419 nm (Inset spectra), which is a characteristic Fe-S cluster spectra of CODHII and $CODH_{Rr}$ (Svetlitchnyi et al, 2001), (Bonam & Ludden, 1987).

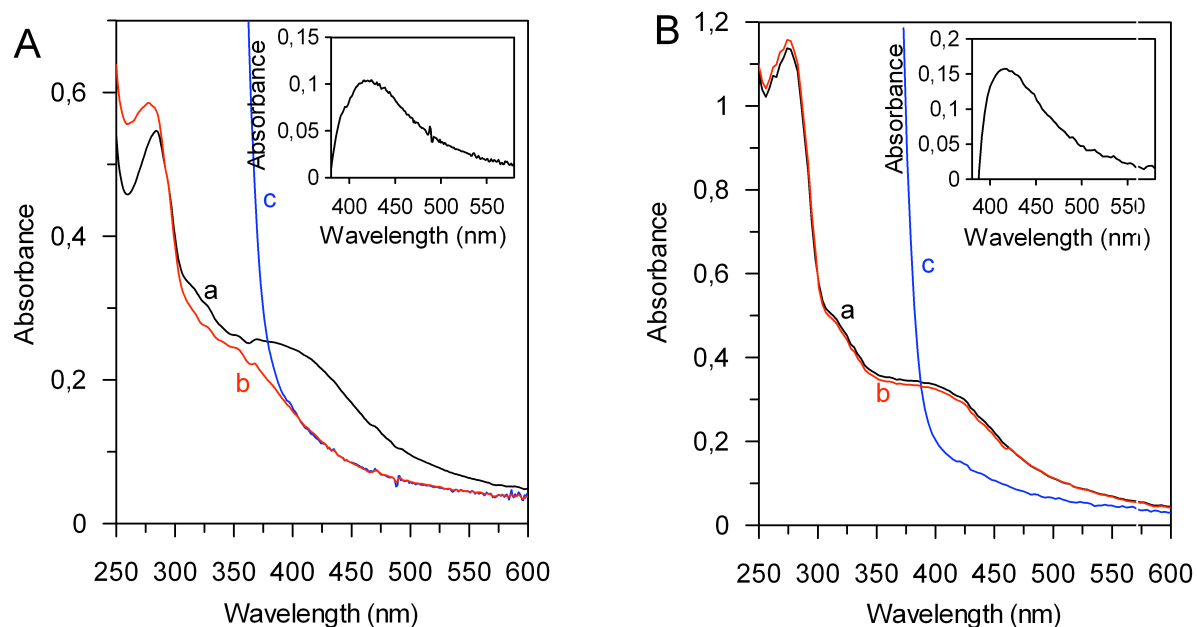


Figure 16. UV-visible absorption spectra of wild-type (A) and cluster C-missing (B) Rec-CODHII. The enzymes (0.38 mg ml^{-1} of wild type and 0.8 mg ml^{-1} of cluster C-missing) were in 50 mM Tris-HCl pH 8.0. Difference spectrum was generated by as-isolated/DT-removed minus DT-reduced and shown in inset. Conditions for each curve: a, as-isolated/DT-removed; b, CO-reduced; c, DT-reduced.

A value was derived from the ratio of absorbance at 419 nm to 280 nm to check for the relative amount of Fe-S clusters in Rec-CODHII, compared to 0.45 of the native CODHII (Svetlitchnyi et al, 2001). Values of 0.42 and 0.28 were obtained for wild-type and C-miss proteins, respectively. This value of wild-type protein is close to that of the native protein, but the cluster C-missing protein showed only two third of that from the native protein. Bleaching of this Fe-S cluster shoulder was observed by treatment of either enzyme with CO or DT. However, incubation of cluster C-missing enzyme with CO could not reduce the characteristic shoulder even though DT reduced it. This indicates that the cluster C-missing species have no metals at

the active site, especially nickel responsible for CO binding and contains approximately three [4Fe-4S] clusters out of five [4Fe-4S].

5. Spectroscopic Determination of Ni-binding and Ni-titration of CooC1

In a previous study, CooC_{Rr} does not contain metal in the native form and nickel binding by the protein was not reported (Jeon et al, 2001). To identify whether CooC1 can bind nickel, an attempt to characterize the Ni-binding property of CooC1 was performed using UV-visible spectroscopy. Fig. 17A shows the spectrum of wild-type CooC1 before and after addition of 0.5 equivalent of NiCl₂ to the as-isolated protein. As-isolated CooC1 shows only a characteristic peak derived from one tryptophan residue at 280 nm. It was previously reported that CooC_{Rr} is not a Fe-S cluster protein (Jeon et al, 2001), and also CooC1 has no characteristic Fe-S cluster maximum around 420 nm. Addition of up to 1 equivalent of nickel to wild-type CooC1 dimer in the presence of 1 mM TCEP under anaerobic condition produced a characteristic peak with a maximum at 330 nm, indicative of nickel bound to the protein. To characterize the Ni-binding activity of CooC1, titration of the protein with Ni(II) was performed. Inset in Fig. 17A shows the difference spectra of nickel titration with increasing of the two maxima at 280 and 330 nm. The intensity and position of two peaks with no appreciable absorption at lower energies suggest that the spectral peaks can be attributed to ligand-to-metal charge transfer (LMCT) bands (300 – 550 nm) of Cys-S_v⁻ → Ni(II) (Kozlowski et al, 1987; Pereira et al, 1998; Jeffrey S. Iwig & Chivers, 2008) and are characteristic of four-coordinate nickel ligated in a square-planar or distorted square-planar geometry (Lever, 1984). This observation of the increase in intensity at 330 nm upon Ni-addition suggests that CooC1 binds nickel via the conserved cysteines of a highly conserved CXC motif found in all of CooC homologues as shown in Fig. 26.

The differences in absorption at 330 nm (Fig. 17B) and 280 nm (Fig. 17B, inset) from the titration resulted in nonlinear curves. Number of binding sites (*n*) and dissociation constant (*K_d*) were calculated from nonlinear fitting equation (Eq. 5, Tab. A9). Wild-type CooC1 binds 0.9 ± 0.01 mole of Ni(II) per dimer with a *K_d* of 0.4 ± 0.05 μM. During titration of CooC1 with Ni(II), there was no strong indication of protein precipitation in all range of Ni(II) concentration used when TCEP is present. However, addition of nickel below the equivalent concentration caused precipitation of the protein in the absence of TCEP under anaerobic condition and even in the presence of 5 mM glycine working as a weak metal chelator. As-isolated CooC1 has identical Ni-binding properties as the protein anaerobically treated with EDTA for two days at 17°C. Therefore, as-isolated CooC1 is equivalent to apo-protein.

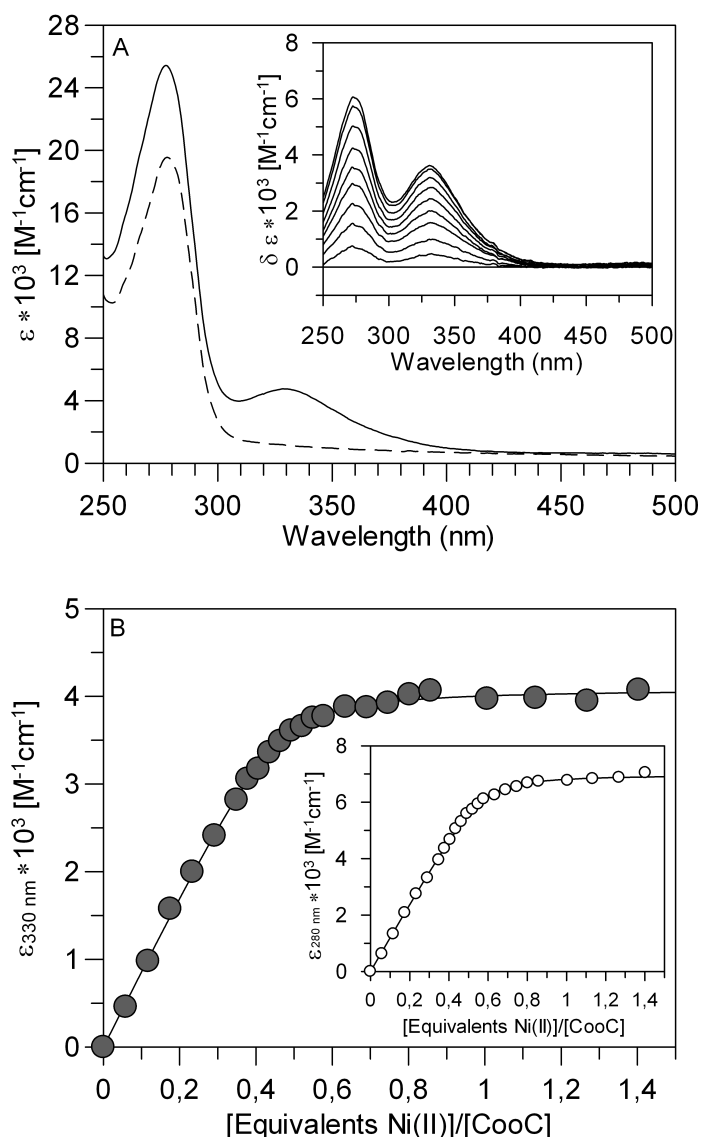


Figure 17. UV-visible spectra of wild-type apo-CooC1 in the absence of nucleotides. (A) UV-visible spectrum of 34 μM monomer of apo-CooC1 (—) dissolved in 50 mM Tris-HCl pH 8.0, 100 mM NaCl and 1 mM TCEP. The spectrum does not show characteristic peaks other than at 280 nm. Addition of 0.5 equivalent nickel resulted in a new maximum at 330 nm (—). A difference spectrum (Inset) was generated by subtracting the signal of wild-type apo-CooC1 from that of CooC1 titrated with up to 0.5 equivalent nickel with increasing of approximately 2 μM Ni(II) in each spectrum. (B) Titration curves of wild-type CooC1 at 330 nm (\bullet) and 280 nm (\circ , inset) with up to 1.5 equivalent nickels.

In order to determine the influence of nucleotides on the binding of nickel to CooC1, the wild-type protein was titrated with Ni(II) in the presence of 100 μM ATP or ADP (Fig. 18A). Binding of 0.5 equivalent of Ni(II) to apo-CooC1 with both nucleotides showed new maxima around 340 and 620 nm, and a shoulder at 380 nm. With a careful examination by difference spectrum (Fig. 18B), arising of new maxima during the Ni-titration of CooC1 in the presence of ATP was visible at 286, 295 and 341 nm with a shoulder around 380 nm. Spectral features of the protein in the presence of Ni and ADP were practically identical to the features with Ni and ADP.

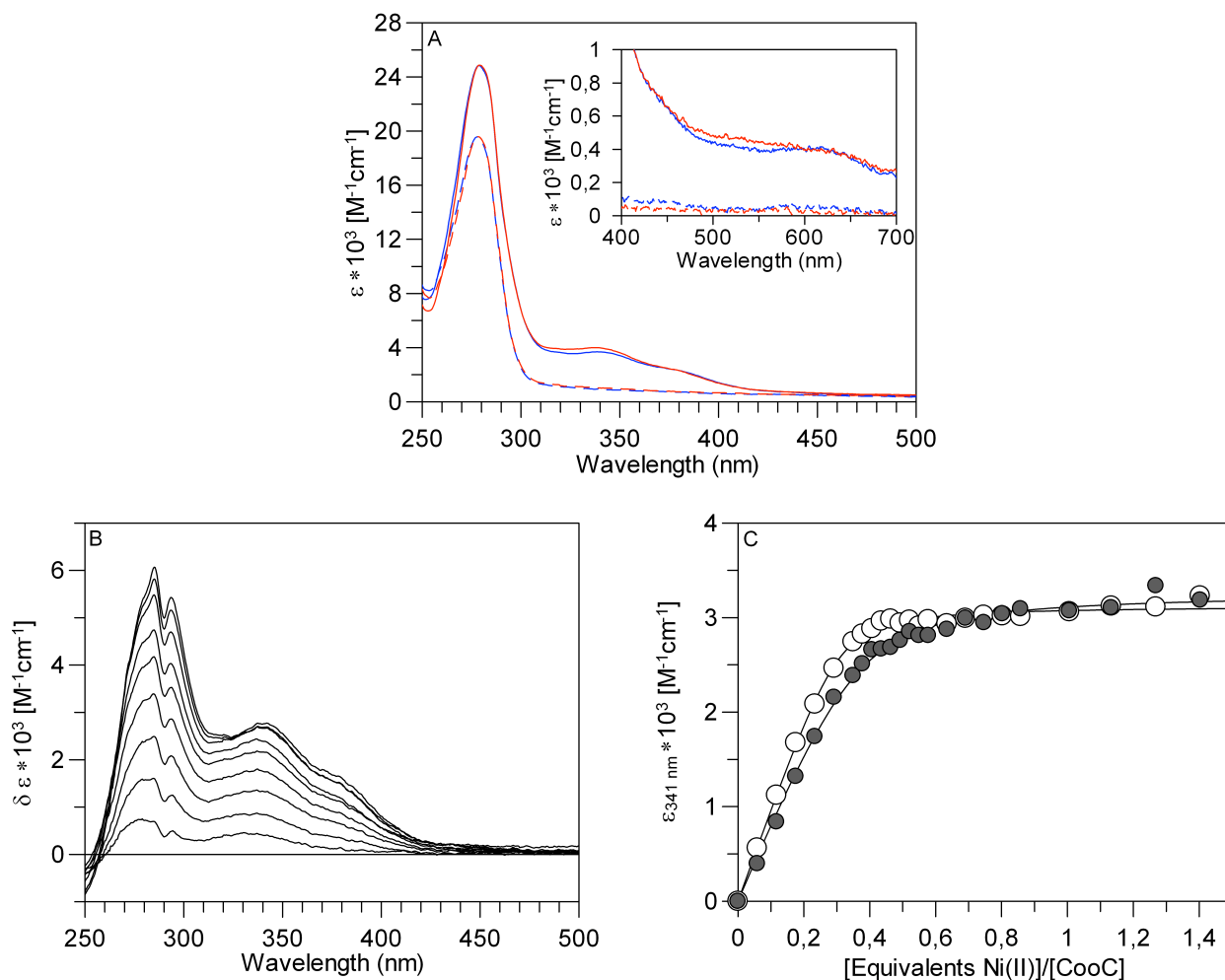


Figure 18. UV-visible spectra of wild-type apo-CooC1 in the presence of nucleotides. (A) UV-visible spectra of 34 μM monomer of apo-CooC1 (---) dissolved in 50 mM Tris-HCl pH 8.0, 100 mM NaCl and 1 mM TCEP containing 100 μM ATP (blue) and 100 μM ADP (red) are practically identical to that without nucleotides (see Fig. 17). Addition of 0.5 nickel equivalents resulted in a new maximum around at 341 nm and a shoulder around 380 nm for both (—). Inset shows a peak and a shoulder at 620 nm with ATP and ADP, respectively. New maxima were clearly visible from a difference spectrum with ATP (B), which was generated by subtracting the signal of apo-CooC1 from that of CooC1 titrated up to 0.5 nickel equivalents with addition of approximately 2 μM Ni^{2+} in each spectrum producing new maxima (286, 295 and 341 nm) and a shoulder at 380 nm. A difference spectrum with ADP showed practically identical feature with maxima as with ATP. (C) Titration curves of wild-type CooC1 at 341 nm with ATP (●) and with ADP (○) titrated with up to 1.5 equivalent nicksels. All these experiments were performed two times independently. Since no large deviation was observed between titrations (Tab. A9), middle values are fitted to a non-linear equation.

These bands at the higher energies (286, 295, 341 and 380 nm) are possibly assignable to LMCT bands of $\text{Cys-S}_\gamma^- \rightarrow \text{Ni(II)}$ or $\text{His-N} \rightarrow \text{Ni(II)}$ (Kozłowski et al, 1987; Pereira et al, 1998; Ruiguang GE, 2006). As shown in the inset of Fig. 18A, a band and a shoulder with low extinction coefficient ($<400 \text{ M}^{-1}\text{cm}^{-1}$) at 620 nm aroused additionally in the presence of ATP and ADP, respectively, in which a band at the lower energies (600 – 700 nm) is the distinct $d-d$ transition of Ni(II) and suggestive of high coordinated Ni(II) (Kozłowski et al, 1987; Cavet et al, 2003). The quantity of Ni-binding to wild-type CooC1 in the presence of ATP or ADP was

studied. A plot of the absorbance difference at 341 nm, where mostly prominent LMCT bands of $\text{Cys-S}_V^- \rightarrow \text{Ni(II)}$ (Kozłowski et al, 1987) are detected, resulted in a non-linear fitting curve with increasing Ni concentration (Fig. 18C). In both conditions less amount of Ni(II) were required to saturate binding sites in wild-type CooC1 with 0.68 and 0.63 per CooC1 dimer for ATP and ADP, respectively (Tab. A9). However, the affinity of the protein for Ni(II) in the presence of ATP decreased to 1.17 μM , while the protein with ADP showed the same affinity for Ni(II) as in the absence of nucleotides (Tab. A9). The influence of ATP observed is due to the binding itself, and is not from the hydrolysis because CooC1 was not able to hydrolyze ATP in the absence of the Mg ion (Fig. 15B).

6. Far-UV CD Spectra and Thermal Unfolding Transitions followed by CD of CooC1

To investigate the effect of ligand binding to changes in secondary structure of CooC1, far-UV CD spectra and thermal stabilities of apo-CooC1 were measured in the absence and presence of Ni or nucleotides. The far-UV CD spectra of CooC1 exhibited characteristic features of α -helical proteins, identified from two minima at 208 and 222 nm (Fig. 19A). All far-UV CD spectra showed practically identical features among the different conditions used (Fig. 19A). The protein secondary structure showed little perturbation in the presence of nickel, ATP or ADP, indicating a minimal net change in secondary structure due to ligand binding.

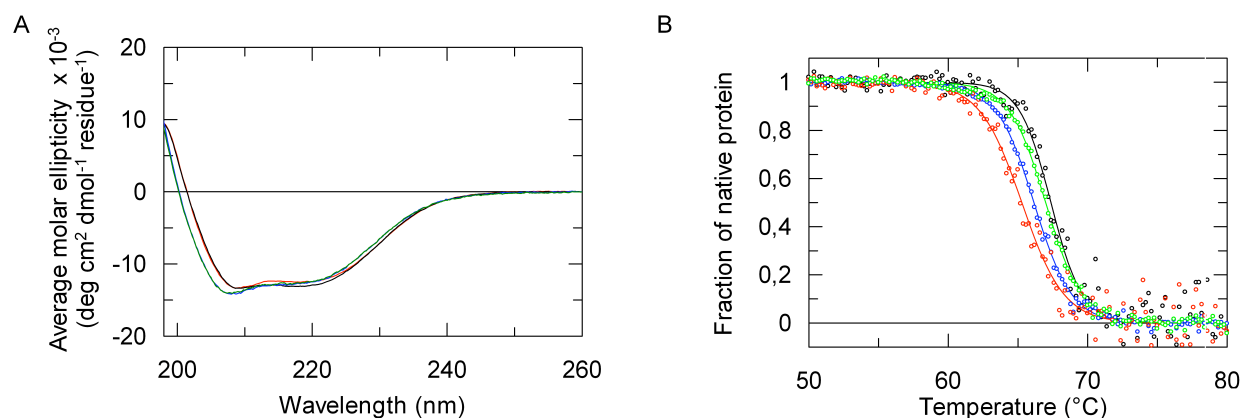


Figure 19. Far-UV CD spectra (A) and thermal denaturation profile (B) of apo-CooC1 (*blue*) in the presence of 10 μM NiCl_2 (*green*), 200 μM ATP (*black*) or 200 μM ADP (*red*). In measurements, 5 μM and 1 μM apo-CooC1 monomer was dissolved in 20 mM Na-Phosphate pH 7.5 containing 100 mM NaCl and 2 mM TCEP with or without a ligand. For the far-UV CD spectra, ten individual scans taken from 190 to 260 nm were added, averaged and subtracted from the solvent CD signal, followed by normalization (Materials and Methods 8.2.1). Thermal denaturation profiles were measured following the signals of CD_{222} for apo- and Ni-CooC1 and CD_{225} for ATP- and ADP-CooC1 over a linear temperature gradient from 20 to 80 $^{\circ}\text{C}$ at 60 $^{\circ}\text{C}/\text{h}$.

The little difference shown in the CD spectra (Fig. 19A) probably originates from different protein purifications, where difference spectra of these CD measurements did not show

significant change. As-isolated apo-CooC1 had a melting temperature (T_m) of 66.4 °C (Fig. 19B), while binding of Ni or ATP increased T_m by approximately 1 °C and binding of ADP decreased T_m by 1 °C compared to that of apo-CooC1. This result suggests that the binding of these ligands does not dramatically influence the thermal stability of CooC1. Binding of ATP or ADP leads to aggregation of the proteins at denaturation temperature higher than 70 °C, resulting in larger deviation than apo- and Ni-incubated CooC1.

7. Oligomeric States of CooC1 studied by Gel Filtration

CooC1 has a calculated molecular weight of 28 kDa (ProtParam in <http://www.expasy.org/tools>). In the presence of TCEP, the as-isolated and EDTA-treated wild-type CooC1 exhibited only a peak assigned to be monomer with molecular weight of 32 kDa from gel filtration experiment (Fig. 20A). The size of CooC1 in solution was slightly bigger than that from the calculation. In the absence of a disulfide bond reducing agent, DTT or TCEP, CooC1 was present in multiple oligomeric states during gel filtration and SDS-PAGE (data not shown). According to the result of Ni-titration, CooC1 showed that it is able to bind one mole of nickel per dimer. To test whether CooC1 forms a dimer depending on nickel, gel filtration was performed in the presence of NiCl_2 . Ni-incubated wild-type CooC1 exhibited two fractions corresponding to monomer (32 kDa) and dimer (54 kDa) with running buffer containing 2 mM NiCl_2 . However, there was only a monomer profile visible when the protein was incubated with nickel and ran over the gel filtration without NiCl_2 or with small amount of nickel (0.5 mM) in the running buffer (data not shown). This indicates that the dimerization of CooC1 by the Ni-binding only occurs when Ni is present in excess, which might explain why the Ni-incubated CooC1 showed two peaks (monomer and dimer). However, nickel induces dimerization of CooC1 in solution, albeit weakly, as observed from the gel filtration experiments.

CooC1 homologues in the MinD family of the SIMIBI class proteins, NifH, MinD and Soj, are ATPases characterized by the presence of a deviant Walker A motif containing a conserved signature lysine at the beginning of the P-loop (Fig. 26). It has been shown that the signature lysine is important in ATP hydrolysis and is involved in the formation of a stable ATP-driven dimer by interaction of the lysine from one molecule with ATP in the other molecule (Schindelin et al, 1997; Zhou et al, 2005; Leonard et al, 2005). The influences of nucleotides on the oligomeric state of wild-type and K8A CooC1 were also examined by gel filtration. In the presence of ADP, wild-type showed 53 kDa and 35 kDa of two states (Fig. 20B). The former corresponds to the dimer but the later is slightly bigger than the monomer of apo-CooC1 (Fig. 20A).

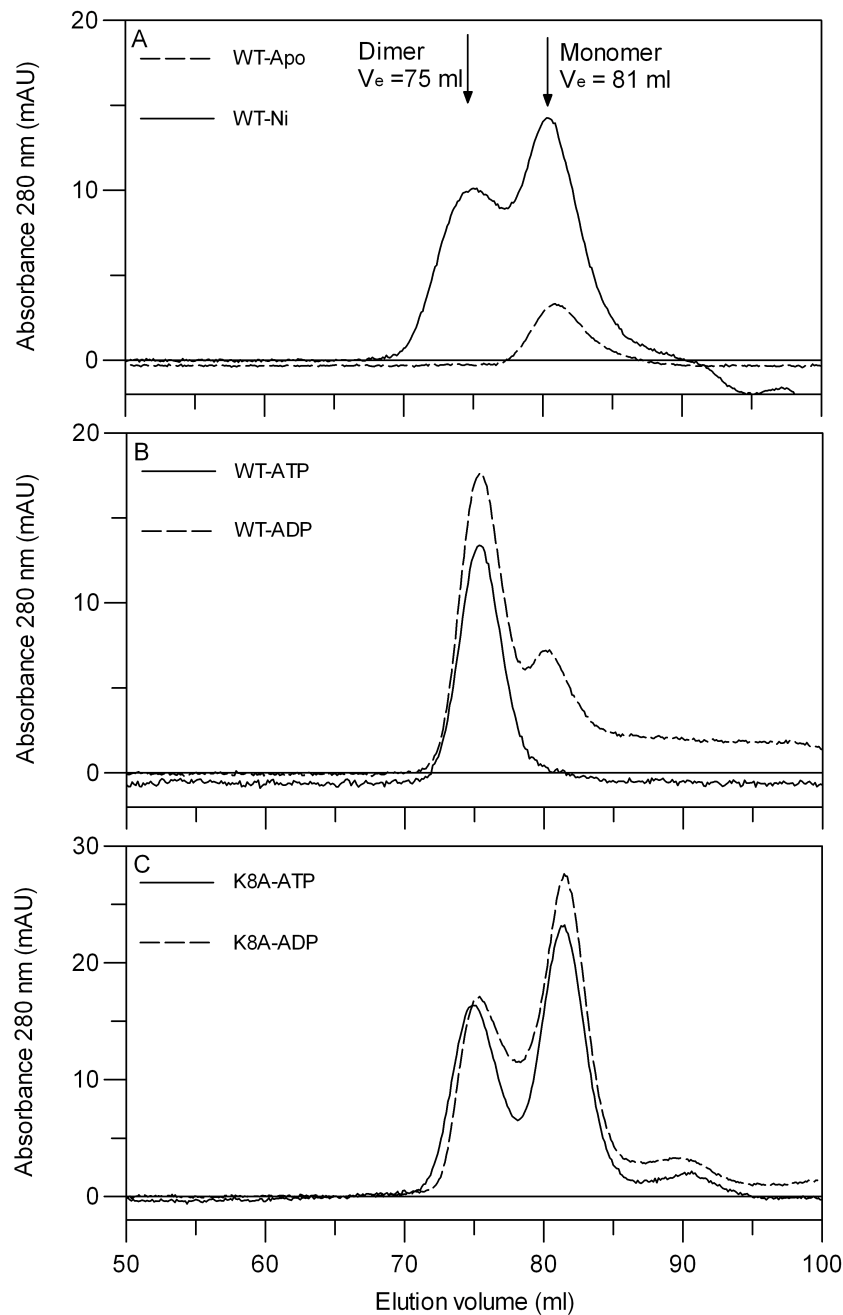


Figure 20. Analysis of nickel- and nucleotide-dependent dimerization of CooC1 by gel filtration chromatography. Approximately, 2 and 3 mg of wild-type and K8A CooC1, respectively, were injected onto Superdex™ 200 prep-grade column in the metal-free running buffer (50 mM Tris-HCl pH 8.0, 100 mM NaCl, and 2 mM TCEP) with or without an effector and run with 1 ml/min of flow rate. Elution profiles were recorded by absorption at 280 nm. (A) Elution profiles of wild type apo-CooC1 (---) in the absence of EDTA and apo-CooC1 (—) treated with 2 mM NiCl_2 prior to run for 10 h at 17 °C and run on gel filtration in the presence of 2 mM NiCl_2 are shown. (B) Wild-type and (C) K8A CooC1 dissolved in running buffer without nucleotides loaded on the column equilibrated in the presence of 1 mM ATP (—) or ADP (---). All experiments were performed twice independently. Since fractions possessing two states were varied between experiments, only one experimental result of dimer and monomer equilibrium is shown here. Molecular weights of proteins from elution profile were calculated by known-molecular weight standards (Fig. A4).

In the other independent gel filtration experiment with ADP, wild-type showed tailing of the dimer peak (data not shown). The 35 kDa species of ADP-bound wild-type might undergo fast equilibrium between monomer and dimer. However, wild-type CooC1 in the presence of ATP presented only a monodisperses symmetric peak assigned as dimer (53 kDa). Figure 20C shows the influence of the mutation of the signature lysine in the P-loop of CooC1 on dimerization in the presence of ATP or ADP. K8A CooC1 showed equilibrium between monomeric and dimeric states in the presence of ATP (54 kDa and 32 kDa) and ADP (53 kDa and 31 kDa), indicating the absence of a stable dimer formation in the presence of ATP in contrast to wild-type. According to the gel filtration analysis, CooC1 undergoes Ni- and nucleotide-dependent dimerization in the presence of Ni²⁺, ATP or ADP, even though the other homologues, MinD and Soj, dimerized solely in an ATP-dependent manner (Zhou et al, 2005; (Leonard et al, 2005).

8. Crystallization

8.1. *Crystallization of CooC1*

CooC1 can be crystallized in numerous conditions, for example, 34 hits from 96 conditions of the index screening (Hampton Research). All crystallization conditions were relatively sensitive to the protein concentration in the drop and the protein purification. Fig. A5 shows crystals used for structure determinations of CooC1. All crystals of CooC1 had no color. Fundamentally, it was hard to differentiate crystals by their appearance because they have completely different shape. For example, crystals of apo-forms (Fig. A5A and D) have same space group ($P3_221$) with same cell constants even though their shapes and growth conditions differ. Appearances of crystals shown in Fig. A5C, D and E were similar with hexagonal setting with a longest axis of approximated 0.4 mm length, but they showed different space groups ($C2$, $P3_221$ and $P2_12_12_1$, respectively). Interestingly, metal-bound forms of crystals (Fig. A5B and C) only obtained with the protein purified aerobically (see Materials and Methods 6.1.). The size and diffraction quality of crystals were not proportional. The highest diffraction was obtained with a crystal of Fig. A5B (~ 0.2 mm in length of long axis) which diffracted up to 1.9 Å with in-house X-ray source, which showed flat shape with no sharp edges and was looking like a seed of sunflower or pumpkin. Crystallizations with AMPPNP (non-hydrolysable ATP analogue) were attempted to get a structure of ATP-bound form. However, most crystals from different conditions with AMPPNP did not diffract well. One crystal with an appearance (Fig. A5E) was obtained with protein preincubated in solution containing 4 mM AMPPNP and 20 mM MgCl₂ equilibrated in reservoir buffer (0.2 M sodium malonate pH 5.0, 15 – 18% (w/v) PEG3350 and 2 mM TCEP) and diffracted to 2.7 Å, but the resulting structure was the same as the ADP-bound form.

8.2. Crystallization of *Rec-CODHII*

Crystals of recombinantly expressed CODHII can be obtained in numerous crystallization conditions. All crystals showed brown color indicating the presence of Fe-S clusters and crystals with a size bigger than 0.2 mm in the longest axis diffracted from 1.90 up to 1.40 Å resolution on a rotating anode X-ray generator and have the same space group (C2) with cell dimensions ($a = 112$ Å, $b = 74$ Å, $c = 70$ Å and $\beta = 111^\circ$) as previously determined for native CODHII_{Ch} crystals (Dobbek et al, 2001), despite the different crystallization conditions used (see Materials and Methods 11.1.). Among them, two conditions (*formate* and *sulfate conditions*) were at least reproducible and produced well diffracting crystals. Crystals from the formate condition appeared and grown in shorter time than the sulfate condition (Fig. A6), but the later condition having well defined crystal shape with sharp edges showed much better diffraction quality than the former. However, the sulfate condition was not highly reproducible by the hanging-drop method, but was obtained by streak seeding method with horsehair. Even though the shapes at the maximum growth are different between the two conditions, morphology of parallelogram shape between them was identical when crystal from the formate condition grew in single small crystals (figure not shown). Optimization of the formate condition to get single bigger crystals by using different sizes of PEGs and different buffers was not successful. Nevertheless, crystals from the formate condition were very useful in a practical aspect to test various soaking conditions in short time.

9. Structures of *Rec-CODHII*

9.1. Overall Structure of *Rec-CODHII*

The overall structures of all types of *Rec-CODHII* reported here are practically identical to the structure of native CODHII (Fig. 4A) isolated from *C. hydrogenoformans* (Dobbek et al, 2001; Dobbek et al, 2004).

9.2. Structures of Three-Redox States in Reversible CO₂-Reduction

Rec-CODHII crystals were poised at a defined redox potential of -600 mV for 3 hours using Ti(III) citrate. These crystals were either directly frozen in liquid N₂ generating the -600 mV state or oxidized via incubation with methylviologen (MV_{ox}) and DTT. The oxidized crystals further incubated with DTT alone to give the -320 mV state. The crystals incubated at -600 mV state were held in the -600 mV solution with NaHCO₃ as CO₂ source generating the -600 mV+CO₂ state.

Under two of the conditions, the -600 mV state, which is equivalent in its redox potential to the $C_{\text{red}2}$ state, and the -320 mV state, which is equivalent to the $C_{\text{red}1}$ state, practically identical structures for cluster C have been determined (Fig. 21A and C). In both structures the Ni ion is coordinated by three sulfur ligands with distorted T-shaped coordination geometry and a deviation from linearity along the C526 S^Y-Ni-S₃ axis of 24° (Tab. A10). Although distorted T-shaped ML_3 complexes are rare, they are not unusual for diamagnetic d^8 metals like Ni²⁺ (Jean, 2005). Fe1 is coordinated by His₂₆₁, Cys₂₉₅, a μ_3 -sulfido ligand and a monoatomic ligand (Fig. 21A and C, Figs. A7 and A8). In both states, alternative position for Fe1 (Fe1B) is weakly occupied (Tab. A8). The monoatomic ligand is in a distance of 2.7 \AA from the Ni ion and occupies the position that would complete the square-planar geometry around the Ni. The electron density of the ligand can be modeled as a light atom (C, N, or O) with occupancies of approximately 60 to 70% or a sulfur atom with 30% occupancy. However, the observed bond lengths of 1.93 - 1.95 \AA between Fe1 and the monoatomic ligand are inconsistent for Fe-S bonds, whereas a water/hydroxo ligand is consistent with the refined bond length, the relative occupancies of ligand and Fe1 (Fig. A7 and Tab. A8) and spectroscopic investigations of the $C_{\text{red}1}$ state (DeRose et al, 1998). The long distance between Ni and the ligand suggests a weak Ni-OH_x interaction. The water/hydroxo ligand in the -320 mV state is in agreement with the OH_x ligand at a high spin Fe²⁺ ion called ferrous component II (FCII) detected in the $C_{\text{red}1}$ state (DeRose et al, 1998; Hu et al, 1996), so the crystal structure is consistent with Fe1 in the -320 mV state being FCII. The presence of the water/hydroxo ligand in the -600 mV state (equivalent to $C_{\text{red}2}$) has not been detected by ENDOR spectroscopy (DeRose et al, 1998). However, as the oxidation state of the water/hydroxo coordinating FCII remains the same in $C_{\text{red}1}$ and $C_{\text{red}2}$, a change of redox potentials may not result in ligand exchange at FCII. In both states, the water/hydroxo ligand is stabilized by hydrogen bond with Lys₅₆₃ (K563) (Fig. 21A and C).

In contrast to high turnover rate of CO oxidation ($31,000 \text{ s}^{-1}$) catalyzed by monofunctional Ni, Fe-CODHases, the enzyme also catalyze the reduction of CO₂ in the presence of appropriate reducing agents with high affinity for CO₂ and turnover numbers less than 100 s^{-1} , making the CO₂ reduction more suitable to accumulate substrate, intermediate or product bound states (Ensign, 1995). Incubating CODHII crystals with CO₂ in the presence of Ti(III) citrate (redox potential of -600 mV in the crystal soaking buffer with pH 8.0) places an electron donor of sufficiently low redox potential together with an oxidizing substrate to allow catalytic CO₂ reduction and generates the $-600 \text{ mV} + \text{CO}_2$ state. In the structure of $-600 \text{ mV} + \text{CO}_2$ state a triatomic ligand bridging Ni and Fe1 was observed, which replaces the water/ hydroxo ligand at Fe1 in the -600 mV state (Fig. 21B and Fig. A7B). The ligand was modelled as CO₂ that fully satisfies the observed electron density maps. However, modeling of the ligand with one or two atoms is not consistent. The B factors of CO₂ are comparable to the other atoms of cluster C (Tab. A8).

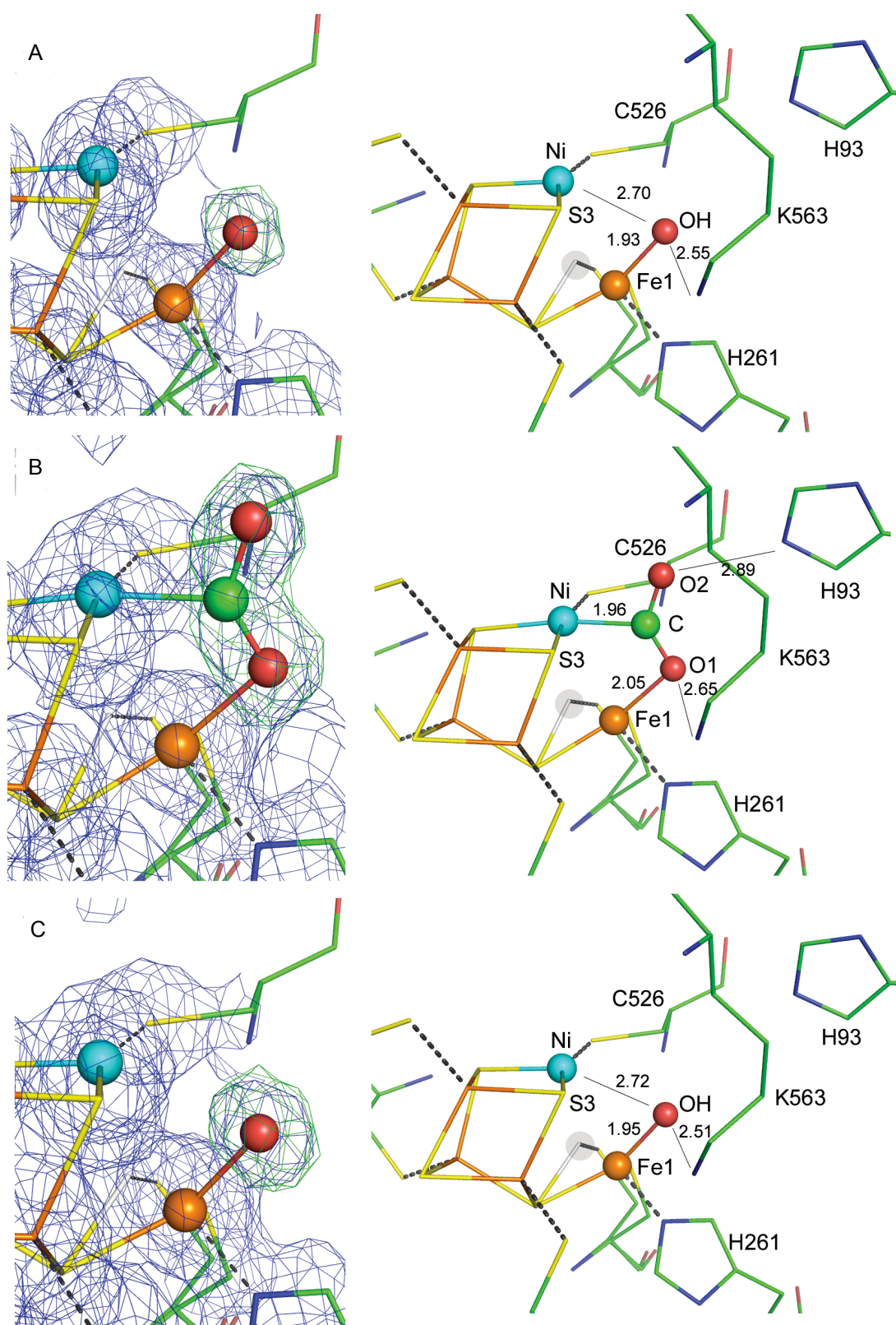


Figure 21. Three-redox states of cluster C: -600 mV (A), -600 mV+CO₂ (B) and -320 mV (C). $2F_{obs} - F_{calc}$ maps and $F_{obs} - F_{calc}$ are shown in *blue* and *green* with contour level at 1σ and at 4.5σ , respectively. The $F_{obs} - F_{calc}$ maps were calculated by removing the OH_x ligand [(A) and (C)] and the CO₂ ligand (B) from the model. An alternative position observed for Fe1 (Fe1B) with estimation of 10 to 30% occupancies is shown in transparent *light gray*. Selected distances are shown in Å. For more details on the geometry of the three states, see Figs. A7. Picture taken from the reference (Jeoung & Dobbek, 2007).

CO₂ bound to cluster C acts as a η^1 OCO ligand at Ni²⁺ with a Ni-C distance of 1.96 Å and completes the square-planar coordination geometry typically found for Ni²⁺ ions. CO₂ acts as a η^1 OCO ligand at Fe1 with an Fe1-O1 distance of 2.05 Å, resulting in a μ_2 - η^2 binding mode of CO₂ bridging the Ni and Fe1 ions (Fig. 21B, see Tab. 1). Like the water/hydroxo ligand in the –600 mV and –320 mV states, O1 and O2 of CO₂ interact to Lys₅₆₃ and to His₉₃, respectively, through hydrogen bonding (Fig. 21B). O1 of CO₂ is in the same position as the water/hydroxo ligand found in the other two states. Only minor changes in the geometry of cluster C were observed by binding of CO₂ to the cluster (Fig. 22). CO₂ binding to cluster C changes geometry at the Ni from the distorted T-shaped to the square-planar coordination, which induces a small shift in the Ni position of approximately 0.2 Å and enlarges the Cys₅₂₆S^Y-Ni-S₃ angle by 12° (Tab. A11).

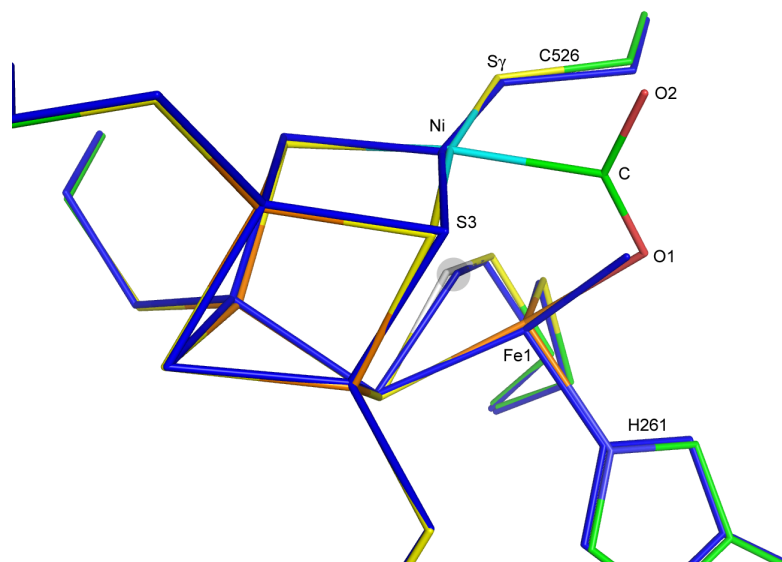


Figure 22. Superposition of the –600 mV (*blue*) and –600 mV+CO₂ (element colors) states. Picture is taken from the reference (Jeoung & Dobbek, 2007).

In all three states the ligand around Fe1 shows small bond angles between 84° and 101° (Tab. A10). The alternative position found for Fe1 (Fe1B) in Tab. A10 is very close to the Ni ion (2.3~2.4 Å) and is most likely only occupied when the Ni ion in cluster C is absent. In contrast to Ni, CO₂ binding does not affect the coordination geometry and position of Fe1 (Fig. 22) and generates structurally more homogenous Fe1 with a lower occupancy for the Fe1B position than in the –600 mV and –320 mV states (Fig. 21 and Tab. A8). When one compares the [NiFe₄S₄OH_x] cluster with the [NiFe₄S₅] cluster (PDB ID: 1SU8) containing four sulfur ligands, the opening of the C₅₂₆S^Y-Ni-S₃ angle from 157° to 176° (Fig. A9 and Tab. A10), respectively, is even more obvious.

The high turnover rate of CO oxidation at cluster C depends on the fast replenishment and removal of substrates and products. A network of water molecules has been found in the direct vicinity of the water/hydroxo ligand at Fe1, which may participate in refilling the substrate waters

at Fe1 once CO₂ has been liberated. The semi-conserved histidines have been proposed to act as proton relay system (Kim et al, 2002). The water network and an effect of one histidine mutation in the proton transfer channel will be discussed in the next section.

9.3. Proton Channel Mutant H96D and Water Network in Rec-CODHII

The oxidation of CO with water at cluster C of CODH produces CO₂, electrons and protons (Eq. 2). While two electrons are believed to transfer through [4Fe-4S] clusters (cluster B and/or cluster D), two protons are suggested to leave via semi-conserved histidine residues (Fig. 32) (Drennan et al, 2001; Kim et al, 2004). Figure 23A shows a putative proton channel in Rec-CODHII comprised of conserved histidines (H93, H96, H99) and ionizable basic residue (N262) near cluster C. Although a previous mutational study proposed that H122 of CODH_{Mt} (H102 in CODHII) has an essential role in the proton transfer system (Kim et al, 2004), a careful examination of Rec-CODHII structures (Fig. 23A) implied that the H102 might not function in proton transfer, which is supported by the following observations. First, H102 is the least conserved residue among CODHs (Fig. 31). Second, this residue is positioned approximately 7 Å away without mediating water or other residues from H99 that is already in contact with the solvent. The residue E368, conserved in CODHs could function instead of H102 in CODHII by abstracting a proton from H99 via water (Fig. 23A). The comparison of Rec-CODHII structures obtained in different oxidation states showed one conserved water molecule (W2 in Fig. 23A), coordinated by the closest water to cluster C (W1 in Fig. 23A) and H96 in different oxidation states. The closest water to OH_x ligand of cluster C of -320 mV state, which is absent in -600 mV+CO₂, might function as a reservoir to replenish water after a turnover of CO-oxidation reaction and/or function as a base to abstract protons during the catalysis (distance of OH_x-W1 = 2.53 Å). Examination of the H96D Rec-CODHII structure showed no change of cluster C and its surrounding residues upon mutation of His₉₆ to Asp (Fig. 23B), indicating that the abolished activity shown in Fig. 14 was not due to protein misfolding or the absence of metal clusters in CODH. The observed low activity of this mutant may be due to the lowering of the pK_a value by changing histidine (pK_a = 6.03) to aspartic acid (pK_a = 3.9), which is observed in 37-fold diminished activity of the mutant (Fig. 14). Furthermore, a water molecule is observed in the position occupied by N^{ε2} of His₉₆ of wild-type. This water is close to Asp₉₆, which suggests that it may compensate the replacement of His by Asp₉₆ (Fig. 23B).

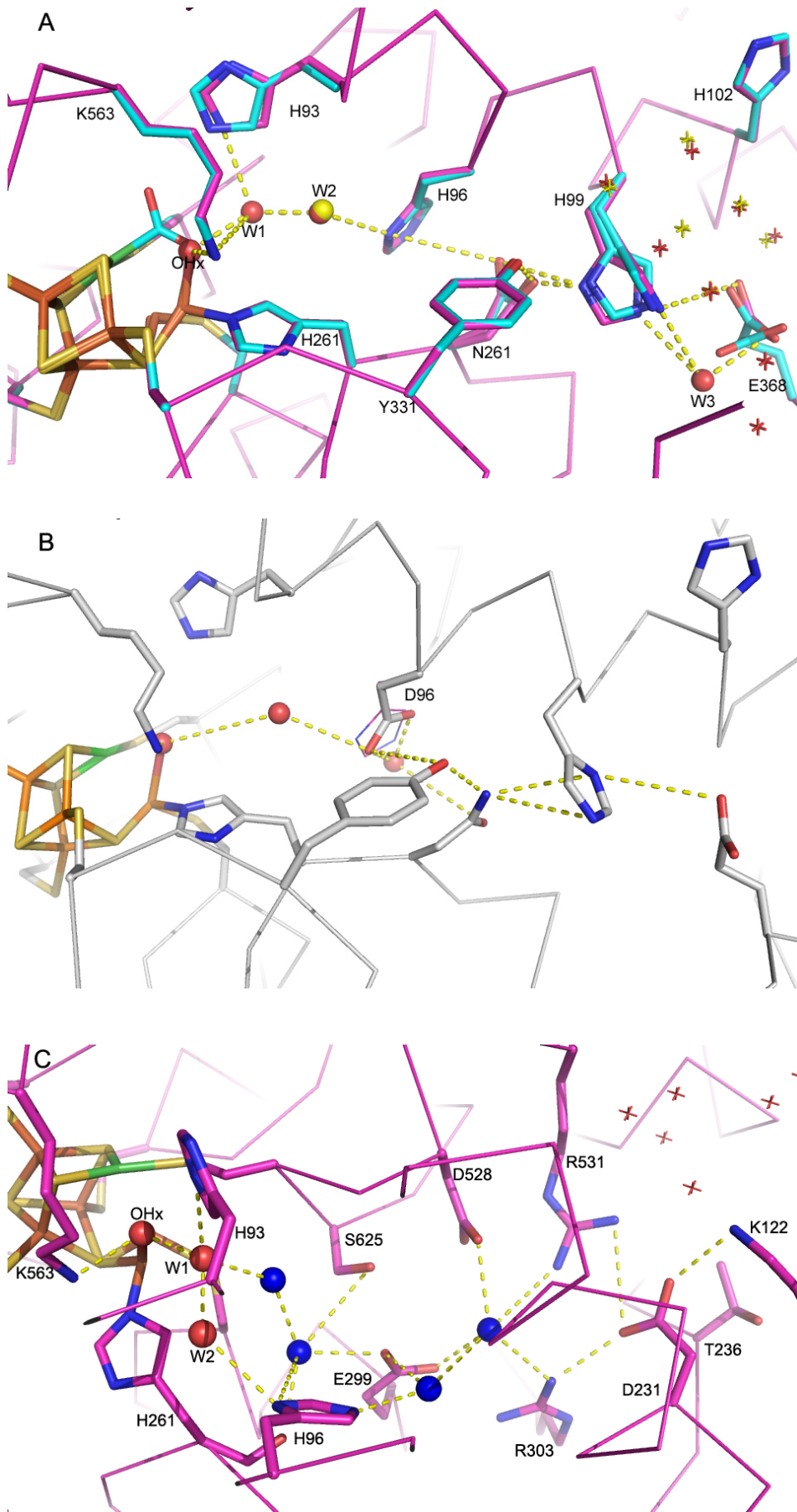


Figure 23. Figure legend is shown in the next page.

Figure 23. Proton channel and water network in Rec-CODHII structures. (A) A putative proton channel shown by superposition of -320 mV (*magenta*) and -600 mV+CO₂ (*cyan*) structures. Waters interacting with residues in the channel are depicted as *red* spheres for -320 mV and *yellow* spheres for -600 mV+CO₂. (B) Appearance of a new water in H96D Rec-CODHII at 1.7 Å resolution. (C) A putative and conserved substrate water network close to the OH_x ligand of cluster C. Here shown is the water network of the -320 mV state. Waters in the proton channel and in substrate water network are shown as *red* and *blue* spheres, respectively. Other solvent waters are shown as asterisks in (A) and (C). Dotted *yellow* lines indicate interactions at a distance of less than 4.4 Å.

After CO oxidation, protons and electrons are released from the protein, and CO and water should be replenished from the solvent. A putative substrate water network with an extension of approximately 16 Å is found nearby the OH_x ligand of cluster C and is mediated via conserved residues (Fig. 23C). These linearly arranged water molecules are well ordered in the CODHII structures reported in this study even though different crystallization conditions and oxidation states were analyzed.

9.4. Structure of Cluster C-missing Rec-CODHII

The crystal structure of cluster C-missing Rec-CODHII was refined at 1.6 Å resolution (Tab. A7-2) and is practically identical to other CODH structures of this study. The presence of completely occupied clusters B and D as judged by B-values of the constituting ions (data not shown) is consistent with the result of UV-vis spectroscopy (approximately three [4Fe-4S] clusters were estimated in Fig. 16B).

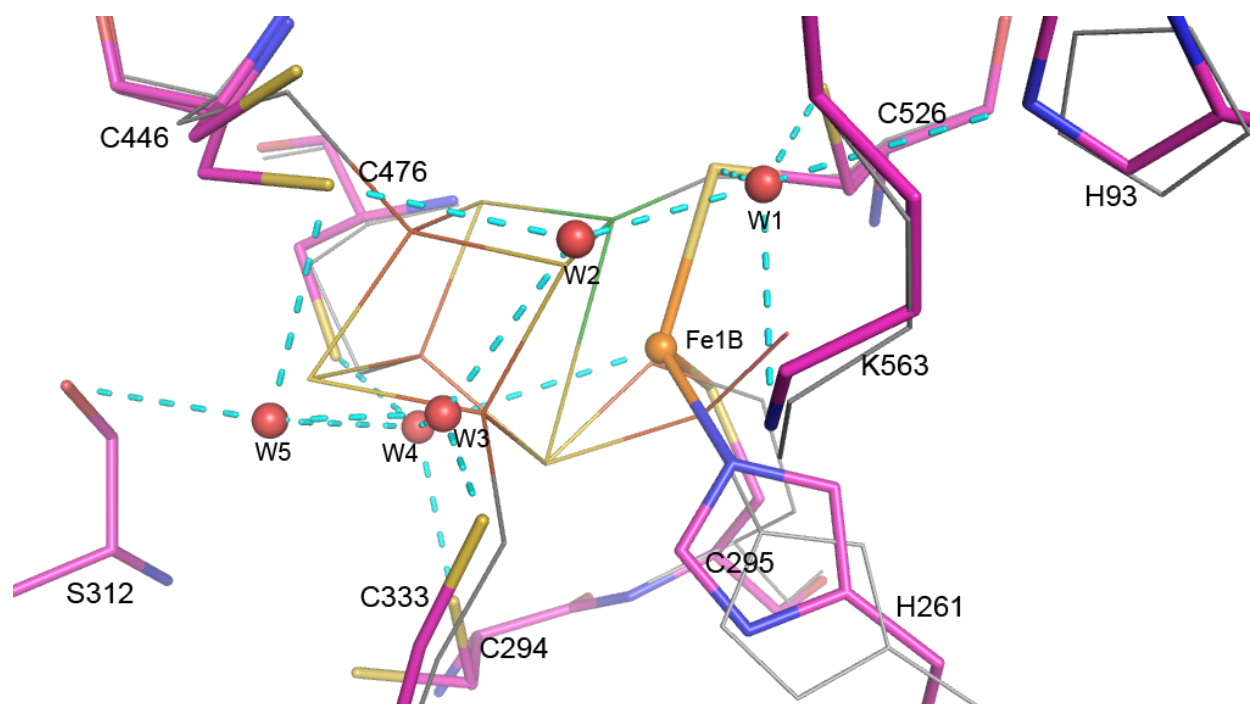


Figure 24. Structure of active site of cluster C-missing Rec-CODHII in superposition with cluster C of -320 mV structure (Fig. 21B) by COOT (Emsley & Cowtan, 2004). The residues of cluster C-missing of Rec-CODHII are drawn in sticks with element color and Fe1B in *orange* sphere. Water molecules are shown in *red* sphere with ionic interactions to surrounding residues (dotted-*cyan*). Cluster C of -320 mV structure is shown as same in Fig. 21B with coordinating residues in *gray*.

Five water molecules and one metal occupy the cavity of cluster C. The metal was modeled as Fe due to anomalous absorption at this position, albeit weakly (data not shown), and a tetrahedral coordination geometry. Fe is ligated by two cysteines (C295 and C526), one histidine (H261) and one water (W3). Interestingly, Fe was found at an alternative position of Fe1 (Fig. 21), termed Fe1B, which has been speculated to be occupied only when the Ni ion is absent (Dobbek et al, 2004). The other residues coordinating the metals of cluster C displayed the same location compared to those of wild-type (Fig. 24) except that H261 moved approximately 1 Å to coordinate Fe1B, resulting in a small displacement of the following residues N262 to D267 (data not shown). This observation again emphasizes that the rigidity of cluster C (Fig. 22) is supported by the protein framework.

10. Structures of CooC1

10.1. Overall Structures

The gene encoding CooC1 from *C. hydrogeniformans* was cloned and overexpressed in *E. coli* and the protein CooC1 was purified to homogeneity and crystallized. CooC1 has a molecular weight of 27.96 kDa. The Phasing of the structure was done with the SIRAS method using a thiomersal-derivatized crystal (Tab. A5). The crystal structures of CooC1 in different states, Apo monomer, and dimers of Metal/ADP-bound, ADP-bound, and Metal-bound states, were solved at 2.3, 2.4, 2.3 and 1.9 Å resolutions, respectively (Tab. A6). The final refined structural models contain different numbers of molecules in the crystallographic asymmetric unit, consisting of all 254 amino acids residues of the monomer.

Fold topology of the polypeptide of all states of CooC1 structures showed basically an α - β - α layered architecture, in which the central core is comprised of a twisted arch of an eight-stranded β -sheet surrounded by α -helices with seven parallel and one antiparallel β -strands (Figs. 25 and 26). The α -helices are assembled on either side of the core β -sheet. This topology is a variation of the typical Rossmann-fold conserved structurally in many other nucleotide-binding proteins, especially, analogous to those of the NTPases in the SIMIBI class. Three major regions in all CooC1 states are structurally flexible, independent of the presence or absence of ADP and/or metal (Figs. 25A and D, and Fig. A10). Region 1 is a cap-loop placed between α 5- and α 6-helices, region 2 is an extended loop from the COOH-terminus of β 5-strand to the NH₂-terminus of the α 7-helix (MBS-loop), and region 3 is at the COOH-terminus of α 12-helix. The adenosine moiety of the bound-ADP lies at a pocket surrounded by two α -helices (α 1 and α 9) and the COOH-terminus of two β -strands (β 8 and β 9), and the diphosphates are recognized by the P-loop nucleotide-binding site located between β 1 and α 1 (Fig. 25B and D,

and Fig. 26). The metal-binding site (MBS) is positioned at the COOH-terminal side of a flexible loop connecting $\beta 5$ -strand and $\alpha 7$ -helix (Figs. 25C and D, and Fig. 26).

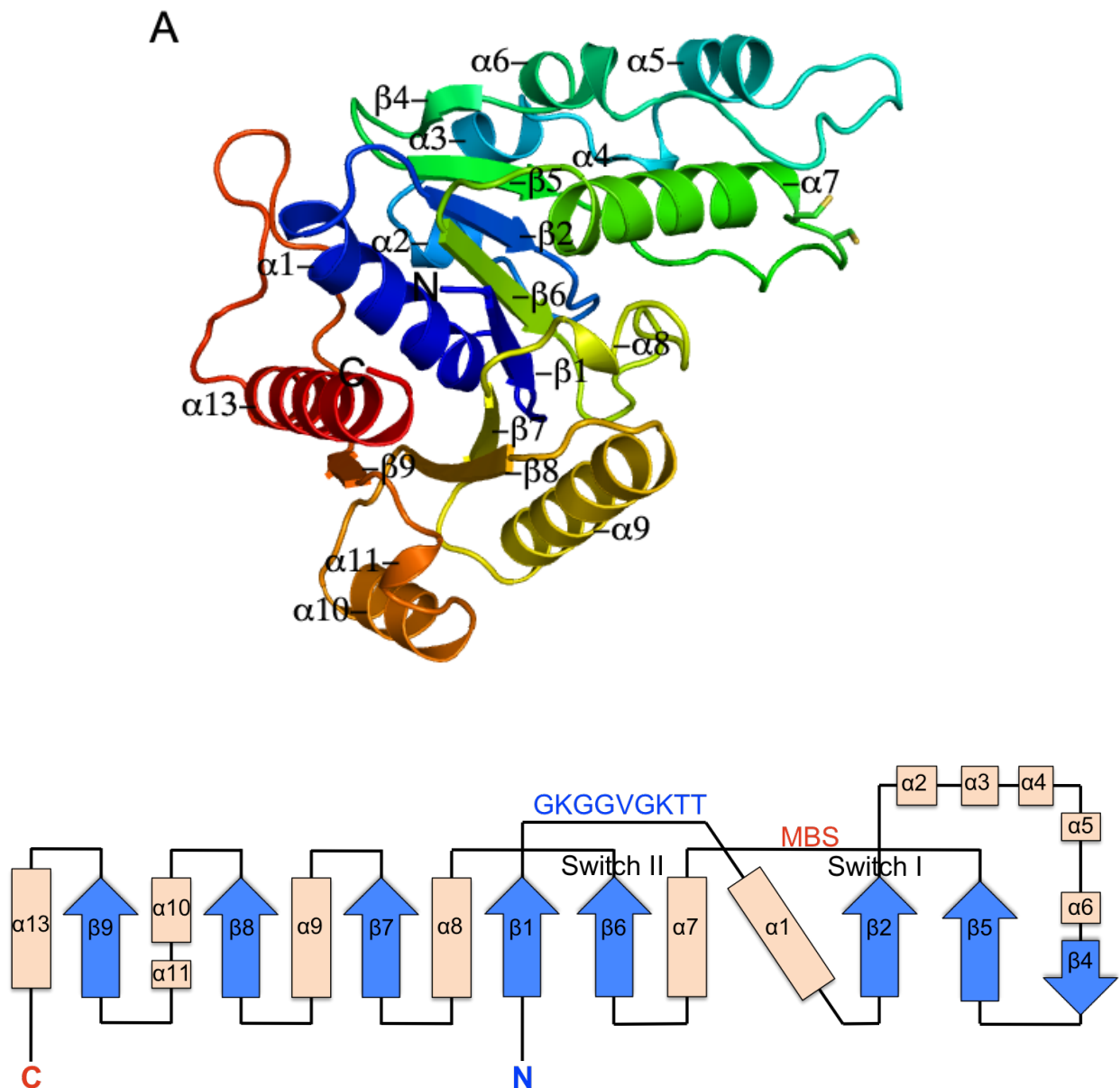


Figure 25. Three-dimensional cartoon presentations of the CooC1 structures. (A) Crystal structure of CooC1 in the monomeric apo-form at 2.3 Å resolution with schematic presentation of topology diagram, which was generated manually in analogy to proteins of the MinD family (see Fig. 9). (B) Dimer of ADP-bound state at 2.4 Å. (C) Dimer of Metal-bound state at 1.9 Å. (D) Dimer of Metal/ADP-bound state at 2.3 Å. Structures are shown in two orientations (side-view in upper and top-view in lower picture by 90° rotation). The structures are colored from *blue* at the NH₂-terminus via *green* through *yellow* to *red* at its COOH-terminus. α -helices and β -strands are numbered from $\beta 1$ and $\alpha 1$ at the NH₂-terminus to $\beta 9$ and $\alpha 13$ at the COOH-terminus in (A). Dimer structures (B, C and D) are shown with surface presentation of Pymol (DeLano). Additional secondary structures are indicated in (B) and (D). Bound ADP is shown as ball-and-stick model in element color (B and D). Bound-metal is shown in *orange* spheres (C and D) with the coordinations through the conserved cysteines (Cys₁₁₂ and Cys₁₁₄). The conserved sequence GKGGVgKTT in the P-loop depicted in topology (A) is shown in *blue*, MBS (Metal-binding site) in *red*, and Switch I and II are shown in *black*. The two-fold non-crystallographic axis is depicted for the dimer structures, (B), (C) and (D).

Figure 25. (continued)

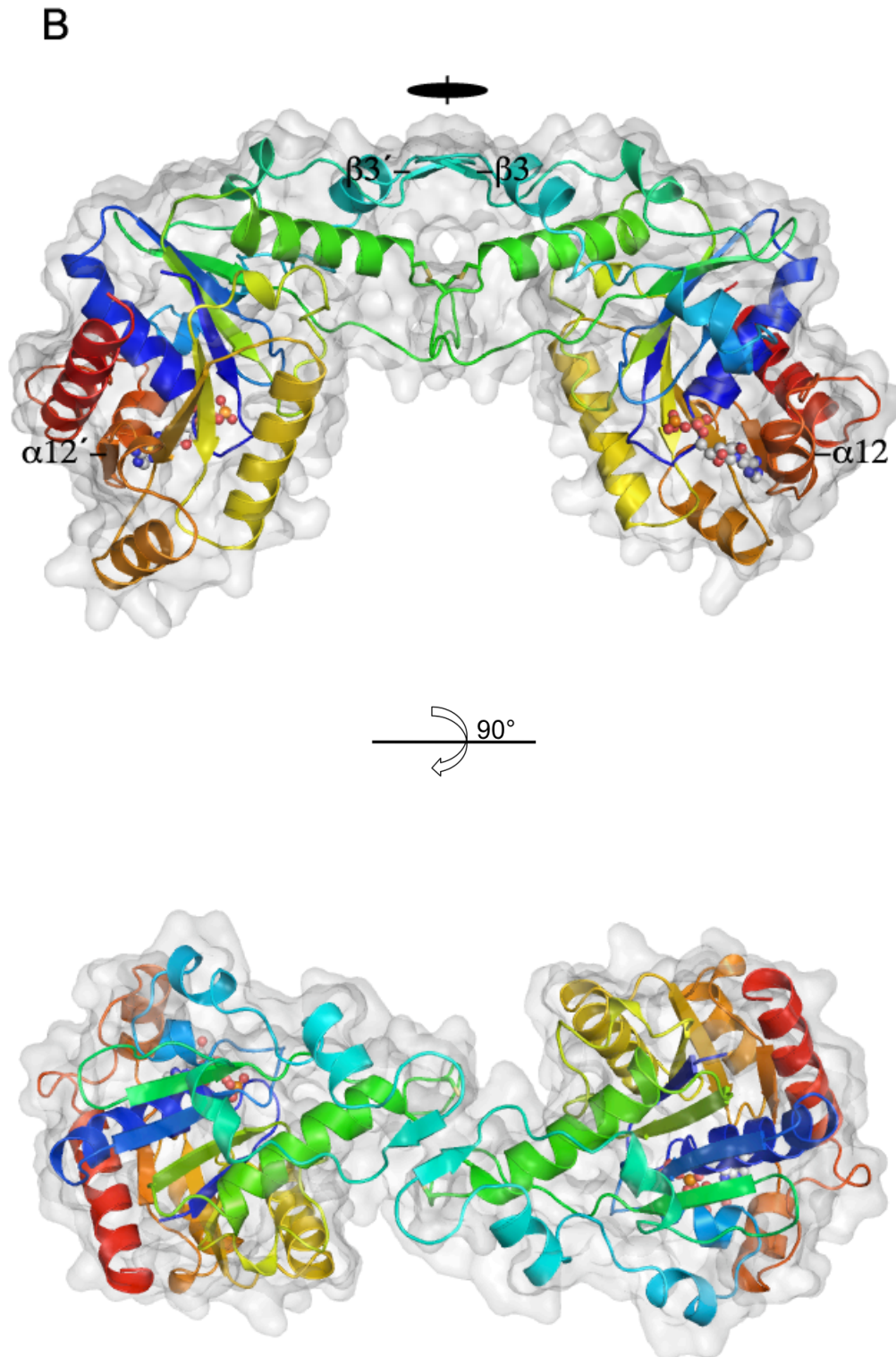


Figure 25. (continued)

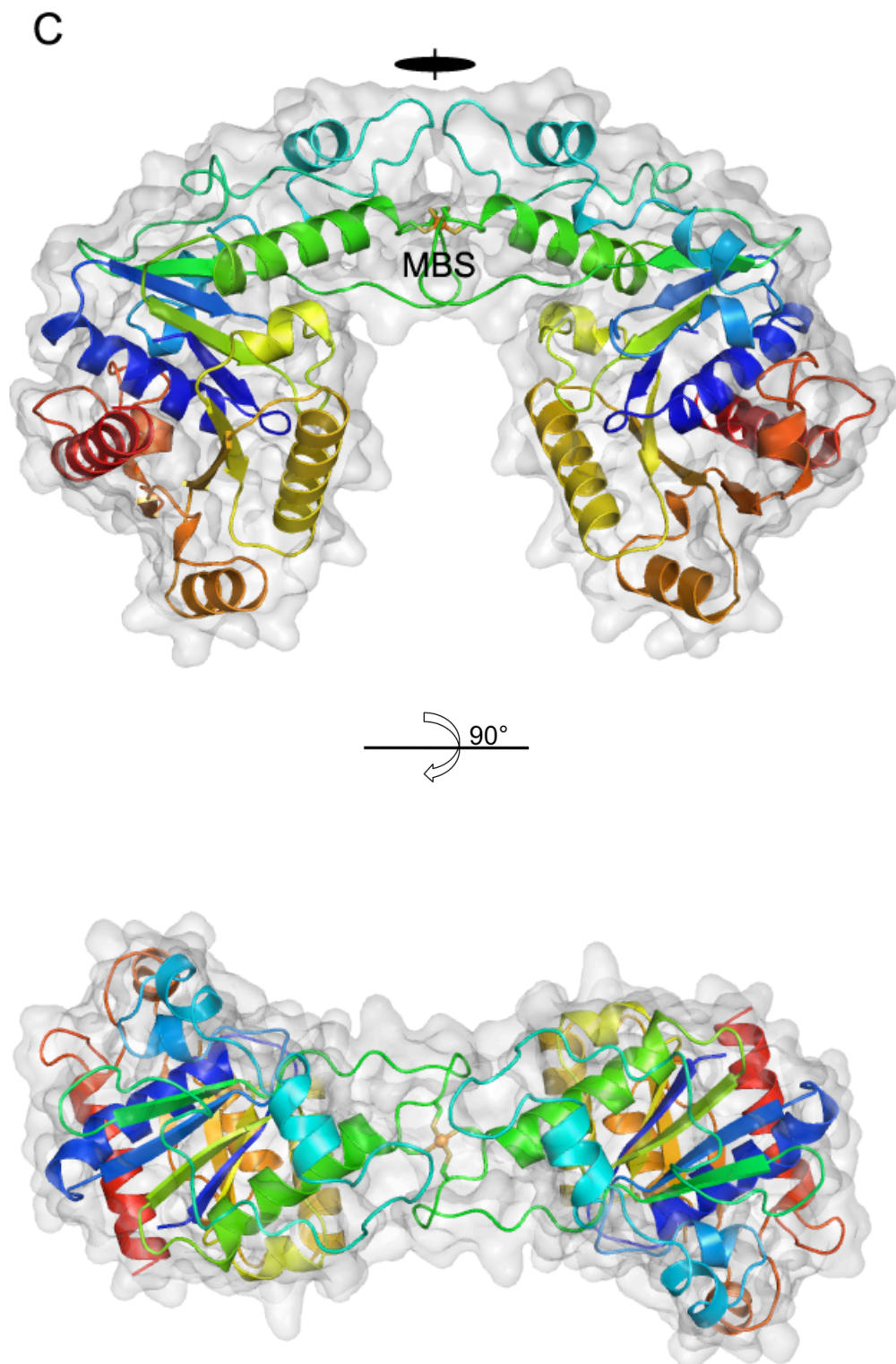
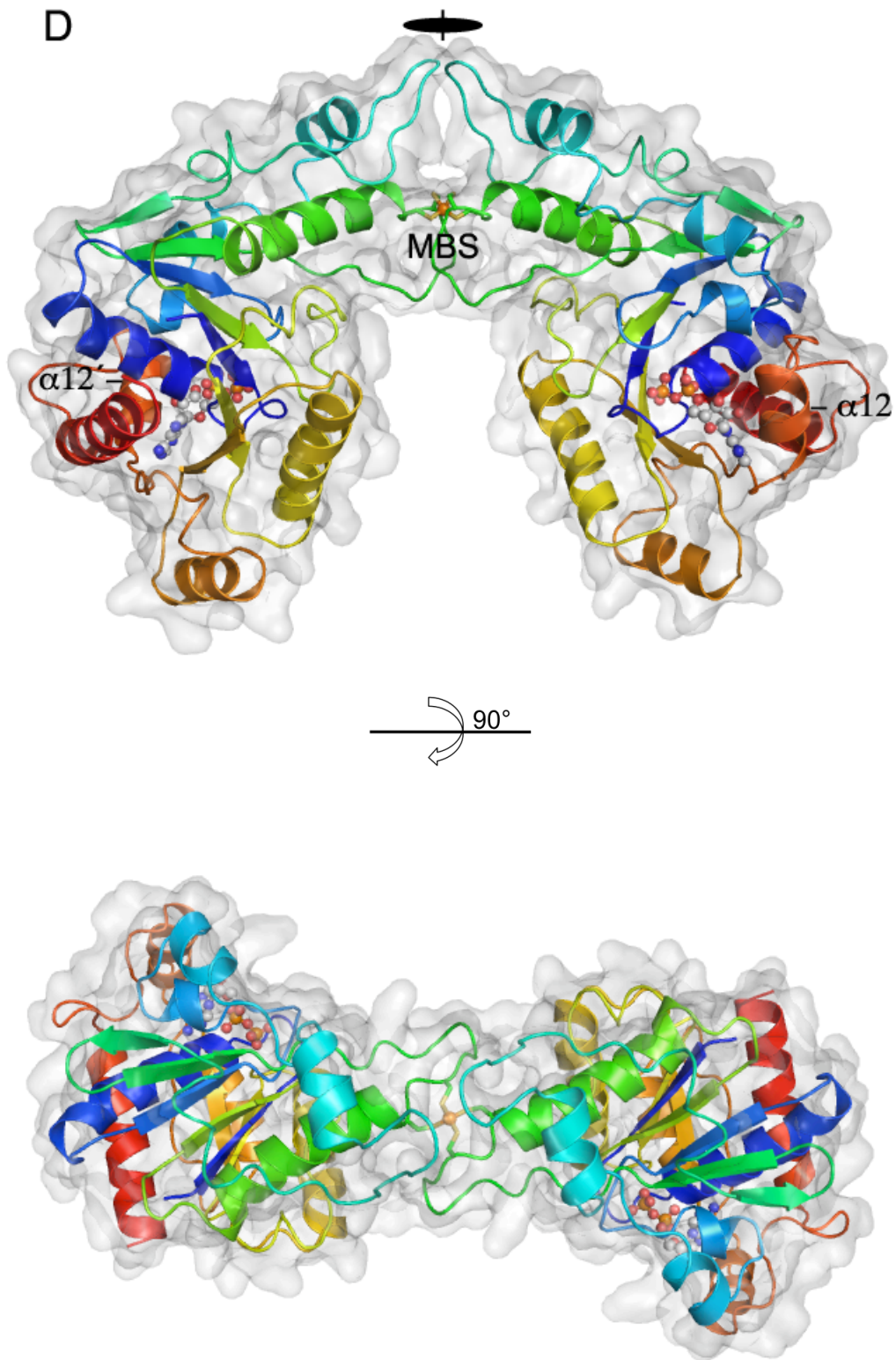


Figure 25. (continued)



A structural similarity search using DALI (Holm & Sander, 1993) shows that the structure of CooC1 is related to the members of the MinD family in the SIMIBI class: MinD (PDB ID: 1HYQ with Z score of 19.3 (Cordell & Lowe, 2001) and 1G3Q with Z score of 19.0 (Hayashi et al, 2001), NifH (PDB ID: 1G1M with Z score of 19.0 (Strop et al, 2001) and 1CP2 with Z score of 18.7 (Schlessman et al, 1998), Soj (PDB ID: 1WCV with Z score of 18.3 and 2BEK with Z score of 17.3 (Leonard et al, 2005), and ArsA (PDB ID: 1II9 with Z score of 12.6 (Zhou et al, 2001) and 1IHU with Z score of 10.8 (Zhou et al, 2000). The core parallel seven-stranded β -sheet (β 1-2 and β 5-9) and a β -strand (β 4) in the CooC1 structure are identically arranged as those found in NifH, MinD, ArsA and Soj proteins (Figs. 9 and 25A, topology diagram). Dethiobiotin and CTP synthetases, proteins of the BioD family in the SIMIBI class (Leipe et al, 2002), showed primarily amino acid sequence similarity to CooC1, and the DALI search also found that these proteins are structurally related (dethiobiotin synthetase, PDB ID: 1DAD with Z score of 11 and CTP synthetase, PDB ID: 2AD5 with Z score of 10.8). Superpositions of dethiobiotin synthetase and the synthetase domain of CTP synthetase with CooC1 show a good agreement with the central core β -sheet and the nucleotide binding sites being highly conserved. In addition to the structural similarity to SIMIBI class proteins, CooC1 shows similarity to the elongation factor Tu (EF-Tu, PDB ID: 1HA3 with Z score of 10.8 (Vogelely et al, 2001) that is a member of the superfamily of translation factor proteins (TRAFAC class (Leipe et al, 2002)). Additionally, EF-Tu has a several characteristic structural similarity to the nucleotide binding site of CooC1, even though the TRAFAC and SIMIBI class proteins exhibit a different topology (Leipe et al, 2002). The structural analysis of CooC1 with primary sequence similarity fully supports that CooC1 is classified as a member of the MinD family of the SIMIBI class.

A superposition of the monomeric CooC1 structure in four different states does not show larger conformational changes in C α -trace, except in the three flexible regions (Fig. 27A). Binding of ADP induced the formation of an additional α -helix (α -12) that enclosed the bound ADP in the ADP-bound structures (Figs. 27B). Although the α 12-helix was modeled in structure refinement of the Metal-bound state, it was not assignable as an α -helix because the electron density was not well defined in this region. Both Metal-bound and Metal/ADP-bound states did not show additional secondary structure in the dimer interface upon metal binding (Figs. 25C and D). The residues around the nucleotide-binding site and MBS in CooC1 are relatively flexible including the Walker A, switch I and II motifs, α 9, α 12 and the NH₂-terminus of MBS-loop, as reflected in the temperature factors (B-factor) of backbone atoms (Fig. A10). In contrast to the helices around the central core β -sheet, the core β -sheet exhibits lower B-factors in all structures, indicating the formation of a general rigid core structure regardless of ADP and/or metal binding. A previous structural analysis of MinD revealed that the regions including the Walker A, switch I and II motifs and α 7-helix (α 9 in CooC1) were mobile upon binding of ATP or ADP in monomer structure (Hayashi et al, 2001). These regions are placed at the dimer interface upon binding of

ATP or ATP-transition state analogue in NifH (Georgiadis et al, 1992) and Soj (Leonard et al, 2005).

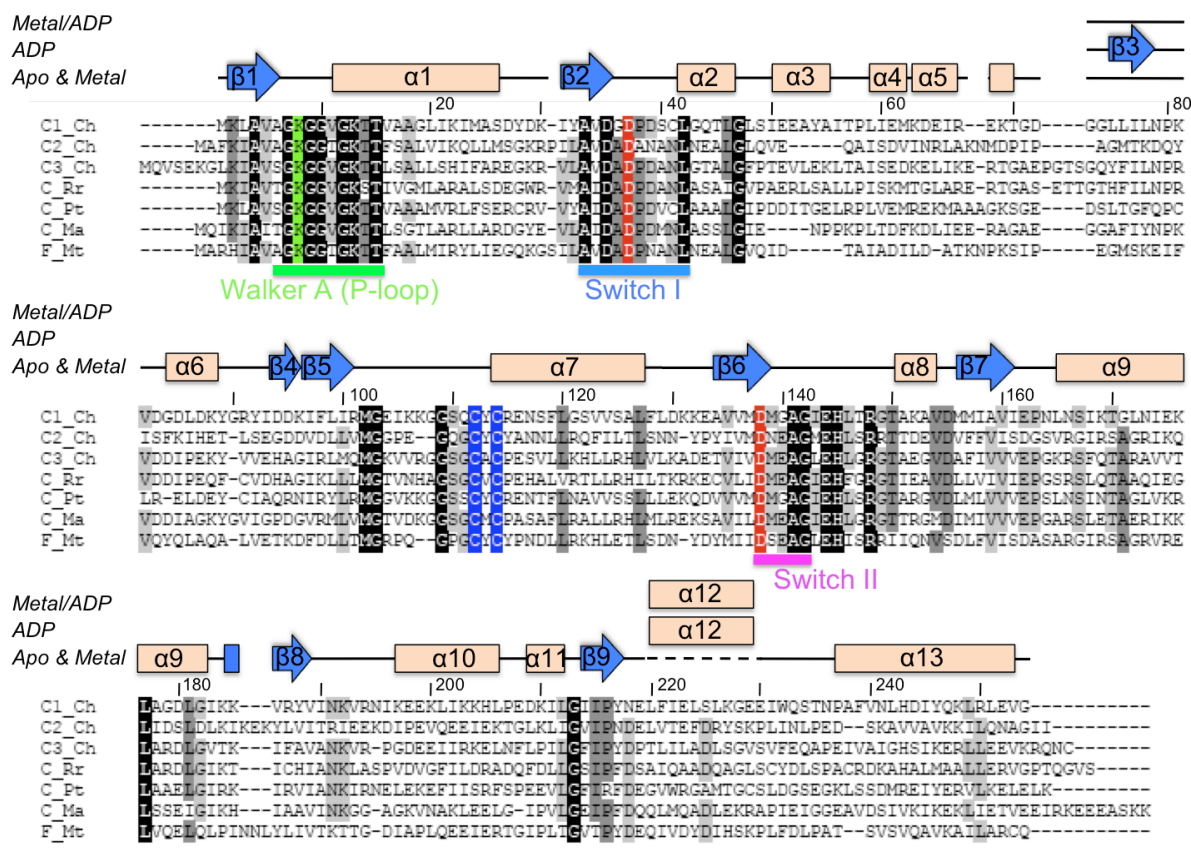


Figure 26. Multiple sequence alignment of CooC homologues. Conserved Walker's motifs are underlined: Walker A motif in green, switch I (Walker A') in cyan and switch II (Walker B) in pink. The conserved CXC motif for metal-binding is marked in blue. Secondary elements are presented above the sequence alignments. Amino acids sequences were aligned with ClustalW (Chenna et al, 2003) and highlighted manually as identity in box: 100%, black; over 85%, dark-gray and over 70%, light-gray. Sequence identity of CooC1_Ch to others are 25% to CooC2_Ch, 38% to CooC3_Ch, 32% to CooC_Rr, 42% to CooC_Pt, 40% CooC_Dh, 35% CooC_Ma and 20% AcsF_Mt. Ch, *C. hydrogenoformans*; Rr, *Rhodospirium rubrum*; Pt, *Pelotomaculum thermopropionicum* SI; Ma, *Methanosarcina acetivorans* C2A; Mt, *Moorella thermoacetica*.

The ADP-bound state of CooC1 form a dimer through a weak interaction with a short β -strand formed by hydrophobic residues (Leu₇₅–Leu₇₆–Ile₇₇) (Fig. 25B), which was not assigned as a strand by PROCHECK (Laskowski et al, 1993) but can be denoted as β -strand because of the characteristic hydrogen bonds between the β -strands from each monomer molecule building an antiparallel β -strand (β 3) in Fig. 25B, top view. The metal-bound states (Fig. 25C and D) form the tight dimer through covalent-linkage of the bound metal by two highly conserved cysteines from each molecule (Cys₁₁₂ and Cys₁₁₄). The dimer interfaces of three different states coincide with the crystallographic 2-fold axis. This type of metal-dependent dimer formation is similar to NifH protein, where a [4Fe-4S] metal cluster is linked via cysteine residues in α 7 and α 8 (numbering in CooC1 structure), forming a covalent dimer structure (Georgiadis et al, 1992; (Schindelin et al, 1997).

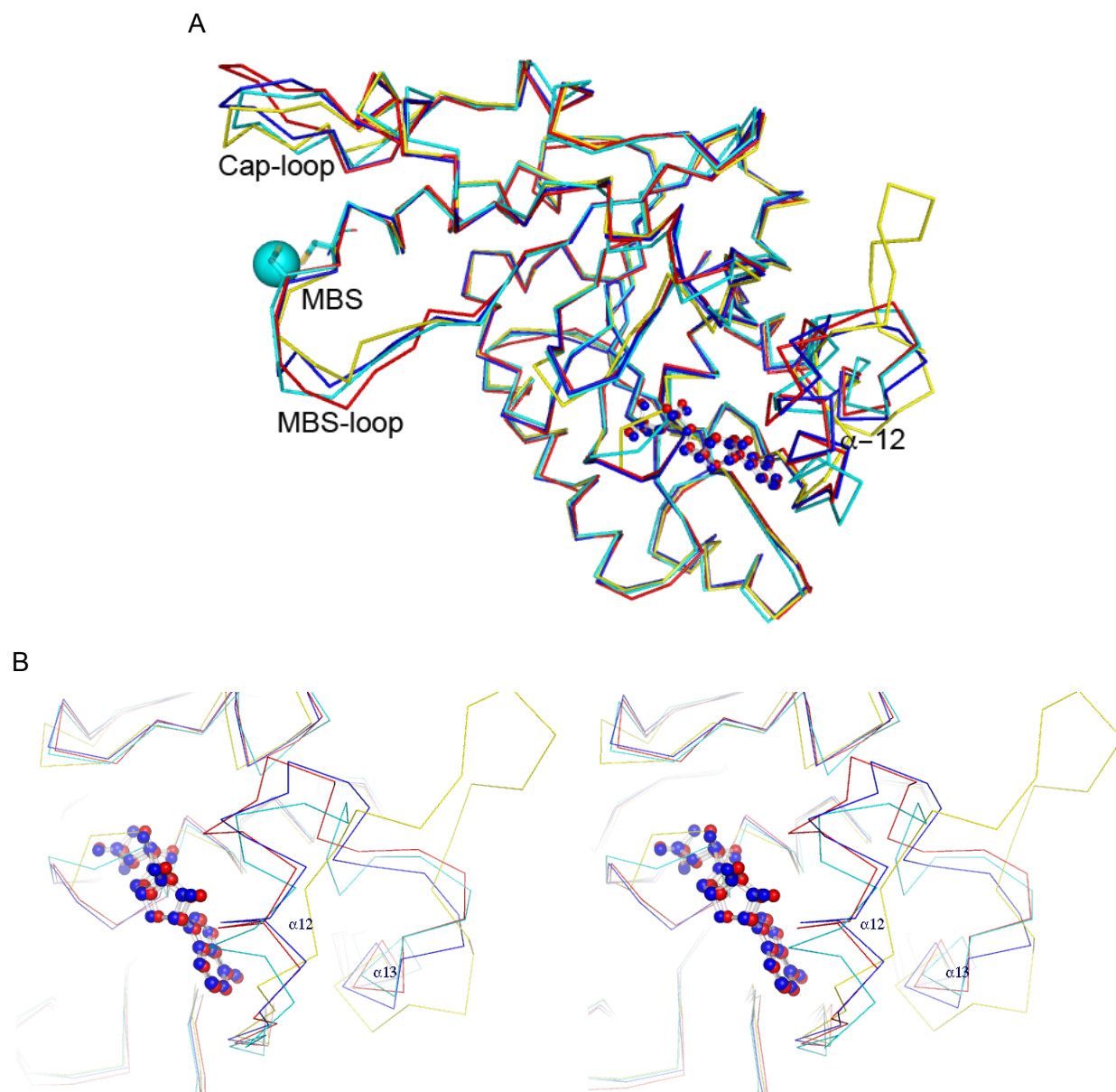


Figure 27. Superposition of C α -traces of monomers between different CooC1 structures (A) and stereo presentation of the movement of α 12-helix upon ADP binding (B). Apo-state is colored in *yellow*, ADP-bound in *blue*, metal/ADP-bound in *red*, and metal-bound in *cyan*. Metals in sphere and ADP in ball-and-stick model are colored according to the corresponding molecule.

Despite no large structural difference in the monomeric molecules of different states, comparison of dimeric states shows that CooC1 undergoes a large movement (Fig. 28), depending on the type of bound ligand. In the Metal-bound state, an angle of approximately 140° between two molecules was found (measured between the α 7-helices). The structure of Metal/ADP-bound CooC1 showed conformational change by widening the angle $\sim 18^\circ$ compared to the Metal-bound state, while no change in distance between the nucleotide-binding sites can be detected (~ 35 Å measured by C α -carbon of Lys₈). A large conformational change was observed in the ADP-bound state, where the structure moved $\sim 60^\circ$ in angle and ~ 5 Å in distance compared to the Metal-bound state, resulting in a more open dimer structure (~ 41 Å).

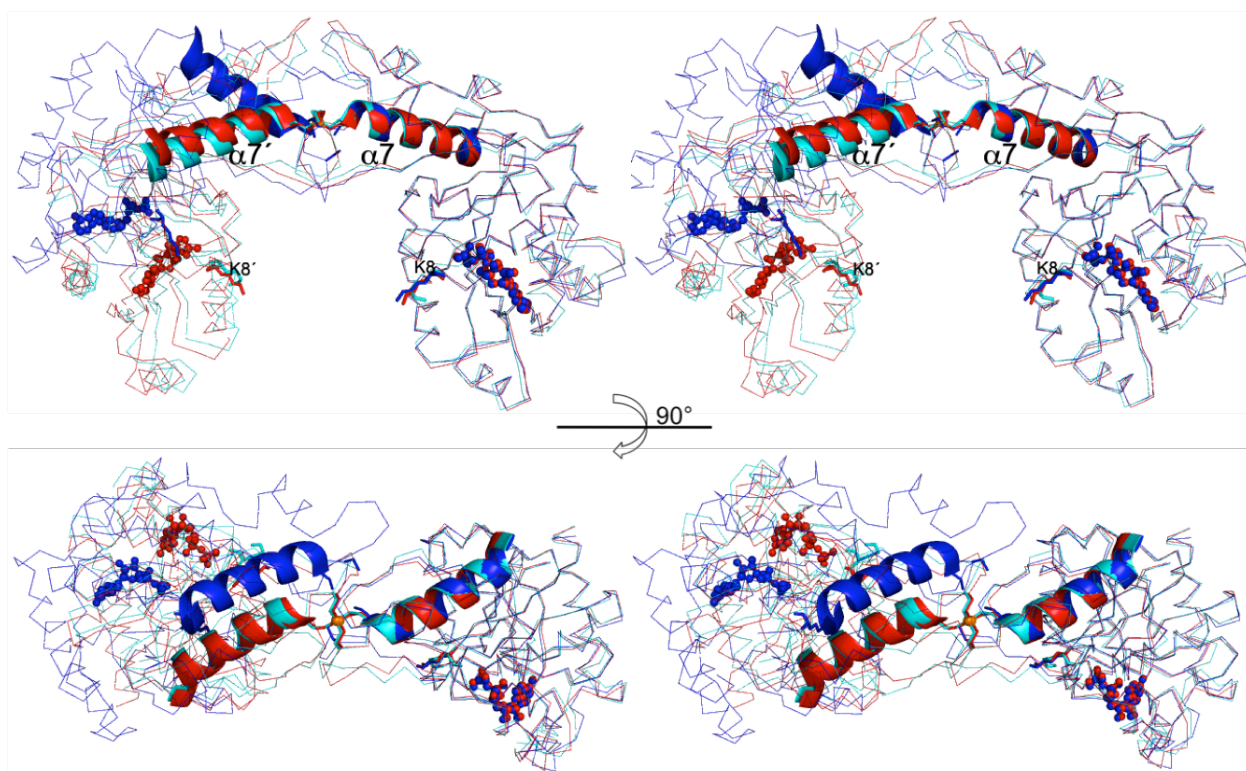


Figure 28. Stereoview presented superposition of the dimer structures of CooC1 in different states, side-view in upper and top-view in lower picture. Structures of ADP-bound in *blue*, metal/ADP-bound in *red*, and metal-bound in *cyan* are superimposed in one molecule (right side). The $\alpha 7$ -helix is shown in cartoon presentation. The two conserved cysteines and Lys₈ are shown as stick-models and coloured according to the molecule they are part of. The metal is depicted as *orange* sphere. ADP molecules are in ball-and-stick.

10.2. Nucleotide Binding Site

The previously reported structures of MinD (Hayashi et al, 2001), NifH (Schindelin et al, 1997), ArsA (Zhou et al, 2000), and Soj (Leonard et al, 2005), all members of the MinD family NTPase, showed a highly conserved xKGGxxK[T/S] motif (x denotes any amino acid). The motif is known as the deviant Walker A motif (P-loop, see Fig. 35B) that adapts to the diphosphate moiety of the bound nucleotide (Lutkenhaus & Sundaramoorthy, 2003). Analysis of two ADP-bound structures of CooC1 in the presence or absence of the bound-metal (ADP-bound and Metal/ADP-bound states) confirmed the common role of the Walker A motif. The conserved GKGGVGKTT (Walker A motif in CooC1, Fig. 26) found in residues 7 to 15 (P-loop) that recognizes nucleotide-bound phosphate (Figs. 29 and A11), forming a layered $\beta 1$ -strand–loop– $\alpha 1$ -helix structure. The backbone amide nitrogens from the residues comprising the Walker A motif (Gly₁₀, Val₁₁, Gly₁₂ and Thr₁₄) stabilize the α - and β -phosphates oxygens in both states. The Lys₁₃, known to interact with β -phosphate oxygens in the homologues of MinD family ATPases (Zhou et al, 2000; Schindelin et al, 1997; Sakai et al, 2001), showed the conserved contact to the phosphate. Ser₄₀ in CooC1, which is conserved among the MinD family, is

hydrogen-bonded to the oxygens of α - and β -phosphates through its carbonyl oxygen and side chain hydroxyl group. Oxygens of the α -phosphate in the ADP-bound state are in contact to the protein through carbonyl oxygen of Gly₁₂ and a hydroxyl group of Ser₄₀ residues, while the hydroxyl groups of Thr₁₅ and Ser₄₀ of the Metal/ADP-bound structure interact with the α -phosphate of the bound ADP. The Thr₁₅ residue is well conserved in the MinD family, except for ArsA where it is replaced with Ser, and showed an equivalent function in the binding of nucleotide (Sakai et al, 2001; Schindelin et al, 1997; Hayashi et al, 2001; Zhou et al, 2000).

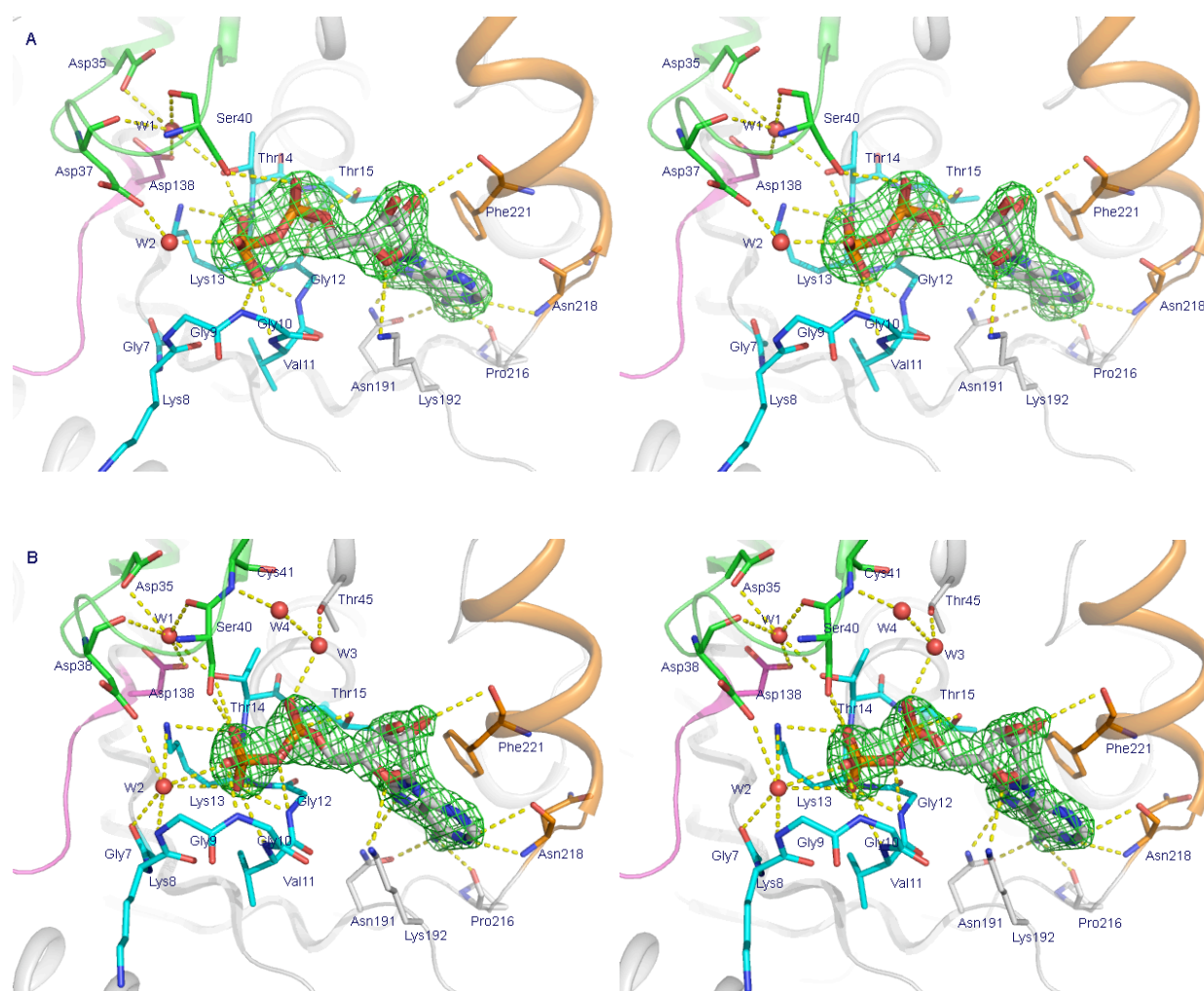


Figure 29. Stereoview of a cartoon presentation of the ADP-binding sites of the ADP-bound (A) and Metal/ADP-bound (B) states. The P-loop (residue 7–15) is shown in *cyan*, switch I region (residue 33–42) in *green*, switch II (residue 138–142) in *pink*, and α 12-helix (residue 218–228) in *brown*. The $F_{obs}-F_{calc}$ omit maps of the ADP molecule are contoured at 5σ in *green*. Water molecules are shown as *red* spheres. Interactions are indicated by *yellow* dotted lines.

While the P-loop usually binds the α - and β -phosphates of the nucleotide, the conserved motifs of switch I and II, also known as the Walker A' and B motifs, respectively, sense the presence or absence of γ -phosphate and the bound Mg ion directly or indirectly. Even though the Mg ions were not found in two CooC1 structures of the ADP-bound states, the conserved residues in the

switch I and II motifs are interacting with the bound ADP via water and/or through residues in the P-loop motif (Figs. 29 and A11). The numbers of water molecules interacting with the phosphate moiety of ADP are different in the different CooC1 structures. Two additional waters (water-3 and -4) are found in the Metal/ADP-bound structure, where water-3 binds directly to the oxygen of α -phosphate by interacting with the hydroxyl group of Thr₄₅ and water-4 is in hydrogen-bonding distance to the amide group of backbone of Cys₄₁.

The switch I region of CooC1 contains residues AVDGDPSCL (33–42) and is between β 2-strand and α 2-helix (Fig. 26). The carboxyl oxygen of the highly conserved residue Asp₃₇, even in structurally not-related ATPases (Walker et al, 1982), interacts with water-2 that is in hydrogen bonding distance to an oxygen of the β -phosphate in both CooC1 structures. This water molecule is in a similar position to the γ -phosphate of the bound-ATP of MinD (Hayashi et al, 2001) and Soj (Leonard et al, 2005), and the Al ion of bound-AlF₄⁻-ADP in NifH (Schindelin et al, 1997). Asp₃₇ is frequently coordinating the Mg ion in many ATP- and GTP-binding proteins including proteins of the MinD family (Fig. 35), and is known to be essential for the ATPase activity (Walker et al, 1982; Schindelin et al, 1997; Georgiadis et al, 1992; Sprang, 1997; Leonard et al, 2005). Water-2 in the Metal/ADP-bound state is additionally hexa-coordinated through oxygen atoms of Gly₇, the β -phosphate and the backbone amides from Gly₉ and Lys₁₃. The carboxyl group of Asp₃₅, conserved in the CooC homologues (Fig. 26 and Fig. 35) (Walker et al, 1982) and the carbonyl oxygen of Ser₄₀ are in hydrogen bonding distance to water-1, thereby interacting indirectly with the phosphate moiety of ADP via the hydroxyl group of Thr₁₄. These two waters are highly conserved in both of ADP-bound CooC1 structures.

The conserved switch II motif (Walker B) is found in a close vicinity of the nucleotide-binding site and contains the conserved sequence of DMGAG (residue 138–142) in both structures of ADP-bound states. The first residue of the switch II motif is the conserved aspartate, which is important in catalysis by coordinating the Mg ion in the ATP-binding proteins (Walker et al, 1982). In both structures, the highly conserved Asp₁₃₈ forms a hydrogen bond with the ordered water-1 molecule that interacts with the hydroxyl group of Thr₁₄ and indirectly interacts with Asp₃₇ through this water molecule.

The conformations of the ribose and adenine rings in both of CooC1 structures show a C2'-*endo* conformation and an *anti*-orientation, respectively, typically found in the nucleotide-binding proteins (Moodie & Thornton, 1993). The ribose 2'-OH in both states interacts with the carbonyl oxygen of Phe₂₂₁, present at the beginning of the α 12-helix. The 4'-O is bound to the amino group of Lys₁₉₂ in the two states. The recognition of the hydroxyl and oxygen in the ribose by hydroxyl and amide groups of backbone of side chains is common in the MinD family proteins. In addition to interactions of N7 and the amide group of the adenine ring with the amide side chain and carbonyl oxygen of Asn₁₉₁, the protein wraps around the ring by interactions of side chains involved in the α 12-helix (residue 218-228) that is formed upon binding of ADP (Fig.

27B). The hydrophobic phenol ring of Phe₂₂₁ stacks on the equatorial position, approximately 3.5 Å apart, of the adenine base of ADP in both structures. The two residues, Pro₂₁₆ and Asn₂₁₈, are in hydrogen bonding distance to the amide group and N1 through carboxy oxygen and amide nitrogen, respectively. An additional interaction of N1 of the ribose to the carboxy oxygen of Asn₂₁₈ was found in the Metal/ADP-bound structure.

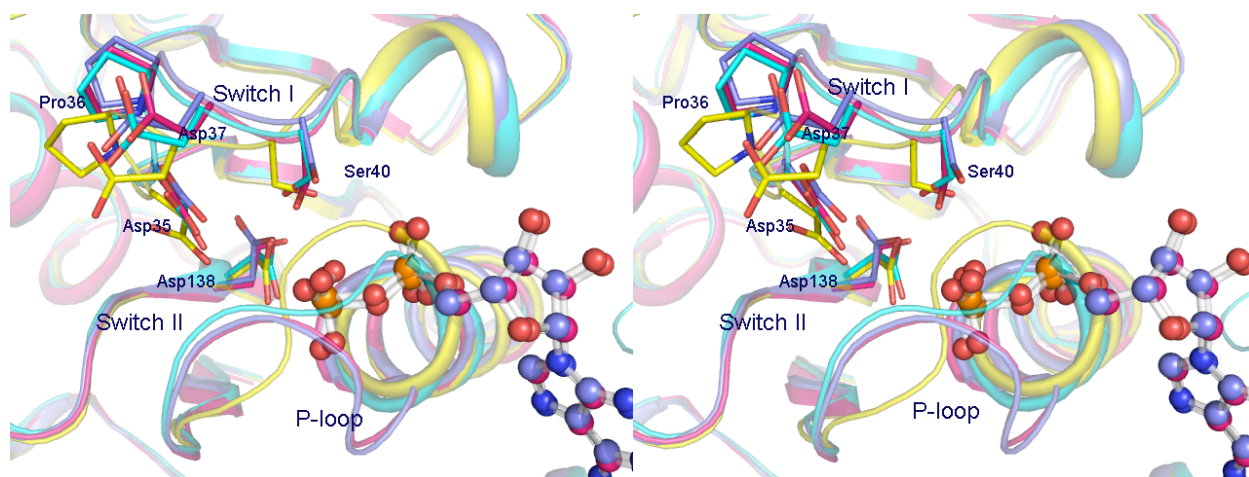


Figure 30. Stereoview of the superposition of ADP-binding sites in different states of the CooC1 structures. The ADP-bound structure is shown in *blue*, the Metal/ADP-bound state in *pink*, the Apo-state in *yellow* and the Metal-bound in *cyan*. ADP molecules are depicted as ball-and-sticks and coloured according to the corresponding structure. Water molecules interacting with the phosphate moiety of ADP and the residues in the motifs are not shown here (See Fig. 29).

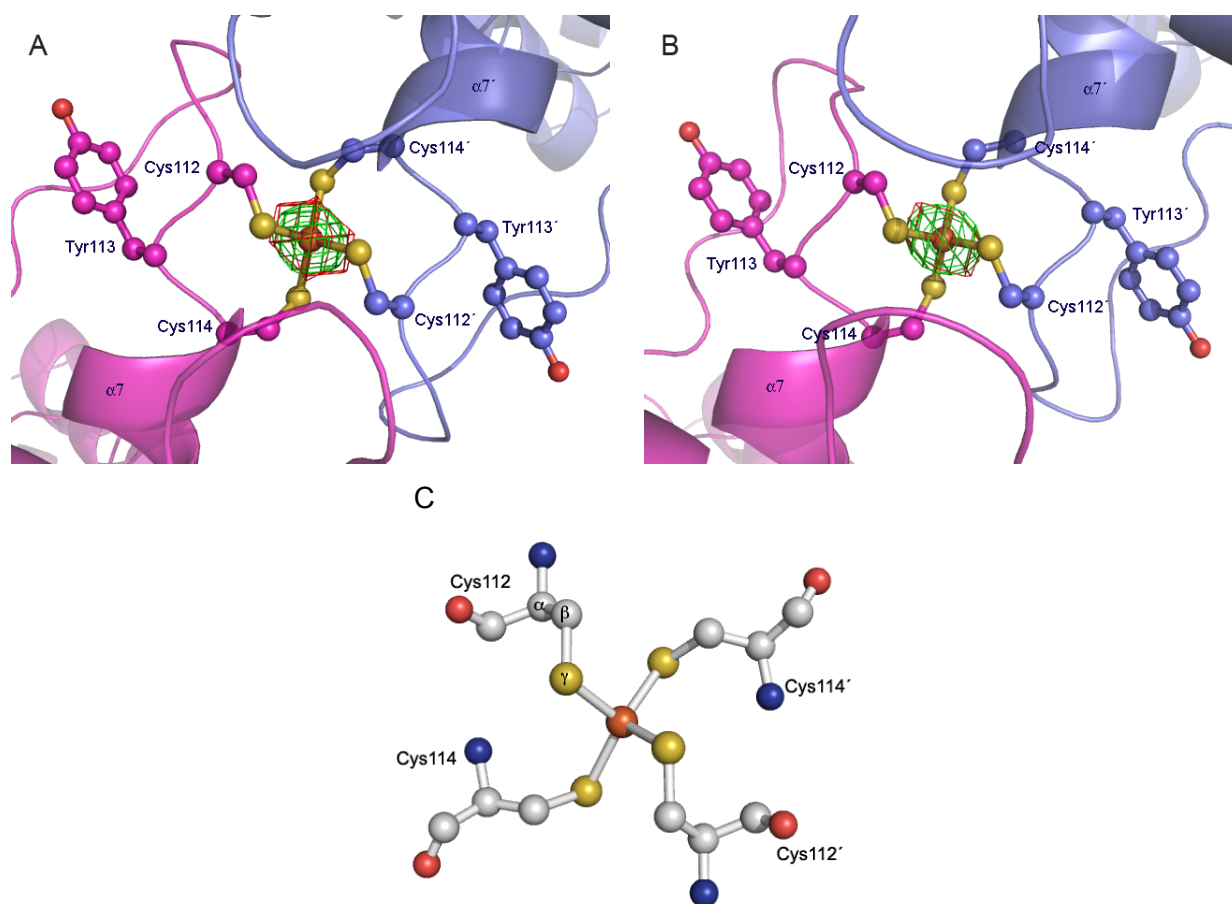
An obvious conformational change upon ADP binding was found in the P-loop region, which is responsible for recognition of the α - and β -phosphates (Fig. 29). The residues Gly₉–Gly₁₀–Val₁₁–Gly₁₂ of the P-loop motif were quite flexible in the absence of ADP as shown in Fig. A10, while ADP-binding induces a structural change for these residues such that they envelope the phosphate moiety and the α 1-helix is extended by one turn. The semi-conserved Pro₃₆ of CooC1 moved ~ 2.5 Å away from the ADP-binding site when ADP is present at the P-loop, inducing a small movement of Asp₃₅ and Asp₃₇ and orientating the hydroxyl group of Ser₄₀ towards the phosphate moiety of the bound ADP (Fig. 30). The switch I motif of Soj was reported to move slightly when comparing the empty, ADP-Mg²⁺-bound and ATP-Mg²⁺-bound states, in which Pro₄₅ (equivalent to Pro₃₆ in CooC1) moved ~ 0.7 Å between the states (Fig. 35) (Leonard et al, 2005). Although the superposition of the C α -atoms of the residues in the switch II motif of CooC1 structures showed no large structural rearrangement, the carboxy group of the highly conserved Asp₁₃₈ is flipped away from the P-loop upon ADP binding (Fig. 30), enabling the coordination of a water molecule (water-1 molecule in Fig. 29).

10.3. *Metal Binding Site*

The aerobically isolated CooC1 protein was crystallized in a metal-induced dimeric state under anaerobic condition in the presence and absence of ADP (Metal-bound and Metal/ADP-bound structures, Figs. 25C and D). One metal ion in the dimer interface of the crystallographic two-fold axis was identified in both structures by its anomalous scattering contribution at the 1.5418 Å wavelength of the rotating Cu-anode (Cu- K_{α}) x-ray source, which allowed to unambiguously identify the presence and position of the metal (Fig 31). Both metals of CooC1 structures were occupied equally and completely, as judged by their B-values (data not shown). The metal is tetrahedrally coordinated by four cysteines, consisting of two sets of two highly conserved cysteines (Cys₁₁₂ and Cys₁₁₄) derived from each molecule. This covalent-linkage generated a stable dimer state. The CXC metal binding motif, which is highly conserved in the functional homologues of CooC1 (Fig. 26), lies at the COOH-terminus of a flexible loop (MBS-loop) connecting the β 5-strand and the α 7-helix. It is interesting that the MBS-loop was largely flexible in the absence and presence of the metal as shown in Fig. A10. The MBS was shielded by a loop above it (cap-loop), which is also flexible in all structures (Fig. 25 and Fig. A10) except in the Apo-form. This cap-loop of the Apo-form was found in a crystal contact region, where the interaction with other molecules in the crystal lattice stabilized its conformation. The copper chaperone for Cu-Zn superoxide dismutase (CCS) delivers copper to the superoxide dismutase (Rosenzweig, 2002). Based on crystallography and spectroscopic data, it was proposed that the conserved CXC motif is responsible for Cu binding (Eisses et al, 2000) (Lamb et al, 2001). The motif, like in the MBS-loop of CooC1, is part of a surface-expanded loop structure following an α -helix (Lamb et al, 2001).

Binding of ADP changed the geometry of the tetrahedrally coordinated metal ion by shortening the metal to S γ -bond length from 2.33 Å in Metal-bound structure to 1.99 Å in the Metal/ADP-bound structure (Fig. 31). This small change in coordination distance resulted in an approximately 18° movement of the α 7- and α 7'-helices, resulting in a wider dimeric structure in the Metal/ADP-bound state (Fig. 28). While the type of metal cannot unambiguously be determined at the moment, the strong anomalous scattering contribution (over $8\sigma = 8e/\text{Å}^3$) at 1.5418 Å wavelength (8,014 eV) indicates that the bound metal could be Fe, Cu or Co. Many transition metals found in metalloproteins occur in their preferred coordination geometries, for example, the Co²⁺ ion prefers an octahedral arrangement over a tetrahedral coordination, while the Cu²⁺ is found mainly in tetrahedral and square planar coordination modes, which both are coordinated commonly by N, O, and/or S atoms (Rulisek & Vondrasek, 1998). A similar tetrahedral coordination geometry of a Fe²⁺ ion by four cysteines has been found in rubredoxin (Chen et al, 2006), where bond length of Fe–S–Cys are 2.30 to 2.33 Å with 104 to 114° of Cys–S–Fe–S–Cys angles. This feature of coordination geometry of iron suggests that the bound

metal of CooC1 structures could be Fe. This is further supported by the bioavailability and abundance of Fe compared to other transition metals (Kaim & Schwederski, 2004).



Metal-bound		Metal/ADP-bound	
Bond (Å)	Angle (°)	Bond (Å)	Angle (°)
2.29 (112S _γ -M)	109 (112S _γ -M-114S _γ)	2.30 (112S _γ -M)	108 (112S _γ -M-114S _γ)
2.33 (114S _γ -M)	104 (114S _γ -M-112'S _γ)	1.99 (114S _γ -M)	110 (114S _γ -M-112'S _γ)
	132 (114S _γ -M-114'S _γ)		123 (114S _γ -M-114'S _γ)
	93 (112S _γ -M-112'S _γ)		90 (112S _γ -M-112'S _γ)

Figure 31. The metal-binding sites in the dimer interface of Metal-bound (A) and Metal/ADP-bound (B) structures are presented as cartoons with residues in the conserved C112YC114 motif shown as ball-and-stick model. These are closer top views of Fig. 25C and D. Anomalous difference (red) and $F_{obs} - F_{calc}$ omit (green) maps of the bound-metal (orange spheres) are contoured at 5σ for the Metal-bound state and 6σ for the Metal/ADP-bound state, respectively. (C) Presentation of the metal coordinations by four cysteines with distances in Å and angles in degree. Because of the two-fold coordination symmetry, only the value of one symmetry equivalent is shown. S is colored in yellow. The prime denotes that the residues and helices originate from the symmetry-related molecule.

Therefore, the reported Metal-bound CooC1 structures were refined using a Fe ion as a model for the metal. However, other metals like Zn and Ni cannot be excluded. A Zn ion with tetrahedral coordination by four cysteine residues with Zn-S-(Cys) bond length of 2.30 and 2.54 Å was observed in a coiled-coil fragment of the Rad50 ATPase from *Pyrococcus furiosus*

(Hopfner et al, 2002) and anaerobic ribonucleotide reductase (Logan et al, 2003). Square planar geometry of dinuclear Ni ions are found in cluster A of ACS_{Ch}, in which one Ni ion is coordinated by three cysteines in 2.1 to 2.2 Å distance and a second Ni is ligated by two cysteines in 2.1 Å and two backbone N atoms (Svetlitchnyi et al, 2004). The Ni ion in the dinuclear Ni-Fe hydrogenase is pentacoordinated (square pyramidal) with four S atoms of Cys residues as equatorial ligands and the bridging S or O atom as an axial ligand (Fontecilla-Camps et al, 2007). Further experiments are necessary to identify the type of metal in the Metal-bound structures of CooC1 and to determine the coordination geometry of the Ni ion in a Ni-bound state.

DISCUSSION

1. Carbon Dioxide Activation at the Ni,Fe-Cluster of Anaerobic CO Dehydrogenase

Carbon dioxide (CO₂) is a key molecule in the development of earth climate and its (Loke et al, 2000) production and consumption is of utmost interest in energy technologies like biological and chemical fuel production (Whitesides & Crabtree, 2007). Activation of CO₂ and other small molecules is complicated by their high local thermodynamic stability. The biological oxidation/reduction of molecules such as CO₂, N₂ and H₂ are essential processes in the global biogeochemical cycles and are catalyzed by enzymes containing complex metal clusters based on iron and sulfur whose detailed function is still poorly understood (Rees & Howard, 2003). CODH catalyzes the reversible reduction of CO₂ using one of the complex metal clusters in biology, called cluster C. During the last decade many biochemical and spectroscopic studies have been carried out to elucidate the mechanism of CO₂-reduction. However, the mechanism remained largely elusive.

The gene (*cooS-II*) encoding CODHII of *Carboxydotherrmus hydrogenoformans* has been cloned. A verified amino acid sequence was aligned to homologous proteins found in bacteria and archaea (Fig. 32). The sequence alignment shows that the residues coordinating the metal clusters in CODH are highly conserved. An interesting result from the alignment is that the proteins from archaea, such as the sulfate-reducing archaeon *A. fulgidus* and the methanogenic archaeon *M. jannaschii*, possess an additional motif to coordinate two [4Fe-4S] clusters, as reported previously (Lindahl & Chang, 2001). The additional region containing this motif in archaeal CODHs resembles the Fe-S cluster motifs found in CooF from bacteria, a polyferredoxin, which interacts with CODH receiving electrons and transfers electrons to hydrogenase through presumably four [4Fe-4S] clusters (Svetlitchnyi et al, 2001; Singer et al, 2006). Alignment of the duplicated two [4Fe-4S] cluster motifs from archaea agrees well with the sequences of CooFs in bacteria, such as *C. hydrogenoformans* and *R. rubrum* (data not shown).

To begin the structural mechanistic study of CO₂-reduction at cluster C, a system for production of a recombinant active CODHII from *C. hydrogenoformans* has been established in *E. coli*. While this is not the first case of the heterologous expression of CODH in *E. coli* (Roberts et al, 1989; Loke et al, 2000), this system provides a method to obtain highly active CODH comparable to the native enzyme using anaerobic expression with the help of co-expressed ISC proteins (Nakamura, 1999) for assembly and insertion of metal clusters in CODH. The main advantage of this expression system is the economical production of CODH using an *E. coli* strain compared to the native production of CODH in *C. hydrogenoformans* and the fast one-

step purification using a small volume of high capacity affinity material, preventing inactivation of the enzyme by oxygen exposure that is often happening during long time purifications.

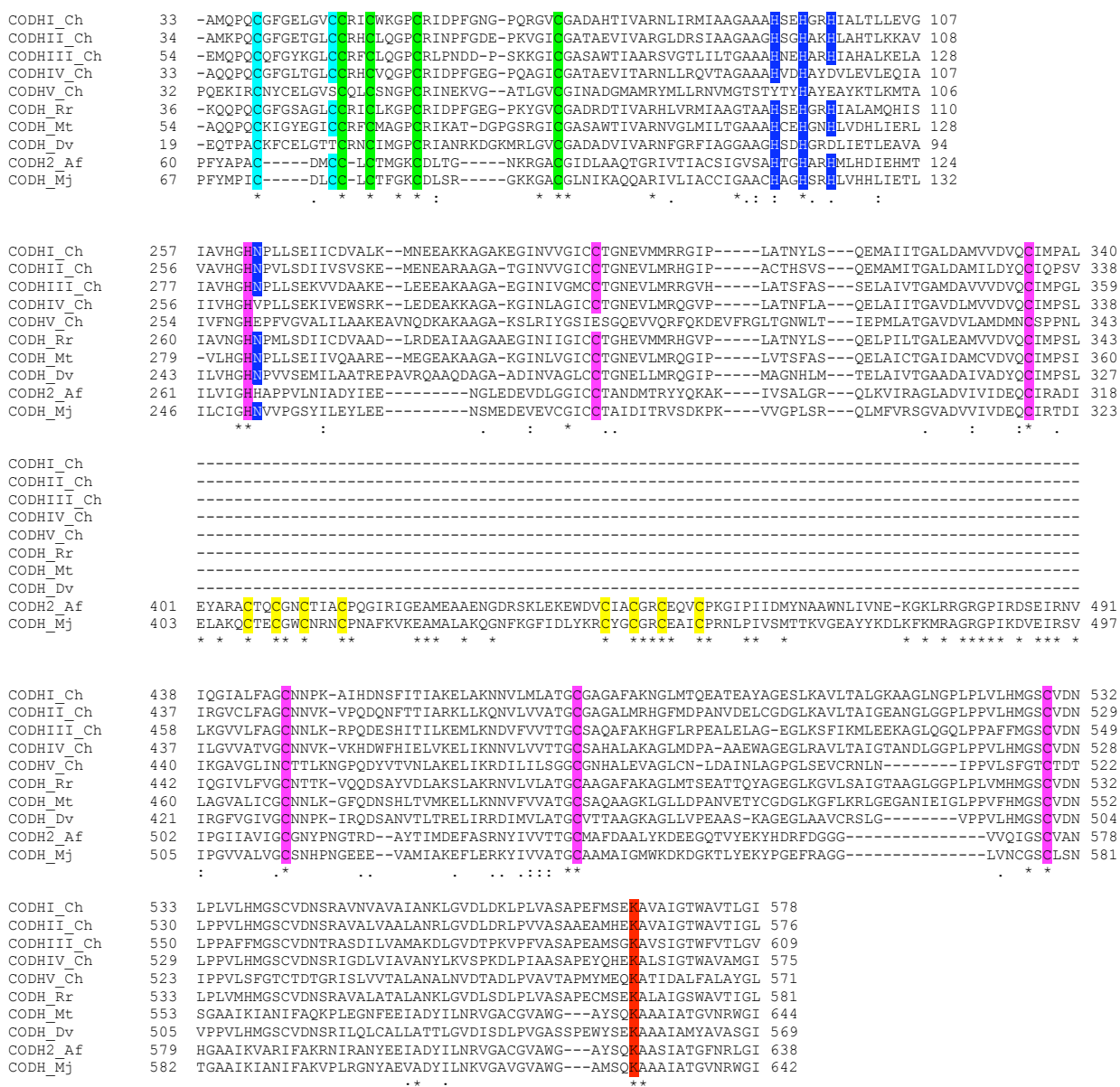


Figure 32. Alignment of amino acid sequences of CODHs. Only the regions with conserved residues coordinating the metals clusters identified structurally (Dobbek et al, 2001), a putative proton channel and lysine residue (Drennan et al, 2001; Lindahl, 2002) are shown here and highlighted in colored boxes: *turquoise*, cluster D; *bright green*, cluster B; *pink*, cluster C, *blue*, conserved residues in the putative proton channel and *red*, a conserved Lys for stabilizing intermediates. CODHs_Ch, CODHs (I-IV) from *C. hydrogenoformans* (Wu et al, 2005); CODH_Rr, CODH from the phototrophic hydrogenogenic bacterium *R. rubrum*; CODH_Mt, β -subunit of ACS/CODH from acetogenic bacterium *M. thermoacetica*; CODH_Dv, CODH from the sulfate-reducing bacterium *Desulfovibrio vulgaris*; CODH2_Af, α -subunit (CdhA2) of ACS/CODH from the sulfate-reducing archaeon *Archaeoglobus fulgidus*; CODH_Mj, α -subunit of ACS/CODH from the methanogenic archaeon *Methanococcus jannaschii*. Additional conserved two Cys-motifs, which can be expected to coordinate two [4Fe-4S] clusters found in archaea is shown and highlighted in *yellow*. Source of these sequences are from (Lindahl, 2002) and references are there in. Amino acids sequences were aligned with ClustalW (Chenna et al, 2003): *, fully conserved residues; : (colon), conservation of strong groups; . (period), conservation of weak groups.

Previous structural characterizations of CODHII isolated from *C. hydrogenoformans* identified a μ^2 -sulfido (μ^2 -S) ligand bridging Ni and Fe1 (See Fig. 4C) (Dobbek et al, 2001; Dobbek et al, 2004). The enzyme with high specific activities of $\sim 14,000$ units mg^{-1} was used for crystallization, as well as the activities of dissolved crystals. Therefore, it was postulated that the μ^2 -S ligand is essential for the catalytic CO oxidation at cluster C (Dobbek et al, 2001; Dobbek et al, 2004). However, observation that sulfide reversibly inactivated CODH_{Rf} and CODH_{Mt} , leading to short lag phases (Feng & Lindahl, 2004b), and no μ^2 -S ligands were identified in the crystal structures of CODH_{Rf} and CODH_{Mt} (Darnault et al, 2003; Drennan et al, 2001) argued the necessity of the bridging ligand for the catalysis. The presented structures of $[\text{NiFe}_4\text{S}_4(\text{OH}_x)/\text{CO}_2]$ clusters without μ^2 -S ligand in crystals with high specific activities (11,000 – 13,500 units mg^{-1}) showed that the μ^2 -S ligand is not required for catalysis. Furthermore, the μ^2 -S ligand occupies the binding site of two substrates (water and CO_2) of Ni,Fe-CODHs. The water/hydroxo ligand observed in -320 mV state requires the same coordination site at Fe1 as the bridging μ^2 -S ligand (Fig. A9), as well as that CO_2 demands the two open coordination sites of Ni and Fe1 for binding. Therefore, the μ^2 -S ligand bridging Ni and Fe1 is absent in catalytic competent enzyme species and can be reductively or chemically replaced, activating the enzyme. It is interesting to note that in the structures of cluster C containing a bridging ligand like CO_2 or the μ^2 -S ligand in the $[\text{NiFe}_4\text{S}_5]$ cluster (Fig. A9), Fe1 showed less structural heterogeneity with lower occupancies for Fe1B. This may be related to the "healing" effect of CO_2 (Anderson & Lindahl, 1996) and the higher specific activities of dissolved crystals after incubation with CO_2 (this work). The beneficial effect of a bridging ligand for Ni,Fe-CODHs activity may be an indication that the μ^2 -S ligand could have a physiological function in restoring or preserving the integrity of cluster C.

Binding modes and structural properties of metal- CO_2 complexes are well documented (Leitner, 1996; Aresta & Dibenedetto, 2007; Gibson, 1996). Coordination of CO_2 at the carbon atom results in a net electron transfer from the metal into the anti-bonding lowest unoccupied molecular orbital of CO_2 . This activation of CO_2 increases the negative partial charges at the oxygen atoms, which are stabilized by binding to electron-deficient centers like transition metals or by forming hydrogen bonds (Leitner, 1996). In the cluster C- CO_2 complex, Ni acts as the Lewis base, and Fe1 is the Lewis acid that together with K563 stabilizes the negative partial charge on O1. H93 contributes to the stabilization of the metal- CO_2 by forming a hydrogen bond with O2. The deviation from linearity along the O-C-O axis with angle of 133° (Tab. A10) is consistent with the activation of CO_2 by binding to cluster C.

The three structures described in this work offer direct evidence for the most important aspects of the reaction mechanism of Ni,Fe-CODHs (Figs. 21 and 33). The $[\text{NiFe}_4\text{S}_4\text{OH}_x]$ cluster determined in the -320 mV state is the functional state to activate CO and has the $\text{H}_2\text{O}/\text{OH}^-$ ligand identified spectroscopically in the C_{red1} state (DeRose et al, 1998). The Ni^{2+} ion is

positioned at the end of the substrate channel and its three sulfido ligands act as π -electron donors to the metal enabling CO to bind to the Ni^{2+} ion (Macgregor et al, 1994). The Ni^{2+} ion has two open coordination sites allowing either an apical binding of CO to form a distorted tetrahedral geometry or an equatorial CO binding to complete the square planar coordination geometry. Based on the structures of CO treated crystals of CODH_{Rr} and CODH_{Mt} , the authors proposed the apical binding of CO on the Ni^{2+} ion (Darnault et al, 2003; Drennan et al, 2001). However, modeling of CO in the apical positions places the carbon atom of bound CO more than 3.5 Å apart from the water/hydroxo ligand and makes further rearrangements necessary for the reaction to proceed as proposed previously (Volbeda & Fontecilla-Camps, 2005). In contrast, the equatorial CO binding in a distorted square planar coordination geometry of the Ni ion would result in a OC-OH_x distance of less than 2 Å (Fig. 33, step II). The binding of CO to a weakly π -electron backbonding metal like Ni^{2+} results in an electrophilic carbon atom and facilitates its reaction with the Fe1-bound water/hydroxo ligand to a metal-carboxylate species as observed in the $-600 \text{ mV} + \text{CO}_2$ state (Figs. 21B and 33, step III). The protein environment, specifically K563 and H93, further stabilizes formation of the metal-carboxylate intermediate. Product release may be assisted by the reversible ligand exchange of CO_2 against H_2O at Fe1 and is accompanied by a two-electron reduction of cluster C, generating the $\text{C}_{\text{red}2}$ state. The water/hydroxo ligand can be replenished through the water network (Fig. 22). The catalytic cycle as described mainly focuses on the Ni-Fe1 dyad whereas the function of the $[\text{Fe}_3\text{S}_4]$ site of cluster C is not directly obvious. A comparison of the $[\text{NiFe}_4\text{S}_4\text{OH}_x]$ with the $[\text{NiFe}_4\text{S}_4(\text{CO}_2)]$ state of cluster C reveals the positions of Ni and Fe1 to be largely unaffected by the presence or absence of the bridging CO_2 ligand (Fig. 22). The $[\text{Fe}_3\text{S}_4]$ site of cluster C appears to serve at least two functions: first, it provides a solid metal-sulfur frame in which Ni and Fe1 are integrated, thereby affording the necessary rigidity to keep both metals in place; second, it serves as an electronic buffer to compensate for the changes at Ni and Fe1 during the catalytic cycle. The small structural changes of cluster C agree well with the low reorganization energy expected for a reaction with turnover rates of $31,000 \text{ s}^{-1}$ and a k_{cat} (catalytic rate constant) / K_m (Michaelis constant) of $1.7 \times 10^9 \text{ M}^{-1} \text{ s}^{-1}$ at $+70^\circ\text{C}$ (Svetlitchnyi et al, 2001).

The structure-based mechanism outlined above agrees in all central aspects with the "bimetallic" mechanism proposed based on EPR-, ENDOR- and Mössbauer-spectroscopy (DeRose et al, 1998; Hu et al, 1996). Evolutionary models based on an autotrophic origin of life propose that the reduction of CO_2 on Ni^{2+} and $\text{Fe}^{2+/3+}$ containing minerals like greigite, which are structurally related to cluster C, were essential first steps in the generation of biological carbon compounds (Russell & Martin, 2004). The model for the catalytic CO oxidation/ CO_2 reduction in Ni,Fe-CODHs is based on neighboring Ni^{2+} and Fe^{2+} ions with open coordination sites. Although the protein matrix assists the channeling of CO/ CO_2 and water, the stabilization of carboxylate intermediate(s) and the transport of protons, it appears to be dispensable for CO oxidation/ CO_2

reduction at moderate rates since all essential functions like substrate binding/activation and turnover, and the two-electron/hydride uptake are mediated by cluster C. Consequently, reaction mechanisms similar to the reduction of CO₂ at cluster C may have promoted the beginning of life.

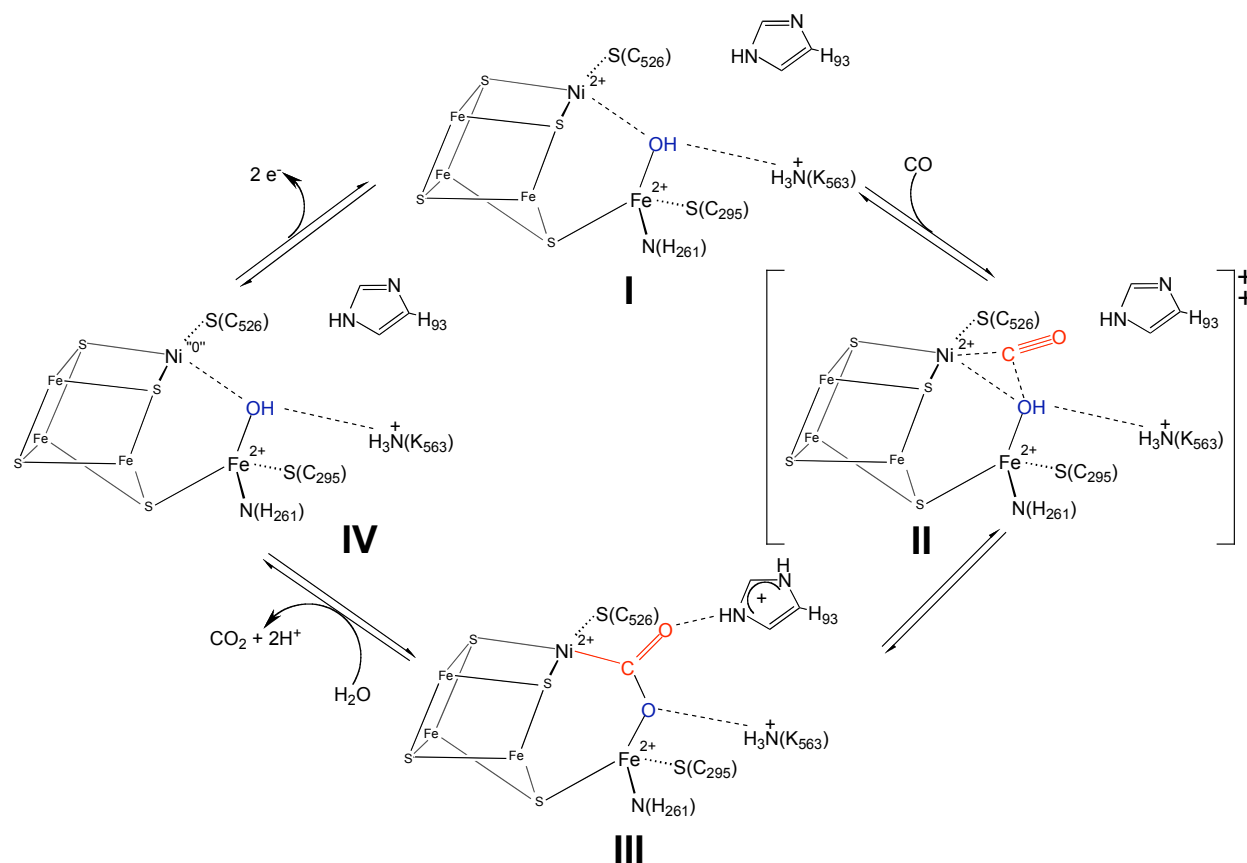


Figure 33. CO oxidation mechanism based on the three-redox states of cluster C. (I) The -320 mV state has been used as model for $C_{\text{red}1}$, the state of cluster C competent of CO oxidation. (II) The proposed transition state of the reaction in which CO binds to the Ni²⁺ ion and reacts with the Fe1-bound OH group. (III) The -600 mV+CO₂ state is used as a model for the stabilization of the metal carboxylate state. (IV) The -600 mV state is used as a model for the $C_{\text{red}2}$ state, which is supposed to contain two additional electrons compared with the $C_{\text{red}1}$ state, denoted as a formal change of the oxidation state of the Ni²⁺ ion. Picture is taken from the reference (Jeoung & Dobbek, 2007).

The remaining question where two electrons reside transiently in the $C_{\text{red}2}$ state of cluster C is elusive and different solutions have been proposed. The [3Fe-4S] subsite of cluster C adopts a comparable geometry to a [4Fe-4S] cluster and appears as a candidate for the uptake / donation of electrons within the sub-cluster. However, Hu *et al.* observed only small differences between $C_{\text{red}1}$ and $C_{\text{red}2}$ by Mössbauer spectroscopy, arguing against larger electronic changes in the sub-cluster (Hu *et al.*, 1996). The Ni ion might act as electron acceptor (Volbeda & Fontecilla-Camps, 2005). However, this proposal is not supported by EXAFS spectroscopy, which did not show changes of the Ni K-edge upon reduction of cluster C (Gu *et al.*, 2004). In

analogy to the industrial water-gas-shift reaction shown in Fig. 2, a hydride species could act as intermediary two-electron sink during the oxidation of CO at cluster C. The absence of a clear ENDOR signal for a metal hydride is so far taken as indicator that hydride formation is not part of the mechanism of CODH (DeRose et al, 1998). However, the weak hydrogen-evolving activity of reduced CODH would be in agreement with intermediary hydride formation. Further investigations will be needed to determine the storage form of the two additional electrons distinguishing $C_{\text{red}2}$ from $C_{\text{red}1}$.

2. Substrate and Product Transfer Pathways in CO Dehydrogenase

CODHII uses a $[\text{NiFe}_4\text{S}_4\text{OH}_x]$ cluster to oxidize CO to CO_2 at the rate of $31,000 \text{ s}^{-1}$ (Fig. 33). In addition to a rigid metal cluster to support such a high turnover rate, CODH requires efficient routes to replenish substrates, CO and water, and to release products, CO_2 , electrons and protons (Eq. 2). A hydrophobic CO channel has been identified in bifunctional ACS/CODH_{Mt} (Doukov et al, 2008), which consists of mainly hydrophobic residues and spans 138 Å from cluster C of the CODH β -subunit (CO generation) to cluster A of the CODH α -subunit (acetyl-CoA production) to allow for intermolecular CO transport. However, monofunctional CODHs are less conflicting in substrate/products routes as the reversible CO oxidation occurs in the monomer. Cavity calculation with the first CODH structure of *C. hydrogeniformans* suggested a putative hydrophobic CO channel in the COOH-terminal domain of the protein, which points to the apical coordination site of the Ni ion (Dobbek et al, 2001). Dobbek and co-authors also found a hydrophilic positively charged cavity filled with water molecules near the subunit interface. However, a putative water channel found in this study is placed in opposite direction to that of Dobbek and co-authors (Dobbek et al, 2001) and directly ends at a water/hydroxyl ligand on the Fe1 site (Fig. 34). Although there is no conclusive data to prove this, the fact that the residues involved in this linear pathway are conserved in most CODHs and are located roughly in a line between cluster C and the protein exterior supports this finding. After CO-oxidation, CO_2 , electrons and protons should leave the protein. The gaseous product CO_2 might exit through the channel found to connect cluster C and C' (Tan et al, 2006) or released through a hydrophilic channel near the CODH dimer interface (Dobbek et al, 2001). Observations of the abolished activity and structurally invariable cluster C of H96D CODHII reported in this study supports the previous mutagenesis studies of CODH_{Mt} on proton channel histidines (Kim et al, 2004), suggesting that protons pass through this putative proton channel in CODH. As the final step of the CO-oxidation reaction, two electrons are presumably transferred from cluster C via cluster B and/or D to an external electron acceptor, polyferredoxine CooF (Lindahl, 2002). However, at this stage, all hypotheses for substrate/product channels described have not been

substantiated and more experimental evidences are necessary using the biochemical and structural analysis of mutants.

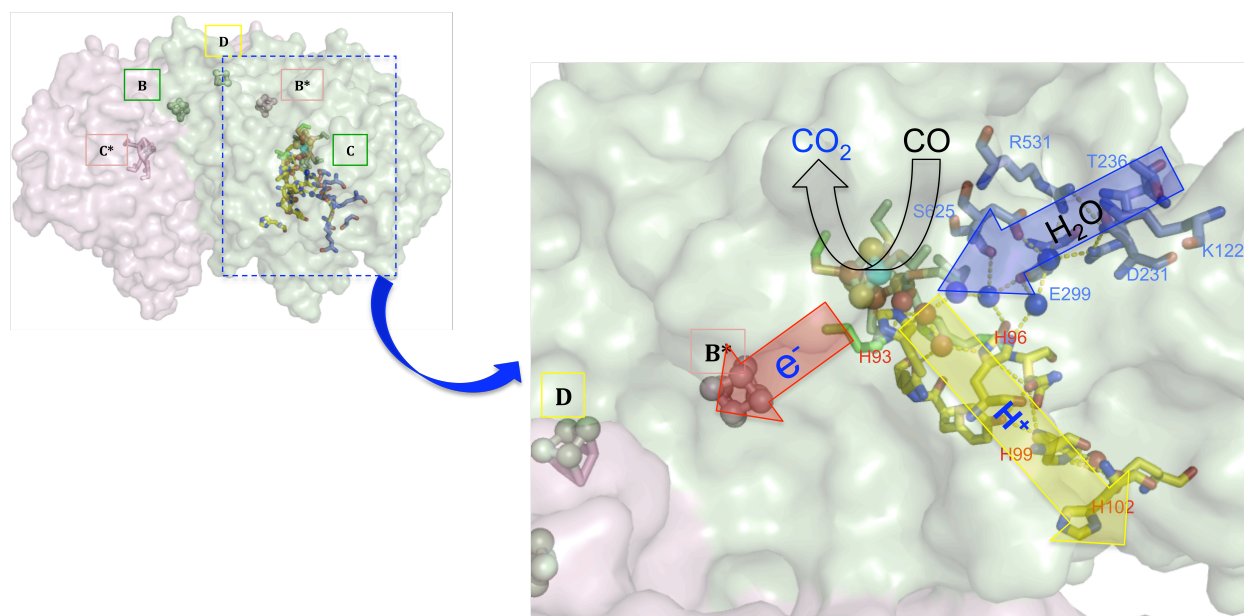


Figure 34. Surface presentation of the water and proton transfer pathways in CODHII. Figure 23A (proton transfer) and 23C (water transfer) are shown as surface model. Residues involved in water and proton channel are shown in *blue* and *yellow*, respectively. Each monomer is depicted in a different color.

3. Implications of Cluster C-missing CO Dehydrogenase

Heterogeneity of cluster C of CODHs from different organisms have been reported in several cases depend on the history of the sample (Lindahl, 2002). Hu and co-authors suggested that this heterogeneity is originating from multiple binding modes of the Ni, which was supported by observations of mixed and homogeneous spin quantitations of cluster C of wild-type and Ni-deficient CODH, respectively, by EPR spectroscopy (Hu et al, 1996). However, the movement of His261 to coordinate Fe1B in cluster C-missing CODH in this study (Fig. 23) and the observation of an alternative position of Fe1 (Fe1B) in this study (Tab. A8) together with the previous report (Dobbek et al, 2004) suggest that the heterogeneity of cluster C may originate from dual conformations of Fe1, and may depend on the occupation of the Ni position.

The biosynthesis of proteins containing metal clusters requires the complex function of specific accessory proteins. It was surprising that CODH containing such complex metal clusters (cluster B, C, and D) can be expressed heterologously in *E. coli*, although it does not naturally contain CODH. However, the heterologous expression of cluster C-missing Rec-CODHII in *E. coli* is not surprising result. It is assumed that *E. coli* does not have specific machinery for

cluster C assembly, but it does assemble and insert conventional [4Fe-4S] of cluster B and D using the ISC (Nakamura, 1999) or SUF machinery (Takahashi & Tokumoto, 2002). The next intriguing question aroused about how cluster C was assembled *in vivo*, especially how nickel is inserted in the cluster. HypB, a homolog of CooC and AcsF, is involved in inserting Ni into the Ni-Fe hydrogenase in *E. coli* (Hausinger, 1997). However, expression of ACS_{Ct} in an *E. coli* strain lacking HypB produced active protein as long as nickel is supplemented during growth, suggesting that HypB was not a surrogate for AcsF to insert Ni into cluster A (Loke & Lindahl, 2003). Ni-deficient CODH from *R. rubrum* (Jeon et al, 2001) and AcsAB from *C. thermoaceticum* (Loke et al, 2000) were activated simply by incubating the enzymes with Ni²⁺ *in vitro*. High concentration of Ni ions in the growth media of *E. coli* might overcome the requirement of a specific Ni-insertion system for cluster C and A of CODH and ACS. Successful expression and crystallization of the cluster C-missing Rec-CODHII, similar to the wild-type protein, provides at least two implications. Firstly, it supplies a prototype structure for studying cluster C assembly by meaning of *in vitro* metal cluster reconstitution. Secondly, it implies that *E. coli* might be capable of production of Ni-deficient CODH, which again provides a tool to study the role of CooC in Ni-insertion of cluster C. As a begin of investigation how cluster C is assembled, the isolated CooC1, a nickel-binding ATPase, was characterized biochemically and structurally, as discussed below.

4. CooC1 is an ATPase

Display of the nucleotide hydrolysis is common in homologous proteins of CooC involved in diverse biological functions: metalcenter assembly, cell division and electron transfer. As-isolated CooC1 is intrinsically an ATPase and a monomer (32 kDa) in solution. These properties are in contrast to *R. rubrum* CooC (Jeon et al, 2001), which is a homodimer in solution (61 – 63 kDa) with an approximately 15-fold higher ATPase activity than CooC1. Conversely, the ATPase activity of AcsF from *C. thermoaceticum* (Loke & Lindahl, 2003), the putative Ni-insertase of ACS and a homologue of CooC2_{Ch} (Fig. 26), was similar to those observed in CooC1, with low ATPase activity and no GTP hydrolysis activity. While NifH of *A. vinelandii* (Ryle & Seefeldt, 2000) and HypB of *E. coli* (Maier et al, 1995) are NTPases, HypB protein from *Bradyrhizobium japonicum* (Fu et al, 1995) hydrolyzes GTP but not ATP. GTPases of the Mrp/MinD family of the SIMIBI class show a highly conserved NKXD motif, which is not present in ATPases of this class. In a GTP_γS-bound HypB structure from *Methanocaldococcus jannaschii*, a carboxylate group of aspartate in the conserved NKXD motif stabilizes N1 and an amide group of the guanosine moiety (Gasper et al, 2006). A sequence alignment shown (Fig. 26) that N191 and K192 of CooC1 are conserved among CooC proteins, which interact with the adenosine moiety in ADP-bound structures of CooC1, but the last aspartate is not conserved in

CooC homologues. This could explain why CooC1 does not show GTP hydrolysis activity, albeit very poorly in CooC_{Rr}, which is unable to stabilize the binding of GTP. The difference in ATPase activity between CooC_{Rr} and CooC1 might arise from different temperatures used in activity measurements as *C. hydrogenoformans* grows at 70 °C (Svetlitchnyi et al, 2001) and CooC1 is a thermostable protein with an approximate melting temperature of 68 °C. The observed low ATPase activity of CooC1 is a typical feature of nucleoside-dependent proteins like HypB (Gasper et al, 2006), MinD (Ma et al, 2003), Soj (Leonard et al, 2005) and NifH (Bulen & LeComte, 1996), which bind to and stabilize other proteins in conformations required for subsequent processing. Acceleration of ATP hydrolysis of CooC1 may occur only when the protein meets its appropriate protein substrate, which is not yet identified, or this acceleration may be not required for CooC1. This is still an open question for future investigations. Despite of using different nucleoside triphosphate of the CooC homologous proteins, there is a common feature that their nucleotide hydrolysis is related to their diverse cellular functions in cell segregation, electron transfer and metallocenter assembly processes.

5. CooC1 is a Nickel-Binding Protein

In nature, various proteins are capable to bind metal ions. Proteins, for examples metalloregulatory proteins, metalloenzymes, and metallochaperones, bind metal ions nearly exclusively via coordination by three types of atoms, sulfurs (Cys and Met), nitrogen's (His), and oxygen's (Asp and Glu). Various spectroscopic and magnetic methods are applied to study these coordination structures in combination with protein crystal structures.

CooC is an essential protein for the activation of Ni-deficient CODH *in vivo* (Jeon et al, 2001), where strains carrying a deletion or P-loop mutations in the *cooC* gene required an elevated concentration of nickel in the grow media to grow with CO as carbon source. However, there was no direct evidence whether CooC can bind nickel *in vivo* and *in vitro* up to date. In the present study, the nickel-binding property of CooC1 was investigated using UV-vis spectroscopy. The most surprising result is that CooC1 binds Ni, which was not observed in the previous study of CooC_{Rr} and AcsF_{Ct} (Jeon et al, 2001; Loke & Lindahl, 2003). CooC1 can bind one nickel per dimer under reducing conditions in the absence of dioxygen with nanomolar affinity (Fig. 17). A spectroscopic investigation of Ni-binding to CooC1 showed a characteristic band for an S⁻(Cys) to nickel LMCT. In addition, the involvement of cysteine residues for binding of nickel is supported by the high sensitivity to rapid oxidation leading to an inability to bind nickel and resulting in various oligomeric states via formation of disulfide-bridges in absence of reducing agents. Although the structures of Metal-bound states of CooC1 could not directly show the Ni-binding site and coordination geometry of the Ni ion, the highly conserved CXC metal binding motif among CooC proteins (Fig. 26) together with the biochemical studies

suggest that this cysteine motif is responsible for nickel binding. Metallochaperones use cysteine motifs to chelate metal ions in metal delivery or insertion during maturation processes. The most prominent CooC homologue with a function in Ni-insertion is HypB from *E. coli*, which is involved in Ni-assembly of Ni-Fe hydrogenase and possesses two metal binding sites with high and low affinity for Ni (Leach et al, 2005). HypB from *E. coli* is differing from archeal HypB proteins, the former contains an N-terminal CXXCGC motif comprising the high-affinity Ni-binding site with sub-picomolar affinity and the later lacks this motif. Both HypB proteins have a similar metal binding motif (CHX_nC) that is the second weak binding site in the G-domain of *E. coli* HypB. The structure of archeal HypB from *M. jannaschii* showed that this motif binds two Zn ions by forming the dimer interface (Gaspar et al, 2006). Mutational and spectroscopic Ni-binding studies identified that *E. coli* HypB binds to nickel by this conserved cysteine motif (Leach et al, 2005). The cysteine-containing metal-binding motif is also found in the copper metallochaperone (CCS) of Cu-Zn superoxide dismutase (SOD) (Lamb et al, 2001), which contains a CXXC motif in domain I and a CXC motif in domain III. Structural and *in vivo* studies suggested that the domain I motif is not essential while the domain III CXC motif might contribute to deliver Cu ions to the SOD active site (Lamb et al, 2001) (Rosenzweig, 2002). However, metal-bound structures of *E. coli* HypB and CCS have not been reported yet. The metal ion selectivity of metal-binding proteins is at least partly achieved by the coordination number/geometry of the metal-protein complex (Pennella et al, 2003), and by ligand selection (Iwig et al, 2008). The question how CooC1 selectively binds nickel should be further examined. The assembly of the nickel-center in Ni-Fe hydrogenase and urease is a complex process requiring many accessory proteins (Hausinger, 1997). Although *R. rubrum* CODH needs at least three proteins, CooCTJ, for the activation of Ni-deficient CODH_{Rr} *in vivo* (Jeon et al, 2001), *C. hydrogenoformans* does not contain homologues of CooT and CooJ proteins in the genomic DNA (Wu et al, 2005). Regardless of involvement of different complexes of accessory proteins, all Ni-assembly systems require two common related events, a nickel-binding and a nucleotide-binding/hydrolysis. The present study showed that the presence of ATP or ADP influenced the Ni-binding characteristic of CooC1 (Fig.18). ADP-binding of CooC1_{Ch} lead to a similar Ni(II)-affinity as that in the absence of ADP but decreased the binding capacity. However, upon binding of ATP, without hydrolysis due to the absence of Mg (Fig. 15B), CooC1 showed an increase in K_d and a decrease in binding capacity for Ni(II). The results indicate that the two binding processes, Ni- and ATP-binding, are tightly connected even though with opposing effects, and that the binding of ATP itself is not sufficient to release Ni. Although the influence of ATP hydrolysis on Ni-binding was not examined in the present study, it can be assumed that the hydrolysis leads to a dramatic change in the Ni-binding/releasing event. It is postulated that CooC requires an additional factor that activates ATP hydrolysis, likely in the

stimulation of ATP hydrolysis in MinD and NifH by MinE and Mo-Fe proteins, respectively, and should be further investigated.

A

```

CooC1_Ch -----MKLAVAGKGGVGRKTTVAAGLIKIMASDYDKIYAVDGGPDSCLGQTLGLSIEEAYAITPLIEMKDEIREKTGD---GGLLILNP: 80
CooC_Rr -----MKIAVTCKGCVGRSTIVGMLARALSDGWRVMAIDAPDANLASAIGVPAERLSALLPISKMTGLARERTGASETTGTHFILNP: 84
MinD -----MGRIIISIVSGKGGTGTVTANLSVALGDRGRKVLAVDGG-----LTMANLSVLGVDDPDVTLHD-----VLAG: 65
Soj MLRAKVRRIALANCKGGVGRKTTTAINLAAYLARLGRVLLVDL-----PQGNATSGLVRAERG-----VYHL: 64
NifH -----AMRQCAIYCKGCGKSTTTQNLVAALAEMGKVMIVGCG-----PKADSTRLLIHSKAQNTIMEMAA-----EAGT: 66
                P-loop                               Switch I

CooC1_Ch KVDGDLDKYGRYIDDKIFLIRMGKIEIKKGGSCCMRENSFLGSVVSALFLDK-KEAVVMCMGAGIEHLTRGTAKA---VDMMAVIEPNLNS: 167
CooC_Rr RVDDIPEQFCVDHAG-IKLLMGTVNHAGSGCVGPEHALVRTLLRHILTKR-KECVLIDMEAGIEHFGRGTIEA---VDLLVIVIEPGSRS: 170
MinD EANVEDAIYMTQFDN--VYVLPQAVD---WEHVLKADPRKLPEVIKSLKDK-FDFILIDCPAGLQDAMSAMLS---GEEALLVTNPEISC: 147
Soj LQGEPLLEGLVHPVDG--FHLLPATPDLVGATVELAGAP---TALREALRDEGYDLVLLDAPPSPSPLTLNALAA---AEGVVVVPQAEYYA: 147
NifH VEDLELEDVLKAGYGGVKCVESGPEPGVCAGRGVITAINFLEEEGAYEDDLDFVFDVLDGVVCGGFAMPIRENKAQEIVIVCSGEMMA: 157
                Switch II

CooC1_Ch IKTGLNIEKLAGDLG-----IKKVRYVINKVRN---IKE--EKLIKHLPEDKILGIIIPYNELFIELSLKGEIHWQSTNPFAVNLHDIYQ: 247
CooC_Rr LQTAAQTEGLARDLG-----IKTICHIANKLAS---PVD--VGFILDRADQFDLLGSIPEFDSAIAQADQAGLSCYDLSFACRDKAHALMA: 250
MinD LTDTMKVGIVLKKAG-----LAILGFVLRVRYGR---SDRDIPPEAAEDVMEVPLLAVIDPEDPAIREGTLEGIPAVKYKPEP--KGAKAFV: 230
Soj LEGVAGLLATLEEVRAGNPRRLRLGLVVTMYDGRLLAQQVEAQLRAHFGEKVFWTVIPRNVRLAEAPSFCKTIAQHAPTS--PGAHAYR: 236
NifH MYAANNISKGIVKYAN--SGSVRLGGLICNSRNT---DREDELI IALANKLGTQMIHFVPRDNVVQRAEIRRMTVIEYDKA--KQADEYR: 241
                *

CooC1_Ch KLRLEVG-----: 254
CooC_Rr ALLERVGPTQGV-----: 263
MinD KLAEEIEKLA-----: 240
Soj RLAEEMARVQEAGS-----: 251
NifH ALARKVVDNKLVLIPNPITMDELEELLMFEGIMEVEDESIVGKTAEV: 289

```

B

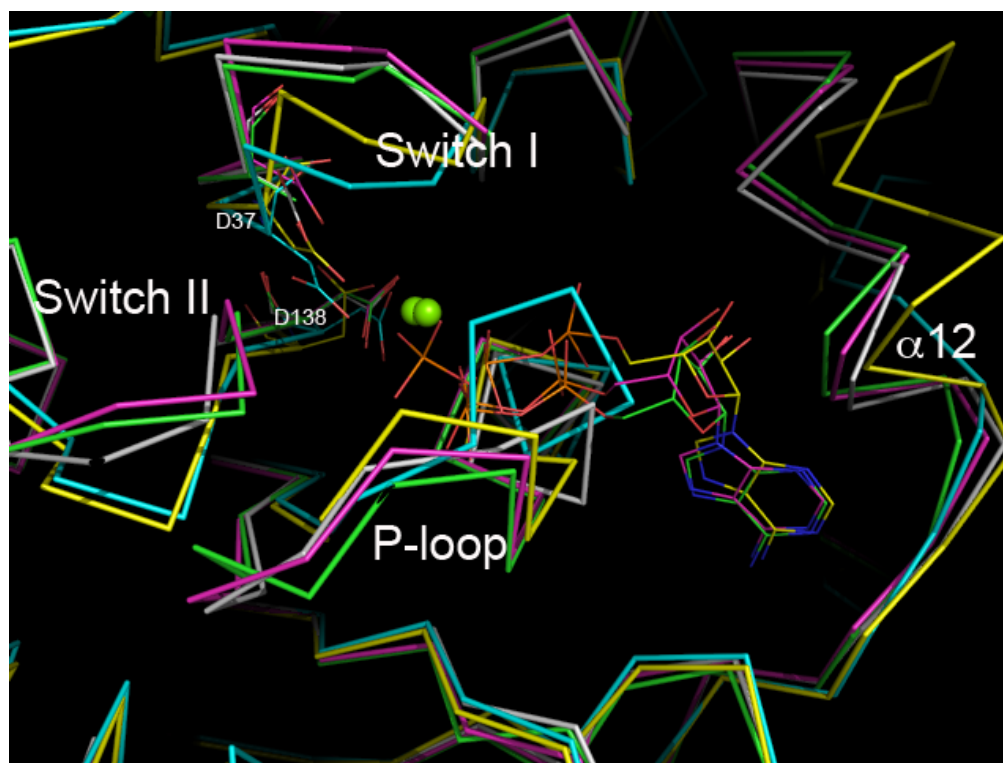


Figure 35. (A) Amino acid sequence alignment of CooC1 with its homologues in the SIMIBI class NTPases. Conserved sequence motifs, P-loop, switch I and II, are underlined. The signature lysine is shaded in *green*, CXC motif marked in *blue*, and conserved D37 and D138 residues (numbering by CooC1) in *red*. A conserved Asn found in NKxD for GTP specificity of GTPases is labeled with a star. Amino acids sequences were aligned with ClustalW (Chenna et al, 2003) and manually modified as identity in box: 100%, *black*; over 85%, *dark-gray* and over 70%, *light-gray*. (B) Comparison of the nucleotide binding sites of CooC1 structures to Soj structures by superposition of the main chain using COOT (Emsley & Cowtan, 2004). Soj-ATP is shown in *green*, Soj-ADP in *pink*, Soj-apo in *gray*, CooC1-apo in *cyan*, and CooC1-ADP in *yellow*. Mg^{2+} ion is shown in *green* sphere. Nucleotides are shown in line with the element color of corresponding proteins.

6. CooC1 undergoes Ni- and Nucleotide-Dependent Dimerization

The present study revealed that CooC1 forms a dimer to coordinate a Ni ion by the four conserved cysteines in a CXC motif from each molecule, which was identified by gel filtration (Fig. 20) and supported by one nickel binding site per dimer (Fig. 17). Structural analysis of the metal-binding site in CooC1 confirmed that the conserved CXC motif promotes metal-dependent dimerization between CooC molecules by forming a tight dimer interface in the metal-binding site, while leaving nucleotide-binding site in an open state (Figs. 25C and D). Inter-molecular bridging via cysteine-mediated metal coordination plays an important role in structure and function and is often found in metalloproteins and metal-binding proteins. For example, CODH (Dobbek et al, 2001) and NifH (Schindelin et al, 1997) form a dimer via covalent-linkage through of a [4Fe-4S]. Crystal structure of Rad50 protein (an ABC type ATPase involved in DNA recombination and repair) showed that a conserved CXXC motif in a hook shape domain dimerizes by binding to a Zn ion, which tethers two DNA molecules in the Mre11 complex (Wiltzius et al, 2005; Hopfner et al, 2002).

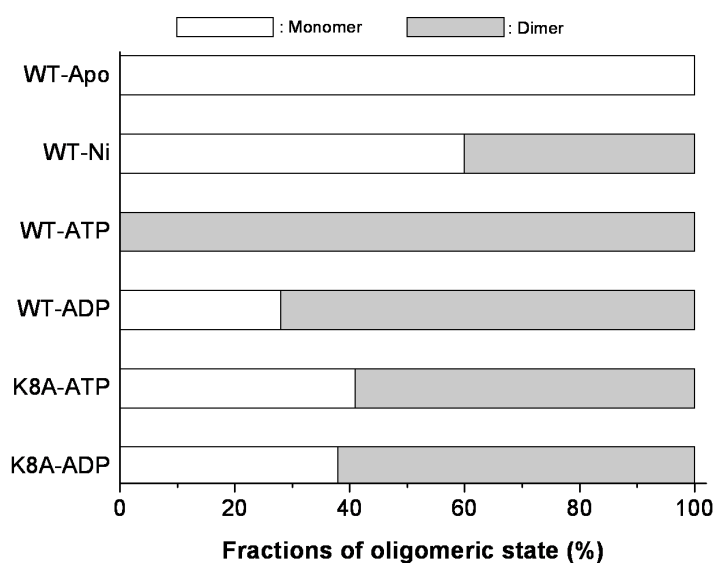


Figure 36. Fractions of monomeric and dimeric states of CooC1 from the gel filtration experiments.

However, gel filtration experiment of CooC1 (Fig. 36) showed that the protein is in an equilibrium between monomer and dimer in the presence of ADP, while it forms a stable dimer in the presence of ATP. CooC1 carrying a mutation in the signature lysine (K8A) showed a completely abolished ATPase activity and behaves similarly to the ADP-bound wild-type protein regardless of nucleotides bound. The mixture of monomeric and dimeric states of ADP-bound CooC1 observed by analytic gel filtration suggests that the ADP-bound CooC1 crystal structure shows only one out of several existing conformational states in solution. This is also in

agreement with small dimer interface formed by the weak hydrogen-bonding interaction of a β -strand in the cpa-loop (Fig. 25B). Structures of CooC1 homologues in the MinD family did not show big conformational changes for the nucleotide binding motifs independent of the binding of ATP, ADP, or ATP-analogues (Fig. A13). The structures of Soj protein either with ADP or ATP, or without bound nucleotide showed that the switch regions are not changed upon binding of different nucleotides. This is similar to what we observed in CooC1 structures of Apo-, ADP-, and Metal/ADP-bound structures, where the conserved aspartate residues in switch I and II regions (Asp₃₈ and Asp₁₃₈) are also structurally conserved (Fig. 35B).

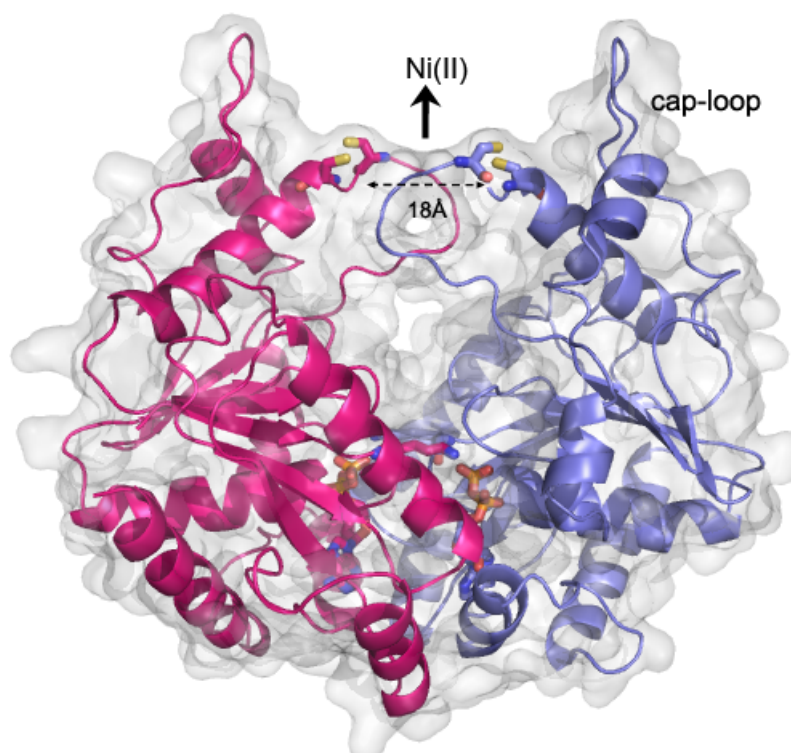


Figure 37. Model structure of ATP-induced dimer CooC1 with surface presentation generated by a superposition of a monomer of Metal/ADP-bound CooC1 to the Soj dimer structure (Leonard et al, 2005) by COOT (Emsley & Cowtan, 2004). Cysteines in the Metal-binding CXC motif, the signature lysine and ADP are shown as sticks with element color according to corresponding molecule. The distance in the open form of the MBS was measured between C α -carbons of Cys₁₁₄.

Based on the similarity of primary sequence with absolutely conserved signature lysine and structure in nucleotide binding motifs (Walker A, switch I, and switch II motifs shown in Fig. 35A and B), CooC1 could form a similar ATP-induced dimer as previously reported structures of NifH (Schindelin et al, 1997) and Soj (Leonard et al, 2005). Since NifH is a covalent dimer formed by an iron-sulfur cluster independent on ATP binding, the structure of Soj was used to model the ATP-induced CooC1 structure (Fig. 37). In this model structure, the highly conserved signature lysine is directed to the position of the β -phosphate of ADP in the other molecule. A striking conformational change was observed in the regions of the MBS and cap-loop. The ATP-driven dimer structure of CooC1 opens the metal-binding site by approximately 18 Å in contrast

to the structure of the Metal-bound state, which opens the nucleotide binding site. Additionally, the flexible cap-loops stand to open a gate that presumably transfer Ni to a partner since the other side (bottom of MBS) are closed. The observation that the binding of ATP or ADP to CooC1 in solution did not show any significant change in the secondary structure (Fig. 19) and the ATP-driven dimerization, suggests that CooC1 changes conformation upon binding/hydrolysis of ATP by opening the MBS site, while closing the nucleotide-binding site, or *vice versa* to bind Ni.

7. Functional Model for Ni-Processing of CooC1_{Ch}

Based on the structures of CooC1 observed in this study and a model structure of an ATP-induced dimer together with biochemical data presented, a functional model of Ni-processing by CooC in the assembly of cluster C of Ni,Fe-CODH can be postulated (Fig. 38). CooC1 is present as monomer in the absence of any ligand (Fig. 38, state-I), Once Ni(II) is available in solution, CooC binds to Ni(II), forming a Ni-induced dimeric structure (Fig. 38, state-II), in which the cap-loop is protecting the bound-Ni by shielding the MBS. The results of Ni-titration in the presence of ADP and the structure of Metal/ADP-bound CooC1 suggest that ADP-bound CooC (Fig.38, state-V) also is able to bind Ni(II), but this is not a fully competent state for Ni-binding. Even though the Ni-binding site is not clearly identified by the presented structures of CooC1, spectroscopic and gel filtration data support a dimer conformation by Ni-binding with an open nucleotide-binding site. It is not yet fully understood how CooC binds selectively Ni(II), but it is speculated that a square planar coordination geometry, which is mainly found for stable low spin Ni(II) complex in metalloproteins (Rulisek & Vondrasek, 1998), would be supportive. To release Ni(II), ATP binds to CooC1 and leads to a conformational change driving dimerization (Fig. 38, state-III). However, ATP-binding itself is not sufficient to release Ni(II) efficiently, which was shown in Ni-titration of CooC1 in the presence of ATP (this study) and ATP-hydrolysis dependent activation of Ni-deficient CODH_{Rf} by CooC_{Rf} (Jeon et al, 2001). The ATP hydrolysis of CooC might provide free energy for a conformational change, Ni-insertion, and subsequent dissociation of the protein from a partner protein. It is believed that concomitant ATP hydrolysis with acceleration completely releases and transfers Ni(II) to a partner (Fig. 38, state-IV). However, whether interaction of CODH and CooC occurred directly or indirectly through additional unknown factor is still elusive. While the details of metal insertion are also unclear, an intermediate involving cysteines from the CXC motif of CooC and the metal accepting ligands in CODH interact to transfer the metal to the active site of CODH. Dimerization and activation of ATP hydrolysis by interacting partner are common events found in proteins of the MinD family in the SIMIBI class. Soj dimerizes upon binding to ATP, while the stimulation of ATP hydrolysis

does not occur until it is in contact with the interacting protein SpoJ (Leonard et al, 2005), similar to the MinD ATPase that requires MinE (Ma et al, 2003).

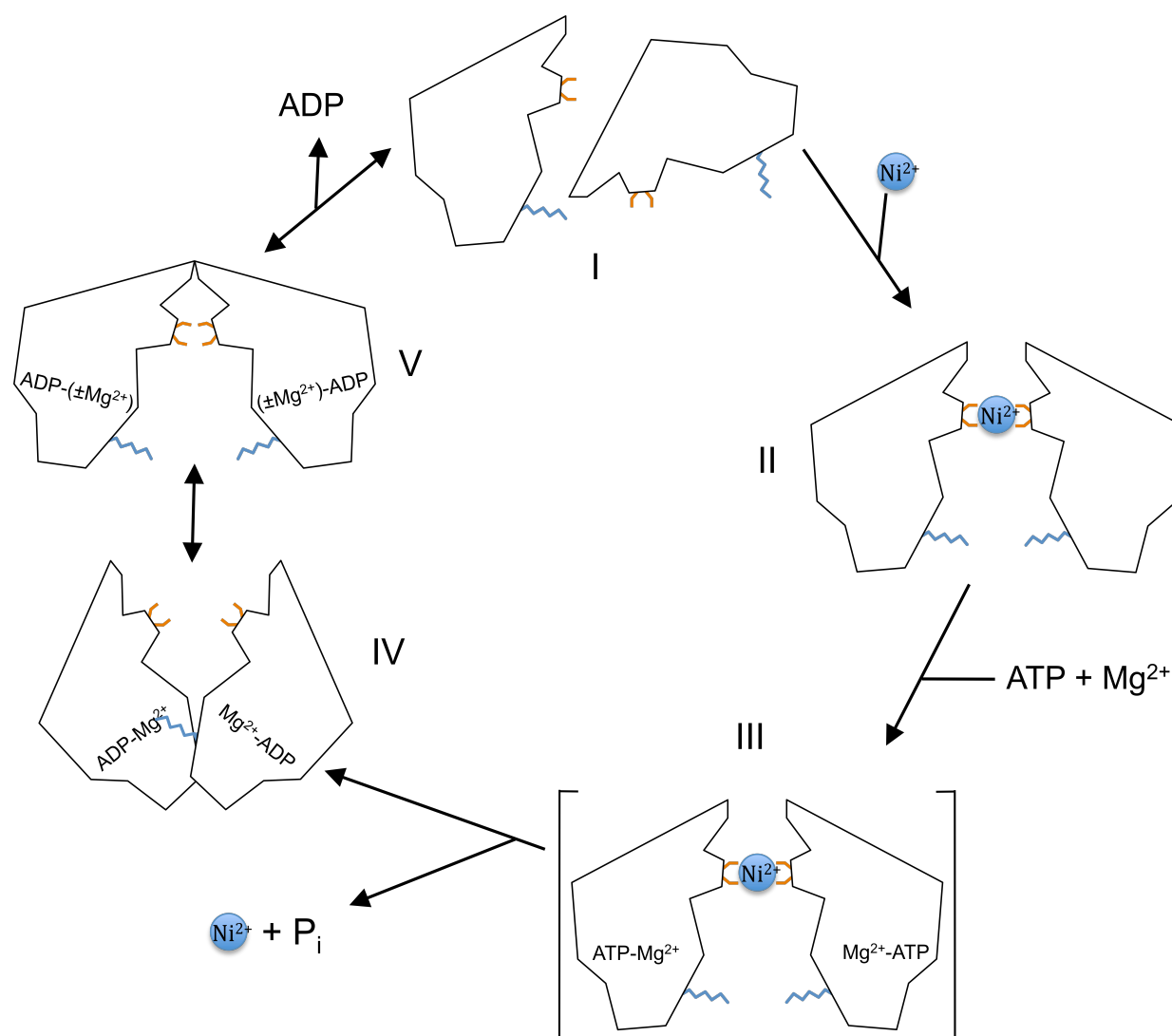


Figure 38. Functional model of CooC1 during Ni-processing. (I) Monomeric state of CooC1 in the absence of nickel has been modeled from the structure of Apo-CooC1 and results from gel filtration. (II) The structure of Metal-bound CooC1 is used as a model for the Ni-bound dimer. (III) Transition state of dimer where ATP and Ni(II) are bound to CooC1. (IV) ATP hydrolysis releases Ni(II) and forms a dimer that is drawn by modeling of an ATP-driven dimer of CooC1. (V) An equilibrium state dimer form between ATP-driven dimer and monomer, which was modeled from the structure of ADP-bound CooC1. The cysteines in the Cys-X-Cys motif are shown in *orange* and the signature lysine in *blue*.

NifH is the iron protein of the nitrogenase complex that catalyses the ATP-dependent reduction of nitrogen. NifH alone does not catalyze ATP hydrolysis at appreciable rates. Bound to the MoFe proteins, hydrolysis is accelerated (Bulen & LeComte, 1996). Based on the striking similarities between CooC and those proteins and the very low rate of ATP hydrolysis even under conditions of dimer formation, a similar missing factor can be expected for CooC1. After releasing Ni(II), CooC might undergo three different conformational changes (Fig. 38, states-IV, -V, and -I) depending on affinity to ADP. While low nucleotide affinities with dissociation

constants (K_d) in the micromolar range are common for the SIMIBI class proteins, where nucleotide exchange is not required for catalytic activation, the TRAFAC class proteins possess high affinities for nucleotide with picomolar to nanomolar K_d , which require a nucleotide exchange factor *in vivo* (Gasper et al, 2008). *E. coli* and *M. jannaschii* HypB proteins, members of the SIMIBI class, showed dissociation constants for GDP and GTP in the micromolar range, and they have affinities that are much lower than those found in most Ras proteins. CooC_{Rf} showed an even lower affinity for ATP (Jeon et al, 2001), indicating that this type of proteins can in principle freely exchange nucleotide without the help of nucleotide exchange factors.

OUTLOOK

The result of heterologous expression system of CODHII in *E. coli* is greatly advantageous for the future at least in three purposes. First, it affords a useful tool to study different CODHs that are difficult to obtain from the native microorganisms. Numerous bacteria and archaea contain CODHs (Lindahl & Chang, 2001) for their survival in CO-rich environments. Comparisons of structural and biochemical properties of CODHs could be interesting in the future research. The genome of *C. hydrogenoformans* encodes five CODHs of which three (CODHI-III) have been isolated from *C. hydrogenoformans* (Svetlitchnyi et al, 2001) (Svetlitchnyi et al, 2004). Two additional CODHs (CODHIV and CODHV) have not been described and may only be expressed under specific conditions or with low abundance. As the sequence and genetic context of CODHIV and CODHV sets them off from the other three CODHs of *C. hydrogenoformans*, different properties and biological functions for them can be expected.

Second, it provides a convenient method for the production of site-directed mutants, which can be used in spectroscopic and/or crystallographic studies about the detailed function of the individual metal centers, especially at clusters B and D, and ways of exploring channels required in CO-oxidation by CODH, such as how substrates are coming and products are leaving. The missing structure in the CO-oxidation mechanism of CODH is how CO interacts with cluster C. Due to the fact that CO-oxidation by CODH is extremely fast ($31,000 \text{ s}^{-1}$), inhibitors, which are structural and chemical analogous of CO like cyanide and mutations allowing to stabilize a CO-bound intermediate may be advantageous. Cyanide (CN⁻) binding has been reported for C_{red1}, but not for C_{red2} (Anderson & Lindahl, 1996). Based on ENDOR spectroscopy it has been argued that the cyanide ion does not act like the isoelectronic substrate CO, but that it binds at the same site as the H_xO species found in C_{red1}, thereby acting as an inhibitor of water activation (DeRose et al, 1998). Other inhibitors that have been studied spectroscopically, such as N₃, n-BIC and CS₂ are interesting to study how they bind/interact with cluster C.

Third, it also supports studies on the assembly of cluster C. The presented studies introduced some biochemical and structural properties of CooC1. However, how CooC inserts nickel into cluster C and how it overcomes the free energy barrier by using ATP hydrolysis are unclear and should be further investigated biochemically and structurally, followed by the production and characterization of Ni-deficient CODH.

REFERENCES

Microcal(TM) Origin. Microcal Softwar, Inc., One Roundhouse Plaza, Northampton, MA USA.

PrimeView based on:UNICORN V4.00.16. GE Health Care.

Anderson ME, Lindahl PA (1996) Spectroscopic states of the CO oxidation/CO₂ reduction active site of carbon monoxide dehydrogenase and mechanistic implications. *Biochemistry-U S* **35**(25): 8371-8380

Aresta M, Dibenedetto A (2007) Utilisation of CO₂ as a chemical feedstock: opportunities and challenges. *Dalton Trans* **28**: 2975-2992

Ascone DS, Marcy NE (2005) Non-fire carbon monoxide deaths associated with the use of consumer products 2002 Annual Estimates. *U S Consumer Product Safty Commission*

Atanassova A, Zamble DB (2005) *Escherichia coli* HypA is a zinc metalloprotein with a weak affinity for nickel. *J Bacteriol* **187**(14): 4689-4697

Bartholomew GW, Alexander M (1979) Microbial metabolism of carbon monoxide in culture and in soil. *Appl Environ Microb* **37**(5): 932-937

Benini S, Rypniewski WR, Wilson KS, Miletti S, Ciurli S, Mangani S (1999) A new proposal for urease mechanism based on the crystal structures of the native and inhibited enzyme from *Bacillus pasteurii*: why urea hydrolysis casts two nickels. *Structure* **7**(2): 205-216

Bonam D, Ludden PW (1987) Purification and characterization of carbon monoxide dehydrogenase, a Nickel, Zinc, Iron-Sulfur protein, from *Rhodospirillum rubrum*. *J Biol Chem* **262**(7): 2980-2987

Bradford MM (1976) Rapid and sensitive method for quantitation of microgram quantities of protein utilizing principle of protein-dye binding. *Anal Biochem* **72**(1-2): 248-254

Brunger AT, Adams PD, Clore GM, DeLano WL, Gros P, Grosse-Kunstleve RW, Jiang JS, Kuszewski J, Nilges M, Pannu NS, Read RJ, Rice LM, Simonson T, Warren GL (1998) Crystallography & NMR system: A new software suite for macromolecular structure determination. *Acta Crystallogr D* **54**: 905-921

Bulen WA, LeComte JR (1996) The Nitrogenase system from Azotobacter: Two-enzyme requirement for N₂ reduction, ATP-dependent H₂ evolution, and ATP hydrolysis. *Proc Natl Acad Sci USA* **56**: 979-986

Cavet JS, Graham AI, Meng WM, Robinson NJ (2003) A cadmium-lead-sensing ArsR-SmtB repressor with novel sensory sites - Complementary metal discrimination by NMTR and CMTR in a common cytosol. *J Biol Chem* **278**(45): 44560-44566

Chen CJ, Lin YH, Huang YC, Liu MY (2006) Crystal structure of rubredoxin from *Desulfovibrio gigas* to ultra-high 0.68 angstrom resolution. *Biochem Bioph Res Co* **349**(1): 79-90

Chenna R, Sugawara H, Koike T, Lopez R, Gibson TJ, Higgins DG, Thompson JD (2003) Multiple sequence alignment with the Clustal series of programs. *Nucleic Acids Res* **31**(13): 3497-3500

- Cordell SC, Lowe J (2001) Crystal structure of the bacterial cell division regulator MinD. *FEBS Lett* **492**(1-2): 160-165
- Darnault C, Volbeda A, Kim EJ, Legrand P, Vernede X, Lindahl PA, Fontecilla-Camps JC (2003) Ni-Zn-[Fe₄-S₄] and Ni-Ni-[Fe₄-S₄] clusters in closed and open subunits of acetyl-CoA synthase/carbon monoxide dehydrogenase. *Nat Struct Biol* **10**(4): 271-279
- deLacey AL, Hatchikian EC, Volbeda A, Frey M, Fontecilla-Camps JC, Fernandez VM (1997) Infrared spectroelectrochemical characterization of the [NiFe] hydrogenase of *Desulfovibrio gigas*. *J Am Chem Soc* **119**(31): 7181-7189
- DeLano WL. PyMol. DeLano Scientific, San Carlos, CA.
- DeRose VJ, Telser J, Anderson ME, Lindahl PA, Hoffman BM (1998) A multinuclear ENDOR study of the C-cluster in CO dehydrogenase from *Clostridium thermoaceticum*: Evidence for H₂O and histidine coordination to the [Fe₄S₄] center. *J Am Chem Soc* **120**(34): 8767-8776
- Dibenedetto MAA (2002) CO₂ conversion and utilization of greenhouse gases. In *ACS Symposium*, Vol. Series 852, p 169. Washington, DC
- Dixon NE, Gazzola C, Blakeley RL, Zerner B (1975) Jack-bean urease (EC 3.5.1.5) - metalloenzyme - simple biological role for Nickel. *J Am Chem Soc* **97**(14): 4131-4133
- Dobbek H, Gremer L, Kiefersauer R, Huber R, Meyer O (2002) Catalysis at a dinuclear [CuSmO(=O)OH] cluster in a CO dehydrogenase resolved at 1.1 angstrom resolution. *Proc Natl Acad Sci USA* **99**(25): 15971-15976
- Dobbek H, Gremer L, Meyer O, Huber R (1999) Crystal structure and mechanism of CO dehydrogenase, a molybdo iron-sulfur flavoprotein containing S-selenylcysteine. *Proc Natl Acad Sci USA* **96**(16): 8884-8889
- Dobbek H, Huber R (2002) The molybdenum and tungsten cofactors: A crystallographic view. *Met Ions Biol Syst* **39**: 227-263
- Dobbek H, Svetlitchnyi V, Gremer L, Huber R, Meyer O (2001) Crystal structure of a carbon monoxide dehydrogenase reveals a [Ni-4Fe-5S] cluster. *Science* **293**(5533): 1281-1285
- Dobbek H, Svetlitchnyi V, Liss J, Meyer O (2004) Carbon monoxide induced decomposition of the active site [Ni-4Fe-5S] cluster of CO dehydrogenase. *J Am Chem Soc* **126**(17): 5382-5387
- Doukov TI, Blasiak LC, Seravalli J, Ragsdale SW, Drennan CL (2008) Xenon in and at the end of the tunnel of bifunctional carbon monoxide dehydrogenase/acetyl-CoA synthase. *Biochemistry-US* **47**(11): 3474-3483
- Doukov TI, Iverson TM, Seravalli J, Ragsdale SW, Drennan CL (2002) A Ni-Fe-Cu center in a bifunctional carbon monoxide dehydrogenase/acetyl-CoA synthase. *Science* **298**(5593): 567-572
- Drapal N, Bock A (1998) Interaction of the hydrogenase accessory protein HypC with HycE, the large subunit of *Escherichia coli* hydrogenase 3 during enzyme maturation. *Biochemistry-US* **37**(9): 2941-2948
- Drennan CL, Heo JY, Sintchak MD, Schreiter E, Ludden PW (2001) Life on carbon monoxide: X-ray structure of *Rhodospirillum rubrum* Ni-Fe-S carbon monoxide dehydrogenase. *Proc Natl Acad Sci USA* **98**(21): 11973-11978

- Eisses JF, Stasser JP, Ralle M, Kaplan JH, Blackburn NJ (2000) Domains I and III of the human copper chaperone for superoxide dismutase interact via a cysteine-bridged dicopper(I) cluster. *Biochemistry-U.S.* **39**(25): 7337-7342
- Emsley P, Cowtan K (2004) Coot: model-building tools for molecular graphics. *Acta Crystallogr D* **60**: 2126-2132
- Ensign SA (1995) Reactivity of carbon-monoxide dehydrogenase from *Rhodospirillum rubrum* with carbon dioxide, carbonyl sulfide, and carbon disulfide. *Biochemistry-U.S.* **34**(16): 5372-5381
- Ermler U, Grabarse W, Shima S, Goubeaud M, Thauer RK (1997) Crystal structure of methyl coenzyme M reductase: The key enzyme of biological methane formation. *Science* **278**(5342): 1457-1462
- Feng J, Lindahl PA (2004a) Carbon monoxide dehydrogenase from *Rhodospirillum rubrum*: Effect of redox potential on catalysis. *Biochemistry-U.S.* **43**(6): 1552-1559
- Feng J, Lindahl PA (2004b) Effect of sodium sulfide on Ni-containing carbon monoxide dehydrogenases. *J Am Chem Soc* **126**(29): 9094-9100
- Fontecilla-Camps JC, Volbeda A, Cavazza C, Nicolet Y (2007) Structure/function relationships of [NiFe]- and [FeFe]-hydrogenases (vol 107, pg 4273, 2007). *Chem Rev* **107**(11): 5411-5411
- Ford PC, Rokicki A (1988) Nucleophilic activation of carbon monoxide - Applications to homogeneous catalysis by metal-carbonyls of the Water Gas Shift and related reactions. *Adv Organomet Chem* **28**: 139-217
- Fraser DM, Lindahl PA (1999) Evidence for a proposed intermediate redox state in the CO/CO₂ active site of acetyl-CoA synthase (carbon monoxide dehydrogenase) from *Clostridium thermoaceticum*. *Biochemistry-U.S.* **38**(48): 15706-15711
- Fu CL, Olson JW, Maier RJ (1995) HypB protein of *Bradyrhizobium japonicum* Is a metal-binding GTPase capable of binding 18 divalent Nickel ions per dimer. *Proc Natl Acad Sci USA* **92**(6): 2333-2337
- Gasper R, Meyer S, Wittinghofer A (2008) G-proteine, Lob der Zweisamkeit: neue Mechanismen der GTPase-Aktivierung. *BIOspectrum* **14. Jahrgang**: 128-133
- Gasper R, Scrima A, Wittinghofer A (2006) Structural insights into HypB, a GTP-binding protein that regulates metal binding. *J Biol Chem* **281**(37): 27492-27502
- Georgiadis MM, Komiya H, Chakrabarti P, Woo D, Kornuc JJ, Rees DC (1992) Crystallographic Structure of the nitrogenase iron protein from *Azotobacter vinelandii*. *Science* **257**(5077): 1653-1659
- Gibson DH (1996) The organometallic chemistry of carbon dioxide. *Chem Rev* **96**(6): 2063-2095
- Gibson DH (1999) Carbon dioxide coordination chemistry: metal complexes and surface-bound species. What relationships? *Coordin Chem Rev* **186**: 335-355
- Goodno CC (1979) Inhibition of myosin ATPase by vanadate ion. *Proc Natl Acad Sci USA* **76**(6): 2620-2624

- Grahame DA, Demoll E (1995) Substrate and accessory protein-requirements and thermodynamics of Acetyl-CoA synthesis and cleavage in *Methanosarcina barkeri*. *Biochemistry-U.S.* **34**(14): 4617-4624
- Gremer L, Kellner S, Dobbek H, Huber R, Meyer O (2000) Binding of flavin adenine dinucleotide to molybdenum-containing carbon monoxide dehydrogenase from *Oligotropha carboxidovorans* - Structural and functional analysis of a carbon monoxide dehydrogenase species in which the native flavoprotein has been replaced by its recombinant counterpart produced in *Escherichia coli*. *J Biol Chem* **275**(3): 1864-1872
- Gu WW, Seravalli J, Ragsdale SW, Cramer SP (2004) CO-Induced structural rearrangement of the C cluster in *Carboxydotherrmus hydrogenoformans* CO dehydrogenase - Evidence from Ni K-edge X-ray absorption spectroscopy. *Biochemistry-U.S.* **43**(28): 9029-9035
- Ha NC, Oh ST, Sung JY, Cha KA, Lee MH, Oh BH (2001) Supramolecular assembly and acid resistance of *Helicobacter pylori* urease. *Nat Struct Biol* **8**(6): 505-509
- Hänzelmann P, Dobbek H, Gremer L, Huber R, Meyer O (2000) The effect of intracellular molybdenum in *Hydrogenophaga pseudoflava* on the crystallographic structure of the seleno-molybdo-iron-sulfur flavoenzyme carbon monoxide dehydrogenase. *J Mol Biol* **301**(5): 1221-1235
- Hausinger RP (1997) Metallocenter assembly in nickel-containing enzymes. *J Biol Inorg Chem* **2**(3): 279-286
- Hayashi I, Oyama T, Morikawa K (2001) Structural and functional studies of MinD ATPase: implications for the molecular recognition of the bacterial cell division apparatus. *EMBO J* **20**(8): 1819-1828
- He MM, Clugston SL, Honek JF, Matthews BW (2000) Determination of the structure of *Escherichia coli* glyoxalase I suggests a structural basis for differential metal activation. *Biochemistry-U.S.* **39**(30): 8719-8727
- Hille R (1996) The mononuclear molybdenum enzymes. *Chem Rev* **96**(7): 2757-2816
- Holm L, Sander C (1993) Protein-structure comparison by alignment of distance matrices. *J Mol Biol* **233**(1): 123-138
- Hopfner KP, Craig L, Moncalian G, Zinkel RA, Usui T, Owen BAL, Karcher A, Henderson B, Bodmer JL, McMurray CT, Carney JP, Petrini JHJ, Tainer JA (2002) The Rad50 zinc-hook is a structure joining Mre11 complexes in DNA recombination and repair. *Nature* **418**(6897): 562-566
- Hu ZG, Spangler NJ, Anderson ME, Xia JQ, Ludden PW, Lindahl PA, Munch E (1996) Nature of the C-cluster in Ni-containing carbon monoxide dehydrogenases. *J Am Chem Soc* **118**(4): 830-845
- Iwig JS, Leitch S, Herbst RW, Maroney MJ, Chivers PT (2008) Ni(II) and Co(II) sensing by *Escherichia coli* RcnR. *J Am Chem Soc* **130**(24): 7592-7606
- Jabri E, Carr MB, Hausinger RP, Karplus PA (1995) The Crystal-structure of urease from *Klebsiella aerogenes*. *Science* **268**(5213): 998-1004
- Jabri E, Karplus PA (1996) Structures of the *Klebsiella aerogenes* urease apoenzyme and two active-site mutants. *Biochemistry-U.S.* **35**(33): 10616-10626

- Jean Y (2005) *Molecular Orbitals of Transition Metals Complexes*, Oxford: Oxford University Press.
- Jeffrey S. Iwig SL, Robert W. Herbst, Michael J. Maroney, and, Chivers PT (2008) Ni(II) and Co(II) sensing by *Escherichia coli* RcnR *J Am Chem Soc* **130**(24): 7592-7606
- Jeon WB, Cheng JJ, Ludden PW (2001) Purification and characterization of membrane-associated CooC protein and its functional role in the insertion of nickel into carbon monoxide dehydrogenase from *Rhodospirillum rubrum*. *J Biol Chem* **276**(42): 38602-38609
- Jeoung J-H, Dobbek H (2007) Carbon dioxide activation at the Ni,Fe-Cluster of anaerobic carbon monoxide dehydrogenase. *Science* **318**(30): 1461-1464
- Kabsch W (1993) Automatic processing of rotation diffraction data from crystals of initially unknown symmetry and cell constants. *J Appl Crystallogr* **26**: 795-800
- Kaim W, Schwederski B (2004) *Bioinorganic Chemistry*: John Wiley & Sons.
- Kerby RL, Ludden PW, Roberts GP (1997) *In vivo* nickel insertion into the carbon monoxide dehydrogenase of *Rhodospirillum rubrum*: Molecular and physiological characterization of *cooCTJ*. *J Bacteriol* **179**(7): 2259-2266
- Kim EJ, Feng J, Bramlett MR, Lindahl PA (2004) Evidence for a proton transfer network and a required persulfide-bond-forming cysteine residue in Ni-containing carbon monoxide dehydrogenases. *Biochemistry-U S A* **43**(19): 5728-5734
- Koonin EV (1993) A superfamily of ATPases with diverse functions containing either classical or deviant ATP-binding motif. *J Mol Biol* **232**(3): 1013-1013
- Kozlowski H, Decocklereverend B, Ficheux D, Loucheux C, Sovago I (1987) Nickel(II) complexes with sulfhydryl containing peptides - potentiometric and spectroscopic studies. *J Inorg Biochem* **29**(3): 187-197
- Kuchar J, Hausinger RP (2004) Biosynthesis of metal sites. *Chem Rev* **104**(2): 509-525
- Kutzelnigg W *Einführung in die Theoretische Chemie*: Wiley-VCH.
- Laemmli UK (1970) Cleavage of structural proteins during assembly of head of bacteriophage-T4. *Nature* **227**(5259): 680-685
- Lamb AL, Torres AS, O'Halloran TV, Rosenzweig AC (2001) Heterodimeric structure of superoxide dismutase in complex with its metallochaperone. *Nat Struct Biol* **8**(9): 751-755
- Lanzetta PA, Alvarez LJ, Reinach PS, Candia OA (1979) Improved assay for nanomole amounts of inorganic-phosphate. *Anal Biochem* **100**(1): 95-97
- Laskowski RA, Macarthur MW, Moss DS, Thornton JM (1993) Procheck - a program to check the stereochemical quality of protein structures. *J Appl Crystallogr* **26**: 283-291
- Leach MR, Sandal S, Sun HW, Zamble DB (2005) Metal binding activity of the *Escherichia coli* hydrogenase maturation factor HypB. *Biochemistry-U S A* **44**(36): 12229-12238
- Leach MR, Zamble DB (2007) Metallocenter assembly of the hydrogenase enzymes. *Curr Opin Chem Biol* **11**(2): 159-165

- Leatherbarrow RJ. (2001) GraFit Version 5 (Ltd., E. S., ed). Horley, UK.
- Lee MH, Pankratz HS, Wang S, Scott RA, Finnegan MG, Johnson MK, Ippolito JA, Christianson DW, Hausinger RP (1993) Purification and characterization of *Klebsiella aerogenes* UreE protein - a nickel-binding protein that functions in urease metallocenter assembly. *Protein Sci* **2**(6): 1042-1052
- Leipe DD, Wolf YI, Koonin EV, Aravind L (2002) Classification and evolution of P-loop GTPases and related ATPases. *J Mol Biol* **317**(1): 41-72
- Leitner W (1996) The coordination chemistry of carbon dioxide and its relevance for catalysis: A critical study (vol 153, pg 257, 1996). *Coordin Chem Rev* **155**: 247-247
- Leonard TA, Butler PJ, Lowe J (2005) Bacterial chromosome segregation: structure and DNA binding of the Soj dimer - a conserved biological switch. *EMBO J* **24**(2): 270-282
- Lever ABP (1984) *Inorganic electronic spectroscopy*, 2nd ed. edn. New York: Elsevier Science.
- Lindahl PA (2002) The Ni-containing carbon monoxide dehydrogenase family: Light at the end of the tunnel? *Biochemistry-Ur* **41**(7): 2097-2105
- Lindahl PA, Chang B (2001) The evolution of acetyl-CoA synthase. *Origins Life Evol B* **31**(4): 403-434
- Lindahl PA, Munck E, Ragsdale SW (1990a) CO dehydrogenase from *Clostridium thermoaceticum* - EPR and electrochemical studies in CO₂ and argon atmospheres. *J Biol Chem* **265**(7): 3873-3879
- Lindahl PA, Ragsdale SW, Munck E (1990b) Mössbauer study of CO dehydrogenase from *Clostridium thermoaceticum*. *J Biol Chem* **265**(7): 3880-3888
- Logan DT, Mulliez E, Larsson KM, Bodevin S, Atta M, Garnaud PE, Sjöberg BM, Fontecave M (2003) A metal-binding site in the catalytic subunit of anaerobic ribonucleotide reductase. *Proc Natl Acad Sci USA* **100**(7): 3826-3831
- Loke HK, Bennett GN, Lindahl PA (2000) Active acetyl-CoA synthase from *Clostridium thermoaceticum* obtained by cloning and heterologous expression of acsAB in *Escherichia coli*. *Proc Natl Acad Sci USA* **97**(23): 12530-12535
- Loke HK, Lindahl PA (2003) Identification and preliminary characterization of AcsF, a putative Ni-insertase used in the biosynthesis of acetyl-CoA synthase from *Clostridium thermoaceticum*. *J Inorg Biochem* **93**(1-2): 33-40
- Lutkenhaus J, Sundaramoorthy M (2003) MinD and role of the deviant Walker A motif, dimerization and membrane binding in oscillation. *Mol Microbiol* **48**(2): 295-303
- Lutz S, Jacobi A, Schlenz V, Böhm R, Sawers G, Bock A (1991) Molecular characterization of an operon (Hyp) necessary for the activity of the 3 Hydrogenase Isoenzymes in *Escherichia coli*. *Mol Microbiol* **5**(1): 123-135
- Ma LY, King G, Rothfield L (2003) Mapping the MinE site involved in interaction with the MinD division site selection protein of *Escherichia coli*. *J Bacteriol* **185**(16): 4948-4955

- Macgregor SA, Lu Z, Eisenstein O, Crabtree RH (1994) Why nickel(II) binds CO best in trigonal bipyramidal and square pyramidal geometries and possible consequences for CO dehydrogenase. *Inorg Chem* **33**(16): 3616-3618
- Magalon A, Bock A (2000) Dissection of the maturation reactions of the [NiFe] hydrogenase 3 from *Escherichia coli* taking place after nickel incorporation. *FEBS Lett* **473**(2): 254-258
- Maier T, Lottspeich F, Bock A (1995) GTP hydrolysis by HypB is essential for nickel insertion into Hydrogenases of *Escherichia coli*. *Eur J Biochem* **230**(1): 133-138
- Matias PM, Soares CM, Saraiva LM, Coelho R, Morais J, Le Gall J, Carrondo MA (2001) [NiFe] hydrogenase from *Desulfovibrio desulfuricans* ATCC 27774: gene sequencing, three-dimensional structure determination and refinement at 1.8 angstrom and modelling studies of its interaction with the tetrahaem cytochrome c(3). *J Biol Inorg Chem* **6**(1): 63-81
- Mayr LM, Landt O, Hahn U, Schmid FX (1993) Stability and folding kinetics of ribonuclease-T(1) are strongly altered by the replacement of *cis*-proline-39 with alanine. *J Mol Biol* **231**(3): 897-912
- Mccoy AJ, Grosse-Kunstleve RW, Adams PD, Winn MD, Storoni LC, Read RJ (2007) Phaser crystallographic software. *J Appl Crystallogr* **40**: 658-674
- McIndoe PJDaJS (2000) *Transition Metal Carbonyl Cluster Chemistry*, Amsterdam: Gordon and Breach Science.
- McPherson A (1982) *Preparation and analysis of protein crystals*: New York: John Wiley & Sons.
- Meyer O, Gremer L, Ferner R, Ferner M, Dobbek H, Gnida M, Meyer-Klaucke W, Huber R (2000) The role of Se, Mo and Fe in the structure and function of carbon monoxide dehydrogenase. *Biol Chem* **381**(9-10): 865-876
- Mobley HLT, Island MD, Hausinger RP (1995) Molecular-biology of microbial ureases. *Microbiol Rev* **59**(3): 451-480
- Moncrief MBC, Hausinger RP (1997) Characterization of UreG, identification of a UreD-UreF-UreG complex, and evidence suggesting that a nucleotide-binding site in UreG is required for *in vivo* metalcenter assembly of *Klebsiella aerogenes* urease. *J Bacteriol* **179**(13): 4081-4086
- Montet Y, Amara P, Volbeda A, Vernede X, Hatchikian EC, Field MJ, Frey M, FontecillaCamps JC (1997) Gas access to the active site of Ni-Fe hydrogenases probed by X-ray crystallography and molecular dynamics. *Nat Struct Biol* **4**(7): 523-526
- Moodie SL, Thornton JM (1993) A study into the effects of protein-binding on nucleotide conformation. *Nucleic Acids Res* **21**(6): 1369-1380
- Murshudov GN, Vagin AA, Dodson EJ (1997) Refinement of macromolecular structures by the maximum-likelihood method. *Acta Crystallogr D* **53**: 240-255
- Nakamura M, Saeki, K. & Takahashi, Y. (1999) Hyperproduction of recombinant ferredoxins in *Escherichia coli* by coexpression of the *ORF1-ORF2-iscS-iscU-iscA-hscB-hscA-fdx-ORF3* gene cluster. *J Biochem (Tokyo)* **126**: 10-18
- Ogata H, Mizoguchi Y, Mizuno N, Miki K, Adachi S, Yasuoka N, Yagi T, Yamauchi O, Hirota S, Higuchi Y (2002) Structural studies of the carbon monoxide complex of [NiFe] hydrogenase

- from *Desulfovibrio vulgaris* Miyazaki F: Suggestion for the initial activation site for dihydrogen. *J Am Chem Soc* **124**(39): 11628-11635
- Pace CN, Vajdos F, Fee L, Grimsley G, Gray T (1995) How to measure and predict the molar absorption-coefficient of a protein. *Protein Sci* **4**(11): 2411-2423
- Page CC, Moser CC, Chen X, Dutton PL (1999) Natural engineering principles of electron tunneling in biological oxidation-reduction. *Nature* **402**: 47-52
- Park IS, Hausinger RP (1995) Requirement of carbon-dioxide for in-Vitro assembly of the urease nickel metallocenter. *Science* **267**(5201): 1156-1158
- Pearson MA, Michel LO, Hausinger RP, Karplus PA (1997) Structures of Cys319 variants and acetohydroxamate-inhibited *Klebsiella aerogenes* urease. *Biochemistry-Us* **36**(26): 8164-8172
- Pennella MA, Shokes JE, Cospers NJ, Scott RA, Giedroc DP (2003) Structural elements of metal selectivity in metal sensor proteins. *Proc Natl Acad Sci USA* **100**(7): 3713-3718
- Pereira E, Gomes L, de Castro B (1998) Synthesis, spectroscopic and electrochemical study of nickel(II) complexes with tetradentate asymmetric Schiff bases derived from salicylaldehyde and methyl-2-amino-1-cyclopentenedithiocarboxylate. *Inorg Chim Acta* **271**(1-2): 83-92
- Pochapsky TC, Pochapsky SS, Ju TT, Mo HP, Al-Mjeni F, Maroney MJ (2002) Modeling and experiment yields the structure of acireductone dioxygenase from *Klebsiella pneumoniae*. *Nat Struct Biol* **9**(12): 966-972
- Rabalais JW, McDonald JM, Scherr V, McGlynn SP (1971) Electronic spectroscopy of isoelectronic molecules. Part II. linear triatomic groupings containing 16 valence electrons. *Chem Rev* **71**(1): 73-108
- Ragsdale SW (2004) Life with carbon monoxide. *Crit Rev Biochem Mol* **39**(3): 165-195
- Ragsdale SW (2006) *Encyclopedia of Inorganic Chemistry: Nickel Enzymes and Cofactors*: John Wiley & Sons, Ltd.
- Ragsdale SW (2007) Nickel and the carbon cycle. *J Inorg Biochem* **101**(11-12): 1657-1666
- Ragsdale SW, Kumar M (1996) Nickel-containing carbon monoxide dehydrogenase/acetyl-CoA synthase. *Chem Rev* **96**(7): 2515-2539
- Rees DC, Howard JB (2003) The interface between the biological and inorganic worlds: Iron-sulfur metalloclusters. *Science* **300**(5621): 929-931
- Reissmann S, Hochleitner E, Wang HF, Paschos A, Lottspeich F, Glass RS, Bock A (2003) Taming of a poison: Biosynthesis of the Ni,Fe-hydrogenase cyanide ligands. *Science* **299**(5609): 1067-1070
- Roberts DL, Jameshagstrom JE, Garvin DK, Gorst CM, Runquist JA, Baur JR, Haase FC, Ragsdale SW (1989) Cloning and expression of the gene-cluster encoding key proteins involved in Acetyl-CoA synthesis in *Clostridium thermoaceticum* - CO dehydrogenase, the corrinoid Fe-S protein, and methyltransferase. *Proc Natl Acad Sci USA* **86**(1): 32-36
- Rosenzweig AC (2002) Metallochaperones: Bind and deliver. *Chem Biol* **9**(6): 673-677

- Ruiguang GE RMW, Xuesong Sun, Julian A. Tanner, Qing-Yu He, Jian-Dong Huang and Hongzhe Sun (2006) Expression and characterization of a histidine-rich protein, Hpn: potential for Ni²⁺ storage in *Helicobacter pylori*. *Biochemical Journal* **393**: 285-293
- Rulisek L, Vondrasek J (1998) Coordination geometries of selected transition metal ions (Co²⁺, Ni²⁺, Cu²⁺, Zn²⁺, Cd²⁺, and Hg²⁺) in metalloproteins. *J Inorg Biochem* **71**(3-4): 115-127
- Russell MJ, Martin W (2004) The rocky roots of the acetyl-CoA pathway. *Trends Biochem Sci* **29**(7): 358-363
- Ryle MJ, Seefeldt LC (2000) Hydrolysis of nucleoside triphosphates other than ATP by nitrogenase. *J Biol Chem* **275**(9): 6214-6219
- Sakai N, Yao M, Itou H, Watanabe N, Yumoto F, Tanokura M, Tanaka I (2001) The three-dimensional structure of septum site- determining protein MinD from *Pyrococcus horikoshii* OT3 in complex with Mg-ADP. *Structure* **9**(9): 817-826
- Sambrook J, E. F. Fritsch & T. Maniatis (1989) *Molecular Cloning: a laboratory Manual*, Vol. 2nd edn: Cold Spring Harbor, NY: Cold spring Harbor Laboratory.
- Schindelin N, Kisker C, Sehlessman JL, Howard JB, Rees DC (1997) Structure of ADP-AIF(4)⁻-stabilized nitrogenase complex and its implications for signal transduction. *Nature* **387**(6631): 370-376
- Schlessman JL, Woo D, Joshua-Tor L, Howard JB, Rees DC (1998) Conformational variability in structures of the nitrogenase iron proteins from *Azotobacter vinelandii* and *Clostridium pasteurianum*. *J Mol Biol* **280**(4): 669-685
- Schubel U, Kraut M, Morsdorf G, Meyer O (1995) Molecular characterization of the gene-cluster *coxMSL* encoding the molybdenum-containing carbon-monoxide dehydrogenase of *Oligotropha carboxidovorans*. *J Bacteriol* **177**(8): 2197-2203
- Seefeldt LC, Ensign SA (1994) A Continuous, spectrophotometric activity assay for nitrogenase using the reductant titanium(III) citrate. *Anal Biochem* **221**(2): 379-386
- Sheldrick GM, Schneider TR (1997) SHELXL: High-resolution refinement. *Method Enzymol* **277**: 319-343
- Shelver D, Kerby RL, He YP, Roberts GP (1997) CooA, a CO-sensing transcription factor from *Rhodospirillum rubrum*, is a CO-binding heme protein. *Proc Natl Acad Sci USA* **94**(21): 11216-11220
- Singer SW, Hirst MB, Ludden PW (2006) CO-dependent H₂ evolution by *Rhodospirillum rubrum*: Role of CODH : CooF complex. *BBA-Bioenergetics* **1757**(12): 1582-1591
- Soriano A, Colpas GJ, Hausinger RP (2000) UreE stimulation of GTP-dependent urease activation in the UreD-UreF-UreG-urease apoprotein complex. *Biochemistry-Us* **39**(40): 12435-12440
- Soriano A, Hausinger RP (1999) GTP-dependent activation of urease apoprotein in complex with the UreD, UreF, and UreG accessory proteins. *Proc Natl Acad Sci USA* **96**(20): 11140-11144
- Spain A (2003) Implications of microbial heavy metal tolerance in the environment. *Reviews in Undergraduate Research* **2**: 1-6

- Sprang SR (1997) G protein mechanisms: Insights from structural analysis. *Annu Rev Biochem* **66**: 639-678
- Strop P, Takahara PM, Chiu HJ, Angove HC, Burgess BK, Rees DC (2001) Crystal structure of the all-ferrous [4Fe-4S]⁰ form of the nitrogenase iron protein from *Azotobacter vinelandii*. *Biochemistry-US* **40**(3): 651-656
- Svetlichny VA, Sokolova TG, Gerhardt M, Ringpfeil M, Kostrikina NA, Zavarzin GA (1991) *Carboxydotherrnus hydrogenoformans* Gen-Nov, Sp-Nov, a CO-utilizing thermophilic anaerobic bacterium from hydrothermal environments of Kunashir-island. *Syst Appl Microbiol* **14**(3): 254-260
- Svetlitchnyi V, Dobbek H, Meyer-Klaucke W, Meins T, Thiele B, Romer P, Huber R, Meyer O (2004) A functional Ni-Ni-[4Fe-4S] cluster in the monomeric acetyl-CoA synthase from *Carboxydotherrnus hydrogenoformans*. *Proc Natl Acad Sci USA* **101**(2): 446-451
- Svetlitchnyi V, Peschel C, Acker G, Meyer O (2001) Two membrane-associated Ni, Fe, S-carbon monoxide dehydrogenases from the anaerobic carbon-monoxide-utilizing eubacterium *Carboxydotherrnus hydrogenoformans*. *J Bacteriol* **183**(17): 5134-5144
- Takahashi Y, Tokumoto U (2002) A third bacterial system for the assembly of iron-sulfur clusters with homologs in archaea and plastids. *J Biol Chem* **277**(32): 28380-28383
- Tan XS, Volbeda A, Fontecilla-Camps JC, Lindahl PA (2006) Function of the tunnel in acetylcoenzyme A synthase/carbon monoxide dehydrogenase. *J Biol Inorg Chem* **11**(3): 371-378
- Teixeira M, Moura I, Xavier AV, Moura JGG, Legall J, Dervartanian DV, Peck HD, Huynh BH (1989) Redox intermediates of *Desulfovibrio gigas* [Nife] hydrogenase generated under hydrogen - Mössbauer and EPR characterization of the metal centers. *J Biol Chem* **264**(28): 16435-16450
- Terwilliger TC, Berendzen J (1999) Automated MAD and MIR structure solution. *Acta Crystallogr D* **55**: 849-861
- Terwilliger TC, Klei H, Adams PD, Moriarty NW, Cohn JD (2006) Automated ligand fitting by core-fragment fitting and extension into density. *Acta Crystallogr D* **62**: 915-922
- Turk D (1992) Weiterentwicklung eines Programms für Molekülgraphik und Elektronendichte-Manipulation und seine Anwendung auf verschiedene Protein-Strukturaufklärungen., Technische Universität München,
- Uden G, Bongaerts J (1997) Alternative respiratory pathways of *Escherichia coli*: Energetics and transcriptional regulation in response to electron acceptors. *BBA-Bioenergetics* **1320**(3): 217-234
- Vogele L, Palm GJ, Mesters JR, Hilgenfeld R (2001) Conformational change of elongation factor Tu (EF-Tu) induced by antibiotic binding - Crystal structure of the complex between EF-Tu-GDP and aurodox. *J Biol Chem* **276**(20): 17149-17155
- Volbeda A, Fontecilla-Camps JC (2005) Structural bases for the catalytic mechanism of Ni-containing carbon monoxide dehydrogenases. *Dalton Trans* **21**: 3443-3450

- Volbeda A, Martin L, Cavazza C, Matho M, Faber BW, Roseboom W, Albracht SPJ, Garcin E, Rousset M, Fontecilla-Camps JC (2005) Structural differences between the ready and unready oxidized states of [NiFe] hydrogenases. *J Biol Inorg Chem* **10**(3): 239-249
- Walker JE, Saraste M, Runswick MJ, Gay NJ (1982) Distantly related sequences in the alpha-subunits and beta-subunits of ATP synthase, myosin, kinases and other ATP-requiring enzymes and a common nucleotide binding fold. *EMBO J* **1**(8): 945-951
- Watt RK, Ludden PW (1998) The identification, purification, and characterization of CooJ - A nickel-binding protein that is CO-regulated with the Ni-containing CO dehydrogenase from *Rhodospirillum rubrum*. *J Biol Chem* **273**(16): 10019-10025
- Watt RK, Ludden PW (1999) Nickel-binding proteins. *Cell Mol Life Sci* **56**(7-8): 604-625
- Whitesides GM, Crabtree GW (2007) Don't forget long-term fundamental research in energy. *Science* **315**(5813): 796-798
- Wilhelm E, Battino R, Wilcock RJ (1977) Low-pressure solubility of gases in liquid water. *Chem Rev* **77**(2): 219-262
- Wiltzius JJW, Hohl M, Fleming JC, Petrini JHJ (2005) The Rad50 hook domain is a critical determinant of Mre11 complex functions. *Nat Struct Mol Biol* **12**(5): 403-407
- Wu M, Ren QH, Durkin AS, Daugherty SC, Brinkac LM, Dodson RJ, Madupu R, Sullivan SA, Kolonay JF, Nelson WC, Tallon LJ, Jones KM, Ulrich LE, Gonzalez JM, Zhulin IB, Robb FT, Eisen JA (2005) Life in hot carbon monoxide: The complete genome sequence of *Carboxydotherrmus hydrogenoformans* Z-2901. *Plos Genet* **1**(5): 563-574
- Wuerges J, Lee JW, Yim YI, Yim HS, Kang SO, Carugo KD (2004) Crystal structure of nickel-containing superoxide dismutase reveals another type of active site. *Proc Natl Acad Sci USA* **101**(23): 8569-8574
- Xu QP, Schwarzenbacher R, Krishna SS, McMullan D, Agarwalla S, Quijano K, Abdubek P, Ambing E, Axelrod H, Biorac T, Canaves JM, Chiu HJ, Elsliger MA, Grittini C, Grzechnik SK, DiDonato M, Hale J, Hampton E, Han GW, Haugen J, Hornsby M, Jaroszewski L, Klock HE, Knuth MW, Koesema E, Kreuzsch A, Kuhn P, Miller MD, Moy K, Nigoghossian E, Paulsen J, Reyes R, Rife C, Spraggon G, Stevens RC, Van den Bedem H, Velasquez J, White A, Wolf G, Hodgson KO, Wooley J, Deacon AM, Godzik A, Lesley SA, Wilson IA (2006) Crystal structure of acireductone dioxygenase (ARD) from *Mus musculus* at 2.06 Å resolution. *Proteins* **64**(3): 808-813
- Zambelli B, Stola M, Musiani F, De Vriendt K, Samyn B, Devreese B, Van Beeumen J, Turano P, Dikiy A, Bryant DA, Ciurli S (2005) UreG, a chaperone in the urease assembly process, is an intrinsically unstructured GTPase that specifically binds Zn. *J Biol Chem* **280**(6): 4684-4695
- Zhang JW, Butland G, Greenblatt JF, Emili A, Zamble DB (2005) A role for SlyD in the *Escherichia coli* hydrogenase biosynthetic pathway. *J Biol Chem* **280**(6): 4360-4366
- Zhou HJ, Schulze R, Cox S, Saez C, Hu ZL, Lutkenhaus J (2005) Analysis of MinD mutations reveals residues required for MinE stimulation of the MinD ATPase and residues required for MinC interaction. *J Bacteriol* **187**(2): 629-638
- Zhou TQ, Radaev S, Rosen BP, Gatti DL (2000) Structure of the ArsA ATPase: the catalytic subunit of a heavy metal resistance pump. *EMBO J* **19**(17): 4838-4845

Zhou TQ, Radaev S, Rosen BP, Gatti DL (2001) Conformational changes in four regions of the *Escherichia coli* ArsA ATPase link ATP hydrolysis to ion translocation. *J Biol Chem* **276**(32): 30414-30422

APPENDIX

1. Appendix Tables

Table A1. Primers used in cloning and mutagenesis of *cooC1*.

Name	Sequence	Tm (°C)
Fw_C1 ¹	5'- GGA ATT <u>CCA TAT GAA</u> GTT AGC GGT TGC AGG A -3'	62.0
Rv_C1 ²	5'- CAT <u>GGT CTC</u> GGA TCC TTA TCC CAC CTC CAA ACG CA -3'	68.0
Fw_C1strep ²	5'- ATG GTA <u>GGT CTC</u> AGC GCC ATG AAG TTA GCG GTT GCA GG -3'	70.0
Rv_C1strep ²	5'- ATG GTA <u>GGT CTC</u> ATA TCT TAT CCC ACC TCC AAA CGA A -3'	64.0
Fw_C1K8A ³	5'- GAA GTT AGC GGT TGC AGG <u>AGC</u> AGG CGG AGT GGG-3'	77.0
Rv_C1K8A ³	5'- CCC ACT CCG CCT <u>GCT</u> CCT GCA ACC GCT AAC TTC-3'	77.0

¹ Restriction site for *NdeI* is underlined. ² Recognition site for *Eco31I* is underlined. ³ Mutated nucleotides are indicated as underline.

Table A2. Thermocycler conditions for PCR reactions of cloning and mutagenesis of *cooC1*.

1. Initial denaturation:	98 °C	30 sec
2. Denaturation:	98 °C	10 sec
3. Annealing:	variable ¹	20 sec
4. Extension:	72 °C	variable ²
Go to 2	25 cycles [15 cycles for site-directed mutagenesis]	
5. Final extension:	72 °C	10 min

¹Annealing temperature was used as Tm – 5 °C for gene amplification, 55 °C for site-directed mutagenesis and 50 °C for colony PCR. ²Extension time was basically depended on size of a target DNA (*cooC1*: 0.8 kb) and DNA polymerase's extension rate (*Pfu* DNA polymerase: 2 min/kb, *Taq* DNA polymerase: 0.5 min/kb). For site-directed mutagenesis, 11 min was applied for *Pfu* DNA polymerase to complete synthesis of 6.5 kb pPKC1 plasmid.

Table A3. Primers used in cloning and mutagenesis of *cooSII*.

Name	Sequence	T _m (°C)
Fw_PR1	5'- GTG TGG CAT GGG AAT ATT GG -3'	57.3
Rv_PR2	5'- CTA CCA TGG TAA TCC CAG GCC -3'	61.8
Fw_PR12	5'- GCA AAA TTT AAA GTC TAC CGA CCG -3'	59.3
Rv_PR6 ¹	5'- <u>GCG GAT CCC</u> TAC CAT GGT AAT CC -3'	64.2
Fw_Seq1	5'- ATC GAC CAC GAA ATA GCT GAA -3'	55.9
Fw_Seq2	5'- CAC GTG AAT TTT GCC GAA GAA -3'	55.9
Rv_T7Ter	5'- GCT AGT TAT TGC TCA GCG G -3'	51.0
Fw_140E ²	5'- GGA CAA AAG GAT <u>GAA</u> GAT ATC GCT -3'	59.3
Rv_140E ²	5'- AGC GAT ATC <u>TTC</u> ATC CTT TTG TTC -3'	57.6
Fw_H96D ²	5'- CAT TCC GGG <u>GAT</u> GCG AAA CAC CTG GCT CAT AC -3'	66.3
Rv_H96D ²	5'- GTG TTT CGC <u>ATC</u> CCC GGA ATG TCC TGC TG -3'	66.1
R_missH96D ³	5'- GTA TGA GCC AGG TGT TTC <u>GCA TC</u> -3'	57.0

¹ *Bam*HI restriction site is indicated as underline. ² Mutated nucleotides are underlined as bold. ³ Miss-pairing nucleotide sequences to wild-type are underlined.

Table A4. Thermocycler conditions for PCR reactions of cloning and mutagenesis of *cooSII*.

1. Initial denaturation:	95 °C	1 min
2. Denaturation:	95 °C	30 sec
3. Annealing:	variable ¹	30 sec
4. Extension:	72 °C	variable ²
Go to 2	25 cycles [15 cycles for site-directed mutagenesis]	
5. Final extension:	72 °C	10 min

¹Annealing temperature was used as T_m – 5 °C for gene amplification, 55 °C for site-directed mutagenesis and 50 °C for colony PCR. ²Extension time was basically depended on size of a target DNA (*cooFISII*: 2.5 kb, *cooSII*: 1.9 kb) and DNA polymerase's extension rate (Herculase DNA polymerase: 1 min/kb, *Pfu* DNA polymerase: 2 min/kb, *Taq* DNA polymerase: 0.5 min/kb). For site-directed mutagenesis, 11 min was applied for *Pfu* DNA polymerase to complete synthesis of 7.3 kb pPKS2 plasmid.

Table A5. Statistics on diffraction data, phasing and structure refinement of CooC1 structures used for phasing experiments.

Crystal Name	<i>Native</i>	<i>Thiomersal-derivative</i>
<i>Data Collection</i>		
Wavelength (Å)	1.5418	1.5418
Spacegroup / cell constants (Å ³)	<i>P3₂21</i> / 80.03, 80.03, 77.02	<i>P3₂21</i> / 79.31, 79.31, 77.23
Total / unique reflections	85,822 / 21,595	82,500 / 31,076
R _s ^a (%)	7.7 / 40.6	7.7 / 35.6
Resolution (Å)	10-2.4 (2.5-2.4)	10-2.1 (2.2-2.1)
Completeness (%)	99.9 / 100.0	98.0 / 96.1
(I) / (σI)	16.05 / 3.30	11.75 / 2.98
<i>Phasing</i>		
Number of Mercury	-	3
Phasing power (PP) ^b		
Centric/acentric	-	0.60 / 0.75
R _{Cullis} ^c	-	0.61
FOM after SOLVE	-	0.37
FOM after RESOLVE	-	0.66
<i>Refinement</i>		
Model R / R _{free} -factor (%) ^d	-	22.6 / 27.5
Rms deviation from ideal geometry		
Bonds (Å)	-	0.007
Angles (°)	-	1.120
Ramachandran statistics (%)		
Most favored / additional / generously allowed / disallowed regions	-	92.8 / 6.7 / 0.0 / 0.5

^a $R_s = \sum_h \sum_i |I_i(h) - \langle I(h) \rangle| / \sum_h \sum_i I_i(h)$; where i are the independent observations of reflection h.

^b $PP = \sqrt{\left(\sum_h |F_H(h)|^2\right) / \left(\sum_h |E(h)|^2\right)}$ with $\sum_h |E(h)|^2 = \sum_h (|F_{PHobs}(h)| - |F_{PHcalc}(h)|)^2$

^c $R_{Cullis} = (\sum_h |F_{PH}(h) - F_P(h) - F_{Hcalc}(h)|) / (\sum_h |F_{PH}(h) - F_P(h)|)$

^d The R_{free} factor was calculated from 5% of the data, which were removed at random before the refinement was carried out.

Table A6. Statistics on diffraction data and structure refinements of CooC1 used for structure determination.

<i>Data Collection</i>	<i>Apo-CooC1</i>	<i>M-ADP-CooC1</i>	<i>M-CooC1</i>	<i>ADP-CooC1</i>
Spacegroup /	<i>P3₂21</i> /	<i>C2</i> /	<i>C2</i> /	<i>P2₁2₁2</i> /
cell constants (Å ³)	80.11, 80.11, 76.84	112.63, 81.32, 86.15, β = 128.836	54.26, 82.44, 55.26, β = 102.955	36.69 241.19 72.85
Total / unique reflections	103,418 / 12,969	87,285 / 23,690	96,026 / 17,845	113,133 / 29,710
R _s ^a (%)	4.1 (41.8)	5.8 (52.4)	5.3 (31.1)	5.1 (45.0)
Resolution (Å)	20-2.30 (2.4-2.3)	20-2.30 (2.5-2.4)	20-1.90 (2.0-1.9)	20-2.30 (2.4-2.3)
Completeness (%)	99.6 (99.8)	99.0 (99.6)	95.4 (92.1)	99.5 (99.8)
(I) / (σI)	34.65 (5.1)	16.67 (2.6)	22.40 (5.4)	18.46 (2.93)
<i>Refinement</i>				
Model R /	23.1 / 28.5	24.7 / 30.2	22.7 / 27.9	22.6 / 27.8
R _{free} -factor (%) ^b				
Rms deviation from ideal geometry				
Bonds (Å)	0.004	0.008	0.005	0.009
Angles (°)	1.12	1.47	1.20	1.80
Ramachandran statistics (%)				
Most favored /	90.9	84.8	90.5	87.6
additional /	8.7	14.3	8.2	11.5
generously allowed /	0.5	0.9	1.4	0.9
disallowed regions	0.0	0.0	0.0	0.0

For the refinement statistics Friedel mates were merged.

^a $R_s = \sum_h \sum_i |I_i(h) - \langle I(h) \rangle| / \sum_h \sum_i I_i(h)$; where *i* are the independent observations of reflection *h*.

^b The R_{free} factor was calculated from 5 - 10% of the data, which were removed at random before the refinement was carried out.

Values in parentheses are given for the highest resolution shell.

Table A7-1. Statistics on diffraction data and structure refinements of three-redox intermediates of Rec-CODHII (Jeoung & Dobbek, 2007).

Data set	-600 mV state (Ti-Citrate)	-320 mV state (re-oxidized)	-600 mV state + CO ₂
Total / unique refl.	567,684 / 104,078	315,206 / 81,496	304,202 / 83,938
R _s ^a (%)	7.0 (19.0)	6.0 (33.0)	8.6 (28.1)
Resolution (Å)	30-1.40 (1.45-1.40)	30-1.48 (1.50-1.48)	30-1.50 (1.60-1.50)
Completeness (%)	97.8 (85.8)	90.4 (85.1)	97.1 (94.4)
(I) / (σI)	15.3 (3.2)	13.5 (5.0)	10.0 (4.4)
Model R / R _{free} -factor (%) ^b	15.8 / 18.3 (32.6 / 34.4)	14.6 / 17.8 (24.5 / 31.3)	15.4 / 18.2 (30.3 / 34.6)
Rms deviation from ideal geometry			
Bonds (Å)	0.016	0.017	0.014
Angles (°)	1.91	1.95	1.95
ESU ^c (Å)	0.042	0.053	0.056

Table A7-2. Statistics on diffraction data and structure refinements of cluster C-miss and H96D of Rec-CODHII.

Data set	C-miss	H96D
Total / unique refl.	394,618 / 72,422	240,138 / 59,677
R _s ^a (%)	6.8 (45.4)	9.4 (32.7)
Resolution (Å)	20-1.60 (1.70-1.60)	20-1.70 (1.80-1.70)
Completeness (%)	99.8 (99.7)	98.5 (97.1)
(I) / (σI)	16.08 (3.63)	11.07 (4.54)
Model R / R _{free} -factor (%) ^b	16.1 / 20.4	17.4 / 21.5
Rms deviation from ideal geometry		
Bonds (Å)	0.020	0.018
Angles (°)	1.28	1.82
ESU ^c (Å)	0.061	0.058

Tab. A7.

For the refinement statistics Friedel mates were merged.

^a $R_s = \sum_h \sum_i |I_i(h) - \langle I(h) \rangle| / \sum_h \sum_i I_i(h)$; where *i* are the independent observations of reflection *h*.

^b The R_{free} factor was calculated from 5% of the data, which were removed at random before the refinement was carried out.

^c Estimated overall coordinate error (ESU) based on maximum likelihood.

Values in parentheses are given for the highest resolution shell.

Table A8. Analysis of B factors and occupancies in cluster C. The values given are for the –600 mV state (top line), the –600 mV+CO₂ state (middle line) and the –320 mV state (bottom line), (Jeoung & Dobbek, 2007).

Atom	Ni	Fe _{1(A)}	Fe _{1(B)}	O ₁	C	O ₂	S ₅	S ₃	S ₁	Av. B in Cl. B
B factor (Å ²)	10.8	10.7	8.2	10.2			7.6	8.4	8.6	4.7
	8.3	9.7	7.3	9.7	8.4	8.1	7.4	7.6	6.5	5.1
	13.6	12.6	12.5	10.3			12.6	13.1	11.8	9.0
Occupancy	0.6	0.6	0.3	0.6			0.8	0.8	0.8	1.0
	0.6	0.7	0.1	0.8	0.8	0.8	0.8	0.8	0.8	1.0
	0.6	0.6	0.3	0.6			0.8	0.8	0.8	1.0

Table A9. Maxima and shoulders appeared in the Ni-titration experiments of wild-type CooC1 in the absence and in the presence of ATP or ADP with number of binding site per dimer and K_d for Ni(II).

	Maxima/shoulders [nm]	Number of Binding sites / Dimer	K_d for Ni ²⁺ [μM]
<i>Wild-type</i> ¹	280	1.1 ± 0.01	0.39 ± 0.05
	330	0.9 ± 0.02	0.40 ± 0.05
<i>with ATP</i> ²	286	0.89	0.82 ($n_1 = 0.80, n_2 = 0.84$)
	295	0.99	1.37 ($n_1 = 1.32, n_2 = 1.45$)
	341	0.68	1.17 ($n_1 = 1.10, n_2 = 1.23$)
	380 (sh)	0.99	1.32 ($n_1 = 1.32, n_2 = 1.45$)
	620	-	-
<i>with ADP</i> ²	286	0.88	0.12 ($n_1 = 0.12, n_2 = 0.12$)
	295	0.85	0.29 ($n_1 = 0.29, n_2 = 0.32$)
	341	0.62	0.40 ($n_1 = 0.39, n_2 = 0.40$)
	380 (sh)	0.85	0.29 ($n_1 = 0.31, n_2 = 0.28$)
	620 (sh)	-	-

¹ middle values from the three independent experiments and standard deviations are shown here. ² middle values from two independent experiments are shown here (n , number of experiment). – indicates that peak and shoulders were not used to calculate values.

Table A10. Angles between selected atoms of cluster C in the three states (Jeoung & Dobbek, 2007).

Angle	–600 mV state	–600 mV+CO ₂ state	–320 mV state
C ₅₂₆ S ^Y -Ni-S ₃	156 °	168 °	157 °
C ₅₂₆ S ^Y -Ni-S ₅	94 °	93 °	94 °
C ₅₂₆ S ^Y -Ni-C	-	86 °	-
O ₁ -C-O ₂	-	133 °	-
Ni-C-O ₁	-	119 °	-
Ni-C-O ₂	-	108 °	-
H ₂₆₁ N ^{ε2} -Fe ₁ -O ₁	88 °	84 °	87 °
H ₂₆₁ N ^{ε2} -Fe ₁ -S ₁	100 °	96 °	101 °
Ni-S ₅ -Fe ₃	73 °	79 °	75 °
Ni-S ₃ -Fe ₃	76 °	83 °	75 °
C-O ₁ -Fe ₁	-	105 °	-

2. Appendix Figures

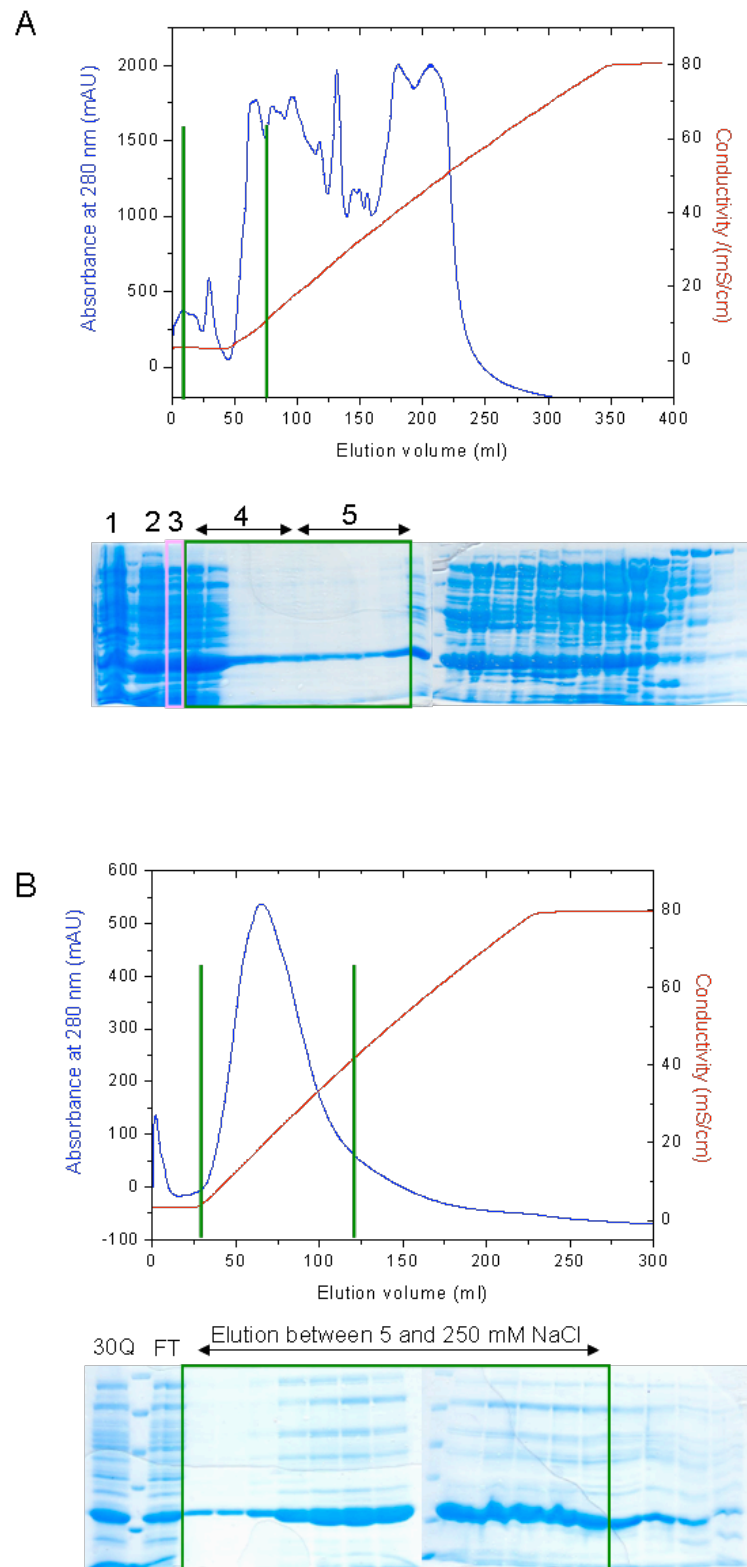


Figure A1. Figure legend is shown in the next page.

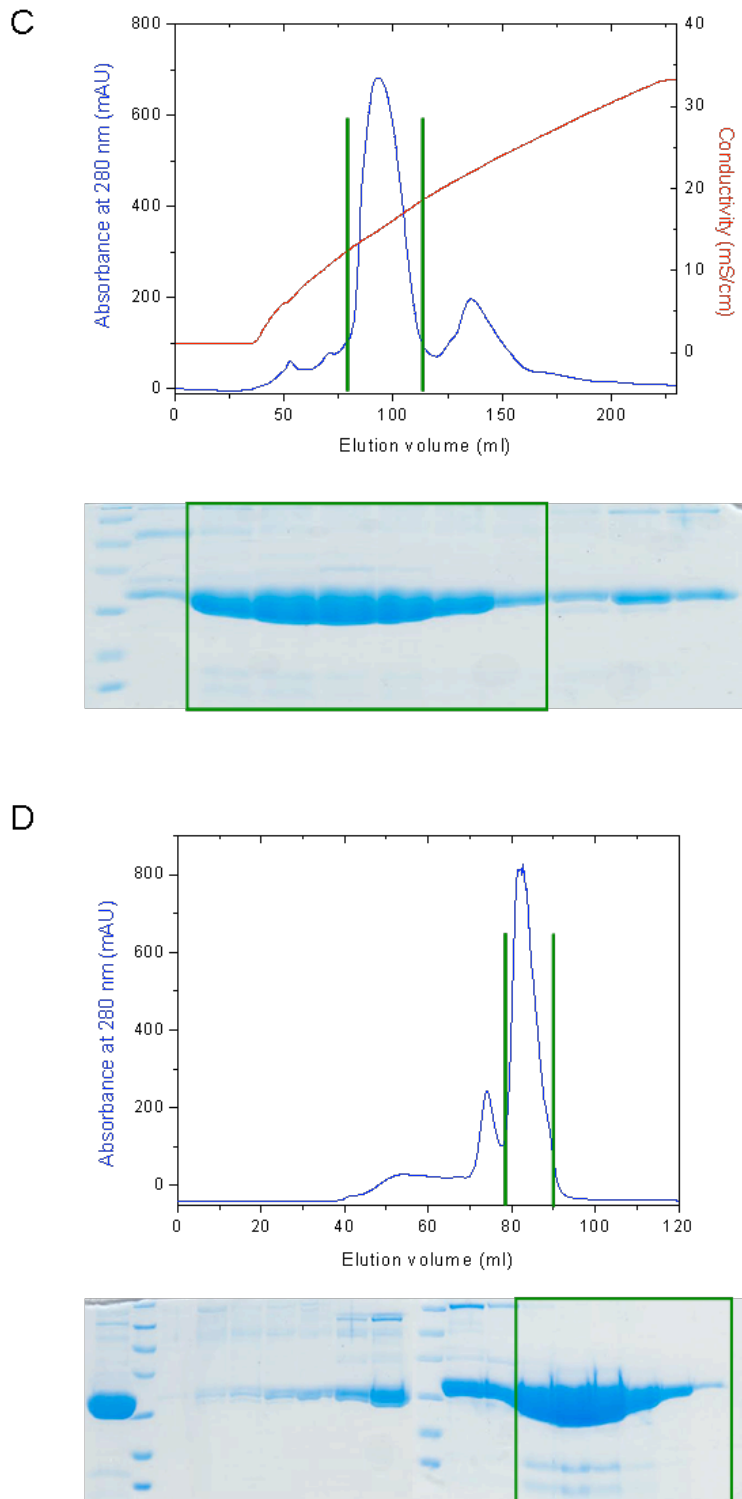


Figure A1. Chromatograms and 12% (w/v) SDS-PAGEs in different steps of CooC1 purification. (A) Source 30Q: Lane 1, pellet; Lane 2, supernatant; Lane 3, flow-through (120 ml); Lane 4, washing fractions (30 ml); Lane 5, elution fractions (15 ml between 0 and 70 mM NaCl), (B) Blue sepharose, (C) Hydroxyapatite and (D) Superdex™ 200 prep-grade. Only elution profiles of each step are shown and corresponding SDS-PAGE are shown under profile of each purification step with Roti-standard size marker. Purities of fractions between *green* lines in elution profiles, which were collected, are shown as *green* boxes in SDS-PAGE.

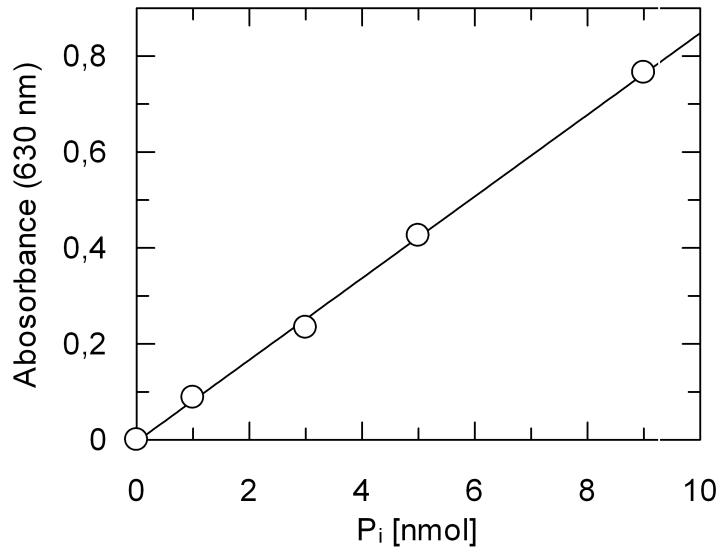


Figure A2. Standard curve for calculation of inorganic [P_i] used in the measurement of NTPase activities of CooC1 by malachite green method. Amount of P_i released was calculated by using equation: $[P_i]_{\text{released}} = (A_{630} + 0.0037)/0.0851$ with correlation coefficient of $R^2 = 0.9995$.

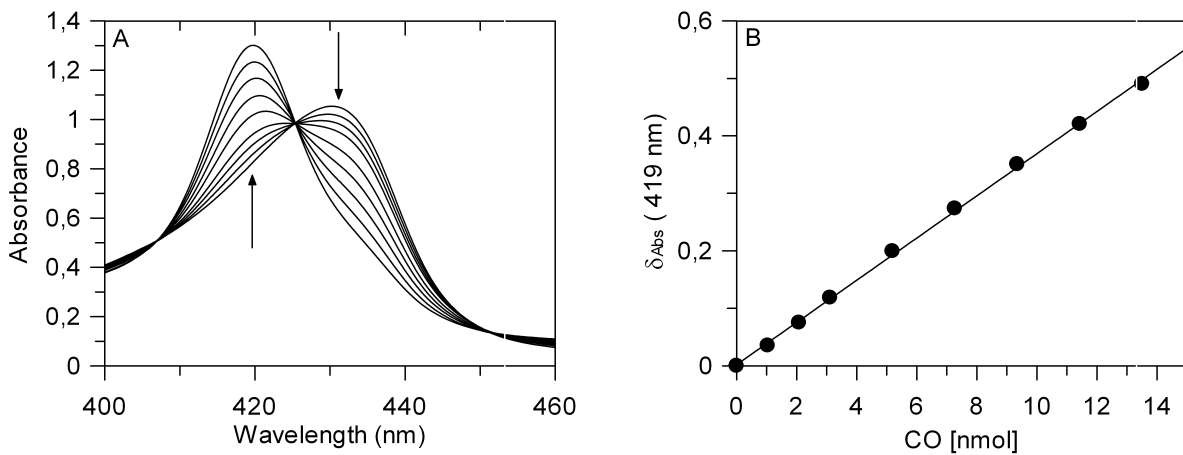
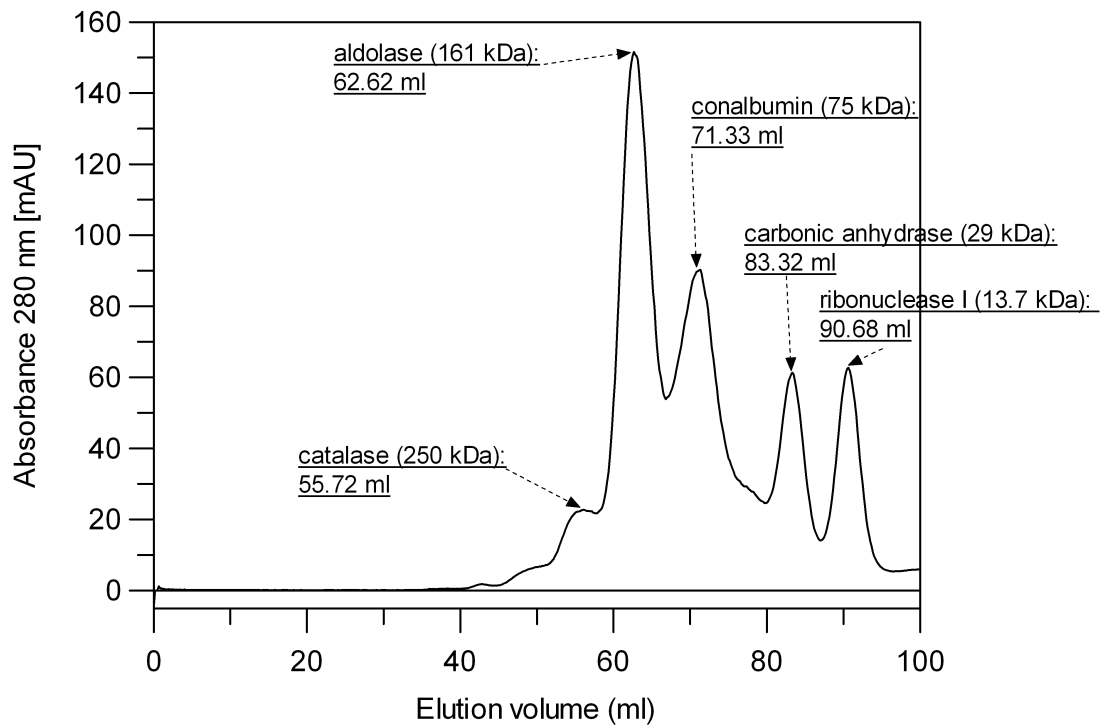


Figure A3. Standard curve of carboxyhemoglobin used to measure CO₂ reduction activity of Rec-CODHIII. (A) Spectral change upon formation of carboxyhemoglobin. Increasing absorbance at 419 nm and decreasing absorbance at 433 nm are indicated in arrow. Spectra were recorded against a buffer without reduced haemoglobin. The first spectrum was measured with reduced haemoglobin in the absence of CO. Each spectrum was recorded after the addition of 1.039 nmol of CO. (B) A linear fitting curve for amount of CO against absorbance change at 419 nm. Amount of CO produced from CO₂ reduction of CODH was calculated by using a linear fitting equation: $\text{nmol of CO} = (\delta_{\text{Abs}} \text{ at } 419 \text{ nm} - 0.0019)/0.0367$ with correlation coefficient of $R^2 = 0.9996$.

A



B

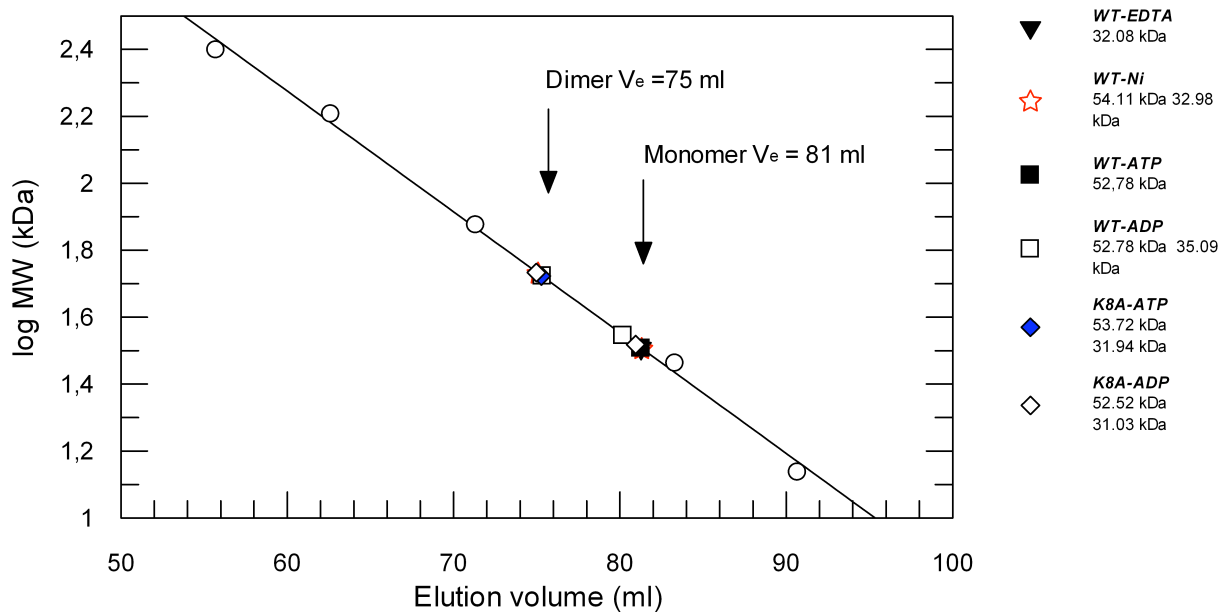


Figure A4. Elution profile (A) and standard curve (B) of molecular sieves used to calculate the molecular weight of CooC1 on Superdex™ 200 prep-grade. Following molecular sieves were dissolved in the running buffer (50 mM Tris-HCl pH 8.0, 100 mM NaCl and 1 mM TCEP): 5 mg/ml catalase (250 kDa), 1 mg/ml aldolase (161 kDa), 1 mg/ml conalbumin (75 kDa), 1 mg/ml carbonic anhydrase (29 kDa) and 1 mg/ml ribonuclease I (13.7 kDa). The standard curve fits to an equation: $\log MW = -0.0361 \times V_e + 4.401$.

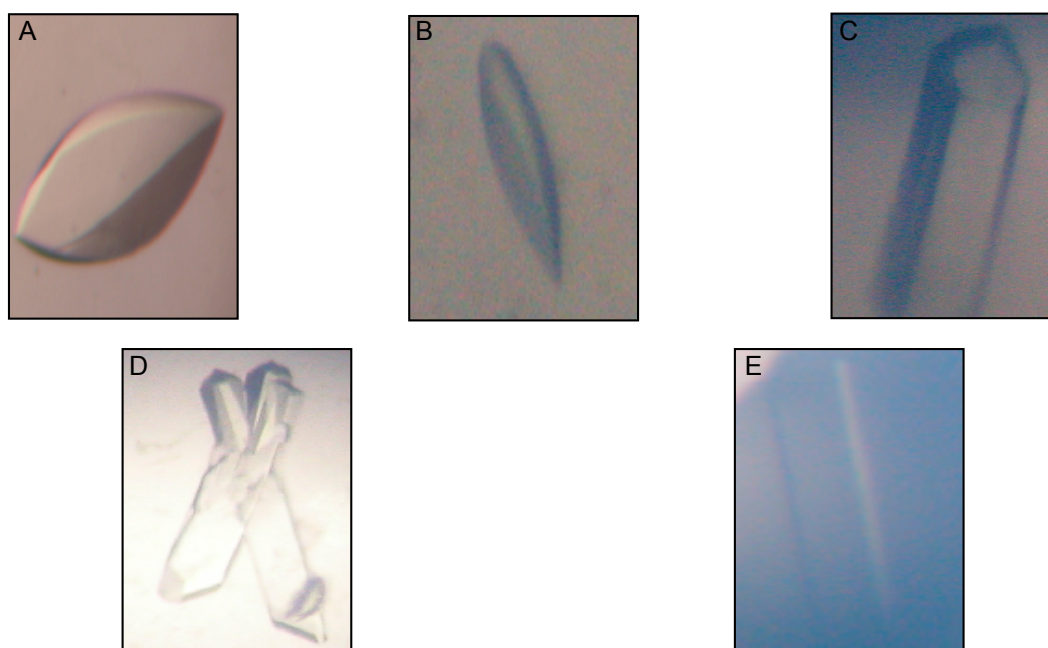
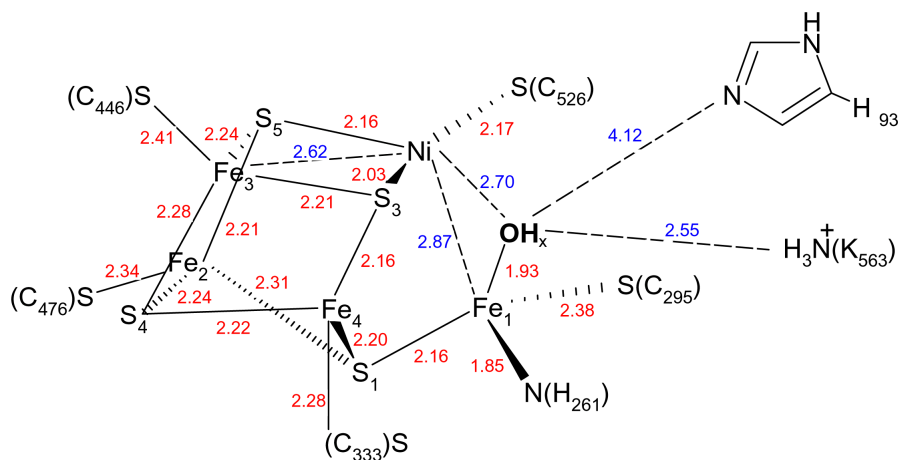


Figure A5. Crystals used in structure determinations of CooC1. In all conditions, 2 μ l of 10 mg/ml protein was mixed with same volume of reservoir buffer and equilibrated with 0.5 ml of reservoir buffer. (A) Crystal for monomeric apo-CooC1 structure used for phasing by thiomersal-derivative. Crystal was obtained in *condition I* (0.1 M tri-ammonium citrate pH 8.0, 15% (w/v) PEG 3350 and 3% (v/v) MPD) and grown up to 0.3 mm within a week. (B) Crystal for dimeric Metal-bound CooC1 structure. Crystals appeared in *condition IV* (0.25 M lithium citrate tribasic tetrahydrate and 14% (w/v) PEG 3350) within a few days and grown up to 0.2 mm after 2 weeks. (C) Crystal for dimeric Metal- and ADP-bound CooC1. Crystals were grown up to 0.4 – 0.5 mm size in *condition V* (0.2 M lithium citrate tribasic tetrahydrate, 10% (w/v) PEG 3350, 5% (v/v) glycerol, 10 mM AlF_4 , 10 mM MgCl_2 and 1 mM ADP) within a week. (D) Crystal for monomeric Apo-CooC1 structure. It was grown to a size of 0.4 – 0.5 mm in *condition II* (0.2 M L-proline, 0.1 M HEPES-NaOH pH 7.5 and 8% (w/v) PEG 3350) in the presence of 2 mM ADP, 10 mM MgCl_2 and 4 mM V_i in a week. (E) Crystal for dimeric ADP-bound CooC1 structure. Crystal appeared in *condition III* (0.2 M lithium citrate tribasic tetrahydrate, 14.5% (w/v) PEG 3350, 5% (v/v) glycerol and 1 mM ADP) within few days and grown up to size of bigger than 0.5 mm after 2 weeks. The sizes of crystals are described as measured in the longest axis.

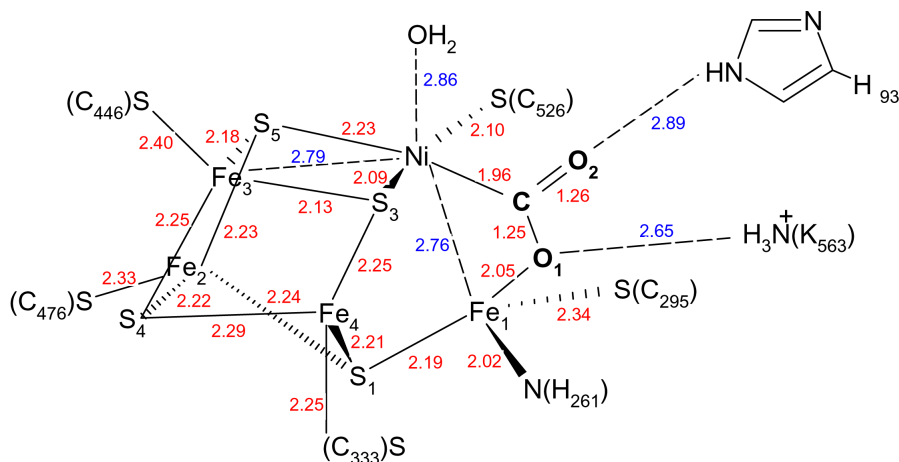


Figure A6. Rec-CODHII crystals grown by hanging drop vapor diffusion method equilibrated in 0.5 ml reservoir buffer containing 2 mM DT. (A) Crystals grown in the *formate condition*: 2 μ l of 10 mg/ml of protein were mixed with 2 μ l of reservoir buffer (0.25 Mg-formate, 16% (w/v) PEG 3350, and 2 mM DT) and grown up to 0.3 mm in length within a week. (B) Crystals from the *sulfate condition*: crystal appeared by mixing of 2 μ l of 10 mg/ml of protein with 2 μ l of reservoir buffer (17% (w/v) PEG 3350, 0.2 M ammonium sulfate, 0.1 M Bis-Tris pH 6.5, and 2 mM DT) or by streak seeding with horse hair at 3 ~ 5 days after setup of crystallization drop. Crystals were grown up to a size of 0.3 \times 0.2 \times 0.05 mm in 10 to 15 days.

A



B



C

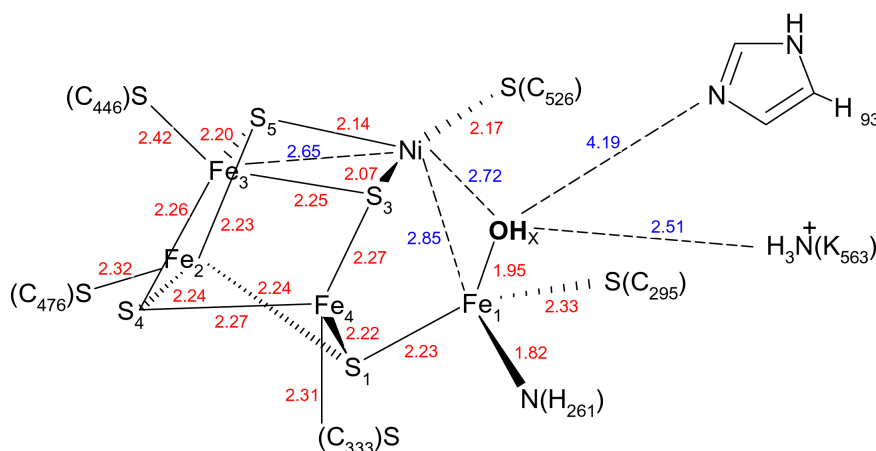


Figure A7. Bond length (red) and additional distances (blue) of cluster C in the -600 mV state (A), the -600 mV + CO₂ state (B): the lengths of both C-O bonds were restrained throughout the refinement, and the -320 mV state (C). Pictures are taken from Jeoung *et al* (Jeoung & Dobbek, 2007).

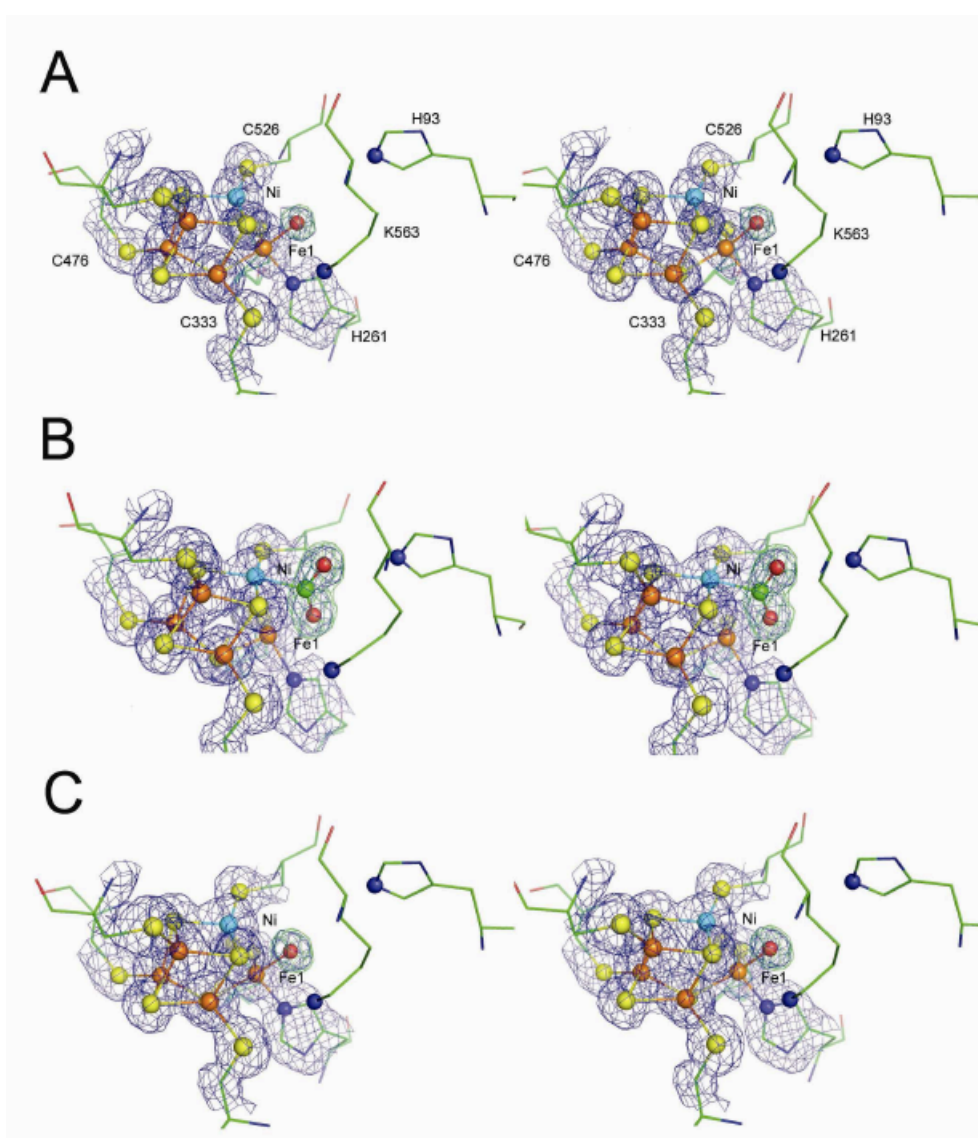


Figure A8. Stereo views on the active site cluster. (A) -600 mV state, (B) -600 mV+CO₂ state and (C) -320 mV state. $2F_{\text{obs}}-F_{\text{calc}}$ maps contoured at 1σ (blue) and omit $F_{\text{obs}}-F_{\text{calc}}$ maps contoured at 5σ for the ligand (OH_x in A and C, CO₂ in B) at Fe1. Pictures are taken from Jeoung *et al* (Jeoung & Dobbek, 2007).

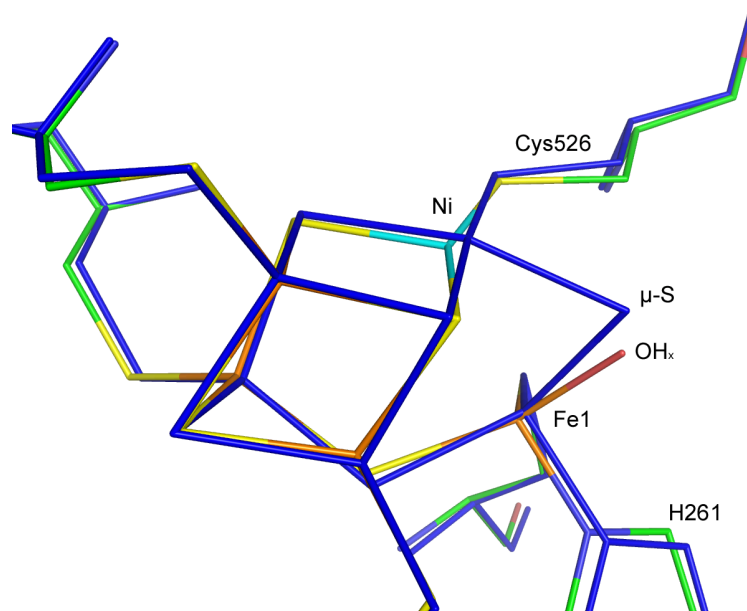


Figure A9. Superposition of the $[\text{NiFe}_4\text{S}_4\text{OH}_x]$ cluster (-320 mV state) in element colors with the $[\text{NiFe}_4\text{S}_5]$ cluster (PDB-code: 1SU8, Dobbek et al, 2004) in *blue*. The positions of the $\mu\text{-S}$ ligand in the $[\text{NiFe}_4\text{S}_5]$ cluster and the OH_x ligand in the $[\text{NiFe}_4\text{S}_4\text{OH}_x]$ cluster are ~ 0.6 Å apart in the superposed structures. Picture is taken from Jeung *et al* (Jeung & Dobbek, 2007).

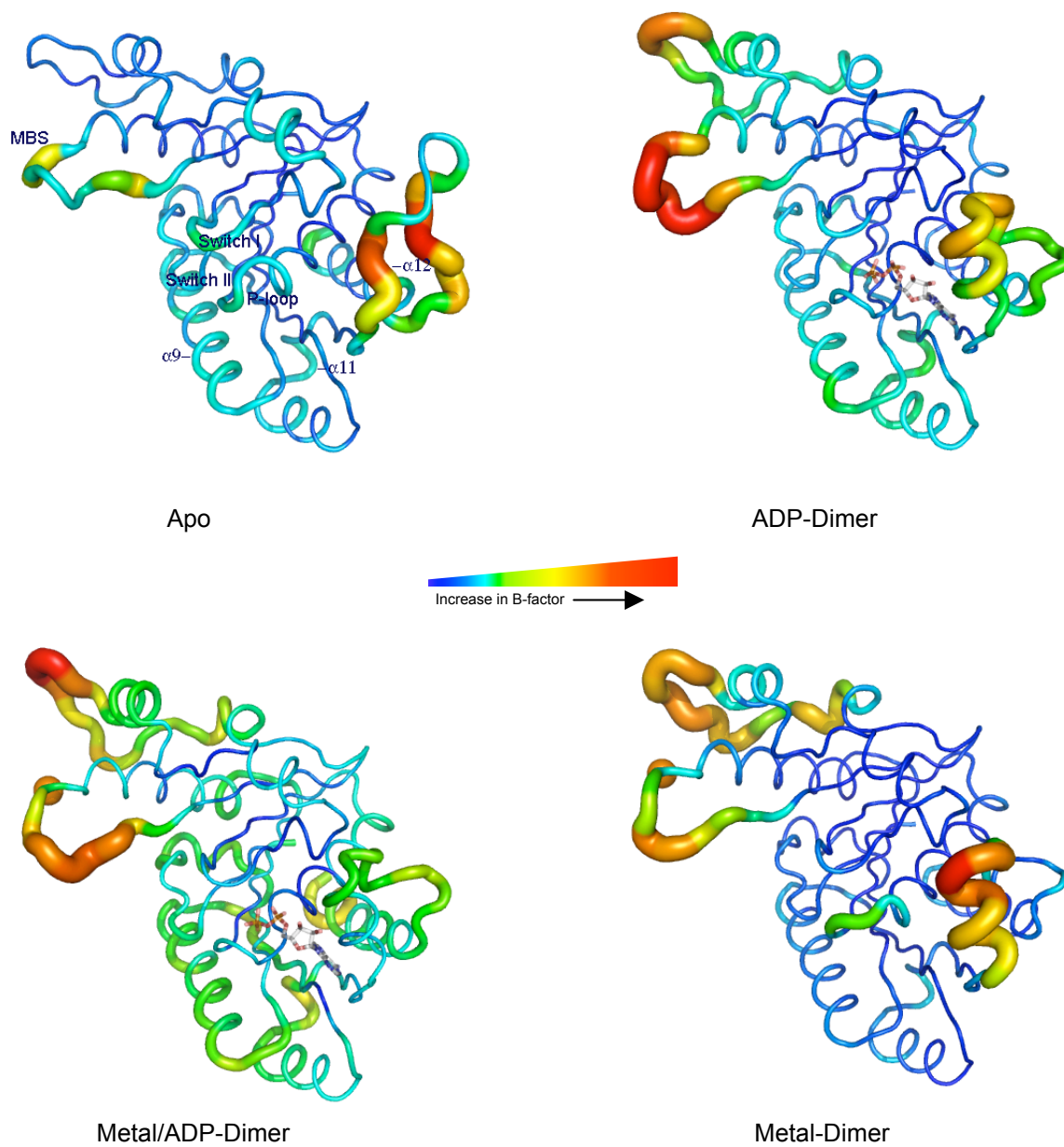


Figure A10. Sausage presentation of CooC1 structures by temperature factors (B-factor).

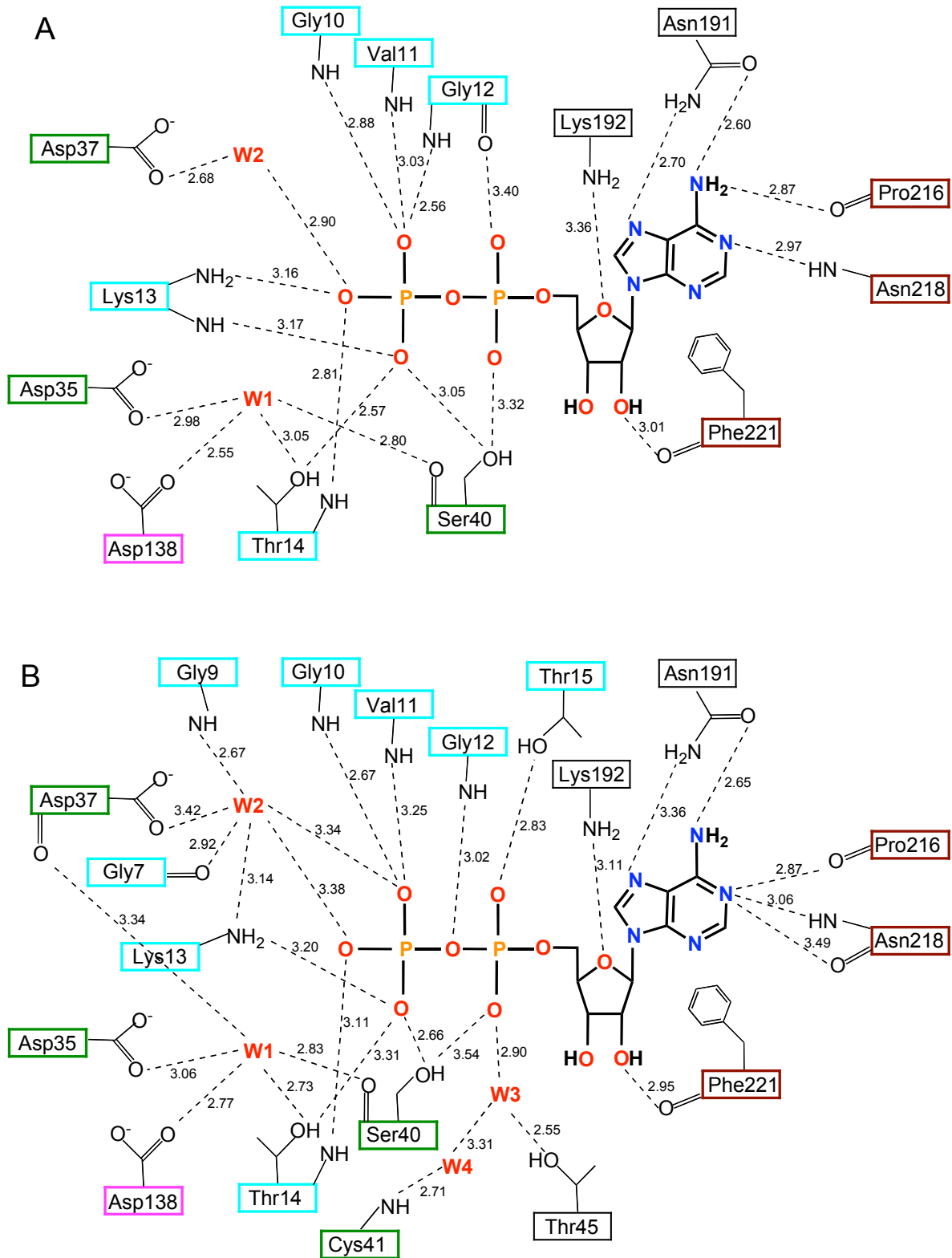


Figure A11. Schematic presentation of ADP-binding sites of ADP-bound (A) and Metal/ADP-bound (B) states of CooC1. The residues involved in the P-loop are boxed in *cyan*, the switch I residues in *green* and the switch II residues in *pink*, and α 12-helix residues in *brown*. Distances are expressed in angstroms.

Hiermit erkläre ich, dass ich die Arbeit selbständig verfasst und keine anderen als die von mir angegebenen Quellen und Hilfsmittel benutzt habe.

Hereby, I declare the fact that I wrote this work independently and used no different data than the sources presented by me.

Ferner erkläre ich, dass ich anderweitig mit oder ohne Erfolg nicht versucht habe, diese Dissertation einzureichen. Ich habe keine gleichartige Doktorprüfung an einer anderen Hochschule endgültig nicht bestanden.

Furthermore, I declare that I did not attempt to submit this thesis elsewhere with or without success. I did not have an equivalent doctor examination at another university.

Bayreuth, den _____